SITE-SPECIFIC PHOTOSYNTHESIS IN WHEAT

(*Triticum aestivum* L.)

A Thesis submitted by

Prabuddha Bandhura Dissanayake Dehigaspitiya

BSc (Agriculture) (Hons), BIT

For the award of

Doctor of Philosophy

2019

Abstract

Global food security is threatened by increasing population growth and the adverse effects of climate change. To sustain the expected global population of 9.5 billion by 2050, food production must increase by at least 60%. Exploitation of the more efficient C_4 mode of photosynthesis of important food crops has been suggested as a resolution for the foreseen risk as most of the cereal crops perform C_3 photosynthesis which is less efficient. Wheat (*Triticum aestivum* L.) is one of the most widely produced cereals globally and accounts for 21% of the world's daily dietary protein intake. Spike photosynthesis is believed to play a vital role in grain filling in wheat, with the contribution from ear photosynthesis to the total yield being 10–44%, depending on genetic and environmental factors. That is, it seems possible that different photosynthetic traits to the main photosynthetic organs may be expressed in specific sites of the same plant, although it is less prominent. Here we refer to this phenomenon as site-specific photosynthesis. It is also hypothesized that, along with photosynthesis, other vital metabolic processes such as sucrose metabolism and nitrogen (N) assimilation vary site-specifically and may play significant roles in grain quality and quantity. The magnitude of this variation in metabolic processes varies even within the same species, indicating a significant genetic difference. In addition, the site-specific variation of metabolic processes in wheat probably depends on ontogeny, being more pronounced during grain filling. Numerous studies have been conducted to elucidate photosynthesis and other metabolic pathways in the flag leaves of wheat. However, there are few site-specific studies of plant metabolic processes, and such information is essential to improve crop yield potential. Therefore, this project aimed to dissect the site-specific, genotypic, and temporal variation of key metabolic processes associated with photosynthesis using pericarps and flag leaves of three wheat genotypes (Huandoy, Amurskaja 75 and Greece25) at different growth stages.

Most gas exchange protocols are designed for leaves. Therefore, to acquire gas exchange properties of wheat spikes, I developed and optimized a new protocol using a LI-COR 6400XT portable photosynthesis system. The newly developed method was used to estimate the biological capacity of carbon (C) assimilation (Vc_{max}: maximum rate of Rubisco carboxylation and J_{max}: maximum rate of photosynthetic electron transport) of wheat spikes at different ontogenies based on carbon dioxide response curves (A-C_i curves). This method could be applied to the irregularly shaped organs

of other species, such as the panicles of rice. The measurements of Vc_{max}, $J_{max,}$ and triose phosphate utilization (*TPU*) of wheat spikes and flag leaves facilitated by using the novel gas exchange protocol, together with expression of genes involved in photosynthesis and sucrose metabolism, demonstrated site-specific variation in the biological capacity of C assimilation at early ontogeny that dissipated by late grain-filling. Transcript abundance of genes related to large and small sub-units of Rubisco (*rbcS* and *rbcL*) in flag leaves was significantly higher than in the pericarps. At early ontogeny, wheat pericarps exhibited a strong, positive correlation between the biological capacity of C assimilation and expression of key genes related to sucrose metabolism. The strong correlation between spike dry weight and the biological capacity of spike photosynthesis along with other observations suggested that metabolic processes in wheat spikes may play a major role in grain filling and thus total yield production. Site-specific, genotypic and temporal variation in the expression pattern of key genes of the C_4 pathway in wheat revealed no evidence for grain-specific C_4 photosynthesis, despite evidence of gene expression related to C_4 pathway enzymes in pericarps and flag leaves. This inference is supported by $\delta^{13}C$ observations. Site-specific, genotypic and temporal patterns of N metabolism suggested that wheat pericarps may play an important role in grain quality (protein concentration) and crop yield potential specifically after leaf senescence. The metabolic responses of wheat spikes in response to elevated temperature showed genotype-dependent differences in target gene expression and proteomics. The proteomic studies revealed that along with photosynthesis, other metabolic processes such as the antioxidant defense system, protein synthesis, and energy production were significantly affected at elevated temperatures. Of the differentially expressed proteins, those related to antioxidant defense systems were more significant in Huandoy than Amurskaja 75, indicating that Huandoy was under greater heat stress than Amurskaja 75. This inter-varietal difference was confirmed by the 60% yield decrease in Huandoy compared with a 5% yield increase in Amursksja 75 at elevated temperatures. That is, my results show that Amursksja 75 is relatively heat tolerant making it a possible candidate for crop improvement programs for future climates. However, the picture about spike metabolic processes in response to elevated temperatures remains incomplete as in both genotypes, there were numerous uncharacterized proteins which may play significant roles in wheat metabolism at a higher temperature.

Findings of this study point to the importance of exploring the site-specific, genotypic, and temporal variation of photosynthesis and other metabolic processes of vital food crops to develop higher-yielding crop varieties in the future.

Certification of Thesis

This Thesis is the work of Prabuddha Dehigaspitiya except where otherwise acknowledged, with the majority of the authorship of the papers presented as a Thesis by Publication undertaken by the student. The work is original and has not previously been submitted for any other award, except where acknowledged.

Principal Supervisor: Professor Saman Seneweera

Associate Supervisor: Professor Gavin Ash

Associate Supervisor: Dr. Anke Martin

Associate Supervisor: Dr. Kiruba Shankari Arun-Chinnappa

Student and supervisors signatures of endorsement are held at the University.

Statement of Contribution

Chapter 2: Exploring natural variation of photosynthesis in a site-specific manner: evolution, progress, and prospects.

Prabuddha Dehigaspitiya, Paul Milham, Gavin J. Ash, Kiruba Arun-Chinnappa, Dananjali Gamage, Anke Martin, Seiji Nagasaka, Saman Seneweera. Planta. 2019 Jun 28:1-8.

Prabuddha Dehigaspitiya (PD) contributed to 55% of the manuscript, consisting of the paper's design, literature collection and interpretation and writing of the manuscript. Saman Seneweera (SS) contributed 20% of the manuscript, consisting of the manuscript's design, revision of the manuscript and editorial input. Paul Milham (PM), Gavin J. Ash (GA), Kiruba Arun-Chinnappa (KA), Dananjali Gamage (DG), Anke Martin (AM) and Seiji Nagasaka (SN) contributed to 25% of the manuscript consisting of revision and editorial input.

Chapter 3: Photosynthesis measurements of wheat spikes: a protocol using LI-COR-6400XT portable photosynthesis system coupled with LI-COR conifer chamber**.**

Prabuddha Dehigaspitiya, Anke Martin, Paul Milham, Gavin J. Ash, Dananjali Gamage, Saman Seneweera. (Prepared for submission)

PD contributed 55%, consisting methodology design, data collection, analysis, writing and revision of the manuscript. SS contributed 20% of the manuscript, consisting of methodology design, data analysis and revision of the manuscript. AM, PM GA, DG contributed to 25% of the manuscript, consisting of revision and editorial input.

Chapter 4: Site-specific, genotypic and temporal variation of gas exchange and its related biochemistry in wheat (*Triticum aestivum* L.)

Prabuddha Dehigaspitiya, Paul Milham, Anke Martin, Gavin Ash, Dananjali Gamage, Saman Seneweera. (Prepared for submission)

PD contributed 55%, consisting of experimental design, data collection, analysis, writing and revision of the manuscript. SS contributed 20% of the manuscript,

consisting of experimental design, data analysis and revision of the manuscript. PM, AM, GA, and DG contributed to 25% of the manuscript, consisting of revision, data collection and editorial input.

Chapter 5: Site-specific, genotypic and temporal characterization of nitrogen metabolism and the expression of key genes of C_4 photosynthesis in wheat (*Triticum aestivum* L.)

Prabuddha Dehigaspitiya, Anke Martin, Paul Milham, Dananjali Gamage, Gavin J. Ash, Kiruba Arun-Chinnappa, Seiji Nagasaka, Kotaro Shirai, Saman Seneweera. (Prepared for submission)

PD contributed 55%, consisting of experimental design, data collection, analysis, writing and revision of the manuscript. SS contributed 20% of the manuscript, consisting of experimental design, data analysis and revision of the manuscript. AM, PM, DG, GA, KA, SN, and Kotaro Shirai, contributed to 25% of the manuscript, consisting of revision, data collection and editorial input.

Chapter 6: A comparative proteomic analysis of wheat (*Triticum aestivum* L.) at high temperatures

Prabuddha Dehigaspitiya, Anke Martin, Paul Milham, Gavin J. Ash, Dananjali Gamage, Kolin Harinda Rajapaksha, Saman Seneweera. (Prepared for submission)

PD contributed 55%, consisting of experimental design, data collection, analysis, writing and revision of the manuscript. SS contributed 20% of the manuscript, consisting of experimental design, data analysis and revision of the manuscript. AM, PM, GA, DG and Kolin Harinda Rajapaksha contributed to 25% of the manuscript, consisting of revision, data collection and analysis, and editorial input.

Acknowledgement

This Ph.D. thesis has been the most amazing undertaking of my life, and I owe a debt of gratitude to all those who have supported me throughout this journey.

First and foremost, I would like to express my special appreciation and sincere gratitude to my principal supervisor, Professor Saman Seneweera for all his contribution of time, ideas, and funding to make my Ph.D. experience productive and stimulating. Besides his role as the principal supervisor, I am also thankful for the excellent example he provided as a successful leader and a good friend to make my Ph.D. journey stressless. Without his guidance and constant feedback, this Ph.D. would not have been achievable. I owe a sincere thank you to Dr. Anke Martin, associate supervisor of my project for all the support, funding, and encouragement she gave me to complete my Ph.D. within three years. Whenever I had doubts and questions, Dr. Martin always made herself available despite her busy schedule. Many thanks to Professor Gavin Ash, associate supervisor of my project for his time and support. I specifically appreciate Professor Ash's prompt responses. Although he is amongst the busiest academics at the university, he always allocated time for me whenever I needed it. I would also like to extend thanks to Dr. Kiruba Shankari for her support at the beginning. I have been lucky enough to have a chance to spend a few years of my life under the excellent supervision of these four exemplary academics.

I gratefully acknowledge the University of Southern Queensland, Australia for providing me the opportunity along with a Postgraduate Research Scholarship to read for my Ph.D. Further, I would also like to extend thanks to Professor Peter Terry, Dean (Graduate Research School), USQ for his kind support during my studies.

I owe a huge debt of gratitude to Professor Paul Milham for all the support and encouragement he gave me during thesis writing. He helped me to improve my writing skills and put a lot of effort to improve the manuscripts/thesis up to this level. I am very much fortunate for the opportunity to work under his guidance.

I am particularly indebted to Dr. Dananjali Gamage, who helped and encouraged me enormously from the very first day of my Ph.D. journey. Her excellent support during experiments and data collection has made an invaluable contribution towards my

Ph.D. Without her help and constant feedback, this thesis would not have been completed on time. Also, thank you so much for being a part of the stunning moments I had during my Ph.D.

I would like to give credit to Professor Seiji Nagasakasa for being an excellent scientist example for me to follow and goals for me to strive for. I also extend my thanks to Dr. Michael Thompson for support with instrumentation and Professor Kolin Harinda Rajapaksha for his excellent provision of the proteomics analysis. Additionally, I would like to thank all the staff members at the USQ who supported me over the years.

I gratefully appreciate the support received through the collaborative work undertaken with University of Tokyo, Japan, National Institute of Fundamental Studies, Sri Lanka, Toyo University, Japan and La Trobe University, Australia, during the final phase of my Ph.D.

I am indebted to all my friends and their families in Toowoomba who opened their homes to me during my time at USQ and who were always so helpful in numerous ways. Special thanks go to Dr. Jay Bandara, Gayani Bandara, Chathurika Gunathunga, Piyum Herath, Mythree Seneweera, Pramesha Madurangi, Indika Herath, Prasanna Kumarathilaka, Madhubashitha Herath, Sachindara Premasiri, Tathsarani Pramasiri, Niroshini Gunathilaka, Arosh Thilakpriya, Chamika Wijerathna, Dumila Perera and Niluka Nakandala.

My sincere thanks also go out to all my friends from the USQ who have been with me throughout my candidature, notably, Ahmed Saad, Motiur Rahaman, Sriram Padmanaban, Barsha Poudel, Joseph Barry, Rian Abdulsada, Sudhan Shah, Mela Aryal, Peter Buyoyu, Chandima Kamaral, and Rudrakshi Sharma.

I would also like to say a heartfelt thank you to my extraordinary Mum, Dad, Pamuditha, Hashini, Irushi, and Sandhuli for always believing in me and encouraging me to follow my dreams. I am particularly indebted to my grandfather, Dr. Ananda Abeysekara, for reading my manuscripts and giving constructive comments.

Last but not least, I wish to give thanks to my wonderful wife, Hansini, for her love, inspiration understanding, and for keeping me sane over the past few months. Thank you for being my editor. But most of all, thank you for being my best friend. I owe you everything.

Table of Content

CHAPTER 1

INTRODUCTION AND LITERATURE REVIEW

1.1 Wheat and its importance for global food security

Global food security is threatened by the current population growth and the adverse effects of climate change (Dehigaspitiya et al. 2019). It is predicted that the global population will have increased to 9.5 billion by 2050 (Alexandratos and Bruinsma 2012). To sustain this increase, global food production must grow by at least 60% (Crist et al. 2017). A dramatic yield improvement in cereal crops like rice (*Oriza sativa* L.) and wheat (*Triticum aestivum* L.) was achieved between the 1950s and 1980s during the Green Revolution, mainly via the introduction of dwarf varieties through molecular breeding (Furbank et al. 2015). Outcomes of the Green Revolution aided to satisfy the global cereal demand for many years. However, feeding the expected global population seems impossible without another massive advance in agriculture as the genetic yield potential of current cereal crops using conventional breeding has almost reached its maximum (Furbank et al. 2015; Dehigaspitiya et al. 2019). Meeting future food production targets has become even more challenging because of the damages to crop and food system infrastructure due to the adverse effects of climate change (Lesk et al. 2016).

As the most cultivated cereal crop in the world, wheat is accountable for one-third of the global annual cereal production and is responsible for 21% of the world's daily dietary protein intake, playing an important role in global food security (Shiferaw et al. 2013). Wheat provides vital components required for human nutrition such as minerals, vitamins, beneficial phytochemicals, and dietary fibre (Shewry 2009). With the projected population of 9.5 billion by 2050, demand for wheat is estimated to increase by at least 50% (Li et al. 2017). Thus it is vital to focus on improving the yield and nutritional properties of wheat (Alexandratos and Bruinsma 2012).

1.2 Site-specific photosynthesis in wheat

Wheat is considered a classical C_3 crop, based on its leaf photosynthesis biochemistry. Improving photosynthetic efficiency of classical C_3 cereals has been suggested as a resolution for future food production targets (Li et al. 2017). One of the different strategies of improving the photosynthetic efficiency, that is bioengineering an efficient photosynthetic pathway into food crops, has been intensely studied (Peterhansel et al. 2013). However, improving photosynthetic efficiency has been challenging due to the complex nature of the photosynthetic processes and inadequate understanding of the genetic mechanisms (Dehigaspitiya et al. 2019).

Spike photosynthesis is believed to play a vital role in grain filling in wheat, with the contribution from ear photosynthesis to the total yield being 10–44%, depending on genetic and environmental factors (Sanchez-Bragado et al. 2014). In food crops, more importance has until now been placed on photosynthesis of the main photosynthetic organs, namely the leaves. However, little attention has been given to the site-specific and temporal variation of photosynthesis and the possibility of utilizing the knowledge of site-specific photosynthesis and photosynthesis-related processes for crop improvement.

Although wheat is considered a classical C_3 cereal based on its leaf photosynthesis, evidence is mounting that a different mode of photosynthesis may operate in wheat spikes compared to leaves (Rangan et al. 2016). This raises the possibility of considering spike photosynthesis as a physiological trait for future crop improvements (Dehigaspitiya et al. 2019). Along with photosynthesis, other vital metabolic processes such as nitrogen assimilation and sucrose metabolism could also vary site-specifically and may play significant roles in grain quantity and protein content (Dehigaspitiya et al. 2019). Therefore, dissecting the site-specific and temporal variation in metabolic processes in wheat and utilizing them for crop improvement appears to be the best way forward. Detailed information about the site-specific variation of photosynthesis and the possibility of utilizing the knowledge of site-specific photosynthesis in crop improvement has been summarised in the published review manuscript entitled "Exploring natural variation of photosynthesis in a site-specific manner: evolution, progress, and prospects" (Chapter 2).

1.3 Objectives of the Study

Wheat genotypes have been characterized based on photosynthesis and other metabolic processes of major photosynthetic organs: leaves. Less attention has been given placed on site-specific variation of photosynthesis and the possibility of using the site-specific variation of plant metabolic processes in crop improvement (Dehigaspitiya et al. 2019). Thus this study focused on investigating site-specific, genotypic and temporal variation in carbon assimilation and other photosynthesis-related processes: sucrose metabolism, nitrogen (N) metabolism, and the expression of C_4 pathway enzymes in wheat using wheat spikes and flag leaves of three wheat genotypes which were grown at different growth stages. Besides, the metabolic changes in wheat spikes at elevated temperatures to determine the adaptability of wheat genotypes to a changing climate was investigated. To achieve this overall aim, this study was broken down into four objectives.

1. Optimize a protocol to measure spike gas exchange of wheat using LI-COR 6400XT portable photosynthesis system (Chapter 3)

Spike photosynthesis is believed to play a vital role in grain filling in wheat and thus the total yield (Sanchez-Bragado et al. 2016). Determining gas exchange parameters of wheat spikes has become increasingly important as a means of elucidating the photosynthetic mechanism and whole plant performance. Although there have been optimized methodologies to determine gas exchange parameters of leaves (Evans and Santiago 2014), protocols for grain gas exchange are less well defined and are not suitable of using protocols of measuring leaf gas exchange for spikes as wheat spikes differ structurally and physiologically from leaves. Thus, the first objective of this project was to optimize a protocol to measure gas exchange parameters of wheat spikes using a portable photosynthesis system.

2. Determine the site-specific, temporal and genotypic variation of photosynthesis and sucrose metabolism in wheat (Chapter 4)

Most of the previous studies investigating photosynthetic parameters of wheat have focussed solely on flag leaves while limited information is available for temporal and genotypic variation of spike photosynthesis (Dehigaspitiya et al. 2019). There also does not appear to be much literature on how sucrose metabolism of wheat pericarps vary over time compared to flag leaves. Therefore, a series of experiments which

involved, molecular, biochemical, and physiological approaches were used to determine the site-specific, genotypic temporal variation of photosynthesis and sucrose metabolism in wheat and the spike contribution to grain filling.

3. Investigate the site-specific, genotypic and temporal variation in the expression of the C_4 pathway and N metabolism in wheat (Chapter 5)

Wheat is considered a classical C_3 cereal. However, recent findings suggested that developing wheat pericarps probably perform a C_4-like photosynthetic pathway (Rangan et al. 2016). The grain protein content of wheat is one of the critical aspects of grain quality which is governed by the N metabolism in plants. Further, plant N metabolism is one of the determining factors of the yield potential (Aben et al. 1999). While it is established that there is a variation in N metabolism in flag leaves of wheat, little is known about the site-specific, genotypic, and temporal variation behind N metabolism (Dehigaspitiya et al. 2019). This chapter focusses on traits related to the C_4 pathway and changes in N metabolism in wheat pericarps (Outer pericarp which includes epidermis and hypodermis) and flag leaves at different growth stages. Identification of important traits of efficient photosynthesis and changes in N metabolism will allow for closer investigations into these changes in future studies to improve grain protein content in wheat.

4. Elucidate the genotypic variation of spike metabolic responses in response to elevated temperatures using gene expression and proteomic approaches (Chapter 6)

Wheat is among the most sensitive crops to heat stress (Wahid et al. 2007). Elevated temperatures may significantly alter the metabolic pathways such as carbon and N assimilation in wheat pericarps (Wahid et al. 2007). Changes in plant metabolism in response to high temperature may have a considerable genotypic effect. Along with carbon and N metabolism associated transcriptome responses, analysis of the whole proteome response of a particular plant organ may provide vital information on metabolic changes occurring in response to elevated temperatures. Therefore, this chapter was designed to investigate the differences in spike metabolic processes of wheat under heat stress and to identify characteristics of possible heat resistant genotypes for crop improvement programs for future climates.

CHAPTER 2

LITERATURE REVIEW

In addition to the literature review in Chapter 1, a review publication entitled 'Exploring natural variation of photosynthesis in a site-specific manner: evolution, progress, and prospects' was published in Planta Journal. This review paper discusses the importance of site-specific changes in photosynthesis and other metabolic processes for crop improvement. The review presents an overview of the foreseen threat to food security due to the population growth, stagnated crop productivity, and climate change. It then explains site-specific photosynthesis, briefly giving some background into natural variation and the evolution of photosynthetic pathways. This chapter is an introduction to the rest of the experimental chapters of this thesis which discuss the importance of site-specific photosynthesis in wheat to improve the crop productivity.

Prabuddha Dehigaspitiya, Paul Milham, Gavin J. Ash, Kiruba Arun-Chinnappa, Dananjali Gamage, Anke Martin, Seiji Nagasaka, Saman Seneweera. Planta. 2019 Jun 28:1-8.

Planta
https://doi.org/10.1007/s00425-019-03223-1

REVIEW

Exploring natural variation of photosynthesis in a site-specific manner: evolution, progress, and prospects

Prabuddha Dehigaspitiya[1] · Paul Milham[2] · Gavin J. Ash[1] · Kiruba Arun-Chinnappa[1] · Dananjali Gamage[1] · Anke Martin[1] · Seiji Nagasaka[1] · Saman Seneweera[1,3]

Received: 27 May 2019 / Accepted: 20 June 2019

Abstract

Main conclusion **Site-specific changes of photosynthesis, a relatively new concept, can be used to improve the productivity of critical food crops to mitigate the foreseen food crisis.**

Abstract Global food security is threatened by an increasing population and the effects of climate change. Large yield improvements were achieved in major cereal crops between the 1950s and 1980s through the Green Revolution. However, we are currently experiencing a significant decline in yield progress. Of the many approaches to improved cereal yields, exploitation of the mode of photosynthesis has been intensely studied. Even though the C_4 pathway is considered the most efficient, mainly because of the carbon concentrating mechanisms around the enzyme ribulose-1,5-bisphosphate carboxylase/oxygenase, which minimize photorespiration, much is still unknown about the specific gene regulation of this mode of photosynthesis. Most of the critical cereal crops, including wheat and rice, are categorized as C_3 plants based on the photosynthesis of major photosynthetic organs. However, recent findings raise the possibility of different modes of photosynthesis occurring at different sites in the same plant and/or in plants grown in different habitats. That is, it seems possible that efficient photosynthetic traits may be expressed in specific organs, even though the major photosynthetic pathway is C_3. Knowledge of site-specific differences in photosynthesis, coupled with site-specific regulation of gene expression, may therefore hold a potential to enhance the yields of economically important C_3 crops.

Keywords Crop improvement · Engineering C_4 into C_3 · Photorespiration · Photosynthesis gene regulation

Introduction

Photosynthesis is the biological process that produces organic carbon compounds by using solar energy, water and atmospheric carbon dioxide (CO_2). In this process, atmospheric CO_2, after going through a series of photosynthetic reduction steps, is converted to carbohydrates (Evans 2013). This biological process is used by autotrophic and semi-autotrophic organisms, being the main driver of food production for heterotrophs for billions of years (Wang et al.

✉ Saman Seneweera
Saman.Seneweera@usq.edu.au

Prabuddha Dehigaspitiya
Prabuddha.DehigaspitiyageDon@usq.edu.au

Paul Milham
P.Milham@westernsydney.edu.au

Gavin J. Ash
Gavin.Ash@usq.edu.au

Kiruba Arun-Chinnappa
Kiruba.ArunChinnappa@usq.edu.au

Dananjali Gamage
Dananjali.Gamage@usq.edu.au

Anke Martin
Anke.Martin@usq.edu.au

Seiji Nagasaka
nagasaka@toyo.jp

[1] Centre for Crop Health, University of Southern Queensland, Toowoomba, QLD 4350, Australia

[2] Hawkesbury Institute for the Environment, Western Sydney University, LB 1797, Penrith, NSW 2753, Australia

[3] National Institute of Fundamental Studies, Hanthana Road, Kandy 20000, Central, Sri Lanka

Published online: 28 June 2019

2011). However, the global production of food for humans has been challenged as a result of increasing population and a potential decrease in food productivity driven by factors related to climate change (Berardy and Chester 2017; Crist et al. 2017).

It is anticipated that the global population will have increased to 9.5 billion by 2050 (Alexandratos and Bruinsma 2012). To sustain this increase, food production must increase by at least 60% (Clay 2011; Crist et al. 2017). Towards the end of 2016, Asia accounted for 59.5% of the global population, and it is undergoing continuous growth (Worldmeters 2017). Tilman et al. (2009) and Sheehy et al. (2008) have suggested that a 60% improvement in the yield of rice (*Oryza sativa* L.) might be needed in order to cater for the growing Asian population in the near future. This translates to catering to 43 people from a hectare of rice instead of the present 27. A dramatic improvement in yield of C_3 cereal crops like wheat (*Triticum aestivum* L.) and rice was achieved between the 1950s and 1980s during the Green Revolution, mainly through the introduction of dwarf varieties via molecular breeding (Furbank et al. 2015). This also improved the fertilizer use efficiency by increasing the grain mass of the crop at the expense of the rest of the above ground biomass (increase in harvest index) (Stapper and Fischer 1990; Evans 2013). Outcomes of the Green Revolution have helped to satisfy the global food demand for many years. However, feeding the projected global population seems impossible without another massive breakthrough as the genetic yield potential of current cereal crops, using conventional breeding, has almost plateaued (Kropff et al. 1994; Furbank et al. 2015; Taylor and Long 2017; Wang et al. 2017b). Meeting future food production goals has become even more challenging because of the predicted and even current changes in climate, such as the increase in global temperature and water scarcity (Elliott et al. 2014). Of the few possible solutions for the upcoming food crisis, increasing the biomass of critical food crops is one of the most intensely studied (Evans 2013; Taylor and Long 2017).

The Green Revolution increased the harvest index with little change to the total aboveground biomass (Austin et al. 1989; Evans 2013; Ort et al. 2015). Evans (2013) suggested that further increases in harvest index may come at the expense of leaves, the major source of carbon fixation, and consequently decreased grain yields. As a corollary, it was argued that total biomass may have to be increased to achieve higher yields (Evans 2013), which would require either enrichment of the light interception of crop plants throughout the growing season and/or an increase in the photosynthetic efficiency (Evans 2013; Taylor and Long 2017). Since there appears little possibility of further improvement to light interception (Evans 2013), increasing photosynthetic efficiency merits investigation.

Of the different strategies for improving photosynthetic efficiency (Fig. 1), engineering a more efficient mode of photosynthesis for food crops is being intensively studied, e.g., by engineering C_4 into C_3 (Gao et al. 2014; Wang et al. 2014; Li et al. 2017); mitigating the functional limitations of the major CO_2 fixing enzyme, ribulose-1,5-bisphosphate carboxylase/oxygenase (RuBisCO) (Cai et al. 2014; Galmes et al. 2014; Sáez et al. 2017); increasing the mesophyll conductance of CO_2 diffusion (Cano et al. 2014; Gu and Sun 2014; Xiong et al. 2017); minimizing the inefficiencies due to dynamic environmental factors (Williams et al. 2014; Retkute et al. 2015; Vialet-Chabrand et al. 2017); and regulating sink–source feedback on photosynthesis (Fatichi et al. 2014; Campany et al. 2017). However, improvement of photosynthetic efficiency is challenging because of the complex nature of photosynthetic mechanisms and inadequate understanding of the genetic processes (Rangan et al. 2016b).

Until now, angiosperms have been divided into functional categories according to the photosynthetic mode of the primary photosynthetic organs, typically the leaves. However, this categorization has been brought into question by the fact that, within the same plant, different organs may perform different modes of photosynthesis (Rangan et al. 2016a, b). We refer to this phenomenon as site-specific or dual biochemistry photosynthesis. The hypothesis of site-specific photosynthesis also includes the possibility that the mode of photosynthesis may change with the environment. Here we mainly focus on the site-specific C_4 photosynthesis since it is the most efficient mode at the current atmospheric conditions. This conceptually novel hypothesis is supported by a growing number of observations, e.g., the cells surrounding the vascular bundles in the stem and petiole of tobacco and celery have C_4-like photosynthetic mechanisms, even though the leaves are C_3, and consequently, that is how the species is categorized (Hibberd and Quick (2002). Furthermore, changes in photosynthesis similar to the C_4 pathway were observed in rice panicles during grain filling (Imaizumi et al. 1990), and evidence for grain-specific C_4 photosynthesis has been reported in the C_3 species, wheat (Rangan et al. 2016b). Further, the existence of different photosynthetic pathways in the husk and foliage leaves of maize (*Zea mays*) is perhaps the most obvious case of site-specific changes in photosynthesis.

The different modes of photosynthesis have been extensively reviewed (Edwards et al. 2004; Kiang et al. 2007; Hibberd and Covshoff 2010), including the possibility of engineering the C_4 pathway into the C_3 (Matsuoka et al. 2001; von Caemmerer 2003; Kajala et al. 2011), and other ways to improve photosynthetic efficiency (Long et al. 2006; Zhu et al. 2010; Blankenship et al. 2011; Ort et al. 2015). However, site-specific photosynthesis and dual-biochemistry photosynthesis have not been sufficiently addressed.

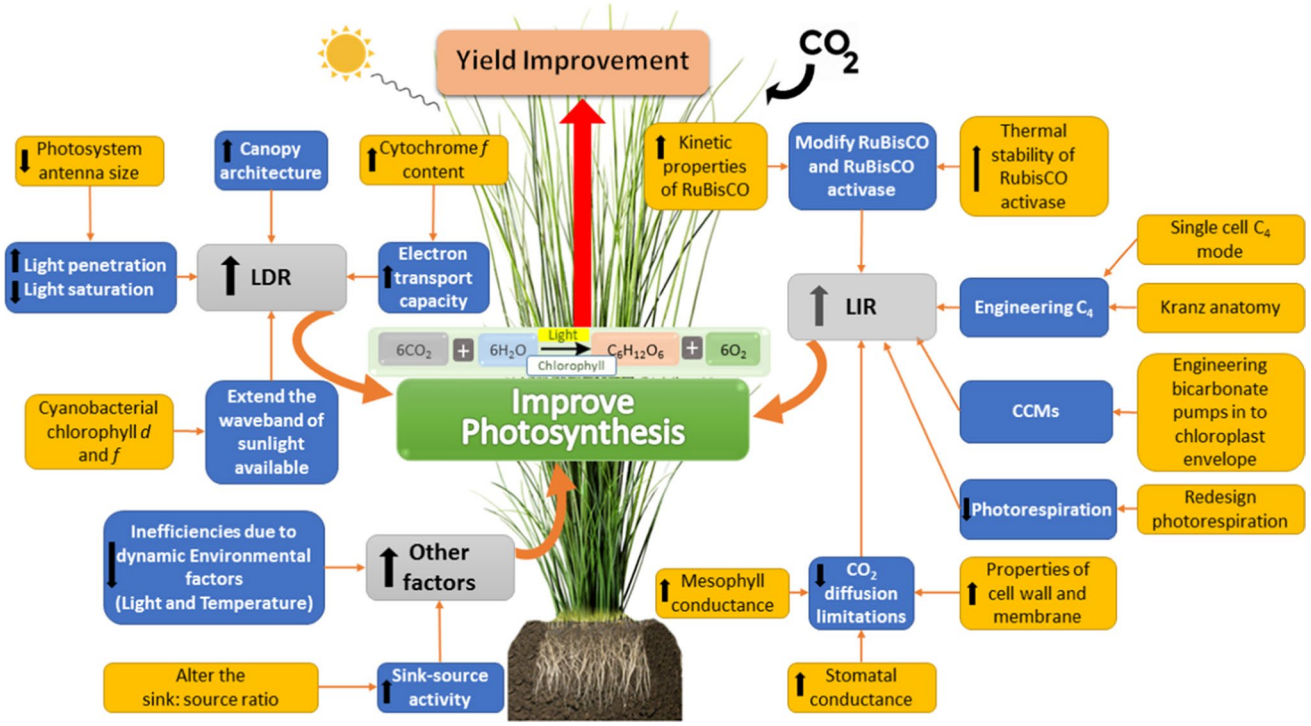

Fig. 1 Possible approaches to improve photosynthesis (upward arrows represent an improvement and downward arrows represent an impairment. LDR and LIR represent light-dependant reactions and light-independent reactions, respectively). Improving the efficiency of the LDR could have an impact on improving the overall efficiency of photosynthesis. Reduction of photosystem antenna size might increase the light penetration and decrease the light saturation of the photosynthetic tissue. In addition, canopy architecture is also important. To expand the available waveband of sunlight, Cyanobacterial chlorophyll d and f can be used and increase the cytochrome f content may lead to increase the electron transport capacity. Moving to the improvement of LIR, modification of RuBisCO is one of the hot research trends. Engineering C_4 mode to C_3, initiate CCMs, redesigning photorespiration and mitigation of the limitations of CO_2 diffusion in photosynthetic tissues are other possible approaches that have been proposed. In addition, alteration of the sink: source ratio and activity; minimize the inefficiencies of photosynthesis due to dynamic environmental factors have also been proposed

In this review, we summarize the literature on site-specific photosynthesis and its importance. We also critically analyze the evolutionary linkage between C_3 and C_4 photosynthesis through photorespiratory modifications, importance of photorespiratory carbon pump as an evolutionary bridge for C_4 pathway, recent approaches that have been taken to improve the efficiency of photosynthesis, photosynthetically efficient physiological traits to understand site-specific photosynthesis, gene-regulatory characteristics of C_4 photosynthesis in a site-specific manner. Also, we discuss the knowledge gaps and the future directions that need to be undertaken to get a better understanding of site-specific photosynthesis. Finally, we summarise the other possible ways of increasing the efficiency of photosynthesis by enhancing the properties of the light-independent and light-dependent reactions.

Natural variation of photosynthesis in angiosperms

Being the most important biochemical light energy using process on earth, photosynthesis converts CO_2 into organic sugars through plants, algae, and photosynthetic bacteria. Photosynthesis consists of two distinct biochemical processes, the light-dependent reaction (LDR) and the light-independent reaction (LIR). The LDR produces ATP (adenosine triphosphate) and NADPH (reduced form of nicotinamide adenine dinucleotide phosphate), which are later utilized by the LIR: the Calvin–Benson cycle. Production of carbohydrates using atmospheric CO_2 and the products of the LDR take place in the Calvin–Benson cycle. Currently, four major photosynthetic mechanisms have been identified in angiosperms: C_3, crassulacean acid metabolism (CAM), C_4, and C_3–C_4 intermediates (Yamori et al. 2014) (Fig. 2). Out of those, the most common photosynthetic mechanism is C_3 where RubisCO fixes atmospheric CO_2 into a three-carbon compound; mainly, phosphoglyceric acid (PGA).

On the other hand, the first stable compound of photosynthesis in the C_4 pathway is the four-carbon molecule, oxaloacetate (OAA). Also, C_4 appears the most efficient form of carbon fixation in the majority of current environmental conditions, i.e., C_4 is theoretically 30% more efficient than C_3 photosynthesis (Zhu et al. 2008). The C_4 grass *Echinochloa polystachya,* growing on the Amazon floodplain,

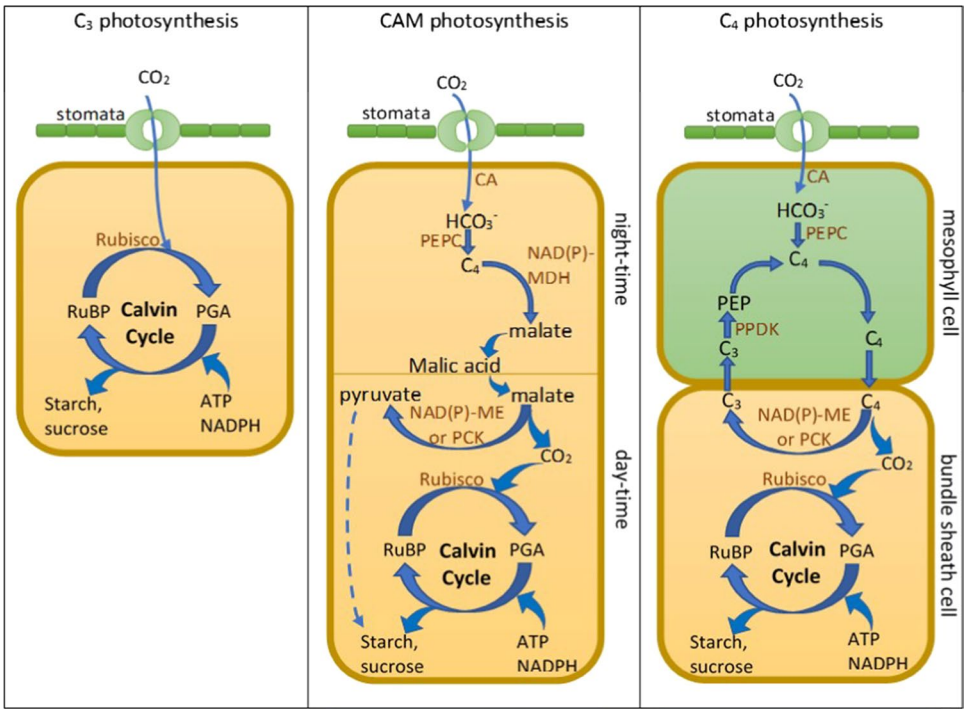

Fig. 2 Schematic diagram of C_3 CAM and C_4 photosynthesis. *Rubisco* ribulose-1,5-bisphosphate carboxylase/oxygenase, *RuBP* ribulose 1,5-bisphosphate, *PGA* phosphoglyceric acid, *ATP* adenosine tri phosphate, *NADPH* nicotinamide adenine dinucleotide phosphate hydrogen, *CA* carbonic anhydrase, *HCO 3* bicarbonate, *NADP* nicotinamide adenine dinucleotide phosphate, *NADP-MDH* NADP-malate dehydrogenase, *NADPME:NADP*-dependent malic enzyme, *PCK* phosphoenolpyruvate carboxykinase, *PEPC* phosphorenolpyruvate carboxylase, *PPDK* pyruvate orthophosphate dikinase, *PEP* phosphorenolpyruvate

holds the record for the highest recorded annual dry-matter productivity, for any terrestrial vegetation, having an average of 100 tonnes per hectare per year (t ha^{-1} $year^{-1}$; productivity is given throughout as mass of oven-dry matter) (Piedade et al. 1991). C_4 forage grass *Pennisetum purpureum* cultivated in El Salvador, recorded the highest annual dry-matter yield for a crop, producing 88 t ha^{-1} $year^{-1}$ (Beadle and Long 1985). Engineering C_4 photosynthesis into critical C_3 food crops has been intensely studied (Kajala et al. 2011; Rangan et al. 2016b; Wang et al. 2017b); however, engineering a complete C_4 pathway into C_3 has proven elusive due to the lack of knowledge of specific gene regulation in both photosynthetic pathways (Wang et al. 2011). Photosynthesis of both C_3 and CAM plants takes place in a single photosynthetic cell. The primary difference between C_4 and CAM is that the CAM pathway expresses a temporal separation of the photosynthetic process (Fig. 2), rather than a spatial separation seen in C_4 Kranz, which will be discussed later.

The evolutionary rise of C_4 photosynthesis through photorespiratory modifications

Current differences in photosynthetic properties of higher plants can be considered as an evolutionary adaptation to diverse ecosystems/niches. The most diverse modifications of photosynthesis occur in the LIRs. However, although there are spatial and temporal differences among photosynthetic modes, the enzyme RuBisCO universally catalyzes the fixation of CO_2 into a stable, three-carbon intermediate. RuBisCO is bifunctional, also binding O_2 in competition with CO_2 and catalyzing a reaction known as photorespiration, which negatively affects the overall efficiency of photosynthesis, and consumes ATP and NADPH (Bowes et al. 1971; Furbank 2011, 2016). At current atmospheric concentrations of CO_2 and O_2, photorespiration can decrease photosynthesis to 30% of its potential (Sharkey 1988; Zhu et al. 2004). This happens mainly by losing assimilated C and N as photorespiratory CO_2 and NH_3 (Fig. 2) (Sharkey 1988; Zhu et al. 2004). However, despite all the inefficiencies that adversely affect photosynthesis, photorespiration is nonetheless the second-most important biochemical reaction on earth, because of its salvage action against 2-phosphoglycolate (2PG): a toxic by-product from oxygenation of RuBisCO (Hagemann et al. 2016). Oxygenation of RuBisCO produces a large amount of 2-PG during the day. Photorespiration is a light-induced biochemical process which converts 2-PG into 3-phosphoglycerate (3-PGA), a Calvin–Benson cycle intermediate (Fig. 2). Therefore, photorespiration is an essential metabolic process for all organisms which perform oxygenic photosynthesis (Somerville 2001). Reactions of photorespiration take place in the chloroplasts, peroxisomes, cytosol and mitochondria. Also, for the main photorespiratory cycle, at least eight enzymes are needed other than a few more auxiliary enzymes (Bauwe et al. 2010).

Photorespiration was not a concern during the early evolutionary stages of photosynthesis when the atmosphere was dominated by CO_2 with only a trace of O_2 (Evans 2013). However, photosynthesis has so successfully reversed that ratio that competition for binding O_2 to RuBisCO has appreciably increased. Hence,

photorespiration may have co-evolved with oxygenic photosynthesis around 3.8–2.5 billion years ago in cyanobacteria that initially lived in O_2-free Precambrian oceans (Canfield 2005; Allen and Martin 2007; Bauwe et al. 2010). The evolution of algae and higher plants may have taken place after the uptake of cyanobacteria into heterotrophs about 1.5 billion years ago (Reyes-Prieto et al. 2007; Bauwe et al. 2010). During this time, C_3 photosynthesis became the dominant carbon assimilation pathway on earth. It is believed that the earth's climate transformed in the past 40 million years from a warm, humid atmosphere having temperate poles, to a less humid atmosphere, with frozen poles, deserts, and grasslands (Zachos et al. 2008). Parallel to this climate shift, the atmospheric CO_2 concentration decreased from over 1000 µmol mol^{-1}, 50 million years ago, to less than 200 µmol CO_2 mol^{-1}, 20,000 years ago (Zachos et al. 2008; Beerling and Royer 2011). In response to this shift, the modern biosphere evolved Bouchenak-khelladi et al. (2009), and two main photosynthetic strategies evolved to deal with the increasing O_2/CO_2. First, carbon concentrating mechanisms (CCMs) evolved in photosynthetic organs to allow RuBisCO to operate in a relatively enriched CO_2/O_2 environment (Hatch and Slack 1966; Sage 2016; von Caemmerer et al. 2017). C_4, CAM, and C_3–C_4 intermediates have CCMs in their photosynthetic pathways. Amongst them, C_4 photosynthesis has the most efficient and complex CCM. Secondly, the kinetic properties of RuBisCO changed to improve its selectivity towards CO_2 relative to O_2 (Evans 2013).

Photorespiratory carbon pump as an evolutionary bridge to the C_4 pathway

There is increasing evidence for the linkage of photorespiration to the evolution of C_4 photosynthesis from its C_3 ancestors (Sage 2004; Hagemann et al. 2016). The development of a photorespiratory carbon pump (Fig. 3), which is commonly seen in C_3–C_4 intermediates, is considered to be an evolutionary bridge for decarboxyacid-based C_4 photosynthesis (Mallmann et al. 2014). The CO_2 released during the decarboxylation in photorespiration may not be a complete loss to the plant since it can be refixed by RuBisCO (Sage and Sage 2009). The photorespiratory carbon pump facilitates efficient refixation of CO_2, by allowing photorespiration to occur in two different types of cells: mesophyll cells (MCs) and bundle sheath cells (BSCs) (Fig. 3). The two-carbon metabolite glycine acts as the CO_2 transporter of this mechanism, which is therefore termed the C_2 pathway. To perform the C_2 pathway more efficiently, a large number of cell-type-specific physiological, biochemical and gene regulatory preconditioning is needed. Localization of mitochondria, which contain glycine decarboxylase (an essential enzyme in photorespiration) into BSCs is one such modification, which forces photorespiratory glycine to migrate from MCs to BSCs (Fig. 3). The CO_2 released by the decarboxylation of glycine at least doubles the CO_2 concentration at BSCs, which creates a favorable condition for BSC RuBisCO to perform at a higher catalytic efficiency and increase photosynthesis. The arrangement of cell organelles linked with photorespiration is also essential for an

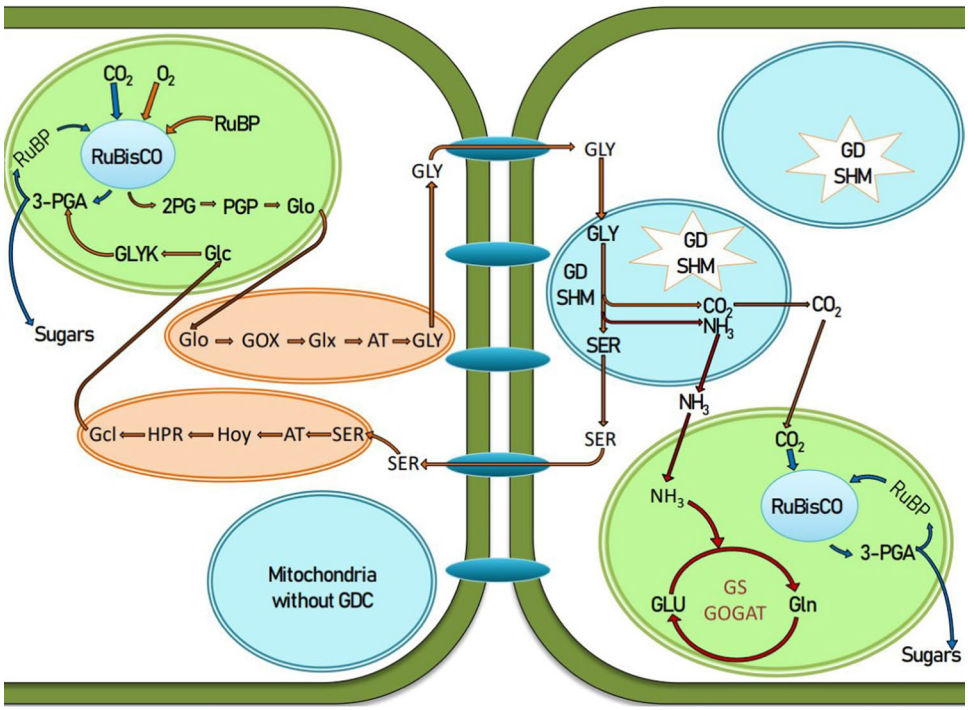

Fig. 3 Schematic diagram of the photorespiratory carbon pump. Green colored circles represent chloroplasts, orange circles represent peroxisomes and blue circles represents mitochondria. *AT* aminotransferase, *GD* glycine decarboxylase, *Glc* glycerate, *Gln* glutamine, *Glo* glycolate, *GLU* glutamate, *GLY* glycine, *GOX* glycolate oxidase, *HPR* Hyp reductase, *Hoy* hydroxypyruvate, *PGP* phosphoglycolate phosphatase, *Pyr* pyruvate, *RuBP* ribulose-1,5-bisphosphate, *SER* serine, *SHM* serine hydroxymethyltransferase, *2-PG* 2-phosphoglycolate, *3-PGA* 3-phospoglycerate

efficient C_2 pathway. The tight arrangement of chloroplasts and mitochondria on the inner cell-walls of BSCs, modifications of chloroplasts to increase their surface area, reduced MC:BSC through increased venation, higher plasmodesmata density connecting adjacent MCs and BSCs, less permeable cell walls of BSCs, and development of mechanisms for photorespiratory NH_4^+ metabolism are some other favorable factors to minimize photorespiratory CO_2 leakage and improve C_2 pathway efficiency (Fig. 3) (Sage and Sage 2009; Busch et al. 2013).

Even though photorespiration has been traditionally regarded as energy wasteful, a process that needs to be redesigned in order to improve photosynthesis, a growing body of evidence suggests otherwise. Biotic and abiotic stresses commonly limit crop productivity throughout the world (Mittler 2006; Kangasjärvi et al. 2012) and it has been reported that photorespiration mitigates their adverse effects. The H_2O_2 produced by the reaction of glycolate oxidase in photorespiration is a useful defense against a wide range of pathogens (Taler et al. 2004; Rojas et al. 2012). Strong correlations between photorespiration and tolerance of abiotic stresses, such as drought (Li and Hu 2015), salt (Hoshida et al. 2000) and exposure to heavy metals (Voss et al. 2013), have also been reported. In addition, recent studies have provided evidence for the interaction of photorespiration with other metabolic activities such as nitrogen assimilation (Rachmilevitch et al. 2004; Linka and Weber 2005; Keys 2006), respiration (Bykova et al. 2005; Tcherkez et al. 2008), one-carbon metabolism and associated purine biosynthesis (Rontein et al. 2003), and redox signaling (Foyer et al. 2009).

Past studies, combined with modern technological advancements, have answered some important questions regarding the photorespiratory pathway, its evolutionary linkage to C_4 photosynthesis and some of its interactions with other metabolic pathways (Bauwe et al. 2010). Yet there are several key areas that still need investigation, e.g., the changes in photorespiration in dynamic environments, how photorespiration interacts with other metabolic pathways (Bauwe et al. 2010) and, most importantly, how photorespiration may change in different photosynthetic organs of the same plant (site-specific changes of photorespiration). In most angiosperms, tissue/organ-specific anatomical, biochemical and gene regulatory differences are prominent. Therefore, expression of differences in metabolic pathways, including site-specific photorespiration, may be possible. For example, the efficiency of photorespiration could be high/low in some photosynthetic organs compared to the leaves of the same plant based on structural and biochemical differences. Understanding photorespiration in a site-specific manner generally is a better approach to address the existing knowledge gap: specifically the transcriptional, post-transcriptional and post-translational regulation of the pathway. This understanding could lead to redesigning of photorespiration in a more energy efficient way to increase the overall photosynthetic productivity of critical C_3 food crops. Knowledge of site-specific photorespiratory changes may also facilitate bio-engineering a photorespiratory carbon pump as in C_3-C_4 intermediates into C_3 plants. This would be an important intermediate step towards bio-engineering a complete CCM as in C_4 plants into critical C_3 food crops.

C_4: the ultimate result of the photosynthetic evolution

The C_4 photosynthetic mechanism was elaborated from the C_3 form simply by the coordination of existing anatomical and biochemical traits that were not efficiently utilized in C_3 plants (Christin and Osborne 2013). The C_4 carbon cycle is the most efficient mechanism for atmospheric CO_2 fixation in higher plants with respect to the use of nitrogen, water and light (Christin and Osborne 2013; Long and Spence 2013). The C_4 pathway may have originated independently up to 60 times during angiosperm evolution (Sage 2004). Most C_4 species are grasses that evolved 30 million years ago, and a lesser number of C_4 dicots that evolved some 20 million years ago (Sage 2004, 2016).

To acquire CCMs in C_4 plants, RuBisCO has to be isolated from the intercellular air spaces. If not, photorespiration takes place because of the high O_2 concentrations in inter-cellular spaces. Although C_4 photosynthesis may take place within a single cell, e.g., in the *Chenopodiaceae* (Voznesenskaya et al. 2002; Chuong et al. 2006), in most cases CCMs of C_4 photosynthesis are a result of distinct metabolic activities of two types of cells, BSCs and MCs, arranged around the vascular tissue (Kranz anatomy), which is supported by a specialized enzymatic activity through gene regulation (Voznesenskaya et al. 2001a). Most of the Calvin cycle enzymes including RuBisCO are localized in BSCs and the arrangement of BSCs around the vascular tissue is known as the photosynthetic carbon reduction (PCR) tissue (Dengler and Nelson 1999). In the majority of C_4 plants, initial CO_2 fixation takes place in MCs, and this carboxylation is catalyzed by phosphoenolpyruvate carboxylase (PEPC). RuBisCO is hardly seen in MCs in C_4, and for this reason, oxygenation activity leading to photorespiration is retarded. The four-carbon acid so produced by PEP is then translocated to the BSCs. This process tends to initiate the CCMs near RuBP by releasing CO_2 from the decarboxylation of the four-carbon acid. The CCM of C_4 increases the CO_2 concentration at the site of RuBisCO about tenfold (Furbank 2011). For example, under high irradiance, C_4 leaves operate with a ratio of the intercellular-to-ambient CO_2 concentration of around 0.3 compared with around 0.7 for C_3 leaves (Wong et al. 1985; Evans 2013). This also

allows the RuBisCO to perform closer to its catalytic maximum (V_{max}) (von Caemmerer and Furbank 2003).

Four subtypes of C_4 photosynthesis have been identified based on the differences in decarboxylation reactions. They are NADP-malic enzyme (NADP-ME), NAD-malic enzyme (NAD-ME), PEP carboxykinase (PEP-CK), and combination of these enzymes (Prendergast et al. 1987). Although each subgroup shows both morphological and biochemical differences, production of OAA, a four-carbon compound from the initial fixation of HCO_3^- by PEPC in MC cytoplasm, is common to all C_4 plants (Prendergast et al. 1987).

Modifications for spatial compartmentation of the C_4 pathway could have indirect impacts on other metabolic processes. For example, large-scale transcriptomic and proteomic studies of some C_4 plants have revealed that metabolic processes other than photosynthesis, such as nitrogen or sulfur assimilation, protein synthesis, and lipid metabolism are also compartmentalized between BSCs and MCs (Majeran and van Wijk 2009). Such modifications of C_4 photosynthesis could perhaps improve overall plant performance. In addition, the Kranz anatomy may also impact on plant defense mechanisms to biotic and abiotic stresses. An experiment by Ku et al. (2000)using transgenic rice plants that overexpressed maize C_4 specific PEPC and pyruvate orthophosphate dikinase (PPDK), highlighted this phenomenon. The importance of the C_4 pathway, and its future potential for mitigating the upcoming food crisis are illustrated by the fact that even though only 3% of all plant species perform C_4 photosynthesis, they contribute to 25% of global photosynthesis (Sage et al. 2012). Because of its higher efficiency, engineering C_4 into the critical C_3 food crops has been studied profoundly during the last two decades (Burgess and Hibberd 2015).

Recent approaches for engineering the C_4 pathway into major C_3 plants and possible insights for success

Changing the mode of photosynthesis of classical C_3 food crops into a more efficient photosynthetic pathway could improve global food production. At least a 30% yield improvement is expected from engineering the C_4 pathway into C_3 food crops (Wang et al. 2017b). However, knowledge about the gene regulation of the complete C_4 photosynthesis is inadequate to achieve this ambitious and challenging goal (Schuler et al. 2016).

Recent advances in techniques of molecular biology, like Next Generation Sequencing, have provided new insights into engineering C_4 into C_3 plants. Complete genome sequencing of critical C_4 crop plants such as: *Zea mays*, *Sorghum bicolor, Setaria italica*, *Amaranthus hypochondriacus and Panicum virgatum*, can be considered as an important step in detailed understanding of C_4 photosynthesis (Paterson et al. 2009; Schnable et al. 2009; Casler et al. 2011; Zhang et al. 2012a; Sunil et al. 2014). Also, new evidence for gene regulation of C_4 biochemistry was revealed by a systems biology approach utilizing transcriptomic data. These transcriptomic data also provided a platform for the computational modeling that facilitated the creation of a metabolic map of the C_4 pathway (Burgess and Hibberd 2015). The first molecular evidence of C_4 Kranz anatomy is one such finding that can be further developed for engineering the C_4 pathway into C_3 plants (John et al. 2014; Li et al. 2015).

Significant earlier approaches to engineering the C_4 pathway into the C_3 focused on the submerged aquatic plant *Hydrilla verticilliata*, which performs a single-cell CCM, C_4-like pathway (Caemmerer et al. 2014). This approach may have been taken as it was thought that engineering a single-cell C_4 pathway into C_3 would be easier than engineering a complete Kranz anatomy. This has, however, been questioned as it requires a large number of structural modifications of the internal organelles, such as chloroplasts and mitochondria, in addition to the necessary biochemistry to minimize carbon leakage (Price et al. 2011).

The requirement of the internal organelles and structural modifications to engineer C_4 photosynthesis into a C_3 pathway was highlighted by Wang et al. (2017a), indicating the evolutionary importance of transitioning from C_3 to "proto-Kranz" anatomy in C_4 precursors (Wang et al. 2017a). Increased organelle volume (chloroplasts and mitochondria) in sheath cells surrounding leaf veins is the crucial characteristic of proto-Kranz anatomy. From the constitutive expression of maize *Golden*2 like genes in C_3 rice, Wang et al. (2017a) were able to induce chloroplast and mitochondrial development in rice vascular sheath cells. Further, increased organelle volume with the accumulation of photosynthetic enzymes and increased intercellular connections were also observed. This can be considered as a critical intermediate step towards engineering a complete C_4 pathway into C_3.

The C_4 rice consortium has initiated many projects to engineer the C_4 mode of photosynthesis into rice (von Caemmerer et al. 2012). The NADP-ME subtype of C_4 in maize was selected as the model pathway, as it was the best characterized of the C_4 subtypes (Kajala et al. 2011; von Caemmerer et al. 2012). Also, of the three biochemical C_4 subtypes, NADP-ME requires the minimum number of enzymes and transporters (Weber and von Caemmerer 2010). To investigate the differences between C_3 and C_4 photosynthetic pathways, Wang et al. (2014) profiled metabolites and transcript abundance of leaves of C_4 maize (*Zea mays*) and leaves of C_3 rice (*Oryza sativa*) using a statistical methodology named the unified developmental model (UDM). Interestingly, the UDM identified possible candidate cis-regulatory elements and transcription factors of

photosynthesis together with the differences between C_3 and C_4 carbon and nitrogen metabolism. One of the crucial aspects of UDM algorithms is the possibility of comparing development in other species. These approaches are useful to close the knowledge gap concerning gene regulation which leads to transforming C_3 into C_4 photosynthesis. Nonetheless, the horizon for releasing a commercial C_4 rice variety is unclear.

Rather than focusing on engineering the entire mode of C_4 photosynthesis into C_3, identification of site-specific changes in photosynthesis and photorespiration, and the induction of efficient C_4-like traits in the specific sites of the plant could improve its photosynthetic efficiency. Also, the site-specific changes in photosynthesis might be used in conventional breeding, especially for crop plants which have just a few C_4-like traits, if only at specific sites. If nothing else, more research on site-specific changes of photosynthesis may not only speed up the process of improving the efficiency of photosynthesis, but also be an intermediate step towards engineering a complete C_4 plant from the C_3.

Evidence for site-specific variation in photosynthesis

Even though the coordination of various anatomical and biochemical C_3 traits was required to evolve a functioning C_4 carbon cycle, all of the traits were present in the ancestral C_3 plants (Christin and Osborne 2013). The evolution of C_4 photosynthesis is a result of transcriptional, post-transcriptional, post-translational and epigenetic regulation. Evolution of Kranz anatomy generally seems to be one of the initial steps towards C_4 photosynthesis (McKown and Dengler 2007). Kranz anatomy facilitates CO_2 concentration at the site of RuBisCO. However, *Bienertia cycloptera* (Chenopodiaceae), which grows under salinity stress in Asian drylands, performs the C_4 mode of photosynthesis in a single chlorenchyma cell, without having Kranz anatomy (Voznesenskaya et al. 2002). This single-cell C_4 mode of photosynthesis is achieved by positioning dimorphic chloroplasts, photosynthetic enzymes, and other cell organelles, like mitochondria and peroxisomes, in distinct places within the cell (Sage and Monson 1998; Voznesenskaya et al. 2002). Voznesenskaya et al. (2002) also showed that the division of labour between the two types of photosynthetic cells (MCs and BSCs) in Kranz anatomy can be achieved by compartmentation within a single chlorenchyma cell. Similar evidence for the single-cell C_4 pathway was shown using *Borszczowia aralocaspica* (subfamily Salsoloideae, family Chenopodiaceae) (Voznesenskaya et al. 2001b; Sage 2002). This takes us to a novel understanding of C_4 photosynthesis, which is that a C_4-like mode of photosynthesis might be engineered in a plant, or at a specific site within it, in the absence of Kranz anatomy.

Possible evidence for site-specific C_4-like photosynthesis was observed by Brown et al. (2010). According to these authors, activation of the C_4 decarboxylation enzymes required for C_4 photosynthesis occurs in the mid-vein region of the classical C_3 plant, *Arabidopsis,* and plays an important role in amino acid and sugar metabolism (Brown et al. 2010). The maximum catalytic activity in isolated mid-veins of *Arabidopsis* leaves, for NADP-ME activity, is six times higher than in the entire leaf, and ten times higher in both NAD-ME and PEPCK on a chlorophyll basis (Brown et al. 2010). The catalytic activities of these decarboxylation enzymes are significantly higher than the values obtained from C_3 plants, and are similar to the catalytic activities in the BSCs of C_4 (Brown et al. 2010). Two transcripts derived from NADP-ME genes of C_4 (*NADP-ME2*, *NADP-ME4*) and transcripts derived from *PCK1 C*$_4$ were identified in mid-vein regions of Arabidopsis; nonetheless, the full-length protein of *NADP-ME4* was not detected (Brown et al. 2010). From work on the mid-vein region of *Arabidopsis*, Brown et al. (2010) further suggested that the high activities of NADP-ME, NAD-ME, and PEPC in veinal cells may provide CO_2 for an efficient photosynthesis. It is also possible that differences in photorespiration may exist at different photosynthetic sites within a plant. Therefore, it is worthwhile to study photorespiration along with photosynthesis in a site-specific manner. Wang et al. (2014) demonstrated the differences in gene expression and metabolites in different sites along the developing leaves of C_4 *Z. mays* (maize) and C_3 *O. sativa* (rice). This would again seem to be an indication of site-specific photosynthesis of plants.

Environmental conditions are also capable of causing both morphological and biochemical changes in photosynthesis. Evolution of C_4 photosynthesis is considered as an adaptation to dry, humid and hot environments, in conjunction with low atmospheric CO_2 levels (Sage 2004; Furbank 2011). Thus environmental extremes may be a way of initiating C_4-like photosynthetic traits (Ueno 1998), e.g., transformation from the C_3 mode to the CAM mode of photosynthesis occurs in some succulent plants (Edwards et al. 1985), while a transformation from C_3 to C_4, again without Kranz anatomy, has been detected in *H. verticillata* (Bowes and Salvucci 1989). The amphibious, leafless sedge, *Eleocharis vivipara*, has a Kranz anatomy and expresses a C_4-like mode of photosynthesis under terrestrial conditions, even though it expresses C_3-like photosynthesis under submerged conditions (Ueno 1998). These findings provide support for the possibility of dual photosynthetic biochemistry and evidence for the impact of environmental factors on the mode of photosynthesis.

Ueno (1998) modified the experiment mentioned in the previous paragraph to analyze the hormonal regulation of the structural and biochemical differentiation of photosynthesis in *E. vivipara*. For this study, submerged *E. vivipara* was

stressed using 5 µM abscisic acid (ABA), which induced the initiation of photosynthetic organs having C_4-like Kranz anatomy, and also, Kranz cells with many organelles (Ueno 1998). Accumulation of large quantities of PEP carboxylase, pyruvate orthophosphate dikinase, and NAD-malic enzyme was also observed at the appropriate sites of the cells, which provided rich evidence for the induced C_4 mode of photosynthesis from ABA exposure. Such results on induced C_4 photosynthesis are also supported by the findings in carbon-14 pulse and carbon-12 chase experiments (Ueno 1998). Solar radiation and temperature are another two factors governing photosynthesis, and it is therefore worthwhile to analyze their impact.

Casati et al. (2000) analyzed the impact of temperature and light on the induction of C_4 photosynthesis in *Egeria densaleaves,* a submerged plant, and observed the expression of PEPC and NADP-malic enzyme (NADP-ME) under two environmental conditions, namely low temperature and low light (LTL) and high temperature and high light (HTL). Plants grown in HTL showed higher expression and activity of both C_4 enzymes than in the plants grown in LTL (Casati et al. 2000).

Rice and wheat are critical to global food security and their leaves photosynthesize using the C_3 pathway (Still et al. 2003; Yuan 2012). It is estimated that in wheat, 10–44% of the photosynthate in grains may arise from photosynthesis in the ear, and about 33–44% from photosynthesis in the grain (Kriedemann 1966; Evans and Rawson 1970; Maydup et al. 2010). The photosynthetic pathway in cereal grains is not well defined; therefore, a fuller understanding of site-specific photosynthesis in immature grains might provide a target for enhanced grain filling.

Data indicative of site-specific differences of photosynthesis in major food crops has been observed for several decades (Nutbeam and Duffus 1976). The evidence of a mode of photosynthesis other than C_3 was observed in wheat, despite the fact that it is categorized as a typical C_3 plant (Nutbeam and Duffus 1976; Rangan et al. 2016b). Duffus and Rosie (1973) reported that there was a 50–100 times higher activity of carbon fixation in PEPC from the barley pericarp organs of developing grains, than in RuBisCO. The possibility of C_4 photosynthesis by the pericarp organs of developing grains was also suggested by Duffus and Rosie (1973), from evidence of the enzyme activity of malate dehydrogenase, malic enzyme, and pyruvate-orthophosphate dikinase. A few years later, clues for the site-specific photosynthesis in wheat were observed by Duffus and Rosie (1973). In their study, the flag leaf and developing grain of wheat showed significantly different carbon isotope discrimination values and had a strong correlation with water usage and transpiration efficiency, even though the values were not comparable with classical C_4 photosynthesis (Merah et al. 2001; Monneveux et al. 2004). However, until the findings of Rangan et al. (2016b) the concept of a C_4 mode of photosynthesis in different wheat organs was not accepted and until now remains contested.

Rangan et al. (2016b) observed the presence and expression of all the genes specific to NAD-ME subtype of C_4 in developing wheat grains, and consequently argued the possibility of a complete C_4 pathway in classical C_3 plants. Subsequent to this, Rangan et al. (2016b) reported the presence of a complete C_4 mode of photosynthesis in the developing wheat grain. This was further supported by evidence of the compartmentalization of C_4 gene expression in the pericarp, which is anatomically fitted to perform C_4 photosynthesis. The C_4 photosynthesis in the wheat pericarp may be an adaptation to heat and water stress in wheat (Rangan et al. 2016a).

One of the most significant outcomes of the study by Rangan et al. (2016b) was the optimal expression of specific C_4 genes in the pericarp during the early- to mid- period of grain filling. Despite the apparent strength of this study, Busch and Farquhar (2016) argued that in the absence of biochemical and physiological data, the evidence was insufficient to support such a conclusion. This opens an avenue for future research, specifically for a biochemical and physiological exploration of the dual biochemistry of photosynthesis in parallel with a molecular analysis.

Interestingly, site-specific photosynthesis occurs in maize (*Z. Mays*), where the foliage uses the C_4 photosynthetic pathway, while the husk surrounding the ear operates through a partial C_3 pathway (Pengelly et al. 2011; Wang et al. 2013). Although high vein density is a prominent feature of C_4 photosynthesis to facilitate efficient transport of C_4 acids from MCs to BSCs (McKown and Dengler 2007), photosynthetically active husk leaves shows a very low vein density as in C_3 plants (Langdale et al. 1989, Wang et al. 2013). Based on the presensce of Rubisco mRNA transcripts, Langdale et al. (1989) inferred that MCs distant from the vascular bundles may perform C_3 photosynthesis. Further, carbon isotope discrimination (^{12}C and ^{13}C) of foliage and husk leaves of maize showed that there was a significant CO_2 fixation in husks through C_3 photosynthesis (Yakir et al. 1991). These findings further highlight the importance of vein density and spacing for the modes of photosynthesis within the same plant.

Identification of C_4-like photosynthesis in C_3 plants and elucidation of the mechanism might be used to induce a similar photosynthetic pathway in other plant organs such as leaves (Fig. 4). This may prove simpler than engineering a complete C_4 pathway into C_3, and improve the yield of critical food crops. Understanding the impact of environmental parameters on the site-specific changes in photosynthesis may also prove to be important. Finally, whether a thorough understanding of site-specific photosynthesis has the potential to mitigate the looming food

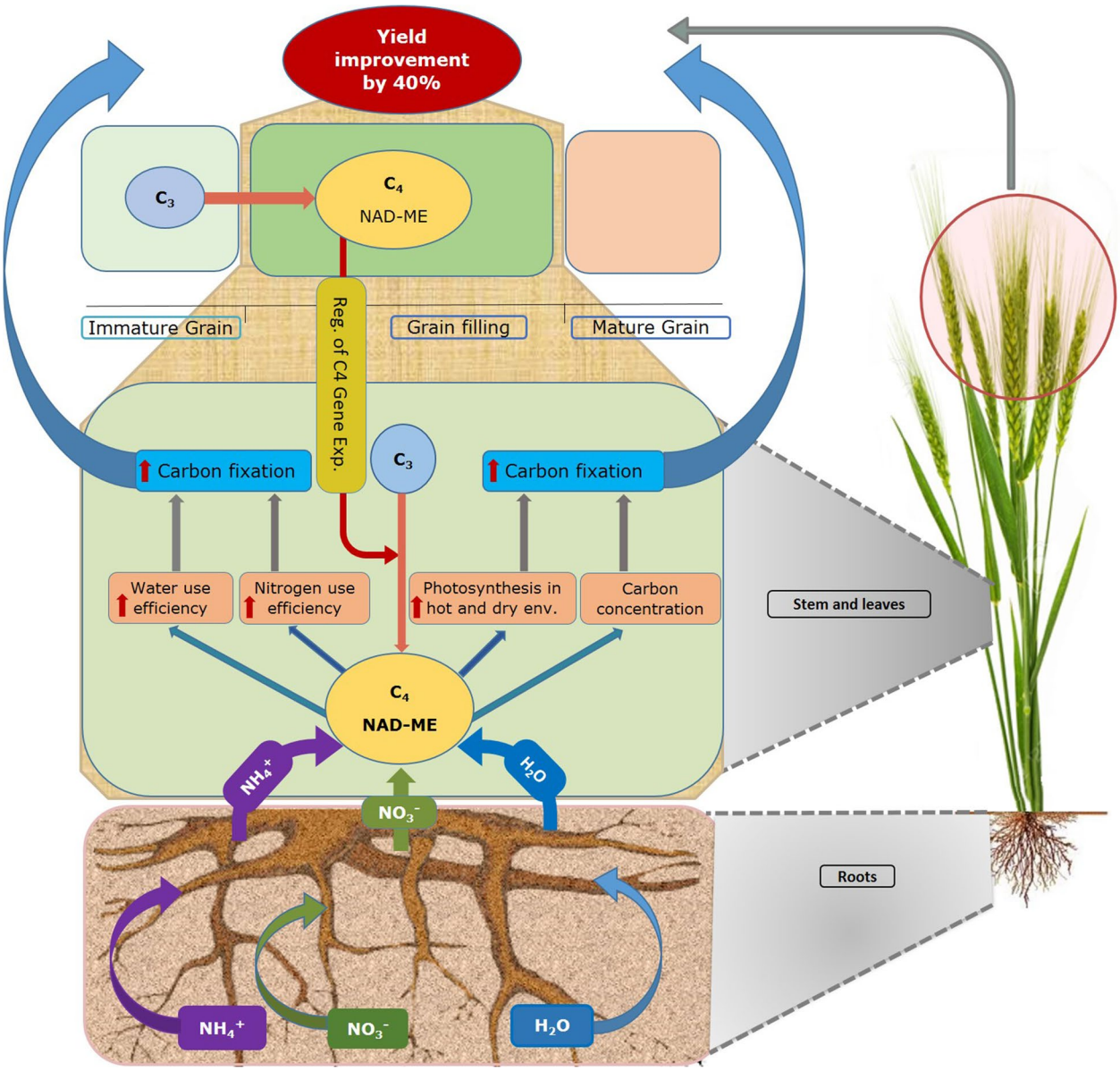

Fig. 4 Utilization of the site-specific C_4 photosynthesis in wheat to increase crop productivity. *Reg.of C_4 Gene Exp* regulation of C_4 gene expression, *env* environment. It has been hypothesized that the developing wheat grain performs NAD-ME subtype C_4 like photosynthesis during mid-grain-filling although it performs C_3 like photosynthesis during its early stages. Understanding this temporal variation of photosynthesis of wheat grain could be highly important to understand the site-specific photosynthesis in wheat. Knowledge of site-specific photosynthesis in wheat can be utilized for an expression of C_4 photosynthesis in major photosynthetic tissues such as leaves. This may facilitate increased efficiency of carbon fixation from the improvement of efficiency in the use of water and nitrogen, and by initiating CCMs. The ultimate outcome would be a yield improvement of ~ 40%

crisis is an open question because the subject has not been intensely studied, the literature is diffuse, and the practical challenges remain unknown. The findings and evidence of the dual biochemistry of photosynthesis/site-specific photosynthesis may provide a novel way of improving the crop yield of critical C_3 food crops such as rice and wheat by increasing the efficiency of photosynthesis by inducing C_4 pathway into specific organs rather than changing the entire mode of photosynthesis in the plant.

Identification of the specific photosynthetic organs which contribute appreciably to crop/grain yield, and the induction of C_4-like traits in those specific organs, could be highly important to yield improvement. Understanding the dual biochemistry of photosynthesis, or site-specific photosynthesis, may be as central to yield improvement as better understanding the contribution of the different anatomical elements of the C_4 pathway to photosynthetically efficient carbon fixation.

Importance of identifying photosynthetically efficient physiological traits to understand site-specific photosynthesis

McKown and Dengler (2007) state that Kranz anatomy had to be fully evolved before a complete C_4 carbon shuttle was initiated in most plants. However, it is possible that the efficiency of photosynthesis might be increased, albeit not to the full potential, without the complete complement of traits. For example, a correlation between higher vein density of leaves and grain yield of rice has been proposed (Feldman et al. 2017; Nawarathna et al. 2017). Below we summarize the literature on photosynthetically efficient physiological traits of C_4 that might improve the efficiency of nett carbon fixation in C_3 crop plants. By altering site-specific gene expression, there is also a possibility of transforming these traits into other photosynthetic organs of the same plant.

Increased vein density as a factor for efficient photosynthesis

To establish an efficient CCM in BSC, the distance between MCs and adjacent BSCs should be a minimum, and placement of each MC directly adjacent to at least one BSC is also important (Sage 2004). High vein density of the photosynthetic organ has a vital role in achieving this unique cell arrangement in C_4 plants (McKown and Dengler 2007). It also increases the mechanical integrity of leaves, which is a favorable trait in windy habitats, and improves the water supply of leaves in dry and hot conditions (Sage 2004). Higher vein density increases the efficiency of C_4 photosynthesis by rapid intercellular diffusion of photosynthetic metabolites between MSs and BSCs (McKown and Dengler 2009). Higher vein density has been hypothesized as an initial step in the evolution of C_4 photosynthesis (McKown and Dengler 2009). Although dense venation is observed in most C_4 leaves, studies using C_3 (*Flaveria robusta*) and C_4 species (*Flaveria bidentis*), showed no difference in major vein density, but a higher density of minor veins in the C_4 plants due to a higher initiation frequency and different patterning (McKown and Dengler 2009). According to McKown and Dengler (2009), earlier termination of MC division and reduced enlargement also cause an increase in the vein density in C_4 plants. Although the gene regulation of vein initiation is not well understood, studies on *A. thaliana* show that vein initiation from ground tissues is induced by the polar auxin flow, mediated by auxin efflux carriers (Scarpella et al. 2006; McKown and Dengler 2009). Conversion of the cells along the auxin transport pathway into procambial cells, followed by development into vascular bundles, has been observed in Arabidopsis (Scarpella et al. 2006). Even though a theoretical optimum for vein density has been suggested (Noblin et al. 2008), vein density varies widely, especially in C_3 plants, in response to the environment (Roth-Nebelsick et al. 2001). Langdale and Nelson (1991) suggested that the veins in C_4 leaves play a vital role in determining cell differentiation, especially for MCs and BSCs. Nonetheless, higher vein density is not invariably a significant character of C_4. For example, Muhaidat et al. (2007) showed that vein density does not differ between some closely related C_3 and C_4 grasses. In this study, these authors also suggested that the vein density might not be a reliable indicator of the C_3 or C_4 photosynthetic pathways in the eudicots as a whole. This is exemplified by higher vein densities in the same species grown in dry environments with low humidity and high solar irradiance, compared to wet environments with high humidity and low solar irradiance (Roth-Nebelsick et al. 2001; Zhang et al. 2012b). Nonetheless, with few exceptions, higher vein density of the photosynthetic organ appears to be an important C_4-like trait that could be the first step in the evolution of Kranz anatomy.

The potential role of MCs and BSCs arrangement in efficient photosynthesis

The increased vein density in C_4 plants is associated with an increase in the ratio between MCs and BSCs (Ku et al. 1974; Gowik and Westhoff 2011). In most C_3 photosynthetic cells, a larger number of chloroplasts is concentrated in the MCs, and MCs of the leaves contribute the most carbon assimilation (Gowik and Westhoff 2011). In contrast, MCs of the C_4 photosynthesis have fewer chloroplasts than in closely related C_3 species (Dengler and Nelson 1999; Stata et al. 2014). The combination of a higher ratio of MCs and BSCs in C_4, with lower chloroplast numbers in MCs, would appear to decrease the potential for photosynthesis in a given area. However, this is not the case, because the photosynthetically active BSCs in C_4 have more, larger chloroplasts (Black and Mollenhauer 1971; Muhaidat et al. 2011; Sage et al. 2011). Differences in the chloroplast distribution of C_3 and C_4 leaves can be seen roughly with the naked eye: the veins are colourless in C_3 and dark green in C_4 (Dengler and Nelson 1999; Maai et al. 2011). The reason for having fewer chloroplasts in MCs of C_4 plants could be that the initial site of carbon fixation is not the chloroplast, but instead, the cytosol of the MC. In contrast, since the chloroplast stroma is the site of carboxylation in C_3 species, a large number of chloroplasts is needed for efficient carboxylation in the MCs (Evans and Loreto 2000; Tholen et al. 2008). In BSCs of C_4 a larger number of mitochondria and peroxisomes are also present (Hylton et al. 1988; Gowik and Westhoff 2011). As a result of the higher number of organelles in BSCs and also because of the higher metabolic activity, the BSCs of C_4 are relatively larger than in closely related C_3 species (Hylton et al. 1988; Stata et al. 2014).

Anatomical and structural changes of MCs and BSCs in different C_4 subtypes

Anatomical and structural differences of MCs and BSCs between the three C_4 subtypes (NADP-ME, NAD-ME, PEP-CK) have also been identified (Kanai and Edwards 1999). Changes in chloroplast placement in the BSCs, grana development of the chloroplasts of BSCs and MCs, the number and the sizes of mitochondria of BSCs, and the initiation of suberin lamella within the BSCs are some of the features that differentiate the three subtypes of C_4 (Hatch et al. 1975; Yoshimura et al. 2004; Ueno et al. 2005). For example, C_4 grasses of the NADP-ME subtype show significantly higher vein density and reduced granal development of chloroplasts in BSCs, with fewer in bundle sheaths, than in the NAD-ME and PEP-CK subtypes. Most of the grasses of NADP-ME subtype also have centrifugally placed chloroplasts in BSCs (Hatch et al. 1975).

Importance of the placement and the relative volume of MCs and BSCs for efficient photosynthesis

In C_4 plants, BSCs are positioned to decrease contact with intercellular air spaces to minimize oxygenation of RuBisCo, which leads to photorespiration. According to Dengler et al. (1994), not only the BSCs in C_4 carbon shuttle, but also MCs have a lesser surface area exposed to intercellular spaces. Also, in both MCs and BSCs in C_4, the ratio between surface area and cell volume is lower than in the closely related C_3 species. The proportions of the MCs and BSCs in C_4 eudicots is also appreciably less than in their closely related C_3 counterparts (Muhaidat et al. 2007). This is partly due to thinner leaves and/or a decreased number of MC layers in the leaf (Muhaidat et al. 2007). The relative volumes of the MCs and BSCs may be significant (Hattersley 1984; Soros and Dengler 1998), because it is important to understand the role of major C_4 characteristics, such as enlarged BSCs and the short diffusion distances for C_4 metabolites between MCs and BSCs (Muhaidat et al. 2007).

Importance of plasmodesmata and their density to efficient photosynthesis

An effective connection between MCs and BSCs is needed for an efficient CCM in photosynthesis, and this connection relies on the plasmodesmata. There are extensive metabolic fluxes between MCs and BSCs through interconnecting plasmodesmata (Danila et al. 2018). Danila et al. (2018) combined scanning electron microscopy and three-dimensional immunolocalization to understand the density of plasmodesmata in C_3 *O. sativa* and C_4 *Z. mays*, revealing that the C_4 species had almost twice the number of plasmodesmata per unit area as the C_3 species. Identification of genetic components responsible for high plasmodesmatal density and engineering them into C_3 crop plants could improve their photosynthetic productivity. Moreover, understanding the differences between MCs and BSCs of both C_3 and C_4 species would seem to have important implications when studying the evolution of the C_4 carbon shuttle.

Site-specific gene regulation of C_4 photosynthesis

Site-specific changes of photosynthesis within plant species have not been sufficiently investigated (Rangan et al. 2016a, b). There may be potential to select crop plants for higher yield based on the occurrence of photosynthetically efficient physiological traits at different sites. Further, it is worth studying the possibility of transferring such traits to major photosynthetic sites such as leaf blades. For this task, a sound knowledge of the genetic regulation of photosynthesis is essential. Since C_4 is the most efficient mode, we summarize the current limited knowledge on C_4 gene regulation, because narrowing the knowledge gap about gene regulation of photosynthesis is another step in understanding site-specific photosynthesis.

The evolution of C_4 photosynthesis from C_3 precursors was a result of large-scale quantitative and spatial modifications in gene expression (Bräutigam et al. 2010). Although understanding the specific gene regulation of C_4 photosynthesis is inadequate, it is believed that it is a result of a multi-level regulation of transcriptional, post-transcriptional, post-translational and epigenetic factors (Sheen 1999; Wang et al. 2011; Fankhauser and Aubry 2016; Lovell et al. 2016; Reeves et al. 2016). Amongst these factors, transcriptional regulation of C_4 is the most extensively studied (Hibberd and Covshoff 2010; Gowik et al. 2016).

Localization of PEPC in MCs exemplifies the transcriptional regulation of C_4 photosynthesis (Taniguchi et al. 2000; Li et al. 2010). It has not yet fully confirmed whether the complete C_4 mechanism is regulated through transcriptional or post-transcriptional controls; however, expression of NADP-ME in BSCs in maize is considered the result of transcriptional regulation (Sheen and Bogorad 1987; Wang et al. 2011). Regulation of pyruvate orthophosphate dikinase, a C_4 enzyme which is required for PEP regeneration in MCs, is another example of the transcriptional regulation of C_4 photosynthesis (Hibberd and Covshoff 2010). In addition, the maize *Golden2* (*Bsd1*) gene is one of the earliest transcription factors identified through genetic studies which could play a role in the C_4 pathway (Langdale and Kidner 1994). Importance of *Golden2* like genes to transform C_3 into proto-Kranz have been reported from the experiments conducted using rice plants (Wang et al. 2017a). Proto-Kranz may have existed even before the C_2 pathway in C_4 evolution.

The C_4 mechanism with Kranz anatomy is the most efficient mode of carbon fixation. Of about 7500 C_4 species, maize is one of the more intensely studied regarding Kranz development (Wang et al. 2013). From histological and cell lineage analysis, the morphological manifestation of Kranz anatomy of maize has been well documented (Langdale et al. 1989). However, much is still unknown about the genetic regulation of Kranz development despite maize *scarecrow* gene (Wang et al. 2013). To provide a much broader insight into the gene regulation of Kranz anatomy, Wang et al. (2013) conducted a genome-wide comparative analysis using Kranz and non-Kranz organs (leaves and husk sheaths, respectively) of maize at different development stages. The analysis revealed cohorts of genes which showed much higher activity during early leaf development. Furthermore, a group of transcription factors linked with the Kranz patterning was identified. This seems to be an important finding since Kranz anatomy may be fundamental to efficient CCM in C_4, and knowledge of its genetic regulation may provide a doorway to transitioning critical C_3 food crops into C_4 (Sedelnikova et al. 2018). From an experiment conducted by Li et al. (2010) used Illumina sequencing throughout a developmental gradient and in mature MSs and BSCs to analyze the transcriptome of the maize leaf. That study identified about 180 transcription factors which were differentially expressed in MCs and BSCs. These transcriptional factors may be highly useful for future studies in functional genomics to dissect the photosynthetic pathways in leaves.

Within the constraints of the limited literature, it is assumed that the post-translational control of C_4 photosynthesis is highly interconnected with protein and enzyme modification, and that it also applies beyond the phosphorylation of PEPC and pyruvate orthophosphate dikinase (Wang et al. 2011). In addition, the results from a study conducted by Naidu et al. (2003) using *Miscanthus giganteus,* suggest that the abundance of pyruvate orthophosphate dikinase may also be regulated through protein turnover. Moving to the epigenetic control of C_4 photosynthesis, it is believed that the expression of PEPC is predominantly epigenetically regulated (Taniguchi et al. 2000; Kausch et al. 2001). Since the knowledge of specific gene regulation in both the C_3 and C_4 pathways is poor, and the rate of accumulation of knowledge in this area is not high, a novel way of addressing this problem might be needed.

The establishment of the C_4 pathway in maize takes place along the developmental axis of the leaf blade which has undifferentiated cells at the leaf base and highly specialized MCs and BSCs at the leaf tip (Majeran et al. 2010) To obtain a system level understanding of the kinetics of maize leaf development and C_4 differentiation, Majeran et al. (2010) measured the accumulation proteome profiles of the leaf along the developmental gradients using mass spectrometry. The results were supported by analyzing structural features, e.g., Kranz anatomy, cell wall, plasmodesmata, and organelles through microscopy. This study identified and functionally annotated more than 4300 proteins. These results can be considered as a well-defined molecular template that demonstrates the metabolic and structural transitions which occur during C_4 differentiation. One year later, Pick et al. (2011) reported that the C_4 pathway in maize leaves is established from sink tissues without having an intermediate phase of C_2 or C_3 channels. Further, Pick et al. (2011) concluded that the evolutionary linkages of C_4 photosynthesis were not recapitulated during C_4 differentiation in maize. Such findings indicate that development of the C_4 pathway may be more complicated than initially thought and that deeper investigation of the processes may be needed to understand C_4 gene regulation.

Understanding the concept of the site-specific photosynthesis appears to be an ideal way to fill the knowledge gap on gene regulation, both in C_3 and C_4 photosynthesis, because there is a possibility of using different organs of the same plant and/or plants grown in different environmental conditions to analyze both the C_3 and the C_4 photosynthetic models. This might complement the model plant approach, which instead uses different organs of the same plant to analyze C_3 and C_4 pathways.

Other possible approaches to improving photosynthesis

Parallel to the concept of site-specific photosynthesis, it is important to know about other possible approaches that might be utilized to improve photosynthesis. Among these are mitigation of the inefficiencies of LDR and LIR (Evans 2013; Sharwood et al. 2016; Niinemets et al. 2017).

Modifying the LDRs is less-well studied compared with the LIRs (Evans 2013). From the limited research, improvement of photosynthetic efficiency by accelerating recovery from photoprotection through genetic manipulation seems to be important as it increased both CO_2 uptake and dry matter productivity by 15% in *Nicotiana* (tobacco) (Kromdijk et al. 2016). Some other approaches that have been studied include (Fig. 1): reduction of light saturation of leaves by improving light penetration by reducing the antenna size of the photosystem (Ort et al. 2011); engineering the pigment-protein complex of higher plants to extend the waveband of sunlight that can be used for photosynthesis using cyanobacterial chlorophyll *d* and *f* (Chen and Blankenship 2011); and improvement of the electron transport capacity by increasing cytochrome *f* content (von Caemmerer and Evans 2010). Improving kinetic properties of RuBisCo (Sharwood et al. 2016) and mitigating limitations to CO_2 diffusion from the atmosphere to the sites of fixation (Tosens et al. 2016) are some of the major challenges of improving the LIR of photosynthesis and these areas also need intensive study.

Photorespiration can reduce photosynthetic productivity by 20–50% depending on the growth temperature. Hence re-engineering photorespiration seems to be a way of improving the efficiency of photosynthesis in C_3 plants and the crop yield. This was simulated by South et al. (2019) altering the photorespiratory pathway in tobacco. Interestingly, after introducing synthetic glycolate metabolic pathways, 20% quantum yield improvement and 40% more biomass productivity were observed in field-grown tobacco. On the other hand, the ratio between the consumption of carbohydrates from the whole plant (sink) and the supply of carbohydrates from leaves (source); sink–source activity has also been considered as a factor that can regulate photosynthesis (Sugiura et al. 2017). Therefore, manipulation of sink–source balance could also be used as a tool to improve the efficiency of photosynthesis at the whole plant level. In addition to these strategies of improving photosynthesis to achieve higher crop yield, it is noteworthy that recent research has highlighted the use of chemical intervention strategies to increase crop yield and resilience. For example, Griffiths et al. (2016) have demonstrated the use of chemical substances to modulate trehalose 6 phosphate (T6P) levels which play a crucial role in sucrose metabolism and sugar sensing pathways of plants. Results of this study revealed that modulation of T6P levels through chemical interventions altered crop growth and development, and thereby the potential yield.

Conclusions

A significant yield improvement of critical food crops is crucial to assure the global food security because of the increasing population and the factors related to climate change. The yield improvement of most food crops by conventional methods has plateaued, thus feeding the future world seems to be impossible without a significant leap in science. Of the many possible approaches, improving the efficiency of photosynthesis of critical food crops is seen as an essential step in addressing the foreseen risk.

Although the hypothesis of site-specific photosynthesis is novel, evidence of the phenomenon has been accumulating for decades. Direction of more attention to site-specific photosynthesis/dual biochemistry of photosynthesis stands to improve the efficiency of photosynthesis per unit area of critical food crops, thereby increasing the crop yield.

The C_4 pathway is considered the most efficient photosynthetic system; consequently, identification and/or induction of C_4 like photosynthesis in specific sites of classical C_3 plants (site-specific C_4 photosynthesis of classical C_3 plants) promises to increase the yield of classical C_3 crops, with no increase in the existing photosynthetic biomass (increase in harvest index). Understanding and optimization of site-specific photosynthesis could also be a useful intermediate step in engineering a complete C_4 pathway into C_3 plants. In addition, investigation of site-specific photosynthesis will help to fill the knowledge gap of the gene regulation of C_3 and C_4 photosynthesis. Lastly, engineering C_4-like photosynthetic pathways into the classical C_3 food crops using genome editing tools like CRISPR/Cas9 would be a novel way of addressing the ambitious goal of increasing the yield of critical C_3 food crops. This venture will probably be the foundation of the next green revolution.

Author contribution statement PD wrote the manuscript. PM, GA, KA, DG, AM, SN and SS each contributed to the design and review of the final manuscript.

Acknowledgements This work was supported by the University of Southern Queensland (USQ), Australia, and the USQ Strategic Research Fund. PD is supported by a USQ International Stipend Research Scholarship and USQ International Fees Research Scholarship.

Compliance with ethical standards

Conflict of interest The authors declare that this study was conducted in the absence of any commercial relationships that could lead to any potential conflict of interest.

References

Alexandratos N, Bruinsma J (2012) World agriculture towards 2030/2050: the 2012 revision. ESA Working paper FAO, Rome

Allen JF, Martin W (2007) Evolutionary biology: out of thin air. Nature 445:610

Austin R, Ford MA, Morgan C (1989) Genetic improvement in the yield of winter wheat: a further evaluation. J Agric Sci 112:295–301

Bauwe H, Hagemann M, Fernie AR (2010) Photorespiration: players, partners and origin. Trends in plant science 15:330–336

Beadle C, Long S (1985) Photosynthesis—is it limiting to biomass production? Biomass 8:119–168

Beerling DJ, Royer DL (2011) Convergent cenozoic CO2 history. Nat Geosci 4:418–420

Berardy A, Chester MV (2017) Climate change vulnerability in the food, energy, and water nexus: concerns for agricultural production in Arizona and its urban export supply. Environ Res Lett 12:035004

Black CC, Mollenhauer HH (1971) Structure and distribution of chloroplasts and other organelles in leaves with various rates of photosynthesis. Plant Physiol 47:15–23

Blankenship RE et al (2011) Comparing photosynthetic and photovoltaic efficiencies and recognizing the potential for improvement. Science 332:805–809

Bouchenak-Khelladi Y, Anthony Verboom G, Hodkinson TR, Salamin N, Francois O, Ni Chonghaile G, Savolainen V (2009) The origins and diversification of C4 grasses and savanna-adapted ungulates. Glob Change Biol 15(10):2397–2417

Bowes G, Salvucci ME (1989) Plasticity in the photosynthetic carbon metabolism of submersed aquatic macrophytes. Aquat Bot 34:233–266

Bowes G, Ogren W, Hageman R (1971) Phosphoglycolate production catalyzed by ribulose diphosphate carboxylase. Biochem Biophys Res Commun 45:716–722

Bräutigam A et al (2010) An mRNA blueprint for C4 photosynthesis derived from comparative transcriptomics of closely related C3 and C4 species. Plant Physiolpp. https://doi.org/10.1104/pp.110.159442

Brown NJ et al (2010) C4 acid decarboxylases required for C4 photosynthesis are active in the mid-vein of the C3 species Arabidopsis thaliana, and are important in sugar and amino acid metabolism. Plant J 61:122–133

Burgess SJ, Hibberd JM (2015) Insights into C 4 metabolism from comparative deep sequencing. Curr Opin Plant Biol 25:138–144

Busch FA, Farquhar GD (2016) Poor evidence for C4 photosynthesis in the wheat grain. Plant Physiol 172:1357

Busch FA, Sage TL, Cousins AB, Sage RF (2013) C3 plants enhance rates of photosynthesis by reassimilating photorespired and respired CO2 Plant. Cell Environ 36:200–212

Bykova NV, Keerberg O, Pärnik T, Bauwe H, Gardeström P (2005) Interaction between photorespiration and respiration in transgenic potato plants with antisense reduction in glycine decarboxylase. Planta 222:130–140

Cai Z, Liu G, Zhang J, Li Y (2014) Development of an activity-directed selection system enabled significant improvement of the carboxylation efficiency of Rubisco. Protein Cell 5:552–562

Campany CE, Medlyn BE, Duursma R (2017) Reduced growth due to belowground sink limitation is not fully explained by reduced photosynthesis. Tree Physiol 37:1042–1054

Canfield DE (2005) The early history of atmospheric oxygen: homage to Robert M. Garrels Annu Rev Earth Planet Sci 33:1–36

Cano FJ, López R, Warren CR (2014) Implications of the mesophyll conductance to CO2 for photosynthesis and water-use efficiency during long-term water stress and recovery in two contrasting Eucalyptus species. Plant Cel Environ 37:2470–2490

Casati P, Lara MV, Andreo CS (2000) Induction of a C4-Like mechanism of co2 fixation in egeria densa, a submersed aquatic species. Plant Physiol 123:1611–1622

Casler MD et al (2011) The switchgrass genome: tools and strategies The Plant. Genome 4:273–282

Chen M, Blankenship RE (2011) Expanding the solar spectrum used by photosynthesis. Trends Plant Sci 16:427–431

Christin PA, Osborne CP (2013) The recurrent assembly of C4 photosynthesis, an evolutionary tale. Photosynth Res 117:163–175

Chuong SD, Franceschi VR, Edwards GE (2006) The cytoskeleton maintains organelle partitioning required for single-cell C4 photosynthesis in Chenopodiaceae species. Plant Cell 18:2207–2223

Clay J (2011) Freeze the footprint of food. Nature 475:287–289

Crist E, Mora C, Engelman R (2017) The interaction of human population, food production, and biodiversity protection. Science 356:260–264

Danila FR, Quick WP, White RG, Furbank RT, von Caemmerer S (2018) CORRECTION: The metabolite pathway between bundle sheath and mesophyll: quantification of plasmodesmata in leaves of C_3 and C_4 monocots. Plant Cell 30(2):tpc.00115.2018

Dengler N, Nelson T (1999) Leaf structure and development in C4 plants. In: Sage RF, Monson RK (eds) C4 plant biology. Academic Press, San Diego

Dengler NG, Dengler RE, Donnelly PM, Hattersley PW (1994) Quantitative leaf anatomy of C3 and C4 grasses (Poaceae): bundle sheath and mesophyll surface area relationships. Ann Bot 73:241–255

Duffus C, Rosie R (1973) Some enzyme activities associated with the chlorophyll containing layers of the immature barley pericarp. Planta 114:219–226

Edwards GE, Ku MSB, Monson RK (1985) C_4 photosynthesis and its regulation. In: Barber J, Baker NR (eds) Photosynthetic mechanisms and the environment. Elsevier Science, Amsterdam, pp 287–327

Edwards GE, Franceschi VR, Voznesenskaya EV (2004) Single-cell C4 photosynthesis versus the dual-cell (Kranz) paradigm. Annu Rev Plant Biol 55:173–196

Elliott J et al (2014) Constraints and potentials of future irrigation water availability on agricultural production under climate change. Proc Natl Acad Sci 111:3239–3244

Evans JR (2013) Improving photosynthesis. Plant Physiol 162:1780–1793

Evans JR, Loreto F (2000) Acquisition and diffusion of CO_2 in higher plant leaves. In: Photosynthesis. Springer, Dordrecht, pp 321–351

Evans L, Rawson HM (1970) Photosynthesis and respiration by the flag leaf and components of the ear during grain development in wheat. Aust J Biol Sci 23:245–254

Fankhauser N, Aubry S (2016) Post-transcriptional regulation of photosynthetic genes is a key driver of C4 leaf ontogeny. J Exp Bot 68(2):137–146

Fatichi S, Leuzinger S, Körner C (2014) Moving beyond photosynthesis: from carbon source to sink-driven vegetation modeling. New Phytol 201:1086–1095

Feldman AB, Leung H, Baraoidan M, Elmido-Mabilangan A, Canicosa I, Quick WP, Sheehy J, Murchie EH (2017) Increasing leaf vein density via mutagenesis in rice results in an enhanced rate of photosynthesis, smaller cell sizes and can reduce interveinal mesophyll cell number. Front Plant Sci 8:1883

Foyer CH, Bloom AJ, Queval G, Noctor G (2009) Photorespiratory metabolism: genes, mutants, energetics, and redox signaling. Ann Rev Plant Biol 60:455–484

Furbank RT (2011) Evolution of the C_4 photosynthetic mechanism: are there really three C4 acid decarboxylation types?. J Exp Bot 62(9):3103–3108

Furbank RT (2016) Walking the C4 pathway: past, present, and future. J Exp Bot 67(14):4057–4066

Furbank RT, Quick WP, Sirault XR (2015) Improving photosynthesis and yield potential in cereal crops by targeted genetic manipulation: prospects, progress and challenges. Field Crops Res 182:19–29

Galmes J, Kapralov MV, Andralojc P, Conesa MÀ, Keys AJ, Parry MA, Flexas J (2014) Expanding knowledge of the Rubisco kinetics variability in plant species: environmental and evolutionary trends Plant. Cell Environ 37:1989–2001

Gao X, Wang C, Cui H (2014) Identification of bundle sheath cell fate factors provides new tools for C3-to-C4 engineering. Plant Signal Behav 9:319–327

Gowik U, Westhoff P (2011) The path from C3 to C4 photosynthesis. Plant Physiology 155:56–63

Gowik U, Schulze S, Saladié M, Rolland V, Tanz SK, Westhoff P, Ludwig M (2016) A MEM1-like motif directs mesophyll cell-specific expression of the gene encoding the C4 carbonic anhydrase in Flaveria. J Exp Bot 68(2):311–320

Griffiths CA, Sagar R, Geng Y, Primavesi LF, Patel MK, Passarelli MK, Gilmore IS, Steven RT, Bunch J, Paul MJ, Davis BG (2016) Chemical intervention in plant sugar signalling increases yield and resilience. Nature 540(7634):574

Gu L, Sun Y (2014) Artefactual responses of mesophyll conductance to CO2 and irradiance estimated with the variable J and online isotope discrimination methods Plant. Cell Environ 37:1231–1249

Hagemann M, Weber AP, Eisenhut M (2016) Photorespiration: origins and metabolic integration in interacting compartments. J Exp Bot 67:2915

Hatch MD, Slack CR (1966) Photosynthesis by sugar-cane leaves: a new carboxylation reaction and the pathway of sugar formation. Biochem J 101:103

Hatch M, Kagawa T, Craig S (1975) Subdivision of C4-pathway species based on differing C4 acid decarboxylating systems and ultrastructural features. Funct Plant Biol 2:111–128

Hattersley P (1984) Characterization of C4 type leaf anatomy in grasses (Poaceae). Mesophyll: bundle sheath area ratios. Ann Bot 53:163–180

Hibberd JM, Covshoff S (2010) The regulation of gene expression required for C4 photosynthesis. Annu Rev Plant Biol 61:181–207

Hibberd JM, Quick WP (2002) Characteristics of C4 photosynthesis in stems and petioles of C3 flowering plants. Nature 415:451–454

Hoshida H, Tanaka Y, Hibino T, Hayashi Y, Tanaka A, Takabe T, Takabe T (2000) Enhanced tolerance to salt stress in transgenic rice that overexpresses chloroplast glutamine synthetase. Plant Mol Biol 43:103–111

Hylton CM, Rawsthorne S, Smith AM, Jones DA, Woolhouse HW (1988) Glycine decarboxylase is confined to the bundle-sheath cells of leaves of C3–C4 intermediate species. Planta 175:452–459

Imaizumi N, Usuda H, Nakamoto H, Ishihara K (1990) Changes in the rate of photosynthesis during grain filling and the enzymatic activities associated with the photosynthetic carbon metabolism in rice panicles. Plant Cell Physiol 31:835–844

John CR, Smith-Unna RD, Woodfield H, Covshoff S, Hibberd JM (2014) Evolutionary convergence of cell-specific gene expression in independent lineages of C4 grasses. Plant Physiol 165:62–75

Kajala K et al (2011) Strategies for engineering a two-celled C4 photosynthetic pathway into rice. J Exp Bot 62:3001–3010

Kanai R, Edwards G (1999) The biochemistry of C4 photosynthesis. In: Sage RF, Monson RK (eds) C4 plant biology. Academic Press, San Diego, pp 49–87

Kangasjärvi S, Neukermans J, Li S, Aro E-M, Noctor G (2012) Photosynthesis, photorespiration, and light signalling in defence responses. J Exp Bot 63:1619–1636

Kausch AP, Owen TP, Zachwieja SJ, Flynn AR, Sheen J (2001) Mesophyll-specific, light and metabolic regulation of the C4 PPCZm1 promoter in transgenic maize. Plant Mol Biol 45:1–15

Keys AJ (2006) The re-assimilation of ammonia produced by photorespiration and the nitrogen economy of C3 higher plants. Photosynth Res 87:165

Kiang NY, Siefert J, Blankenship RE (2007) Spectral signatures of photosynthesis I. Review of Earth Organ Astrobiol 7:222–251

Kriedemann P (1966) The photosynthetic activity of the wheat ear. Ann Bot 30:349–363

Kromdijk J, Głowacka K, Leonelli L, Gabilly ST, Iwai M, Niyogi KK, Long SPJS (2016) Improving photosynthesis and crop productivity by accelerating recovery from photoprotection 354:857–861

Kropff MJ, Cassman KG, Peng S, Matthews RB, Setter TL (1994) Quantitative understanding of yield potential. In: Cassman KG (ed) Breaking the yield barrier. IRRI, Los Banos, Philippines, pp 21–38

Ku S, Gutierrez M, Kanai R, Edwards G (1974) Photosynthesis in mesophyll protoplasts and bundle sheath cells of various types of C4 plants II. Chlorophyll and hill reaction studies. Zeitschrift für Pflanzenphysiologie 72:320–337

Ku MS et al (2000) Photosynthetic performance of transgenic rice plants overexpressing maize C 4 photosynthesis enzymes. Stud Plant Sci 7:193–204

Langdale JA, Kidner CA (1994) Bundle sheath defective, a mutation that disrupts cellular differentiation in maize leaves. Development 120:673–681

Langdale JA, Nelson T (1991) Spatial regulation of photosynthetic development in C4 plants. Trends in Genetics 7:191–196

Langdale JA, Lane B, Freeling M, Nelson T (1989) Cell lineage analysis of maize bundle sheath and mesophyll cells. Dev Biol 133(1):128–139

Li J, Hu J (2015) Using co-expression analysis and stress-based screens to uncover *Arabidopsis* peroxisomal proteins involved in drought response. PloS One 10:e0137762

Li P et al (2010) The developmental dynamics of the maize leaf transcriptome. Nat Genet 42:1060–1067

Li Y et al (2015) Developmental genetic mechanisms of C 4 syndrome based on transcriptome analysis of c 3 cotyledons and c 4 assimilating shoots in haloxylon ammodendron. PloS One 10:e0117175

Li Y, Heckmann D, Lercher MJ, Maurino VG (2017) Combining genetic and evolutionary engineering to establish C4 metabolism in C3 plants. J Exp Bot 68:117–125

Linka M, Weber AP (2005) Shuffling ammonia between mitochondria and plastids during photorespiration. Trends Plant Sci 10:461–465

Long SP, Spence AK (2013) Toward cool C4 crops. Annu Rev Plant Biol 64:701–722

Long SP, ZHU XG, Naidu SL, Ort DR (2006) Can improvement in photosynthesis increase crop yields? Plant Cell Environ 29:315–330

Lovell JT et al (2016) Drought responsive gene expression regulatory divergence between upland and lowland ecotypes of a perennial C4 grass. Genome Res 26:510–518

Maai E, Shimada S, Yamada M, Sugiyama T, Miyake H, Taniguchi M (2011) The avoidance and aggregative movements of mesophyll chloroplasts in C4 monocots in response to blue light and abscisic acid. J Exp Bot 62:3213–3221

Majeran W, van Wijk KJ (2009) Cell-type-specific differentiation of chloroplasts in C4 plants. Trends Plant Sci 14:100–109

Majeran W et al (2010) Structural and metabolic transitions of C4 leaf development and differentiation defined by microscopy and quantitative proteomics in maize. Plant Cell 22(11):3509–3542

Mallmann J, Heckmann D, Bräutigam A, Lercher MJ, Weber AP, Westhoff P, Gowik U (2014) The role of photorespiration during the evolution of C4 photosynthesis in the genus Flaveria. Elife 3:e02478

Matsuoka M, Furbank RT, Fukayama H, Miyao M (2001) Molecular engineering of C4 photosynthesis. Annu Rev Plant Biol 52:297–314

Maydup ML, Antonietta M, Guiamet J, Graciano C, López JR, Tambussi EA (2010) The contribution of ear photosynthesis to grain filling in bread wheat (*Triticum aestivum* L.). Field Crops Res 119:48–58

McKown AD, Dengler NG (2007) Key innovations in the evolution of Kranz anatomy and C4 vein pattern in *Flaveria* (Asteraceae). Am J Bot 94:382–399

McKown AD, Dengler NG (2009) Shifts in leaf vein density through accelerated vein formation in C4 *Flaveria* (Asteraceae). Ann Bot 104:1085–1098

Merah O, Deleens E, Nachit M, Monneveux P (2001) Carbon isotope discrimination, leaf characteristics and grain yield of interspecific wheat lines and their durum parents under Mediterranean conditions. Cereal Res Commun 29:143–149

Mittler R (2006) Abiotic stress, the field environment and stress combination. Trends Plant Sci 11:15–19

Monneveux P, Reynolds M, González-Santoyo H, Pena R, Mayr L, Zapata F (2004) Relationships between grain yield, flag leaf morphology, carbon isotope discrimination and ash content in irrigated wheat. J Agron Crop Sci 190:395–401

Muhaidat R, Sage RF, Dengler NG (2007) Diversity of Kranz anatomy and biochemistry in C4 eudicots. Am J Bot 94:362–381

Muhaidat R, Sage TL, Frohlich MW, Dengler NG, Sage RF (2011) Characterization of C3–C4 intermediate species in the genus Heliotropium L. (Boraginaceae): anatomy, ultrastructure and enzyme activity. Plant Cell Environ 34:1723–1736

Naidu SL, Moose SP, Al-Shoaibi AK, Raines CA, Long SP (2003) Cold tolerance of C4 photosynthesis in Miscanthus ×

giganteus: adaptation in amounts and sequence of C4 photosynthetic enzymes. Plant Physiol 132:1688–1697
Nawarathna R, Dassanayake K, Nissanka S (2017) Is phenotypic variability in leaf vein density in rice associated with grain yield scientific. J Rice Res 1:1–9
Niinemets Ü, Berry JA, Caemmerer S, Ort DR, Parry MA, Poorter H (2017) Photosynthesis: ancient, essential, complex, diverse… and in need of improvement in a changing world. New Phytol 213:43–47
Noblin X, Mahadevan L, Coomaraswamy I, Weitz DA, Holbrook NM, Zwieniecki MA (2008) Optimal vein density in artificial and real leaves. Proc Natl Acad Sci 105:9140–9144
Nutbeam AR, Duffus CM (1976) Evidence for C 4 photosynthesis in barley pericarp tissue. Biochem Biophys Res Commun 70:1198–1203
Ort DR, Zhu X, Melis A (2011) Optimizing antenna size to maximize photosynthetic efficiency. Plant Physiol 155:79–85
Ort DR et al (2015) Redesigning photosynthesis to sustainably meet global food and bioenergy demand 112:8529–8536
Paterson AH et al (2009) The *Sorghum bicolor* genome and the diversification of grasses. Nature 457:551–556
Pengelly JJ, Kwasny S, Bala S, Evans JR (2011) Functional analysis of corn husk photosynthesis. Plant physiol 156:503–513
Pick TR et al (2011) Systems analysis of a maize leaf developmental gradient redefines the current C4 model and provides candidates for regulation. Plant Cell 23:4208–4220
Piedade M, Junk W, Long S (1991) The productivity of the C_4 Grass Echinochloa polystachya on the Amazon floodplain. Ecology 72:1456–1463
Prendergast H, Hattersley P, Stone N (1987) New structural/biochemical associations in leaf blades of C4 grasses (Poaceae). Funct Plant Biol 14:403–420
Price GD, Badger MR, von Caemmerer S (2011) The prospect of using cyanobacterial bicarbonate transporters to improve leaf photosynthesis in C3 crop plants. Plant Physiol 155:20–26
Rachmilevitch S, Cousins AB, Bloom AJ (2004) Nitrate assimilation in plant shoots depends on photorespiration. Proc Natl Acad Sci 101:11506–11510
Rangan P, Furtado A, Henry RJ (2016a) Commentary: new evidence for grain specific C4 photosynthesis in wheat. Front Plant Sci 7:1537
Rangan P, Furtado A, Henry RJ (2016b) New evidence for grain specific C4 photosynthesis in wheat. Sci Rep 6:31721
Reeves G, Grangé-Guermente MJ, Hibberd JM (2016) Regulatory gateways for cell-specific gene expression in C4 leaves with Kranz anatomy. J Exp Bot 68(2):107–116
Retkute R et al (2015) Exploiting heterogeneous environments: does photosynthetic acclimation optimize carbon gain in fluctuating light? J Exp Bot 66:2437–2447
Reyes-Prieto A, Weber AP, Bhattacharya D (2007) The origin and establishment of the plastid in algae and plants. Annu Rev Genet 41:147–168
Rojas CM, Senthil-Kumar M, Wang K, Ryu C-M, Kaundal A, Mysore KS (2012) Glycolate oxidase modulates reactive oxygen species–mediated signal transduction during nonhost resistance in *Nicotiana benthamiana* and *Arabidopsis*. Plant Cell 24(1):336–352
Rontein D, Rhodes D, Hanson AD (2003) Evidence from engineering that decarboxylation of free serine is the major source of ethanolamine moieties in plants. Plant Cell Physiol 44:1185–1191
Roth-Nebelsick A, Uhl D, Mosbrugger V, Kerp H (2001) Evolution and function of leaf venation architecture: a review. Ann Bot 87:553–566
Sáez PL et al (2017) Photosynthetic limitations in two Antarctic vascular plants: importance of leaf anatomical traits and Rubisco kinetic parameters. J Exp Bot 68:2871–2883
Sage RF (2002) C4 photosynthesis in terrestrial plants does not require Kranz anatomy. Trends Plant Sci 7:283–285
Sage RF (2004) The evolution of C4 photosynthesis. New Phytol 161:341–370
Sage RF (2016) A portrait of the C4 photosynthetic family on the 50th anniversary of its discovery: species number, evolutionary lineages, and Hall of Fame. J Exp Bot 67:4039–4056
Sage RF, Monson RK (1998) C4 plant biology. Elsevier
Sage TL, Sage RF (2009) The functional anatomy of rice leaves: implications for refixation of photorespiratory CO2 and efforts to engineer C4 photosynthesis into rice. Plant Cell Physiol 50:756–772
Sage RF, Christin P-A, Edwards EJ (2011) The C4 plant lineages of planet Earth. J Exp Bot 62:3155–3169
Sage RF, Sage TL, Kocacinar F (2012) Photorespiration and the evolution of C4 photosynthesis. Annu Review Plant Biol 63:19–47
Scarpella E, Marcos D, Friml J, Berleth T (2006) Control of leaf vascular patterning by polar auxin transport. Genes Devt 20:1015–1027
Schnable PS et al (2009) The B73 maize genome: complexity, diversity, and dynamics. Science 326:1112–1115
Schuler ML, Mantegazza O, Weber AP (2016) Engineering C4 photosynthesis into C3 chassis in the synthetic biology age. Plant J 87(1):51–65
Sedelnikova OV, Hughes TE, Langdale JA (2018) Understanding the genetic basis of C4 Kranz anatomy with a view to engineering C3 crops. Annu Rev Genet 52:249–270
Sharkey TD (1988) Estimating the rate of photorespiration in leaves. Physiol Plant 73:147–152
Sharwood RE, Ghannoum O, Kapralov MV, Gunn LH, Whitney SM (2016) Temperature responses of Rubisco from Paniceae grasses provide opportunities for improving C3 photosynthesis. Nat Plants 2:16186
Sheehy JE, Ferrer AB, Mitchell P (2008) Harnessing photosynthesis in tomorrow's world: Humans, crop production and poverty alleviation. In: Photosynthesis. Energy from the sun. Springer, Dordrecht, pp 1237–1242
Sheen J (1999) C4 gene expression. Annu Rev Plant Biol 50:187–217
Sheen J-Y, Bogorad L (1987) Differential expression of C4 pathway genes in mesophyll and bundle sheath cells of greening maize leaves. J Biol Chem 262:11726–11730
Somerville CR (2001) An early Arabidopsis demonstration. Resolving a few issues concerning photorespiration. Plant Physiol 125:20–24
Soros CL, Dengler NG (1998) Quantitative leaf anatomy of C3 and C4 Cyperaceae and comparisons with the Poaceae. Int J Plant Sci 159(3):480–491
South PF, Cavanagh AP, Liu HW, Ort DR (2019) Synthetic glycolate metabolism pathways stimulate crop growth and productivity in the field. Science 363:eaat9077
Stapper M, Fischer R (1990) Genotype, sowing date and plant spacing influence on high-yielding irrigated wheat in southern New South Wales II. Growth, yield and nitrogen use. Aust J Agric Res 41:1021–1041
Stata M et al (2014) Mesophyll cells of C4 plants have fewer chloroplasts than those of closely related C3 plants. Plant Cell Environ 37:2587–2600
Still CJ, Berry JA, Collatz GJ, DeFries RS (2003) Global distribution of C3 and C4 vegetation: carbon cycle implications. Glob Biogeochem Cycles 17(1):6–1
Sugiura D, Watanabe CK, Betsuyaku E, Terashima I (2017) Sink-Source Balance and Down-Regulation of Photosynthesis in Raphanus sativus: Effects of Grafting, N and CO2. Plant Cell Physiol 58:2043–2056
Sunil M, Hariharan AK, Nayak S, Gupta S, Nambisan SR, Gupta RP, Panda B, Choudhary B, Srinivasan S (2014) The draft genome and transcriptome of Amaranthus hypochondriacus: a

C4 dicot producing high-lysine edible pseudo-cereal. DNA Res 21(6):585–602
Taler D, Galperin M, Benjamin I, Cohen Y, Kenigsbuch D (2004) Plant eR genes that encode photorespiratory enzymes confer resistance against disease. Plant Cell 16:172–184
Taniguchi M et al (2000) Binding of cell type-specific nuclear proteins to the 5′-flanking region of maize C4 phosphoenolpyruvate carboxylase gene confers its differential transcription in mesophyll cells. Plant Mol Biol 44:543–557
Taylor SH, Long SP (2017) Slow induction of photosynthesis on shade to sun transitions in wheat may cost at least 21% of productivity. Phil Trans R Soc B 372:20160543
Tcherkez G, Bligny R, Gout E, Mahé A, Hodges M, Cornic G (2008) Respiratory metabolism of illuminated leaves depends on CO2 and O2 conditions. Proc Nat Acad Sci 105:797–802
Tholen D, Boom C, Noguchi K, Ueda S, Katase T, Terashima I (2008) The chloroplast avoidance response decreases internal conductance to CO2 diffusion in *Arabidopsis thaliana* leaves. Plant Cell Environ 31:1688–1700
Tilman D et al (2009) Beneficial biofuels—the food, energy, and environment trilemma. Science 325:270–271
Tosens T et al (2016) The photosynthetic capacity in 35 ferns and fern allies: mesophyll CO2 diffusion as a key trait. New Phytol 209:1576–1590
Ueno O (1998) Induction of Kranz anatomy and C4-like biochemical characteristics in a submerged amphibious plant by abscisic acid. Plant Cell 10:571–583
Ueno O, Yoshimura Y, Sentoku N (2005) Variation in the activity of some enzymes of photorespiratory metabolism in C4 grasses. Ann Bot 96:863–869
Vialet-Chabrand S, Matthews JS, Simkin AJ, Raines CA, Lawson T (2017) Importance of fluctuations in light on plant photosynthetic acclimation. Plant Physiol 173:2163–2179
von Caemmerer S (2003) C4 photosynthesis in a single C3 cell is theoretically inefficient but may ameliorate internal CO2 diffusion limitations of C3 leaves Plant. Cell Environt 26:1191–1197
von Caemmerer S, Evans JR (2010) Enhancing C 3 photosynthesis. Plant Physiol 154:589–592
von Caemmerer S, Furbank RT (2003) The C4 pathway: an efficient CO2 pump. Photosynth Res 77:191–207
von Caemmerer S, Quick WP, Furbank RT (2012) The development of C4 rice: current progress and future challenges. Science 336:1671–1672
S Von Caemmerer, Ghannoum O, Pengelly JJ, Cousins AB (2014) Carbon isotope discrimination as a tool to explore C4 photosynthesis. J Exp Bot 65:3459–3470
von Caemmerer S, Ghannoum O, Furbank RT (2017) C4 photosynthesis: 50 years of discovery and innovation. J Exp Bot 68:97–102
Voss I, Sunil B, Scheibe R, Raghavendra A (2013) Emerging concept for the role of photorespiration as an important part of abiotic stress response. Plant Biol 15:713–722
Voznesenskaya EV, Franceschi VR, Kiirats O, Freitag H, Edwards GE (2001a) Kranz anatomy is not essential for terrestrial C4 plant photosynthesis. Nature 414:543–546
Voznesenskaya EV, Franceschi VR, Kiirats O, Freitag H, Edwards GE (2001b) Kranz anatomy is not essential for terrestrial C 4 plant photosynthesis. Nature 414:543
Voznesenskaya EV, Franceschi VR, Kiirats O, Artyusheva EG, Freitag H, Edwards GE (2002) Proof of C4 photosynthesis without Kranz anatomy in *Bienertia cycloptera* (Chenopodiaceae). Plant J 31:649–662
Wang L, Peterson RB, Brutnell TP (2011) Regulatory mechanisms underlying C4 photosynthesis. New Phytol 190:9–20
Wang P, Kelly S, Fouracre JP, Langdale JA (2013) Genome-wide transcript analysis of early maize leaf development reveals gene cohorts associated with the differentiation of C4 K Ranz anatomy. Plant J 75(4):656–670
Wang L et al (2014) Comparative analyses of C4 and C3 photosynthesis in developing leaves of maize and rice. Nat Biotechnol 32:1158–1165
Wang P, Khoshravesh R, Karki S, Tapia R, Balahadia CP, Bandyopadhyay A, Quick WP, Furbank R, Sage TL, Langdale JA (2017a) Recreation of a key step in the evolutionary switch from C3 to C4 leaf anatomy. Curr Biol 27(21):3278–3287
Wang S, Tholen D, Zhu XG (2017b) C4 photosynthesis in C3 rice: a theoretical analysis of biochemical and anatomical factors Plant. Cell Environ 40:80–94
Weber AP, von Caemmerer S (2010) Plastid transport and metabolism of C 3 and C 4 plants—comparative analysis and possible biotechnological exploitation. Curr Opin Plant Biol 13:256–264
Williams M, Rastetter EB, Van der Pol L, Shaver GR (2014) Arctic canopy photosynthetic efficiency enhanced under diffuse light, linked to a reduction in the fraction of the canopy in deep shade. New Phytol 202:1267–1276
Wong S-C, Cowan IR, Farquhar GD (1985) Leaf conductance in relation to rate of CO2 assimilation I. Influence of nitrogen nutrition, phosphorus nutrition, photon flux density, and ambient partial pressure of CO2 during ontogeny. Plant Physiol 78:821–825
Worldmeters (2017) Worldmeters. http://www.worldometers.info/. Accessed 02 Feb 2017
Xiong D, Flexas J, Yu T, Peng S, Huang J (2017) Leaf anatomy mediates coordination of leaf hydraulic conductance and mesophyll conductance to CO2 in Oryza. New Phytol 213:572–583
Yakir D, Osmond B, Giles L (1991) Autotrophy in maize husk leaves: evaluation using natural abundance of stable isotopes. Plant physiol 97:1196–1198
Yamori W, Hikosaka K, Way DA (2014) Temperature response of photosynthesis in C3, C4, and CAM plants: temperature acclimation and temperature adaptation. Photosynth Res 119:101–117
Yoshimura Y, Kubota F, Ueno O (2004) Structural and biochemical bases of photorespiration in C4 plants: quantification of organelles and glycine decarboxylase. Planta 220:307–317
Yuan D (2012) Biotechnological interventions for crop improvement in the context of food security. Doctoral dissertation, Universitat de Lleida
Zachos JC, Dickens GR, Zeebe RE (2008) An early Cenozoic perspective on greenhouse warming and carbon-cycle dynamics. Nature 451:279–283
Zhang G et al (2012a) Genome sequence of foxtail millet (Setaria italica) provides insights into grass evolution and biofuel potential. Nat Biotechnol 30:549–554
Zhang S-B, Guan Z-J, Sun M, Zhang J-J, Cao K-F, Hu H (2012b) Evolutionary association of stomatal traits with leaf vein density in Paphiopedilum, Orchidaceae. PloS One 7:e40080
Zhu XG, Portis A Jr, Long S (2004) Would transformation of C3 crop plants with foreign Rubisco increase productivity? A computational analysis extrapolating from kinetic properties to canopy photosynthesis. Plant Cell Environ 27:155–165
Zhu X-G, Long SP, Ort DR (2008) What is the maximum efficiency with which photosynthesis can convert solar energy into biomass? Curr Opin Biotechnol 19:153–159
Zhu X-G, Long SP, Ort DR (2010) Improving photosynthetic efficiency for greater yield. Annu Rev Plant Biol 61:235–261

CHAPTER 3

PHOTOSYNTHESIS MEASUREMENTS OF WHEAT SPIKES: A PROTOCOL USING LI-COR-6400XT PORTABLE PHOTOSYNTHESIS SYSTEM COUPLED WITH A LI-COR CONIFER CHAMBER

An initial technical hurdle was how to measure gas exchange parameters of wheat spikes as most gas exchange protocols available were designed for leaves. As spikes differ structurally and physiologically from leaves, a new methodology was optimized to measure gas exchange parameters of wheat spikes using a LI-COR-6400XT portable photosynthesis system coupled with a LI-COR conifer chamber. The method that was optimized was used to determine the biological capacity of carbon assimilation of wheat spikes at different stages of ontogeny as discussed in Chapters 4, 5, and 6. This chapter has been prepared as a methods article to be submitted to "Functional Plant Biology".

Photosynthesis measurements of wheat spikes: a protocol using LI-COR-6400XT portable photosynthesis system coupled with a LI-COR conifer chamber

Prabuddha Dehigaspitiya [1], Gavin J. Ash [1], Anke Martin [1], Dananjali Gamage [2], Paul Milham[3], Saman Seneweera [1,4]*

Affiliations

[1] Centre for Crop Health, University of Southern Queensland, Toowoomba, 4350, Queensland, Australia.

[2] Department of Agricultural Biology, Faculty of Agriculture, University of Ruhuna, Sri Lanka.

[3] Hawkesbury Institute for the Environment, Western Sydney University, LB 1797 Penrith NSW, 2753, Australia.

[4] National Institute of Fundamental Studies, Hanthana Rd, Kandy, Sri Lanka.

E-mail addresses:

Prabuddha Dehigaspitiya: Prabuddha.DehigaspitiyageDon@usq.edu.au
Gavin Ash: Gavin.Ash@usq.edu.au
Anke Martin: Anke.Martin@usq.edu.au
Dananjali Gamage: Danajali@agbio.ruh.ac.lk
Paul Milham: P.Milham@westernsydney.edu.au

***Corresponding author**

Saman Seneweera (+61401879853)
Saman.Seneweera@usq.edu.au

Abbreviations

Ci – intercellular carbon dioxide concentration; IRGA - infrared gas analyser; PAR - photosynthetically active radiation.

Abstract

Understanding gas exchange parameters of critical cereals like spikes of wheat and panicles of rice has become increasingly important as a means of elucidating the mechanisms behind grain photosynthesis and whole plant performance. Optimized methods have been established to analyse leaf gas exchange using the LI-COR portable photosynthesis system. However, protocols for grain gas exchange analysis are less well defined. In this study, we have provided a method of analysing gas exchange of wheat spikes/ cereal grains using LI-COR-6400XT portable photosynthesis system coupled with a LI-COR conifer chamber (6400-05). The method discussed here has been optimized for analysing gas exchange parameters of wheat spikes. Further, several means of calculating the photosynthetic area of wheat spikes required in determining gas exchange parameters is provided. Similar protocol with minor changes can easily be utilized to analyse gas exchange parameters of three-dimensional plant organs such as fruits and stems.

Key words: Grain photosynthesis, Portable photosynthesis system, LI-COR, rice and wheat

1. Introduction

Spike photosynthesis is believed to play a vital role in grain filling in wheat, with the contribution from ear photosynthesis to the total yield being 10–44%, depending on the genotypic and environmental conditions (Sanchez-Bragado et al., 2016, Sanchez-Bragado et al., 2014). Furthermore, the possibility of having a different mode of photosynthesis in wheat spikes compared to leaves (Rangan et al., 2016, Dehigaspitiya et al., 2019) raises the possibility of considering spike photosynthesis as a physiological trait for future crop improvements (Molero et al., 2016). Although various approaches have been proposed to measure spike photosynthesis, there is a limitation of having an adequately established methodology (Sanchez-Bragado et al., 2016). The LI-COR-6400XT portable photosynthesis system (Li-COR, Lincoln, Nebraska, USA) is commonly used to analyze gas exchange of leaves; however, wheat spikes differ structurally and physiologically from leaves. To overcome similar issues when studying gas exchange of roots, Aranjuelo et al. (2009) suggested using a hand-made chamber connected in parallel to the sample air hose of the LI-COR-6400. A similar modification was used to measure the gas exchange parameters of wheat spikes (Sanchez-Bragado et al. (2016). However, there are notable difficulties, e.g. the apparatus is difficult to construct; the degree of control of conditions inside the chamber is questionable as is the calculation of the photosynthetic area; and, the respiration rate of the wheat spike generally exceeds that of leaves and changes with the physiological stages of the grain (Evans and Santiago, 2014a).

We address the preceding difficulties by coupling a LI-COR-6400XT with a LI-COR conifer chamber (6400-05: Li-COR, Lincoln, Nebraska, USA) and developing a methodology for calculating the photosynthetic area of the wheat spikes. This calculation can be extended to estimate the area of other thick and uneven photosynthetic organs.

2. Materials and equipment

2.1. Materials and equipment: for gas exchange measurements

- LI-6400 XT portable photosynthesis system
- LI-COR transparent conifer chamber (6400-05)

- CO_2 cartridges and (O-rings) gaskets
- LI-COR portable light meter
- Desiccant
- Soda lime
- LI-6020 battery charger
- Tripod
- Standard RS-232 cable- to download data
- Growth cabinet- to maintain a constant light and other environmental conditions throughout the measurements
- Computer software
    - LI-6400 software
    - LI-6400 Sim program – to recompute data
    - Imaje-J application software
    - Microsoft Excel

2.2.Materials and equipment: for spike area measurements

- Permanent marker, sharp blade, zip-lock bag, ice container
- Metric ruler
- White cardboard sheet that contains 1 cm^2 coloured square
- High-resolution digital camera (6 megapixel or higher)
- Vernier calliper

3. Methodology

3.1.Calculating the area of the spike using Image J software

1. Detach the wheat spike from the plant using a sharp blade, place into a zip-lock bag, and store on ice until commencing the area measurements.
2. Place the wheat spike on white cardboard that contains a 1 cm^2 coloured square. Also, place a metric ruler (cm ruler) next to the wheat spike as shown in Figure 1.01 (The metric ruler and the wheat spike must be parallel to each other and it must be perpendicular to the horizontal axis) (Figure 1.01).

3. Place the digital camera vertically above the middle of the wheat spike and take a high-resolution photograph (1 cm^2 square and the metric ruler must be present in the photograph, and the placement of the rectangle should be closer to the middle of the wheat spike. The height of the camera is not critical as the metric ruler is in the photograph).
4. Transfer the image to a computer which has *ImageJ* application. (Digital Image Analysis Software: Download *ImageJ* software with *Java* application that suits to your computer operating system using the link: http://rsb.info.nih.gov/ij/download.html) (Figure 1.02).
5. Open the image (Step 4) from an image editing software and crop it to remove unnecessary contents/area to get a clear image which contains the spike, metric ruler and the 1 cm^2 square. Save the image.
6. Open the *ImageJ* application. (Double click on the *ImageJ* icon on the desktop or click the start menu and navigate to *ImageJ*).
7. On *ImageJ* application, click "File" menu on the menu bar and click "Open" or press "Ctrl" and "O" keys together on the keyboard to open the relevant image (Figure 1.03, Figure 1.04).
8. From the "Open" window, select the saved photograph of the wheat spike (Figure 1.05, Figure 1.06).
9. Select the "Straight line" tool from the toolbar (Figure 2.07).
10. Then, move cursor to the 1 cm^2 square. Click and drag from one corner to the other (same side) to draw a straight line of 1 cm (Figure 2.08).
11. Click "Analyse" menu and select "Set Scale" (To set the scale of the image which contains the wheat spike) (Figure 2.09).
    a. At "Set Scale" window, type "1" at "Known distance:" (Figure 2.10).
    b. Type "cm" at "Unit of length" (Figure 2.11).
    c. Check "Global" check-box (Figure 2.12) and then click "OK".
12. Click 'Image' Menu → Select 'Type' → Select '8 bit' (to convert the image into grayscale) (Figure 3.13, Figure 3.14).
    a. Click 'Image' → Select 'Adjust' → Click 'Threshold' (to convert the wheat spike into red colour) (Figure 3.15).
    b. Adjust the lower slide bar back and forth to get a minimum amount of red colour in the background and minimum grey on the spike (Figure 3.16).
    c. Click 'Apply' to get a black-and-white (grey scale) image (Figure 3.17).

13. From the ‘Analyze’ menu, navigate to ‘Set Measurements’. Click on ‘Area’, ‘Standard deviation’ and ‘Display label’ to check the relevant check-boxes. Then change the ‘Decimal places’ to ‘2’ (Figure 3.18, Figure 4.19).
14. Navigate to ‘Analyze’→ Select ‘Analyze Particles’ and confirm whether the range within the ‘Size’ is sufficient to get the minimum and maximum areas of the wheat spikes (Figure 4.20, Figure 4.21).
15. Click on check-boxes of ‘Display results’, ‘Clear results’ and ‘Include holes’ (Figure 4.22).
16. Click ‘OK’
17. All the measurements are saved in the ‘Results’ file and displayed in the ‘Results’ window (Figure 4.23).
18. The area of the wheat spike can also be calculated using the ‘ROI Manager’ method in *image J* software
19. Go to ’Analyze’→ select ‘Tools’ → ‘ROI Manager’ (This will open the ROI Manager window) (Figure 5.24, Figure 5.25)
    a. Click on ‘Wand’ (tracing) tool from the toolbar (Figure 5.26)
    b. Click on 1 cm^2 square in the image (Figure 5.27)
    c. Click on ‘Add [t]’ on ROI Manager window (or press ‘t’ key on the keyboard) (Figure 5.28)
    d. Then click on the wheat spike (Figure 6.29)
    e. Click ‘Add [t]’
    f. Click ‘Measure’ (Figure 6.30)
20. Similar to the previous method, all the measurements are saved in the ‘Results’ file and displayed in the ‘Results’ window. Now the individual results can be copied and pasted into an Excel sheet, or else, can be copied after analysing all the images. (Figure 6.31).
    a. Select “File” → Select “Save As” (Figure 6.32).
    b. Save the picture with a separate name to avoid overwriting the original image.
21. The result which derived from this method only gives the two-dimensional area of a single side of the wheat spike. To get the total photosynthetic area of the spike, the result must be multiplied by two. The spike area calculated from this methodology is not very accurate since the wheat spike is a three-dimensional structure rather than two-dimensional as consider in *ImageJ*.

3.2.Calculating the area of the spike using physical methods

In this approach, the wheat spike is considered as an elliptical/oval cylinder (Figure 7)

1. Calculate the average diameter of the major axis (a) of the wheat spike by taking measurements at different places using a Vernier caliper. e.g.: (a = (a_1 + a_2 + a_3)/3) (Figure 7)
2. Calculate the average diameter of the minor axis (b) of the wheat spike following the same method. e.g.: (b=(b_1 + b_2 + b_3)/3) (Figure 7)
3. Measure the length of the wheat spike (L). (Figure 7)
4. Calculate the photosynthetic area of the wheat spike using either of these equations.
    a. Equation 1:

$$A \approx 2\pi L \sqrt{\frac{(a/2)^2 + (b/2)^2}{2}}$$

    b. Equation 2:

$$A \approx \pi L \left[3\left(\frac{a}{2} + \frac{b}{2}\right) - \sqrt{\left(3\frac{a}{2} + \frac{b}{2}\right)\left(\frac{a}{2} + 3\frac{b}{2}\right)}\right]$$

"A" is the photosynthetic area of the wheat spike. a and b denote the diameters of the major axis and minor axis of the oval, respectively (Figure: 7). L is the length of the spike that is used for the photosynthetic measurements.

Equation 1 is more accurate (within 5% of the actual value) when "a" is not more than three times higher than b.

A comparison between spike areas of different varieties at different growth stages derived from Image J software and the equation method is shown in Table 1.

3.3.Installation of LI-6400XT for the measurements

1. Connect the LI-COR conifer chamber (6400-05) to the sensor/infrared gas analyser (IRGA) following the instruction manual.

- A tripod is usually required for taking measurements since the handle on the sensor head has to be removed to accommodate the conifer chamber (6400-05). Also, to determine A/Ci curves, approximately 30 to 40 minutes is required, making it difficult to manually hold the IRGA.
- The manufacturer advises that IRGAs not be interchanged (Manual, 2005).

2. Connect the sensor head/IRGA to the tripod and attach the signal cables.
3. Install the external quantum sensor to the mounting bracket and plug the BNC connector.
4. Connect the power supply or insert batteries to the console and connect the sensor head/IRGA to the console.
5. Change the desiccant and soda lime if needed.
    - Both desiccant and soda lime (CaO and NaOH) give a colour change with the use. The Indicating Drierite (W.A. Hammond Drierite Company, P.O. Box 460, Xenia, OH 45385) is the recommended desiccant for LI-6400/LI-6400XT (Manual, 2005). Colour change of the Drierite is more prominent and easier to observe (blue when dry and pink upon absorption of moisture) indicating the time to replace. However, the colour indicator of most of the soda lime, which is a pH-sensitive ethyl violet, might not give a noticeable colour change upon absorption of CO_2. Also, the efficiency of the soda lime decreases if soda lime becomes too dry as absorption of CO_2 requires moisture. If the soda lime is too dry, open the chemical tube and add about 5–10 mL of water.
6. Connect the CO_2 cylinder/cartridge.
    - Before installing the CO_2 cartridge, check the presence and the condition of the O-ring. It is recommended to use a new O-ring with each new CO_2 cartridge (Manual, 2005).
7. Turn on the machine using on/off switch.
8. From the "Userprefs" menu, select the appropriate configuration.
    - By default, the conifer chamber comes with the caption of "ConiferChmbr Needless EB.xml"
9. Press "Y" to the message regarding the IRGA connected status for navigating to the main menu. Once you press "Y" IRGA starts to warm up.
10. To configure the instrument for the light source that you are using for measurements, navigate to the configuration menu. From there, navigate to light

source controls and then select the appropriate configuration from pick sources and press enter. Press escape to return to the main menu.

Before starting the measurements, it is advisable to go through a preparation checklist to ensure that the instrument is performing satisfactorily.

11. To start this checklist, navigate to new measurements from the main menu.

3.3.1. Preparation checklist

12. Check the temperatures
    - To check temperatures (block temperature, leaf temperature, and air temperature) in LI-COR-6400XT and LI-COR-6400 navigate to the display group h (row h) by pressing “h” from the keypad. There, the three values should be reasonable and within the same range to the working environment. Then, disconnect the leaf thermocouple and compare the leaf and block temperatures. If the difference between the leaf and block temperatures are higher than 0.1°C make sure to adjust the leaf temperature to zero.
13. Check the light source and sensors
    - To check the light sensors (ParIn_µm and ParOut_µm) navigate to the display group g (row g) by pressing “g” and check the response of the sensors when the external light source is illuminated and darkened. If the ParIn_ µm gives a negative value, there is a mismatch between the actual light source and the configured light source at step 10. To correct this, navigate to the configuration menu and reselect the appropriate light source.
14. Check the pressure sensors
    - Navigate to the display group g (row g) by pressing “g” to check the ambient pressure. The value should be reasonable and stable. For example, at sea level 100 kPa, at an altitude of 1000 feet value should be around 97 kPa. These values could also be varied due to weather conditions.
15. Check the leaf fan
    - To check the condition of the leaf fan (to check whether the fan is working or not), navigate to level two by pressing “2” and then press “F1”. Press “o” to turn off the fan and listen to the sound change of the stopping fan

motor. Again, press “f” for turn on the fan. You should be able to hear the fan motor. If you do not hear the sound, there could be a problem in the leaf fan either fused or clogged with debris.

16. Check the flow

- Fix the flow rate into 1000 µmol s^{-1} by navigating to level 2 and pressing “F2” (chamber should be closed). To check the actual maximum flow, go to display group b by pressing “b”. The flow rate should be around 700 µmol s^{-1} if the CO_2 mixer is installed. To check the flow restrictions of chemical tubes, make the soda lime and drierite into full scrub from the full bypass. By doing this, the flow rate should drop from 5 µmol s^{-1} to 10 µmol s^{-1} per tube. If the drops are higher than this, air mufflers of the chemical tubes could be clogged or a problem with the flow diversion tube. If the flow control is within the acceptable range, set the flow to 500 µmol s^{-1}.

Once the IRGA is switched on for about 10 minutes (after warming up), the following steps can be conducted.

17. Check the flow rate

- Turn off the pump by navigating to level 2 by pressing “2”, press “F2” and set the flow to “0”. Next, turn off the chamber fan by navigating to level 2, press “F1” and press “o”. The flow rate should be between 0 µmol s^{-1} and 2 µmol s^{-1}. If the flow does not fall into an appropriate range, navigate to the calibration menu in the main menu, and go to zero flow meter to re-zero the flow rate. Wait for the 10-second countdown. Then the voltage will reach closer to zero. After that, select Ok.

18. Check the reference and sample CO_2 levels (CO_2 IRGA)

- Press “a” and navigate to display group a, to observe reference and sample CO_2 values. Then, make the soda lime and drierite chemical tubes into full scrub and full bypass respectively. The reference CO_2 value should rapidly reach zero. However, it takes more time for sample CO_2 to reach zero. It is acceptable if both the values (reference and sample) are between 0-5 µmol mol^{-1}. If not, CO_2 IRGA must be re-zeroed. (If the working temperatures are not much changing re-zeroing the IRGA is not needed since they are quite stable. However, it has been advised to follow this step every time

you turn on the instrument) Prior to re-zeroing the CO_2 IRGA, both soda lime, and drierite must be replaced with fresh chemicals by putting the device into sleep mode. Navigate to the main menu by pressing "escape". Then select the calibration menu and navigate to IRGA zeroing. Select auto CO_2 (Not auto H_2O or auto all) and observe the values. (It is advisable to record old and new CO_2 IRGA zero values).

19. Check the reference and sample H_2O levels (H_2O IRGA)
    - Observe the reference and sample H_2O levels on display group "a" in the new measurement menu. Turn the drierite chemical tube into the full scrub and observe the changes of the H_2O levels. Reference H_2O must reach zero faster than the sample H_2O does (This takes more time than when zeroing CO_2 IRGA). It is acceptable if the reference H_2O drops down to 0.2-0.3 mmol mol^{-1} within a minute and further falling slowly. Generally, the sample H_2O values are higher than that, but it also should fall down gradually. If these values are not between the above ranges, re-zeroing the H_2O IRGA may be needed. To re-zero H_2O IRGA, navigate to calibration menu, select IRGA zeroing and hit auto H_2O.
    - (To re-zero both CO_2 IRGA and H_2O IRGA at the same time, turn both the chemical tubeless into the full scrub and select auto all in IRGA zeroing menu).
20. Mixer calibration
    - The reason for conducting the mixer calibration is to check the maximum and minimum possible operating CO_2 levels of the instrument. Generally, the maximum CO_2 level should be around 2000 µmol $mol^{-1,}$ and the minimum should be around 40 µmol mol^{-1}. For this, the chamber (conifer chamber) doesn't need to be closed. Turn the soda lime chemical tube into the full scrub. Press "escape" and navigate to the main menu. From there, navigate to calibration menu and select mixer calibration and press "Y" for the prompted message (OK to continue?). Once the calibration is done, the data can be viewed in a graph. Press "escape" to navigate to the main menu and go to new measurements menu.
21. Check for leaks

- Press “a” and navigate to display group a. Close the conifer chamber (this should be empty). Exhale the air around the chamber gasket and observe the fluctuations of the sample CO_2 concentration. If there are no leaks, this should not increase the sample CO_2 concentration for more than 1 µmol mol^{-1}. If there is a fluctuation more than that, check the gasket for damages and replace it.
- Now the instrument is ready for taking measurements

3.3.2. Taking measurements

22. Navigate to level 1 by pressing “1” and open a log file by pressing “F1”. Give an appropriate name to the data file. (It is better to include parameters like date, species, variety, tissue, etc.) And if necessary, add remarks accordingly.
23. Navigate to level 2 by pressing “2” to set the reference CO_2 level and the block temperature
    - Press “F3” and navigate to CO_2 mixer, select CO_2 reference and press “enter”, set the mixer value to 400 µmol mol^{-1} and press keep (this value depends on the environmental condition that you are working on. when you are taking measurements at ambient conditions it should be slightly above the ambient CO_2 level).
    - Press “F4” and navigate to the temperature menu, select the block temperature, press enter and set the block temperature to the desired value (for example, 25°C). (If the entered block temperature is not around the ambient temperature (working temperature), the power consumption of the instrument will be higher than the normal, and if the instrument is operated using batteries, frequent battery changes might be required.)
24. Introduce the wheat plant to a constant artificial light source where the light intensity is around 1000 µmole m^{-2} s^{-1} photosynthetically active radiation (PAR) and keep it for 30 to 45 minutes.
    - It is better to introduce the plant into a controlled growth chamber since other environmental parameters such as temperature and relative humidity can also be maintained at a constant level until the measurement is taken. (Generally, for A/Ci curves it may take approximately 30 to 45 minutes to

complete. So, it is better to have a constant environment throughout this period)

25. Calculate the area of the selected spike part which accommodates into the conifer chamber using the described method and inserts the spike area by navigating to Level 3 by pressing "3". (This also can be done after downloading the data to a computer).
26. Insert the wheat spike to the conifer chamber and wait until the spike reaches to steady-state photosynthesis.
    - Make sure that the conifer chamber is properly sealed.
    - To identify the steady-state photosynthesis, check the graphs of photosynthesis and stomatal conductance by navigating to Level 4 by pressing "4".
27. If graphs are stable, spot measurements of gas exchange can be taken. To log this value, navigate to Level 1 by pressing "1" and press "F1". This value will be saved into the log file which was previously created. (Step: 22).
28. To obtain A/Ci curves, navigate to Level 5 by pressing "5" and select "AUTO PROG". From the list, select "A-Ci Curve". Press "Y" when asked, "Append to current data file?"
29. Insert the desired CO_2 levels to the instrument and press "Enter".
    - E.g. For C_3 plants, 400 300 200 100 50 400 400 600 800 1200 1500 1700
    - For C_4 plants 400 300 200 100 00 400 400 600 800 1200 1500 1700
30. Set minimum and maximum waiting times.
    - Set 120 s and 300 s as the minimum and the maximum waiting time, respectively.
31. Pres "Y" (Yes) to the option "Always Match" and press "Y" for "Stability Definition OK?".
32. Then press "F5" to start the auto-program.
    - Then the program will run automatically for different CO_2 levels, and it will take about 40 minutes depending on the matching time.
    - The star mark (*) at menu 2 indicates the auto-program is running.
33. When the measurements are taken, attention should be paid to the following:
    - Line C: Photo (photosynthesis) should be between -10 and + 30 or higher depending on the CO_2 level, Cond (conductance) should be a positive value

between 0.01 and 1, Ci (intercellular CO_2 level) should be a positive value (negative Ci may be due to a problem associated with leaf temperature or moisture calibration)

- Line D: VpdL should be lesser than 2. Higher values may be due to higher spike and outside temperatures.
- Line H: spike temperature should be slightly less than the air temperature.
- Line I: Indicates the battery charge. Beeping indicates voltage below 10 and should change the batteries.
- At the end of the auto program, the "*" mark in menu 2 will disappear.

34. After the measurement, turn off the light source of the growth chamber while keeping all other parameters unchanged (temperature and relative humidity).
35. Navigate to Level 2 by pressing "2" and set the reference CO_2 level back to 400 µmol mol^{-1}.
    - After the measurement, the reference CO_2 level will be at 1700 µmol mol^{-1}. Thus, it has to be changed back into 400 µmol mol^{-1}.
36. Allow the plant to stay in the dark for 30 minutes.
    - If the artificial light source is not from a controlled growth chamber, cover the entire plant and the conifer chamber with a black cover to stop the light penetration.
37. Take A/Ci curve using the same program used with the light source.
    - If the photosynthesis values in the dark give much lower values than -2, photosynthesis values can be recomputed using the following equation.
    - $P_c = [P_L - P_D]$ where P_c denotes corrected photosynthesis, P_L denotes photosynthesis values under constant light and P_D denotes photosynthesis values in the dark.
38. Download data as described in (Evans and Santiago, 2014b)
39. Recompute data after measuring the entire spike area as described in (Evans and Santiago, 2014b)
40. Gas exchange parameters of wheat spikes under light and dark is tabulated in Tables 2 and 3 respectively.

3.3.3. After measurements

41. Turn off the LI-COR 6400XT as described in Evans and Santiago (2014b)
42. Detach the IRGA from the tripod and loose the leaver of the lid of the conifer chamber to avoid gasket compression during storage.
43. Remove batteries or the external power source.
44. Store appropriately in the storage box

3.4.Concluding remarks

The analyse of gas exchange parameters of the photosynthetic organs is useful to determine the underlying photosynthetic biochemistry and the whole plant performance. In most cereals, protocols for measuring gas exchange parameters of leaves have been fully established. However, less attention has paid shown to the investigation of the gas exchange of minor photosynthetic organs such as wheat spikes and rice panicles. Growing evidence supports the fact that photosynthesis of developing cereals may play an important role in grain filling and thus total yield. Further, there is a high possibility of using spike/panicle gas exchange parameters as a trait of crop improvement. Therefore, characterization of cereals, based on the grain gas exchange seems increasingly important.

An optimized protocol to determine gas exchange parameters of wheat spikes using LI-COR-6400XT portable photosynthesis system coupled with LI-COR conifer chamber is reported. Further, two different methods for the photosynthetic area calculations of wheat spikes, which can further be utilized in crop phenotyping has also been reported. Photosynthetic area values acquired from different methods have been discussed and compared. Similar approaches with slight modifications can be used to assess gas exchange parameters in most other cereals.

Conflict of interest

The authors declare that this study was conducted in the absence of any commercial relationships that could lead to any potential conflict of interest.

Acknowledgment

This work was supported by the University of Southern Queensland (USQ), Australia and the USQ Strategic Research Fund. PD is supported by a USQ International Stipend Research Scholarship and USQ International Fees Research Scholarship.

Tables and figures

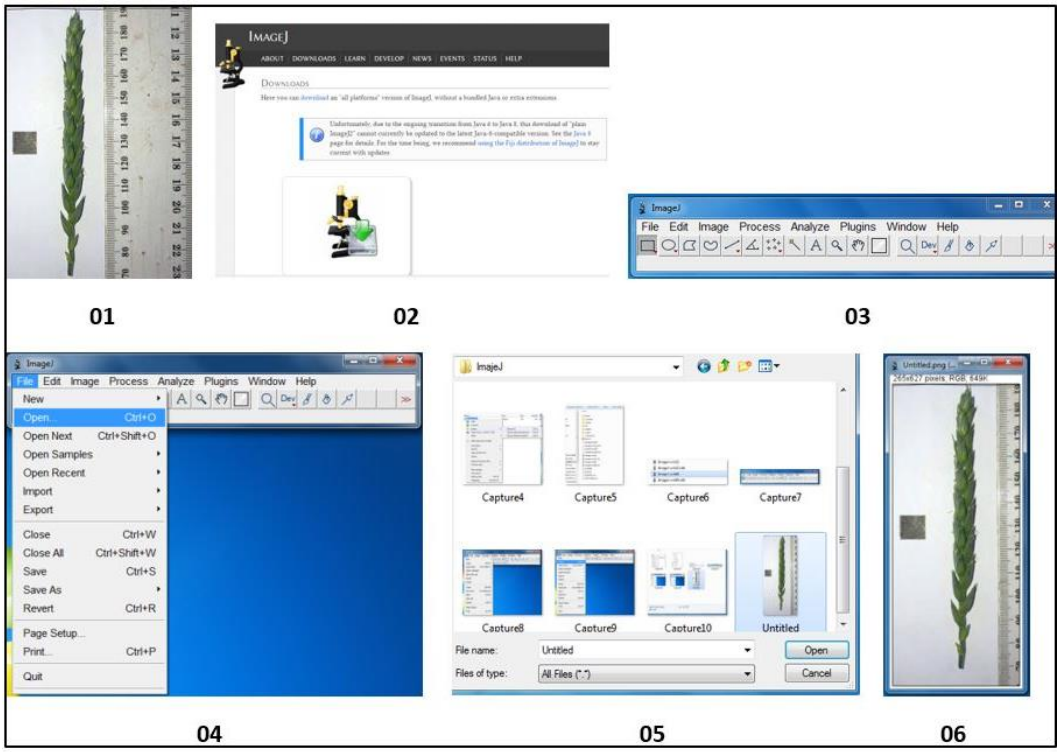

Figure 1

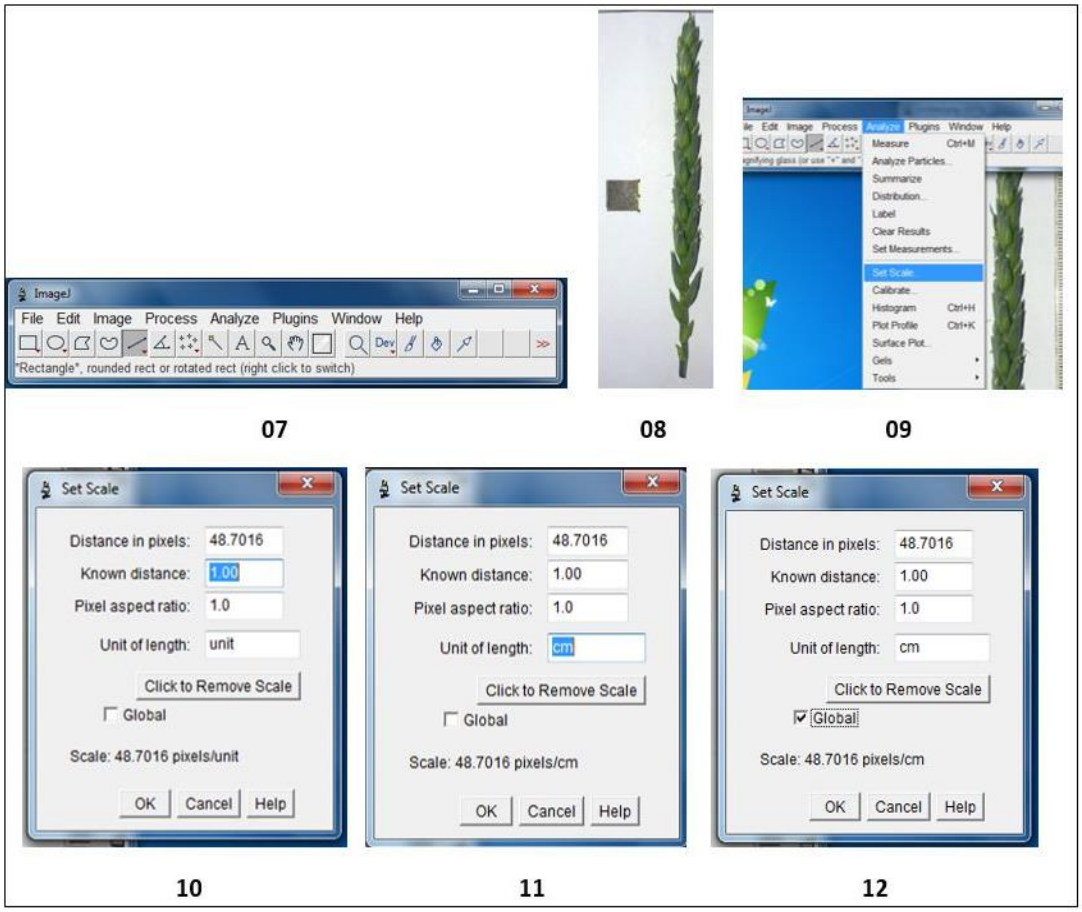
ImageJ
File Edit Image Process Analyze Plugins Window Help
"Rectangle", rounded rect or rotated rect (right click to switch)
07
08
09
Set Scale
Distance in pixels: 48.7016
Known distance: 1.00
Pixel aspect ratio: 1.0
Unit of length: unit
Click to Remove Scale
Global
Scale: 48.7016 pixels/unit
OK Cancel Help
10
Set Scale
Distance in pixels: 48.7016
Known distance: 1.00
Pixel aspect ratio: 1.0
Unit of length: cm
Click to Remove Scale
Global
Scale: 48.7016 pixels/cm
OK Cancel Help
11
Set Scale
Distance in pixels: 48.7016
Known distance: 1.00
Pixel aspect ratio: 1.0
Unit of length: cm
Click to Remove Scale
Global
Scale: 48.7016 pixels/cm
OK Cancel Help
12

Figure 2

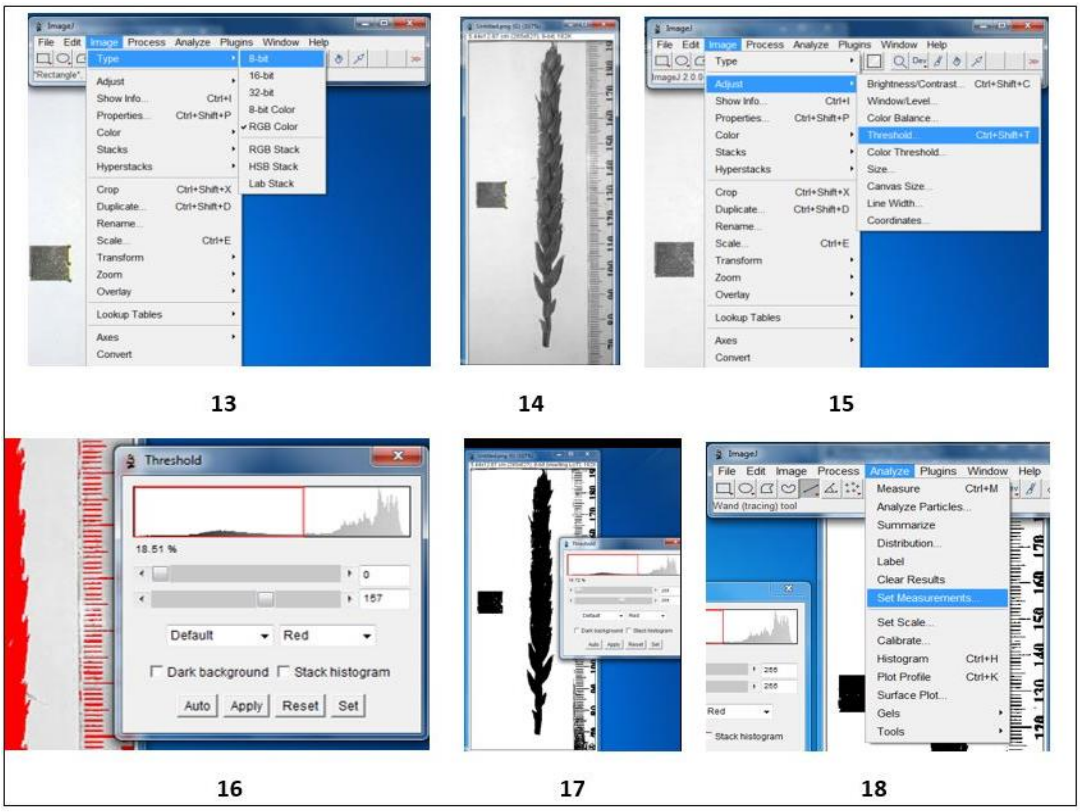

Figure 3

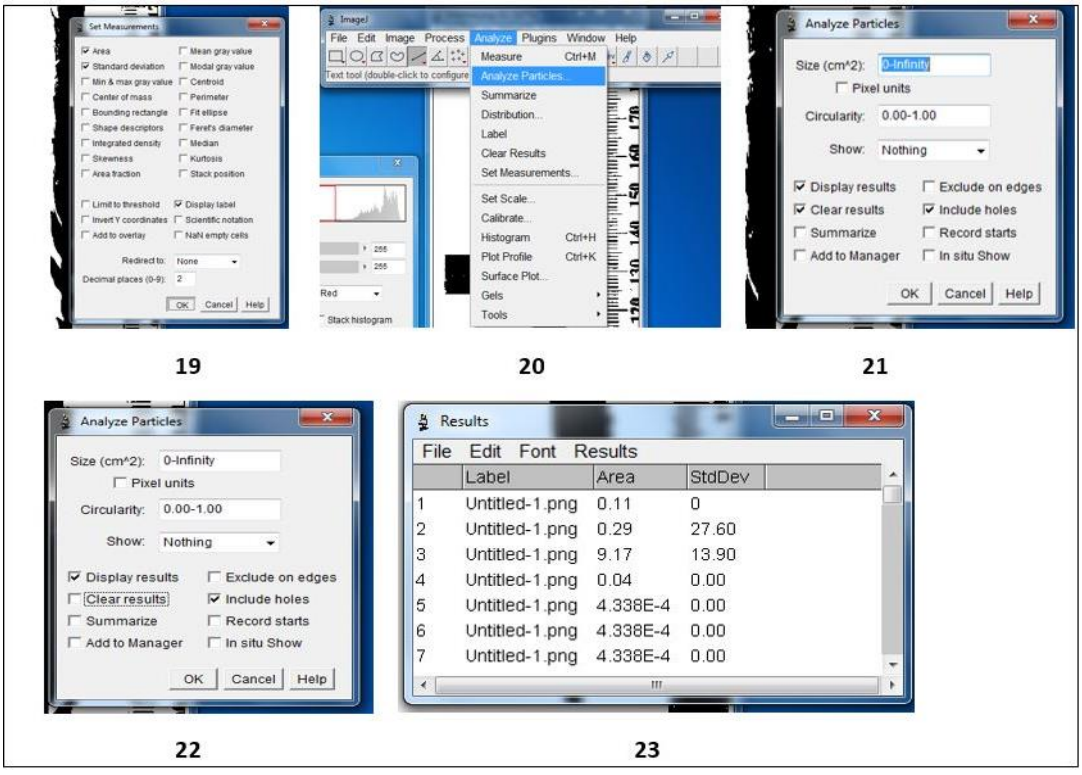

Figure 4

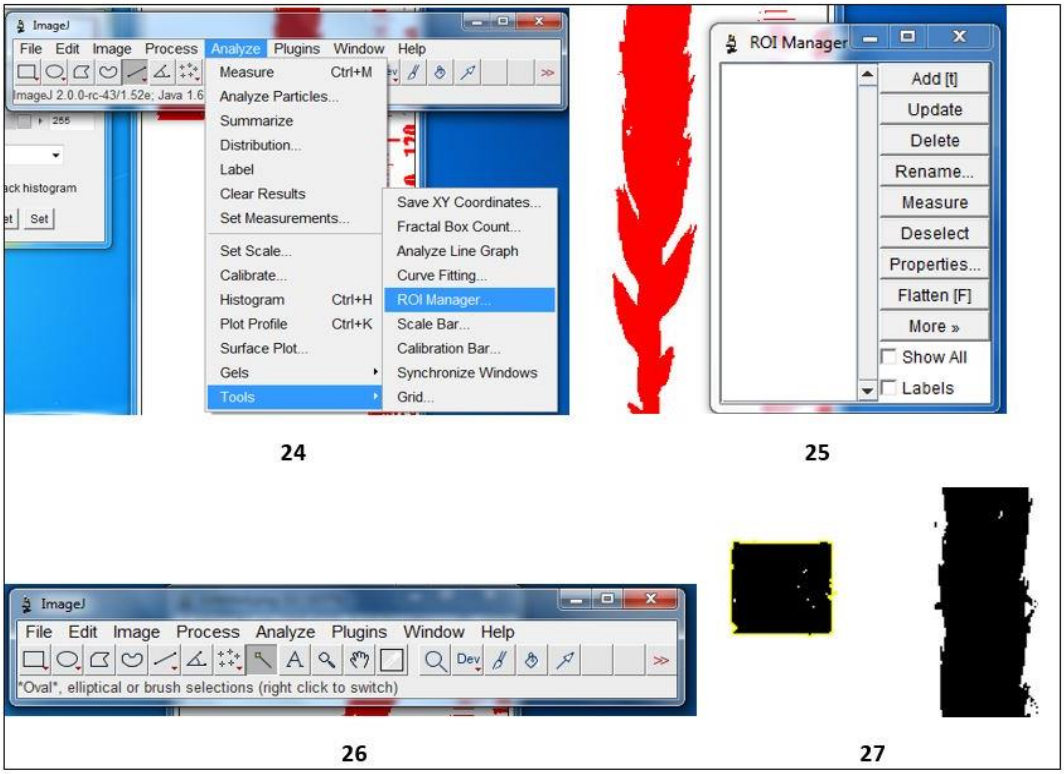

Figure 5

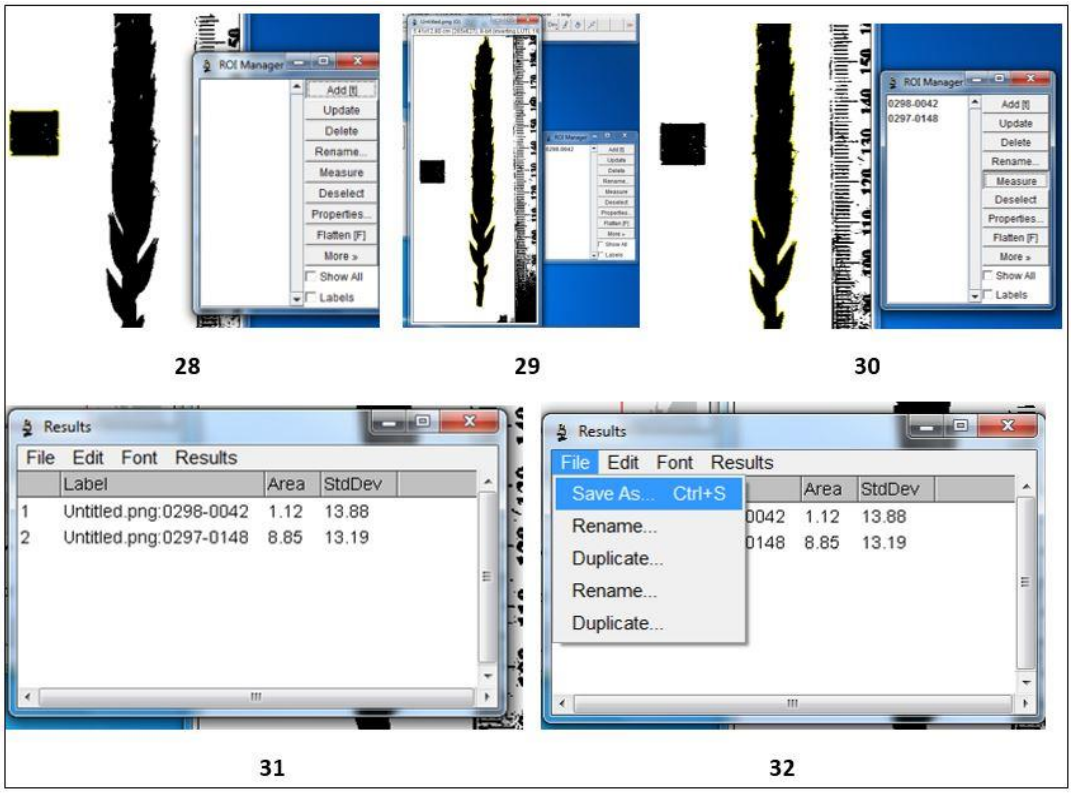

Figure 6

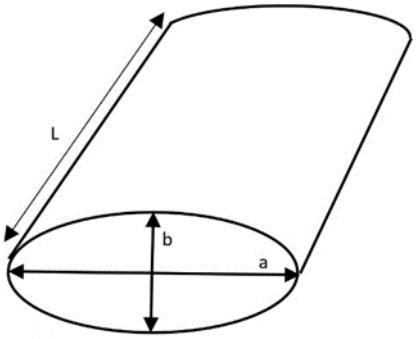

Figure 7. Calculation of the photosynthetic area of the wheat spike considering it as an elliptical cylinder. L denotes the length of the spike. "a" denotes diameter of the major axis and "b" denotes the dimeter of the minor axis. To get much accurate measurements, it is better to take the average value of different a and b values taken at different points of the spike.

Table 1. Differences of photosynthetic areas of wheat spikes from different area measuring methods. Abbreviations: 14-dpa: 14 days post anthesis.

	Method		
Growth stage	**Image J (cm^2)**	**Equation 1 (cm^2)**	**Equation 2 (cm^2)**
Heading	**8**	**10.5**	**10.5**
Heading	**10.34**	**10.76**	**10.75**
Heading	**10.4**	**12.61**	**12.6**
Heading	**16.28**	**14.32**	**14.21**
14-dpa	**19.2**	**20.31**	**20.2**
14-dpa	**20.02**	**16.92**	**16.8**
14-dpa	**21.34**	**17.83**	**17.7**
14-dpa	**21.6**	**19.68**	**19.67**
14-dpa	**23.6**	**18.82**	**18.68**

Table 2. Gas exchange parameters of wheat spike of Huandoy at 14 days post anthesis (14-dpa) under 800 µmole m^{-2} s^{-1} (PAR)

CO_2 level inside the chamber	**Photosynthesis** (µmol m^{-2} s^{-1})	**Stomatal conductance** (mol H_2O m^{-2} s^{-1})	**Intercellular CO_2** (µmol CO_2 mol^{-1})	**Transpiration rate** (mmol H_2O m^{-2} s^{-1})
400	**3.75**	**0.0943**	**320**	**1.63**
300	**2.39**	**0.103**	**249**	**1.76**
200	**0.61**	**0.112**	**184**	**1.89**
100	**-1.50**	**0.12**	**120**	**2.00**
50	**-2.67**	**0.128**	**87.6**	**2.10**
100	**-0.97**	**0.133**	**111**	**2.18**
200	**1.68**	**0.138**	**171**	**2.23**
300	**4.01**	**0.141**	**237**	**2.27**
400	**5.96**	**0.142**	**307**	**2.28**
700	**9.93**	**0.138**	**542**	**2.24**
800	**10.50**	**0.128**	**620**	**2.10**
1200	**12.60**	**0.115**	**961**	**2.10**
1500	**13.80**	**0.107**	**1220**	**1.85**
1700	**14.30**	**0.101**	**1390**	**1.78**

Table 3. Gas exchange parameters of wheat spike of Huandoy at 14 days post anthesis (14-dpa) under dark (0 PAR)

CO_2 level inside the chamber	**Photosynthesis** ($\mu mol\ m^{-2}\ s^{-1}$)	**Stomatal conductance** ($mol\ H_2O\ m^{-2}\ s^{-1}$)	**Intercellular CO_2** ($\mu mol\ CO_2\ mol^{-1}$)	**Transpiration** ($mmol\ H_2O\ m^{-2}\ s^{-1}$)
400	**-8.87**	**0.174**	**492.0**	**2.24**
300	**-9.08**	**0.163**	**402.0**	**2.16**
200	**-9.04**	**0.151**	**311.0**	**2.06**
100	**-8.96**	**0.143**	**218.0**	**1.99**
50	**-8.86**	**0.139**	**171.0**	**1.96**
100	**-8.47**	**0.137**	**215.0**	**1.94**
200	**-8.34**	**0.136**	**312.0**	**1.93**
300	**-8.19**	**0.134**	**409.0**	**1.90**
400	**-8.18**	**0.127**	**511.0**	**1.82**
700	**-7.95**	**0.116**	**809.0**	**1.69**
800	**-8.18**	**0.105**	**921.0**	**1.56**
1200	**-7.79**	**0.096**	**1310.0**	**1.46**
1500	**-7.80**	**0.089**	**1620.0**	**1.36**
1700	**-7.65**	**0.084**	**1810.0**	**1.30**

References

Aranjuelo, I., Cabrera-Bosquet, L., Mottaleb, S. A., Araus, J. L. & Nogues, S. 2009. 13C/12C isotope labeling to study carbon partitioning and dark respiration in cereals subjected to water stress. *Rapid Communications in Mass Spectrometry,* 23**,** 2819-2828.

Dehigaspitiya, P., Milham, P., Ash, G. J., Arun-Chinnappa, K., Gamage, D., Martin, A., Nagasaka, S. & Seneweera, S. J. P. 2019. Exploring natural variation of photosynthesis in a site-specific manner: evolution, progress, and prospects. 1-18.

Evans, J. R. & Santiago, L. S. 2014a. PrometheusWiki Gold Leaf Protocol: gas exchange using LI-COR 6400. *Functional Plant Biology,* 41**,** 223-226.

Evans, J. R. & Santiago, L. S. J. F. P. B. 2014b. PrometheusWiki gold leaf protocol: gas exchange using LI-COR 6400. 41**,** 223-226.

Manual, L. 2005. Using the LI-6400 portable photosynthesis system. LI–COR Biosciences Inc.: Lincoln) Available at https://www. licor. com/env/support/product.

Molero, G., Sukumaran, S. & Reynolds, M. P. 2016. Potential to include spike photosynthesis in breeding programs: Genetic variation for spike photosynthesis and identification of molecular markers.

Rangan, P., Furtado, A. & Henry, R. J. 2016. New evidence for grain specific C4 photosynthesis in wheat. *Scientific reports,* 6**,** 31721.

Sanchez-Bragado, R., Molero, G., Reynolds, M. P. & Araus, J. L. 2014. Relative contribution of shoot and ear photosynthesis to grain filling in wheat under good agronomical conditions assessed by differential organ δ13C. *Journal of experimental botany,* 65**,** 5401-5413.

Sanchez-Bragado, R., Molero, G., Reynolds, M. P. & Araus, J. L. 2016. Photosynthetic contribution of the ear to grain filling in wheat: a comparison of different methodologies for evaluation. *Journal of experimental botany,* 67**,** 2787-2798.

CHAPTER 4

SITE-SPECIFIC, GENOTYPIC AND TEMPORAL VARIATION OF GAS EXCHANGE AND ITS RELATED BIOCHEMISTRY IN WHEAT (*Triticum aestivum* L.)

The site-specific, genotypic, and temporal variation of photosynthesis and sucrose metabolism in flag leaves and spikes of wheat were comparatively investigated. Three winter wheat varieties were grown under glasshouse conditions and analysed at four different stages of ontogeny after heading. To determine the variation in metabolic processes, a multidisciplinary approach was used including gas exchange measurements to determine the biological capacity of carbon assimilation, gene expression profiling, phenotyping, and biochemical assays. Findings of this study can be used to address the current knowledge gaps of site-specific, genotypic and temporal variation of photosynthesis and the importance of spike-metabolic processes for grain filling. This chapter has been prepared as a research manuscript to be submitted to "Planta".

Site-specific, genotypic, and temporal variation of gas exchange and its related biochemistry in wheat (*Triticum aestivum* L.)

Prabuddha Dehigaspitiya[1], Paul Milham[2], Anke Martin[1], Gavin Ash[1], Dananjali Gamage[3], Saman Seneweera[1, 4]*

Affiliations

[1] Centre for Crop Health, University of Southern Queensland, Toowoomba, QLD, 4350, Australia

[2] Hawkesbury Institute for the Environment, Western Sydney University, LB 1797 Penrith NSW, 2753, Australia.

[3] Department of Agricultural Biology, Faculty of Agriculture, University of Ruhuna, Sri Lanka.

4 National Institute of Fundamental Studies, Hanthana Road, Kandy, Sri Lanka.

E-mail addresses:

Prabuddha Dehigaspitiya: Prabuddha.DehigaspitiyageDon@usq.edu.au

Paul Milham: P.Milham@westernsydney.edu.au

Anke Martin: Anke.Martin@usq.edu.au

Gavin Ash: Gavin.Ash@usq.edu.au

Dananjali Gamage: Dananjali@agbio.ruh.ac.lk

***Corresponding author**

Saman Seneweera (+61401879853)
Saman.Seneweera@usq.edu.au

Abbreviations

AGB – above ground biomass; BWS – biomass without spikes; CM – complete maturity; dpa – days post anthesis; HI – harvest index; PAL – photosynthetic area of total leaves; PAS – photosynthetic area of total spikes; PAT - total photosynthetic area; PASM – photosynthetic area of spike of main tiller; Rubisco - Ribulose 1,5-bisphosphate carboxylase/oxygenase; *rbcL* - Ribulose 1,5 –bisphosphate carboxylase/oxygenase (large sub unit); *rbcS* - Ribulose 1,5 – bisphosphate carboxylase/oxygenase (small sub unit); SAI – spike area index; *SPP1* - Sucrose Phosphate Phosphatase 1; *SPS1* - Sucrose Phosphate Synthase 1; *SUS1* - Sucrose Synthase type 1; TB – total biomass; *TPU* – trios phosphate utilization.

Abstract

To determine the importance of wheat spikes for yield we investigated the genotypic and temporal variation of traits related to photosynthesis and sucrose metabolism in the pericarps and flag leaves of three wheat genotypes, Huandoy, Amurskaja75 and Greece 25. Spike biomass, nitrogen (N) concentrations of photosynthetic organs and the photosynthetic area of flag leaves and spikes were measured at heading, and at 14- and 30-days post-anthesis (dpa). Further, the biological capacity of carbon assimilation (Vc_{max} and J_{max}) of spikes and flag leaves were determined using A-C_i curves at heading, and at 3-, 14-, and 30-dpa. Lastly, molecular level changes in photosynthesis and sucrose metabolism at heading, and at 14- and 30-dpa were determined by investigating the transcript abundance of key genes of photosynthesis and sucrose metabolism: *rbcL, rbcS, SPS1, SUS1* and *SPP1*. Significant genotypic and temporal variation in Vc_{max} and J_{max} were observed early in ontogeny that dissipated by late grain-filling. Although the transcript abundance of *rbcS* and *rbcL* in flag leaves was significantly higher than in the pericarps, both organ types displayed a similar expression pattern among growth stages. The N concentrations of pericarps suggest that the greatest amount of Rubisco may be present during grain enlargement; however, gene expression indicated the contrary. From heading to 14-dpa, wheat pericarps exhibited a strong, positive correlation between biological capacity for carbon assimilation and expression of key genes related to sucrose metabolism (*SPS1*, *SUS1* and *SPP1*). Lastly, the strong correlation between spike dry weight and the biological capacity for carbon assimilation suggest that metabolic processes in wheat spikes may have a major role in grain filling and total yield.

Keywords: source and sink interaction, Rubisco, sugar sensing, transcript abundance, grain filling, organ-specific photosynthesis

1. Introduction

Significant yield improvement of critical C_3 cereal crops occurred during the green revolution between the 1950s and 1980s (Furbank et al., 2015) and has sustained the global food demand for a number of decades. However, catering to the estimated global population of 9.8 billion by 2050 (Dillard, 2019) necessitates a 60% yield improvement of critical food crops (Li et al., 2017, White and Gardea-Torresdey, 2018). Reaching that target seems impossible without another huge breakthrough, as the yield potential of most current cereal crops has plateaued (Furbank et al., 2015, Wang et al., 2017). Sustaining global food security is even more precarious given the predicted water scarcity and global warming (Yadav et al., 2019). Increasing the efficiency of photosynthesis is one possible solution to the upcoming food crisis (Kubis and Bar-Even, 2019, van Bezouw et al., 2019); and several different approaches have been suggested. The favored approaches include: engineering C_4 traits into C_3 plants; mitigating the functional limitations of ribulose-1,5-bisphosphate carboxylase/oxygenase (Rubisco); regulation of sink and source feedback of photosynthesis; and minimization of the inefficiencies of photosynthesis due to dynamic environmental factors (Schuler et al., 2016, Jansson et al., 2018, South et al., 2018, Dehigaspitiya et al., 2019). However, inadequate understanding of the complex genetic processes of photosynthesis has minimized improvement in what already are photosynthetically inefficient crop plants (Li et al., 2017).

In angiosperms, more importance has until now been placed on photosynthesis of the major photosynthetic organs, namely the leaves. However, a growing number of observations support the possibility that more efficient modes of photosynthesis may occur in minor photosynthetic organs, a phenomenon described as site-specific changes in photosynthesis (Rangan et al., 2016b, Bachir et al., 2017, Wang et al., 2017). Site-specific changes in photosynthesis in major crop plants merit investigation because of the possibility of transferring those more photosynthetically efficient traits into the leaves.

As a cereal, wheat (*Triticum aestivum* L.) is second in importance only to rice, providing 20% of the daily calories and protein in the developing world (Tadesse et al., 2017). Wheat demand is expected to increase by 50% by 2050 (Li et al., 2017), which requires the annual increment in wheat yield to be boosted from less than 1%

at present, to at least 1.6% (Tadesse et al., 2017). Photosynthesis in wheat leaves has been well studied (Evans and Rawson, 1970, Lawlor et al., 1989). Nonetheless, little is known about how photosynthesis in other organs, e.g. in wheat spikes, which may play an important role in grain-filling (Serrago et al., 2013), contributing perhaps 10–44% of photosynthate depending on genetic and environmental factors (Tambussi et al., 2007, Maydup et al., 2010). The potential contribution of wheat spikes to grain yield is supported by delayed chlorosis in the pericarps, better water supply during late grain filling and the protection provided to the endosperm (Dehigaspitiya et al., 2019). Also, evidence for grain specific C_4 photosynthesis has been recently reported (Rangan et al. (2016b), hence a fuller understanding of spike photosynthesis in wheat may open a new route to enhancement of grain yield.

In C_3 plants, the first step in net photosynthetic CO_2 assimilation and photorespiratory oxidation of carbon (C) is catalyzed by the enzyme Rubisco. Rubisco is the most abundant protein in the C_3 photosynthetic organs and accounts for 15–30% of the total nitrogen (N) in leaves (Makino et al., 1992, Suzuki et al., 2009, Seneweera et al., 2011). Rubisco plays a central role in C assimilation in all photosynthetic pathways: C_3, C_4, CAM and C_3-C_4 intermediates. In the C_3 pathway under high irradiance, the amount of Rubisco is a determining factor for the rate of CO_2 assimilation throughout the life cycle of a photosynthetic organ (Suzuki et al., 2009). In addition, Rubisco content varies widely with the physiological stage of the leaf/ photosynthetic organ, e.g. in leaves, it increases during maturation and gradually declines during senescence (Suzuki et al., 2001). Site-specific variation of Rubisco abundance has also been also reported (Nomura et al., 2000). In higher plants, degradation products of Rubisco are a source of N that is utilized by developing tissues (Makino et al., 1984, Suzuki et al., 2001). The balance between Rubisco synthesis and degradation determines the amount of Rubisco in a photosynthetic organ (Suzuki et al., 2001). The expression patterns of *rbcL* and *rbcS* mRNAs, and their activities, have been intensely studied in wheat leaves (Nie et al., 1995, Demirevska et al., 2009), whereas, less attention has been paid to site-specific/ organ-specific changes of expression of *rbcL* and *rbcS* in wheat pericarps/ spikes.

In C_3 photosynthesis, the maximum rate of Rubisco carboxylation (Vc_{max}) and the maximum rate of electron transport in the light-dependent reactions (J_{max}) regulate the biological capacity of C assimilation. Carbon dioxide response curves (A-C_i curves)

generated from gas exchange parameters of leaves, combined with various fitted models (A-C_i curve fitting methods) provide access to estimates of Vc_{max} and J_{max} (Farquhar et al., 1980, Fan et al., 2011). The biological capacity of C assimilation by leaves of wheat plants has been well-characterized using A-C_i curves. However, it has been suggested that a more efficient photosynthetic system may be expressed in wheat spikes and contribute to crop yield (Rangan et al., 2016b). Thus, it is important to better understand the variation of C assimilation capacity in wheat spikes during grain filling, which until now has not been evaluated in detail.

Photosynthesis correlates highly with plant sucrose metabolism (Vu et al., 2006, Vicente et al., 2015). The quantity of sugars produced from photosynthesis varies among different photosynthetic organs (Koch, 2004), which may lead to initiation of site-specific molecular level changes of the sucrose metabolism. For example, with high rates of photosynthesis, the sugar concentration of the photosynthetic tissue (source) increases and the genes related to source activity of sucrose metabolism are upregulated (Stitt et al., 2010). Subsequently, the produced sugars are translocated to sink tissues while upregulating the genes related to sucrose formation and amino acids synthesis (Paul and Pellny, 2003, Stitt et al., 2010). This sink-source interaction is a determining factor in grain yield of wheat (Rajala et al., 2009). Knowledge of the expression patterns of key genes regulating sucrose metabolism in wheat pericarps during grain filling may therefore illuminate the photosynthetic contribution by the spike to wheat grain yield, and consequently, deserve further exploration.

The main hypotheses of this study are: (i) parameters of C assimilation and sucrose metabolism site-specifically, genotypically and temporally vary; and (ii) spike photosynthesis and sucrose metabolism of wheat pericarps contribute appreciably to grain yield. These hypotheses was tested by observing the physiological and molecular level changes of photosynthesis and sucrose metabolism in wheat spikes and flag leaves of three wheat genotypes through different growth stages after heading.

2. Methods

2.1 Plant materials and growth conditions

Three winter wheat varieties (Amurskaja 75, Greece 25, and Huandoy) were selected based on differences in the expression of genes related to C_4 pathway observed from an experiment conducted by Rangan et al. (2016a). Of the three genotypes, Greece 25 and Huandoy were awned wheat varieties. Seeds were sourced from the Australian Grain Gene Bank, Grains Innovation Park, Horsham, Victoria. Five seeds were sown in each pot filled with 4.2 kg of loam soil. The experimental design was completely randomized with 3 replicates. The pots were placed in a glasshouse at the University of Southern Queensland, Australia (Latitude: 27° 33' 38.02" S and Longitude: 151° 55' 55.20" E) from May 2017 to October 2017. The maximum and minimum temperatures were maintained at 22°C and 14°C respectively. All the pots were randomized weekly to minimize the location effect inside the glasshouse. Germinated seedlings were thinned to two plants per pot 14 days after sowing.

2.2. Plant growth measurements

Three replicates from four growth stages [heading, 14-days post anthesis (14-dpa), 30-dpa and complete maturity (CM)] were used for phenotyping. The traits measured and growth stages of data collection are indicated in Table 1. Areas of leaves were measured using a leaf area meter (LI-COR, USA). Spike area was measured using the method described in (Chapter 2). The harvest index (HI) was calculated by dividing the weight of the total harvest from the total above ground biomass. Spike area index (SAI) was calculated by dividing spike area from the total photosynthetic area. After leaf and spike area measurements, samples were dried at 60°C for 72 h and weighed.

2.3. Gas exchange measurements

Four growth stages of the wheat spikes and flag leaves: heading, 3-dpa, 14-dpa and 30-dpa were selected to assess gas exchange parameters. Spike gas exchange measurements were made using a portable photosynthesis system (LI-6400xt, LI-COR, USA) coupled with LI-COR transparent conifer chamber (LI-COR, Lincoln, NE, USA 6400-05) as described in Chapter 2. Gas exchange measurements of the flag

leaves were carried out as described by Evans and Santiago (2014) between 9 am and 2.30 pm. Wheat plants were introduced into a controlled growth chamber (PGC-105, Percival, USA) at the University of Southern Queensland, Australia at least one h prior to the measurements. The temperature, canopy level light intensity, relative humidity of the controlled growth chamber was maintained at 22°C, 1000 µmol m^{-2} s^{-1} and 70% respectively. Photosynthetic area of the wheat spike was calculated using the method described in (Chapter 2). After connecting the wheat spike to the portable photosynthesis system, spike level temperature and the air flow rate were maintained at 22°C and 500 µmol s^{-1} respectively. The starting reference CO_2 concentration inside the conifer chamber was 400 µmol mol^{-1}. Relative humidity inside the chamber was maintained at 50–70%. Each spike was equilibrated for about 10–15 min to reach steady state gas exchange before measurements commenced. Steady-state gas exchange was identified by observing the fluctuations in graphs of photosynthesis and stomatal conductance. Carbon dioxide response (A-C_i) curves were obtained for wheat spikes and flag leaves in each growth stage.

2.4 Plant carbon and nitrogen analysis

Oven dried pericarps and flag leaves of three genotypes at four growth stages were removed from the plants and ground in a ball mill (Tissue Lyser II, QIAGEN, Australia) to ~100 µm diameter. Carbon and N content of the plant samples was measured using a combustion analyzer (C and N) (Leco CN628, USA).

2.5 Gene expression analysis

It has been suggested that at least nine enzymes are involved in sucrose metabolism which are fructokinase, hexokinase, invertase, phosphoglucomutase, phosphoglucose isomerase, UDP-glucose Purophosphorylase (UDPGP), sucrose synthase (SUS), sucrose phosphate phosphatase (SPP), and sucrose phosphate synthase (SPS) (Jiang et al., 2015). Of these possibilities, we focused on the mRNA abundance of the last three types of enzymes since they may have major roles in sucrose biosynthesis. Along with sucrose metabolism, transcript abundance of key genes of photosynthesis was also tested.

2.5.1. Sample collection and RNA extraction

Three replicates of wheat spikes and flag leaves from the main tiller at heading, 14-dpa, and 30-dpa were harvested between 11.00 am and 1.00 pm, placed in storage tubes and immediately submerged in liquid N_2. Samples were subsequntly stored at -80°C until total RNA extraction.

Uncontaminated and RNase free mortars and pestles were stored at -80°C, in a sealed polythene bag, at least 12 h prior to the extraction. TPS buffer was prepared using 10 mM EDTA, 1 M KCl, and 100mM TRIS-HCl. After adjusting the pH to 8, the buffer was autoclaved and cooled to room temperature. Mortars and pestles were chilled using liquid N_2 before ~200 mg of the outermost layer of the wheat pericarp and flag leaves was dissected and placed into separate chilled mortars. Plant samples were ground to a fine powder using liquid N_2. Five hundred µL of Trizol® Reagent (Invitrogen by Thermo Fisher Scientific, USA) and 700 µL of TPS buffer were added to the ground plant samples and the grinding was continued. The homogenized solutions were collected in 2.5 mL RNase-free, autoclaved microcentrifuge tubes and incubated at room temperature for 10 min. One hundred and twenty µL of chloroform (per 200 mg of plant tissue) was added to the incubated samples and mixed gently. The samples were incubated for another 3 min before being centrifuged for 15 min at 15 000 rpm at 4°C (Eppendorf centrifuge 5424R, Australia). After phase separation, the supernatant was collected in a new set of RNase-free microcentrifuge tubes and 600 µL of ice-cold isopropanol was added (Biotechnology grade, Sigma-Aldrich, USA). The sample tubes were gently mixed and incubated for 10 min. To separate the precipitated RNA, tubes were centrifuged for 10 min at 15 000 rpm at 4°C. After removing the supernatant, 600 µL of 75% ethyl alcohol (Biotechnology grade, Sigma-Aldrich, USA) was added to each tube. To purify RNA pellets, tubes were centrifuged for 5 min at 15,000 rpm at 4°C. After removing ethyl alcohol, samples were air-dried, 30 µL of diethyl pyrocarbonate (DEPC) treated water (Sigma-Aldrich, USA) was added to each tube to dissolve the RNA and the samples were stored at -80°C until further use.

2.5.2. RNA measurement

RNA was quantified using a Qubit Fluorimeter (Invitrogen by Thermo Fisher Scientific, USA) according to the manufacturer's instructions. To ensure RNA integrity, agarose gel electrophoresis stained with "Gel Red" nucleic acid stain (Fisher Biotech, Australia) was conducted and gels were observed using a gel visualization unit (Fisher Biotech, Australia). Concentrations of the RNA samples were adjusted to 1 µg/µL.

All RNA samples were treated with DNase I, Amplification Grade (Invitrogen by Thermo Fisher Scientific, USA) according to the manufacturer's instructions. RNA samples were reverse-transcribed using SensiFAST^{TM} cDNA synthesis kit (Catalogue No – Bio-65054, Bioline, UK) as per the manufacturer's instructions and the samples of 20 µL were introduced into the thermal cycler with the program set at 25°C for 10 min for primer annealing, 42°C for 15 min for reverse transcription and 85°C for 5 min for inactivation of the process. cDNA was stored at -20°C for future use.

2.5.3. Primer selection and quantitative reverse transcription polymerase chain reaction (qRT-PCR)

Nucleic acid sequences for gene-specific primers of key genes in photosynthesis and sucrose metabolism (Supplementary Table S1) were acquired from published literature (Vicente et al., 2015, Bachir et al., 2017). The specificity of the primers for *Triticum aestivum* L. was tested using the Primer-Blast option in the National Centre for Biotechnology Information (NCBI) website (https://www.ncbi.nlm.nih.gov). Primers were sourced from Integrated DNA Technologies, Inc. (Integrated DNA Technologies Pty. Ltd, the Republic of Singapore).

Reactions were carried out in 96-well plates using QuantStudio 3 real-time PCR system (Applied Biosystems, Thermo Fisher Scientific, USA). cDNA were diluted 10 times by adding DEPC treated water (1:9). Each reaction mixture contained 4 µL of diluted cDNA, 4 µL of DEPC treated water, 10 µL of PowerUp™ SYBR™ Green Master (Applied Biosystems from Thermo Fisher Scientific, USA), 1 µL of 10 mM forward primer and 1 µL of 10 mM reverse primer. Three biological replicates were

used for each growing stage of the three wheat genotypes. The PCR programme was set at 95°C for 10 min followed by 40 cycles of 95°C for 15 s and 60°C for 1 min.

2.6 Statistical analysis

Before statistical analysis, the normality of the data set was tested and the data which were not normally distributed were transformed for normality. To determine the significance of different growth stages, organ types and genotypes, ANOVA was carried out at $P < 0.05$ significant level. Tukey's test and standard errors of differences were used to determine the differences between growth stages, organ types and genotypes. Pearson product-moment correlations were used to test potential correlations between spike dry-weights and parameters of the biological capacity of C assimilation and of gene expression related to sucrose metabolism and the parameters of biological capacity of C assimilation. Data analysis was conducted using SPSS statistical software version 23 (IBM, Armonk, NY, USA). GraphPad Prism scientific software version 5.01 (GraphPad Software, San Diego, CA) was used for graphical representation of the data. Primer efficiencies of the reactions of gene expression analysis were determined using the LinRegPCR software v2012. Relative gene expression of three varieties of two organ types at different growth stages was calculated using the comparative threshold cycle (C_t) $2^{-\Delta\Delta Ct}$ method.

3. Results

3.1 Phenotypic changes of the wheat genotypes

The measured phenotypic traits were categorized into three different groups related respectively to growth, photosynthesis and harvest characteristics (Table 1).

3.1.1 Growth-related traits

There were statistically significant interactions between genotype and growth stage on growth related traits, namely: total spike weight ($P < 0.001$), total above ground biomass (AGB) ($P < 0.001$), total biomass (TB) ($P < 0.001$), plant height ($P < 0.01$) and biomass without spikes (BWS) ($P < 0.001$) (Figure 1). Huandoy had the greatest total spike weights at all four growth stages, while the maximum TB was shown by

Amurskaja 75 (Figure 1). Both TB and TAB steadily increased up to 30-dpa, with little or no difference between 30-dpa and CM. Importantly, from heading to 14-dpa, BWS increased steadily, and from 14-dpa to CM, BWS gradually decreased.

3.1.2 Photosynthesis-related traits

Genotype and the growth stage had statistically significant interactions on photosynthetic area of total spikes (PAS) ($P < 0.01$), spike of main tiller (PASM) ($P < 0.01$), photosynthetic area of leaves (PAL) ($P < 0.01$), total photosynthetic area (PAT) ($P < 0.01$), spike area index (SAI) ($P < 0.001$) and the ratio between total spike area and total leaf area (PAS/PAL) ($P < 0.001$) (Figure 2). However, statistically significant interactions between genotype and growth stage were not observed on photosynthetic area of total flag leaves (PAFL) and flag leaf of main tiller (PAFLM) (Figure 2). The maximum PAS was observed in Huandoy at three growth stages: heading, 14-dpa and 30-dpa (Figure 2a). In contrast, the maximum PAFL was observed in Amurskaja 75 (Figure 2b). Similarly, Amurskaja 75 also displayed the highest PAL and PAT (all spikes and leaves) at three growth stages (Figure 2c and 2d). However, the highest SAI and the PAS/ PAL were shown by Huandoy (Figure 2e and 2f).

3.1.3 Harvest-related traits

Genotype affected tiller number ($P < 0.01$), total harvest (TH) ($P < 0.001$) and HI ($P < 0.001$) (Figure 3a, 3c, and 3d), but did not affect spike number (Figure 3.b). Both TH and HI were greater for Huandoy than other genotypes, while Amurskaja 75 had the greatest number of spikes and tillers at maturity (Figure 3). Overall, there were significant interactions among genotypes, growth stage and organ type for Vc_{max}, J_{max}, and *TPU* (Table 2).

3.2 Changes in gas exchange parameters between genotypes and during ontogeny

Overall, there were significant interactions among genotypes, growth stage and organ type for Vc_{max}, J_{max}, and *TPU* (Table 2). For spikes, there was a statistically significant interaction between genotype and growth stage on: C assimilation capacity; Vc_{max} (P

< 0.001), J_{max} (P < 0.001) and *TPU* (P < 0.001) (Figure 4). Both Huandoy and Amurskaja 75 displayed their highest Vc_{max}, J_{max} and *TPU* for spikes at 14-dpa (Figure 4). Except for between 3-dpa and 30-dpa, Vc_{max} of wheat spikes were significantly different among other growth stages (Table 3). When compared to 30-dpa, Vc_{max}, J_{max} and *TPU* at 14-dpa showed increases of 21.2%, 33.2%, and 22.5% respectively for Huandoy and 12.3%, 15.4% and 7.4% respectively for Amurskaja 75. In contrast, highest Vc_{max}, J_{max} and *TPU* of Greece 25 occurred at heading, with a mean increase of 47.2%, 103.74%, and 51.9% respectively compared to 30-dpa. Of the three genotypes, spikes of Greece 25 displayed the highest Vc_{max}, J_{max} and *TPU* for all the growth stages except for 30-dpa (Figure 4).

For flag leaves, growth stage and genotype displayed statistically significant interaction effects on Vc_{max} (P < 0.05), J_{max} (P < 0.01) and *TPU* (P < 0.05) for flag leaves (Figure 5). However, the effect of genotype for the Vc_{max} was not statistically significant (Figure 5). Results from multiple comparisons revealed that growth stage heading and 3-dpa did not show a statistically significant difference for Vc_{max}, $J_{max,}$ and *TPU* (Table 3). Overall, in the studied genotypes, the highest and the lowest flag leaf Vc_{max}, J_{max} and *TPU* were observed at 14-dpa and 30-dpa respectively (Figure 5). The mean increases of Vc_{max}, $J_{max,}$ and *TPU* at 14-dpa compared to 30-dpa was 72.3%, 215.3%, and 82.8%, respectively for Huandoy, 42 %, 100 %, and 61% respectively, for Amurskaja 75 and 87%, 197%, and 70% respectively, for Greece 25.

Photosynthetic parameters of flag leaves (Vc_{max}, $J_{max,}$ and *TPU*) were significantly higher than in spikes at early reproductive stages (heading to 14-dpa) (Figure 6). Interestingly, during late-grain filling (30-dpa), the parameters of C assimilation capacity of spikes and flag leaves was not statistically different (Table 5).

3.3 Site-specific, genotypic and temporal variation of N concentrations

From heading to 14-dpa, N concentration increased in the pericarps and was unchanged in flag leaves (Figure 7). Overall, N concentrations of flag leaves were appreciably higher than in the pericarps. In pericarps and flag leaves, there was a statistically significant interaction between genotype and growth stage on N concentrations (P < 0.001), with the lowest N concentrations occurring at CM (Figure

7). Greece 25 had the greatest N concentration in both pericarps and flag leaves at all four growth stages (Figure 7).

3.4 Expression of genes associated with photosynthesis

The 3-dpa stage was omitted from gene expression analysis since differences in Vc_{max}, J_{max} and *TPU* between heading and 3-dpa were typically minimal. Genotype, organ type and growth stage had a significant interaction with expression of *rbcS* ($P < 0.001$) (Table 6). However, there were no statistically significant interactions on *rbcL* expression between genotype and organ type, and genotype, organ type and growth stage (Table 6).

In pericarps, the expression pattern of *rbcL* and *rbcS* was similar across genotypes at the three growth stages, with a decreasing trend from heading to 30-dpa. Mean relative expression of *rbcL* at heading was 82.9, 37.2 and 20.3-fold greater than the relative expression of *rbcS* at the same growth stage (heading) in Huandoy, Amurskaja 75 and Greece 25, respectively (Table 7). The maximum expression for both *rbcL* and *rbcS* occurred during heading (Table 7). Relative expression of *rbcL* at heading compared with 30-dpa showed 4.4, 8.0 and 2.3-fold increases for Huandoy, Amurskaja 75 and Greece 25, respectively (Table 7). Also, the relative expression of *rbcS* at heading was 6.8, 30.9 and 6.5-fold higher than at 30-dpa for Huandoy, Amurskaja 75 and Greece 25 respectively (Table 7). At heading, Amurskaja 75 and Greece 25 had the highest and the lowest relative expressions for *rbcL*, respectively (Table 7). In contrast, the maximum and the minimum mean *rbcS* expression were observed in pericarps of Greece 25 and Huandoy respectively.

In flag leaves, as with the pericarps, the maximum and the minimum expression for both *rbcL* and *rbcS* occurred at heading and 30-dpa respectively, for all three wheat genotypes (Table 7). Flag leaves at heading displayed 8.6, 6.8 and 7.0-fold increases in *rbcL* expression compared to the expression at 30-dpa for Huandoy, Amurskaja 75 and Greece 25, respectively. And for *rbcS* expression, 6.8, 5.6 and 20.1-fold increases were observed at heading, compared to 30-dpa in Huandoy, Amurskaja 75, and Greece 25, respectively (Table 7). Similar to pericarps, expression of *rbcL* is significantly higher than the expression of *rbcS* at all growth stages in the three genotypes.

To conclude, at all ontogenies of wheat pericarps and flag leaves, both *rbcL* and *rbcS* expression displayed a similar pattern across genotypes, which was a decreasing trend towards 30-dpa. Of the two genes, the relative expression of *rbcL* was significantly higher than *rbcS* between genotypes at all growth stages.

3.5 Expression variation of key genes related to sucrose metabolism

Genotype, organ type and growth stage had a statistically significant interaction effect on the expression of *SPS1* ($P < 0.001$) (Table 6). Likewise, genotype and organ type and, genotype and growth stage showed statistically significant interactions on *SUS1* and *SPP1* expression (Table 6). However, organ type and growth stage did not show a statistically significant interaction effect on *SPP1* expression (Table 6).

In pericarps, expression of *SPS1* and *SUS1* increased with growth stage for Huandoy, while for Amurskaja 75 and Greece 25 the trend was to decrease (Table 8). Generally, the expression of genes of sucrose metabolism was higher in early to mid-reproductive stages (heading and 14-dpa) than later during late-grain filling (30-dpa).

In flag leaves, there were considerable variations in the expression of *SPS1*, *SUS1* and *SPP1* among the three growth stages. As for pericarps, expression of *SPS1* and *SUS1* in Huandoy increased over time, while in Amurskaja 75 and Greece 25 the trend was for *SPS1* expression to decrease.

When comparing two organ types, both pericarps and flag leaves of Huandoy and Amurskaja 75 showed similar expression patterns in *SPS1*, *SUS1* and *SPP1* (Table 8). Generally, the expression of *SPS1* and *SUS1* was much higher in flag leaves than in pericarps (Table 8). In contrast, the expression of *SPP1* was much higher in pericarps than in flag leaves of Amurskaja 75 and Greece 25.

3.6 Strong positive correlations were observed between spike dry weights and parameters of biological capacity of carbon assimilation of wheat spikes multiplied by total spike area

To obtain a holistic idea about the plant photosynthetic parameters, values of Vc_{max}, J_{max} and *TPU* of spikes at different growth stages were multiplied by the total spike

area at considered growth stages. Strong positive correlations between spike dry weight and [Vc_{max}]* [spike area] (r = 0.800, $P < 0.01$), spike dry weight and [J_{max}]*[spike area] (r = 0.720, $P < 0.01$), and, spike dry weight and [*TPU*]*[spike area] (r = 0.813, $P < 0.01$) were observed.

3.7 Strong positive correlations were observed between parameters of biological capacity of carbon assimilation and the expression of genes of sucrose metabolism at early reproductive stages.

At heading in all three genotypes, strong positive correlations were observed between Vc_{max} and the expression of *SUS1* (r = 0.816, $P < 0.01$), Vc_{max} and the expression of *SPP1* (r = 0.946, $P < 0.01$), J_{max} and the expression of *SUS1* (r= 0.851, $P < 0.01$), J_{max} and the expression of *SPP1* (R= 0.959, $P < 0.01$), *TPU* and the expression of *SUS1* (r = 0.799, $P < 0.01$), and, *TPU* and the expression of *SPP1* (r = 0.932, $P < 0.01$). At 14-dpa, strong positive correlations were observed between Vc_{max} and the expression of *SPS1* (r = 0.786, $P < 0.05$), Vc_{max} and the expression of *SPP1* (r = 0.817, $P < 0.01$), J_{max} and the expression of *SPS1* (r= 0.769, $P < 0.05$), J_{max} and the expression of *SPP1* (r = 0.7909, $P < 0.05$), *TPU* and the expression of *SPS1* (r = 0.807, $P < 0.01$), and, *TPU* and the expression of *SPP1* (r = 0.795, $P < 0.05$). However, at later growth stages (30-dpa) in pericarps, this strong correlations between spike photosynthetic parameters and gene expression of sucrose metabolism could not be observed. Likewise, in flag leaves, positive correlations were not observed between photosynthetic parameters and gene expression of sucrose metabolism.

4. Discussion

4.1 Highest biomass accumulation of wheat spikes occurred between 14-dpa and 30-dpa

The greatest rate of biomass accumulation of spikes was between 14-dpa and 30-dpa for all three genotypes. Moreover, during the same period, BWS decreased while TB increased. This means that most of the photosynthetic products from the grain enlargement phase to CM, accumulates in wheat spikes (wheat endosperm).

Furthermore, the degradation products of senescing plant tissues also translocate to wheat spikes and are stored in the endosperm. It has been identified that both starch and protein deposition in the wheat endosperm is controlled by two separate mechanisms (Jenner et al., 1991). Wheat endosperm starts accumulating dry matter during the grain enlargement phase, that is between 15–20-dpa, until the spike reaches maturity (35–40-dpa) (Jenner et al., 1991). The substrate effect on mitotic activity has been considered as the main determinant of biomass deposition in wheat spikes. The genetic, morphological and environmental factors also play an important role in determining the rate and the duration of biomass accumulation (Jenner et al., 1991). More importantly, the rate and the distribution of starch deposition during grain filling is governed mainly by factors related to wheat spikes and/or the grain itself (Jenner et al., 1991).

In general, our results reveal that the biological capacity of C assimilation (Vc_{max} and J_{max}) was higher at 14-dpa than the other growth stages, supporting the fact that wheat spikes may have a prominent role in starch biosynthesis in the endosperm (Figure 8). A strong correlation between Vc_{max} and the tissue N content was reported by Walker et al. (2014). Consistent with this proposition, in the present study, the highest N concentrations for wheat pericarps were observed at 14-dpa, the phase which displayed the highest Vc_{max}, and J_{max}. Rubisco is the key enzyme of C assimilation and plays a central role in C_3 photosynthesis (Suzuki et al., 2001). Also, Rubisco is a significant proportion of the N content of photosynthetic organs; consequently, it is not unreasonable to assume that peaking of the N content in wheat pericarps during grain enlargement reflects peaking of Rubisco.

The remobilization of N from the vegetative organs of the wheat plant to the endosperm takes place during mid- to late-grain filling phase and is dependent on genotypic and environmental factors (Barbottin et al., 2005). In this study, the low N concentrations in flag leaves at late grain filling (30-dpa) are consistent with remobilization. From the current study, considerable variation in organ specific N concentrations among genotypes was recorded. In general, the highest and the lowest N concentrations in wheat pericarps were observed in Greece 25 and Huandoy respectively. However, the variation in N concentrations in wheat flag leaves was not as significant as in the wheat pericarps (Figure 7) indicating organ specific changes in N metabolism.

Lastly, there is a considerable genotypic variation in growth and harvest related factors including: total spike weight, AGB, TB, BWS, HI and TH, as expected from previous research (Darroch and Baker, 1990a). It has also been reported that the duration of grain filling determines the time to maturity and the yield (Darroch and Baker, 1990b).

4.2 Transcript abundance of *rbcL* and *rbcS* varied between organ types, genotypes and organ ontogeny

The expression of both *rbcL* and *rbcS* varied temporally in all three genotypes, with the heading stage generally showing the highest *rbcS* and *rbcL* expression. Similarly, by confirming the genotypic variation of the mRNA abundance, pericarps of Greece 25 and Amurskaja 75 displayed the highest *rbcS* and *rbcL* expression respectively at heading. Likewise, in flag leaves at heading, Greece 25 displayed the highest mRNA abundance for *rbcS*. These genes of *rbcL* and *rbcS* in a photosynthetic organ code for the enzyme Rubisco.

Rubisco limits light-saturated C assimilation under current atmospheric conditions and is important in both C and N metabolism of plants (Suzuki et al., 2009). In higher plants, Rubisco is made up of eight large subunits and eight small subunits. The small and the large subunits of Rubisco are coded from a multigene family *rbcS* in the nucleus, and a single gene *rbcL* in the chloroplast genome respectively (Dean et al., 1989, Suzuki et al., 2009). In grasses, Rubisco content increases during leaf growth, peaks at full expansion, then declines during senescence (Suzuki et al. (2010). The transcript abundance of the Rubisco-encoding genes, *rbcS* and *rbcL*, determines the amount of Rubisco in a photosynthetic organ (Suzuki et al., 2010). In general, our results revealed that the, transcript abundance of *rbcS* and *rbcL* were highest at heading, and the lowest at 30-dpa respectively both in wheat pericarps and flag leaves. A similar expression pattern was documented in leaves of amaranth (Nikolau and Klessig, 1987), pea (Sasaki et al., 1987), bean (Bate et al., 1991) and rice (Suzuki et al., 2001). Although the abundance of *rbcS* and *rbcL* is lower at 14-dpa than at the heading, the highest N concentrations in the pericarps occurred at 14-dpa. These observations suggest that Rubisco content and *rbcS* and *rbcL* abundance in wheat pericarps may not have a strong positive correlation. The reason for this observation may be that at heading, wheat pericarps start producing Rubisco at an increasing rate

and that, although the *rbcS* and *rbcL* expression declines between heading and 14-dpa, Rubisco production may continue. Alternatively, the degradation of Rubisco between heading and 14-dpa may be minimal, in contrast to that in the flag leaves. The N concentrations of flag leaves across growth stages revealed that the highest Rubisco content may occur during leaf expansion as found by Suzuki et al. (2010). Therefore, our results suggest that there is an organ-specific variation in Rubisco biosynthesis/ degradation, N and C metabolism in wheat.

4.3 Carbon assimilation capacity depends on organ types, genotypes and growth stages

A clear difference in Vc_{max}, J_{max}, and *TPU* between wheat spikes and flag leaves was observed in this study. The highest Vc_{max}, J_{max}, and *TPU* were observed in flag leaves at heading to grain enlargement phase (heading to 14-dpa). The photosynthetic capacity of the flag leaves drastically declined while that of the spikes did not, so by 30-dpa there was no significant difference in Vc_{max}, J_{max} and *TPU* between these organs. This collapse in C assimilation by flag leaves coincided with leaf senescence. In both wheat spikes and flag leaves, strong positive correlation among Vc_{max} and J_{max} was found that accords with the results of Wullschleger (1993) based on analysis of A-Ci curves for 109 species. The amount of Rubisco present in a photosynthetic organ decreases during senescence (Suzuki et al., 2001), and loss of Rubisco from flag leaves at late grain-filling could explain the decreased rate of C assimilation at 30-dpa. This assumption is supported by the observation in our next experiment that N concentration in flag leaves decreased in late grain-filling compared to the heading and grain enlargement phases. Since Rubisco contributes for 15-35% of total N of a C_3 photosynthetic organ (Makino et al., 1992, Suzuki et al., 2009), lesser N concentrations in flag leaves at late grain-filling may be due to the existence of a lesser amount of Rubisco due to degradation. Furthermore, there was a significant difference in N concentrations between wheat pericarps and flag leaves. Nitrogen concentrations of flag leaves were much higher than the wheat pericarps around heading and 14-dpa. Similarly, the highest *rbcL* and *rbcS* mRNA expressions were observed in wheat flag leaves compared to wheat pericarps mainly during heading to 14-dpa. Moreover, the ratio of spike photosynthetic area and leaf photosynthetic area was lower at heading than during late grain-filling. The preceding observations support the argument that

flag leaves are the main driver of C assimilation during heading to grain enlargement phase in wheat and that this role may be taken up by the spikes/ pericarps during late grain-filling.

Strong positive correlations between spike dry weight and the product of biological capacity of C assimilation of wheat spikes and spike area were observed. Although the wheat leaves are the main driver of photosynthesis during heading and grain enlargement, C assimilation and sucrose metabolism of wheat spikes/pericarps is likely play an important role later during grain filling (Figure 8). Therefore, the metabolic processes of wheat spikes/pericarps, such as N metabolism and protein biosynthesis, and their contribution to grain quality under different environmental conditions merit further investigation.

In this study, a marked difference was observed in biological capacity of C assimilation between genotypes in both wheat spikes and flag leaves. Similarly, there was a significant variation between plant growth stages on biological capacity of C assimilation. In general, the highest and the lowest Vc_{max}, J_{max} and *TPU* of wheat spikes were observed during grain enlargement and 30-dpa respectively. Genetic variation in biochemical limitations to C assimilation in plants has been recorded (Wullschleger, 1993, Geber and Dawson, 1997). Genetic diversity is one of the governing factors for adaptive evolution in rates of C fixation (Geber and Dawson, 1997). Other than genetic variation, plant development stage, organ type, plant nutrient supply and environmental conditions also influence the rate of C assimilation (Fan et al., 2011, Walker et al., 2014). Therefore, further research is required to elucidate the molecular mechanisms following the site specific, temporal and genotypic changes behind wheat grain filling for a higher yield.

4.4 Expression of key genes associated with sucrose metabolism varied between organ types, genotypes and growth stages

Marked variation in abundance of the mRNAs, *SPS1*, *SUS1* and *SPP1*, among organ types, indicating that the sucrose metabolism varied in a site-specific manner was observed. Further, the growth stage and genotype also had a significant influence on the expression of the above mRNAs. The correlation analysis between the biological capacity of C assimilation in wheat spikes and mRNA abundance in wheat pericarps

at heading showed a strong positive correlation between Vc_{max} and *SPP1*, Vc_{max} and *SUS1*, J_{max} and *SUS1*, and J_{max} and *SPP1*. Similarly, the biological capacity of C assimilation and *SPS1* and *SPP1* in pericarps had strong positive correlations at 14-dpa. Sucrose is the main product of photosynthesis which plays important roles in growth, signal transduction, acclimation, growth, and development in plants (Jiang et al., 2015). The overall steps of sucrose metabolism in higher plants have been clearly documented (Jiang et al., 2015). However, to date, the site-specific and temporal variation of sucrose metabolism in wheat has not been intensely investigated. Translocation of sucrose from its source to sink regulates the source and sink integration of the plant and then determines the plant growth and the yield (Bihmidine et al., 2013).

A number of studies have suggested a correlation between photosynthesis and sucrose biosynthesis (Stitt, 1986, Battistelli et al., 1991, Seneweera et al., 1995). SPS catalyzes the biosynthesis of sucrose-6-phosphate from fructose-6-phosphate and UDP-glucose (Figure 8). Furthermore, SPS has been identified as the main rate-limiting enzyme of sucrose synthesis (Seneweera et al., 1995, Lunn and MacRae, 2003). Moreover, the enzyme SPP is responsible for the final step of sucrose biosynthesis in plants (Figure 8). SPP catalyzes the irreversible reaction of producing sucrose by hydrolyzing sucrose-6-phosphate (Jiang et al., 2015). In most plants, sucrose is the main transport carbohydrate and it forms the interface between C assimilation and utilization at the source and the sink tissues respectively (Baxter et al., 2003). The amount of sucrose present in a photosynthetic organ depends on the rate of sucrose biosynthesis and the rate of sucrose export from the source (Ho and Thornley, 1978, Baxter et al., 2003). The possibility of regulating the gene expression of a number of metabolic pathways including sucrose metabolism from sucrose and its metabolites have been reported (Koch et al., 1996, Baxter et al., 2003). According to our results, the highest photosynthetically active stage of wheat spikes was the heading and the grain enlargement phase. Interestingly, the highest *SPS1* and *SPP1* mRNA expression were also observed among the same growth stages (heading and 14-dpa) (Table 8). This suggests the fact that the sucrose metabolism of wheat pericarps may be regulated through a sugar sensing mechanism as reported by Koch et al. (1996), Baxter et al. (2003). The higher expression of both *SPS1* and *SPP1* may reveal the increased sucrose synthesis in the wheat pericarp which then leads to higher C assimilation. Our

results showed that the biomass accumulation after heading was mainly taking place in wheat spikes. Thus, the sucrose, generated at wheat pericarps may therefore be exported to the wheat endosperm. This was further confirmed by the highest biomass accumulation of wheat spikes which commenced during the grain enlargement phase in all considered wheat genotypes. Because of the strong interdependence of SPP and SPS, similar potential activities and importance in sucrose biosynthesis, Echeverria et al. (1997) suggested that both SPP and SPS act together as a multienzyme complex in sucrose metabolism.

In a photosynthetic organ, sucrose is degraded by either sucrose invertase or SUS. Degradation of sucrose into UDP-glucose is catalyzed by the enzyme SUS while under invertase, sucrose is converted into both fructose and glucose (Jiang et al., 2015). In general, higher SUS activity could be seen in source tissues. However, increased biomass production and/or sucrose content was reported in switchgrass, tobacco, cotton and poplar due to overexpression of SUS enzyme (Coleman et al., 2006, Coleman et al., 2009, Jiang et al., 2012, Poovaiah et al., 2015). Furthermore, phenotypic changes were exhibited in plants which had disabled SUS enzymes by knockout mutations (Craig et al., 1999, Ruan et al., 2003). Consistent with this proposition, in the current study, pericarps of the tested wheat genotypes exhibited an increased *SUS1* expression around grain enlargement phase; the phase which displayed the highest biological capacity of C assimilation and the increased biomass accumulation. This may also occur because at grain enlargement phase, wheat grains exhibit more sink activities such as starch and amino acid biosynthesis. To facilitate those sink activities, sucrose cleavage has to be increased and this is supported by the higher *SUS1* expression at grain enlargement phase in wheat pericarps. The products of sucrose cleaving in the wheat pericarp is then translocated to the wheat endosperm.

Data from this study as well as in other reported studies suggests that sucrose metabolism in wheat is influenced by the genotype, growth stage and organ type. Moreover, sucrose metabolism in wheat pericarps may have a major role in wheat grain filling and thereby influence the total yield (Figure 8). More research in this area is increasingly important to elucidate the complete mechanism of sucrose metabolism in wheat pericarps to understand its contribution for a higher crop yield.

5. Conclusion

In this study, we characterized the properties of the biological capacity of C assimilation in wheat spikes using gas exchange measurements. Comparison between wheat spikes and flag leaves revealed that Vc_{max} and J_{max} of spikes are generally similar to the wheat flag leaves during late grain filling although flag leaves displayed significantly higher rates from early to mid-grain-filling. With the other supporting data (both phenotypic and molecular), we infer that during leaf senescence, wheat spikes may perform a significant role in C assimilation contributing to the total yield. The mRNA abundance of *rbcS* and *rbcL* with N percentages and biological capacity of C assimilation of wheat pericarps and flag leaves revealed that the wheat pericarps and flag leaves act differently during Rubisco biosynthesis. Finally, expression of key genes of sucrose metabolism with the other supporting data provided by us and others also revealed that the genotypic, site-specific and temporal influence on sucrose metabolism in wheat and the influence of the metabolites of sucrose metabolism for altering the gene expression. Interestingly, mRNAs abundance during sucrose metabolism in wheat pericarps further confirmed the fact that spike sucrose metabolism may have a significant role in grain filling and then for the total yield. These observations point towards the importance of the metabolic activities of wheat spikes/pericarps for grain filling. However, it is a challenging task to present a generalised picture of spike contribution to grain filling because of the complex nature of metabolic processes, their interactions and the genotypic variation observed even within the same species. Thus, more focused research is required to elucidate the site-specific changes in the key metabolic processes such as protein biosynthesis, source and sink balance, photosynthesis, sucrose metabolism and N assimilation along with their interactions to get a holistic understanding of grain filling and thereby explore new avenues to improve crop yield in the future.

Conflict of interest

The authors declare no conflict of interest

Acknowledgement

This study was funded by the University of Southern Queensland, Australia.

List of Figures

Figure 6. Comparison between wheat spikes and flag leaves of (a) Huandoy: Vc_{max}, (b) Huandoy: J_{max} (c) Huandoy *TPU* (d) Amurskaja 75: Vc_{max} (e) Amurskaja 75: J_{max} (f) Amurskaja 75: TPU (g) Greece 25: Vc_{max} (h) Greece 25: J_{max} and (i) Greece 25: *TPU*. Data presented are mean values of three replicates. Brackets with lowercase 'a and b' represents statistically not significant. Abbreviations; Hu; Huandoy, Am; Amurskaja 75, Gr; Greece 25, SP; wheat spikes, FL; wheat flag leaves.

Figure 7. Changes in (a) nitrogen percentages in wheat pericarps, and (b) nitrogen concentrations in wheat flag leaves of three wheat genotypes at four growth stages. Data presented are mean values from three replicates. Abbreviations; Hu; Huandoy, Am; Amurskaja 75, Gr; Greece 25, ***; $P<0.001$.

Figure 8. Schematic diagram of the proposed mechanism of spike contribution for grain filling in wheat. Abbreviations; SUC: sucrose, Fruc: Fructose, F6P: fructose 6 phosphate, UDP-Glc: UDP glucose, Suc6P: sucrose 6 phosphate, *rbcL*: ribulose 1,5 – bisphosphate carboxylase/oxygenase (large sub unit), *rbcS*: ribulose 1,5 – bisphosphate carboxylase/oxygenase (small sub unit), SPP: Sucrose Phosphate Phosphatase, SPS: Sucrose Phosphate Synthase, SUS: Sucrose Synthase type 1, C: carbon, LIR: light independent reaction, LDR: light dependent reaction.

List of Tables and Supplememtary Tables

Table 7. Heatmap of transcript abundance of *rbcL and rbcS*genes related to photosynthesis regulation in wheat pericarps and flag leaves at four growth stages. Data presented are the mean values of gene expression. At relative expressions, shades of red denote relatively higher expression, shades of yellow denote average expression, and shades of green denote relatively low expression. At fold changes, dark blue indicates greater fold changes, and light blue indicates moderate fold changes.

Table 8. Heatmap of transcript abundance of *SPS1, SUS1 and SPP1* genes related to carbon metabolism in wheat pericarps and flag leaves at four growth stages. Data presented are the mean values of gene expression. At relative expressions, shades of red denote relatively higher expression, shades of yellow denote average expression, and shades of green denote relatively low expression. At fold changes, dark blue indicates greater fold changes, and light blue indicates moderate fold changes.

Supplementary Table S1. List of primer sequences of genes selected for qRT-PCR

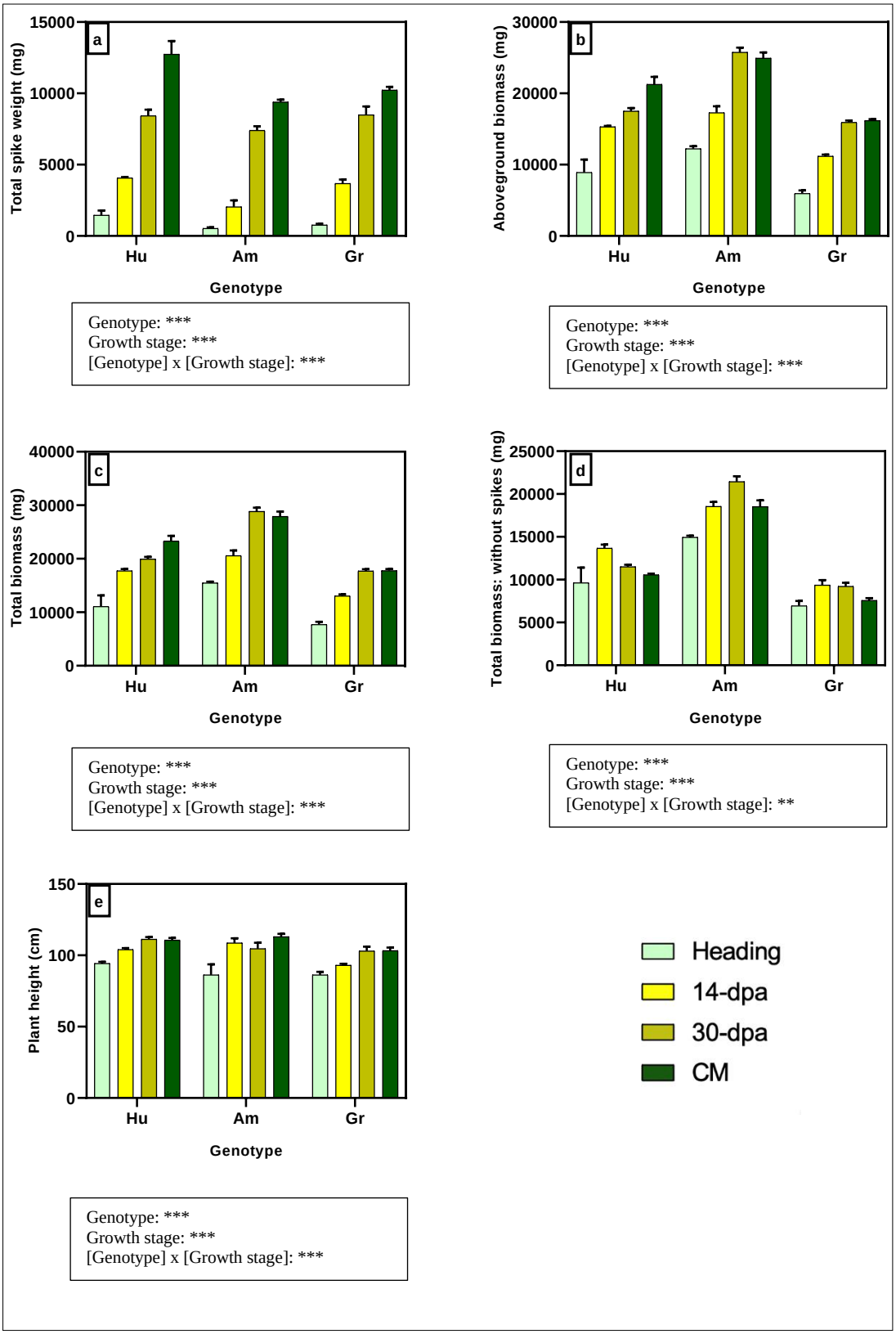
a
Total spike weight (mg)
15000
10000
5000
0
Hu
Am
Gr
Genotype
Genotype: ***
Growth stage: ***
[Genotype] x [Growth stage]: ***
b
Aboveground biomass (mg)
30000
20000
10000
0
Hu
Am
Gr
Genotype
Genotype: ***
Growth stage: ***
[Genotype] x [Growth stage]: ***
c
Total biomass (mg)
40000
30000
20000
10000
0
Hu
Am
Gr
Genotype
Genotype: ***
Growth stage: ***
[Genotype] x [Growth stage]: ***
d
Total biomass: without spikes (mg)
25000
20000
15000
10000
5000
0
Hu
Am
Gr
Genotype
Genotype: ***
Growth stage: ***
[Genotype] x [Growth stage]: **
e
Plant height (cm)
150
100
50
0
Hu
Am
Gr
Genotype
Genotype: ***
Growth stage: ***
[Genotype] x [Growth stage]: ***
Heading
14-dpa
30-dpa
CM

Figure 1

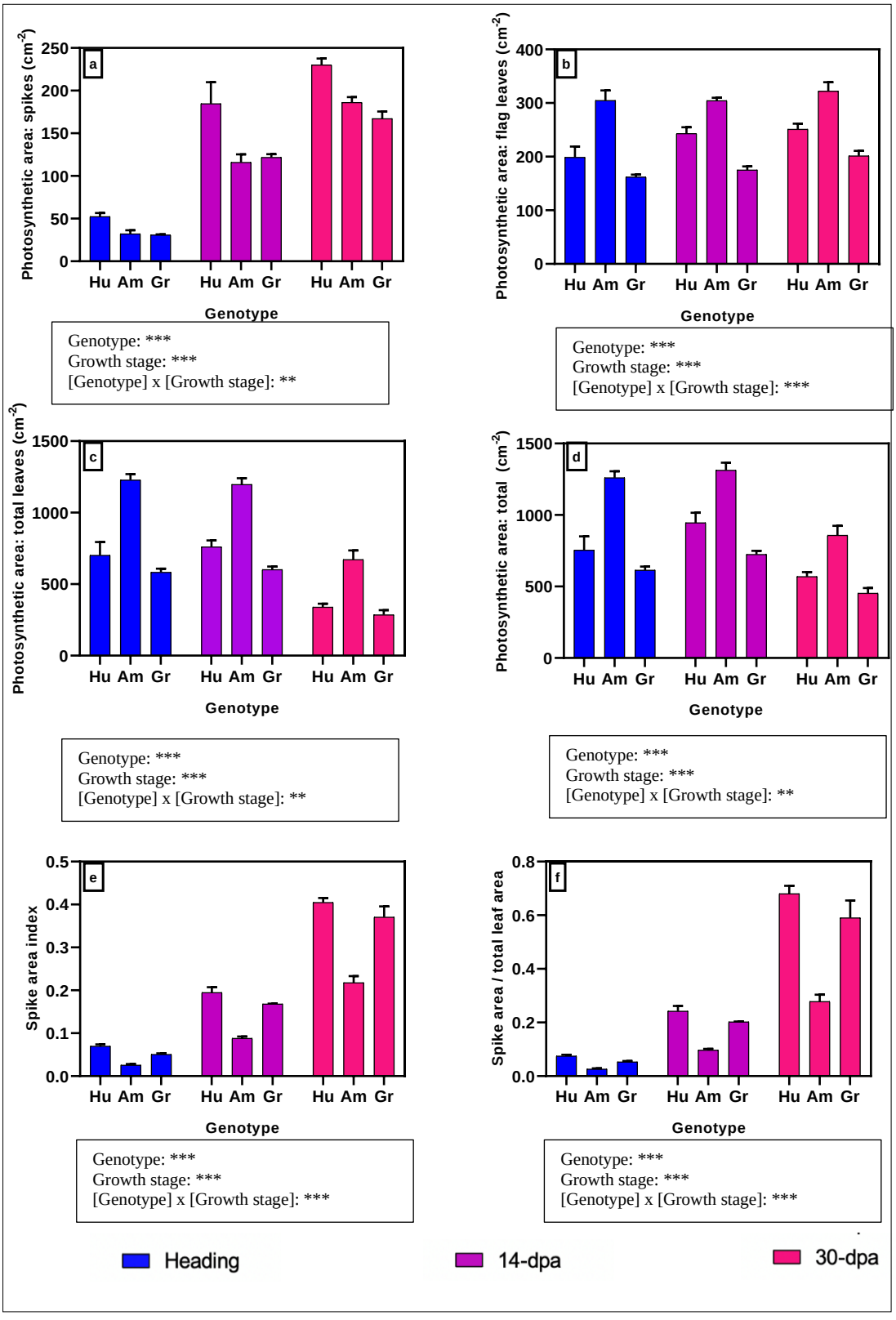
a
Photosynthetic area: spikes (cm-2)
250
200
150
100
50
0
Hu Am Gr Hu Am Gr Hu Am Gr
Genotype
Genotype: ***
Growth stage: ***
[Genotype] x [Growth stage]: **
b
Photosynthetic area: flag leaves (cm-2)
400
300
200
100
0
Hu Am Gr Hu Am Gr Hu Am Gr
Genotype
Genotype: ***
Growth stage: ***
[Genotype] x [Growth stage]: ***
c
Photosynthetic area: total leaves (cm-2)
1500
1000
500
0
Hu Am Gr Hu Am Gr Hu Am Gr
Genotype
Genotype: ***
Growth stage: ***
[Genotype] x [Growth stage]: **
d
Photosynthetic area: total (cm-2)
1500
1000
500
0
Hu Am Gr Hu Am Gr Hu Am Gr
Genotype
Genotype: ***
Growth stage: ***
[Genotype] x [Growth stage]: **
e
Spike area index
0.5
0.4
0.3
0.2
0.1
0.0
Hu Am Gr Hu Am Gr Hu Am Gr
Genotype
Genotype: ***
Growth stage: ***
[Genotype] x [Growth stage]: ***
f
Spike area / total leaf area
0.8
0.6
0.4
0.2
0.0
Hu Am Gr Hu Am Gr Hu Am Gr
Genotype
Genotype: ***
Growth stage: ***
[Genotype] x [Growth stage]: ***
Heading
14-dpa
30-dpa

Figure 2

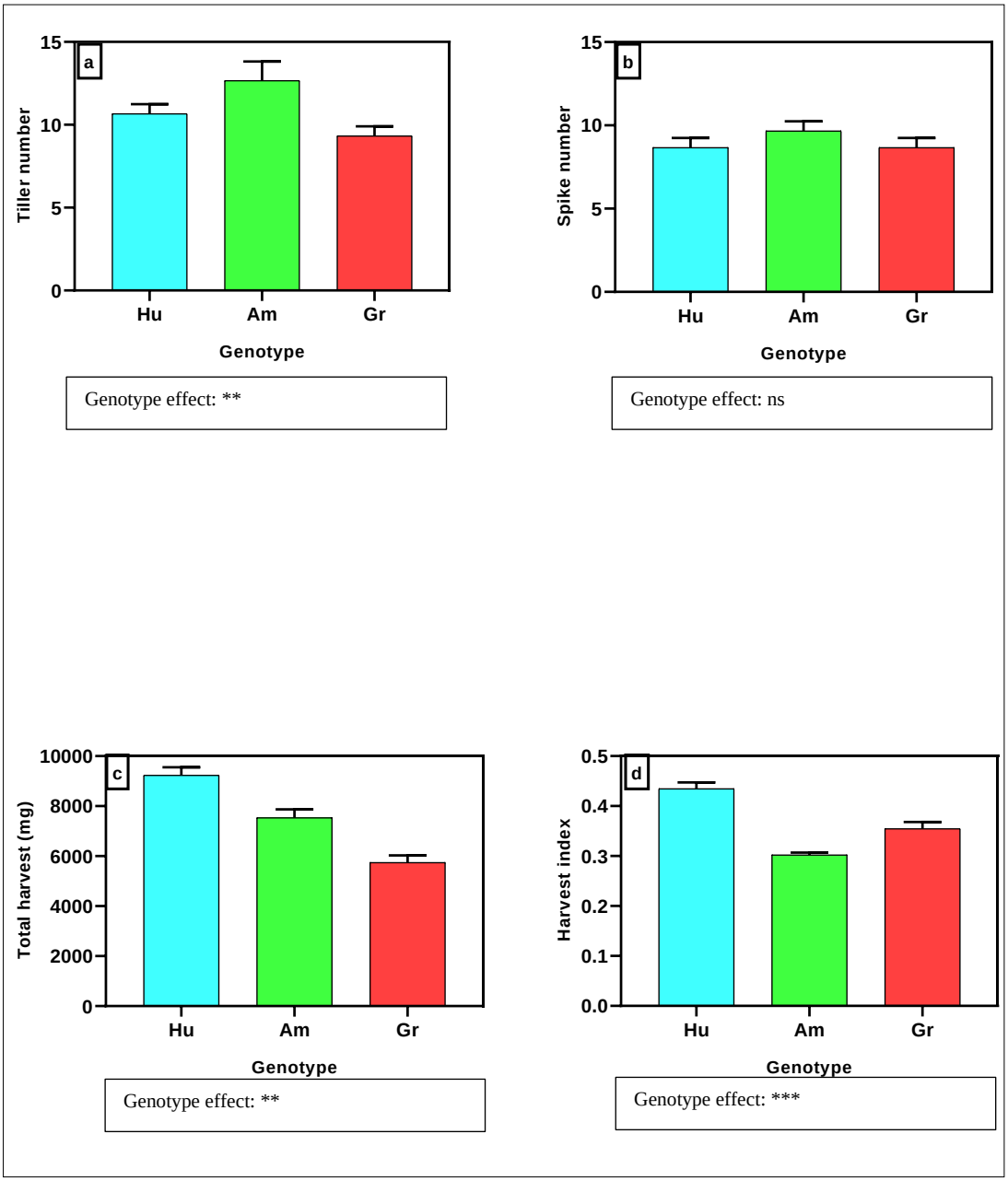
a
Tiller number
15
10
5
0
Hu
Am
Gr
Genotype
Genotype effect: **
b
Spike number
15
10
5
0
Hu
Am
Gr
Genotype
Genotype effect: ns
c
Total harvest (mg)
10000
8000
6000
4000
2000
0
Hu
Am
Gr
Genotype
Genotype effect: **
d
Harvest index
0.5
0.4
0.3
0.2
0.1
0.0
Hu
Am
Gr
Genotype
Genotype effect: ***

Figure 3

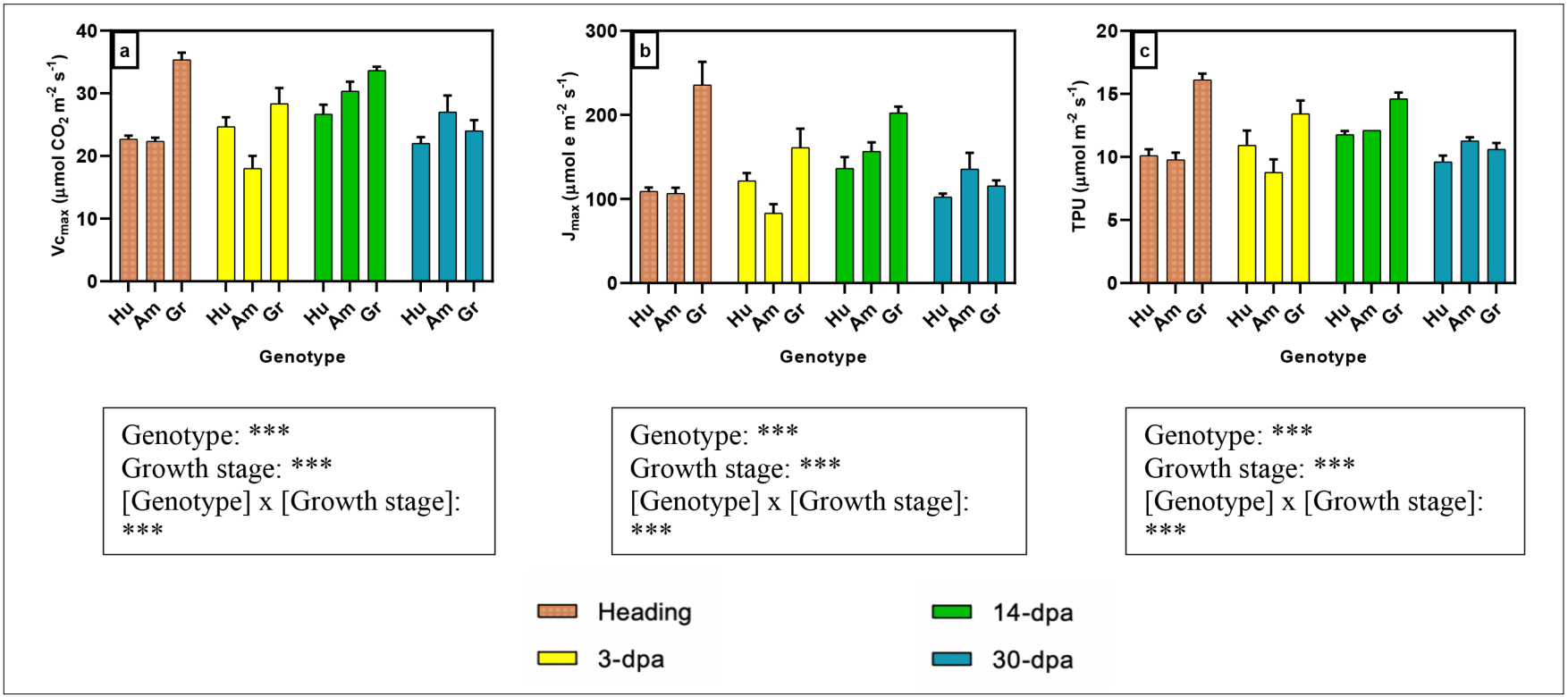
a
b
c
Vcmax (µmol CO2 m-2 s-1)
Jmax (µmol e m-2 s-1)
TPU (µmol m-2 s-1)
Hu
Am
Gr
Genotype
Genotype: ***
Growth stage: ***
[Genotype] x [Growth stage]: ***
Heading
3-dpa
14-dpa
30-dpa

Figure 4

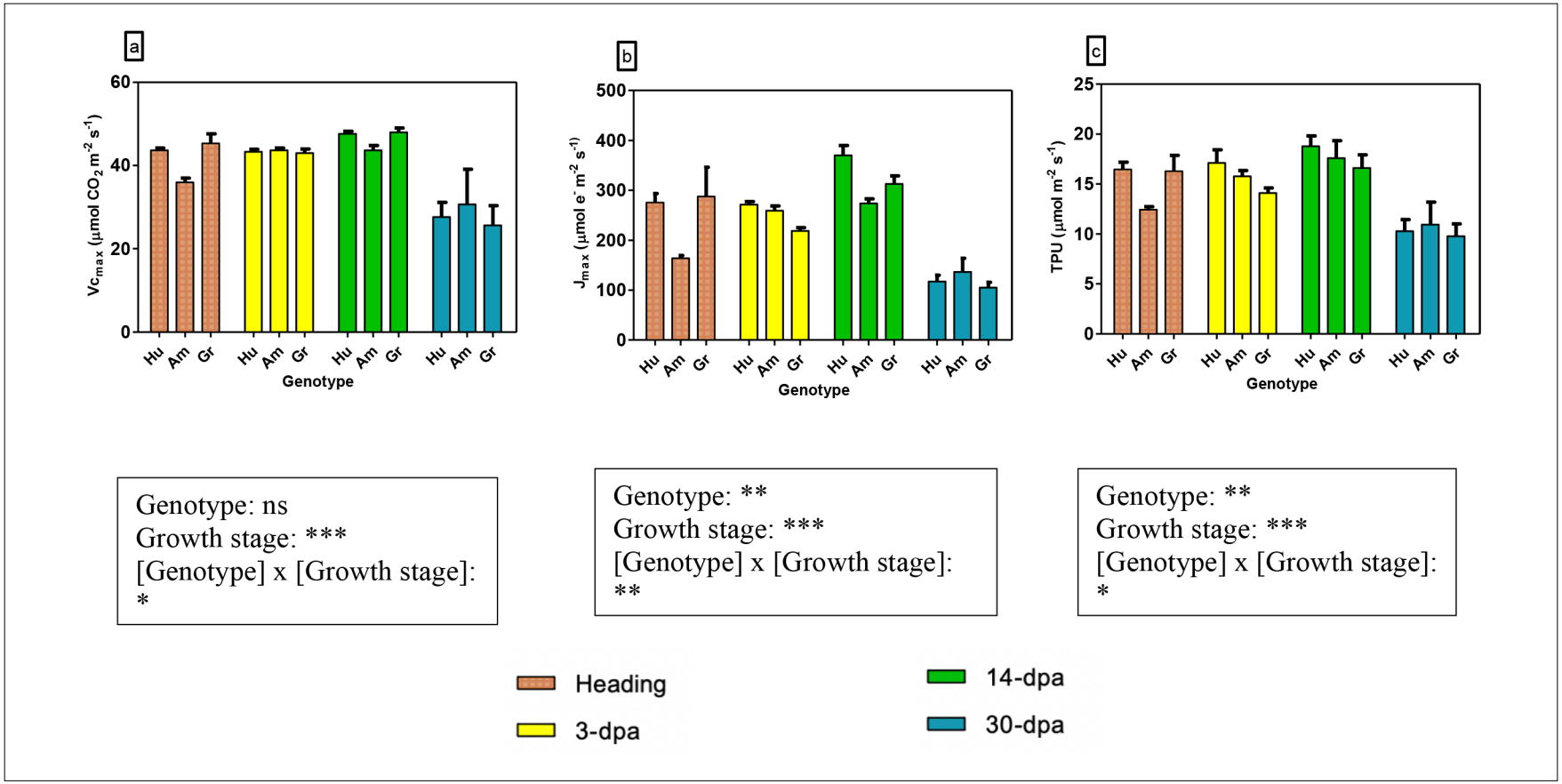
a
b
c
Vcmax (µmol CO2 m-2 s-1)
Jmax (µmol e- m-2 s-1)
TPU (µmol m-2 s-1)
Hu Am Gr Hu Am Gr Hu Am Gr Hu Am Gr
Genotype
Genotype: ns
Growth stage: ***
[Genotype] x [Growth stage]: *
Genotype: **
Growth stage: ***
[Genotype] x [Growth stage]: **
Genotype: **
Growth stage: ***
[Genotype] x [Growth stage]: *
Heading
3-dpa
14-dpa
30-dpa

Figure 5

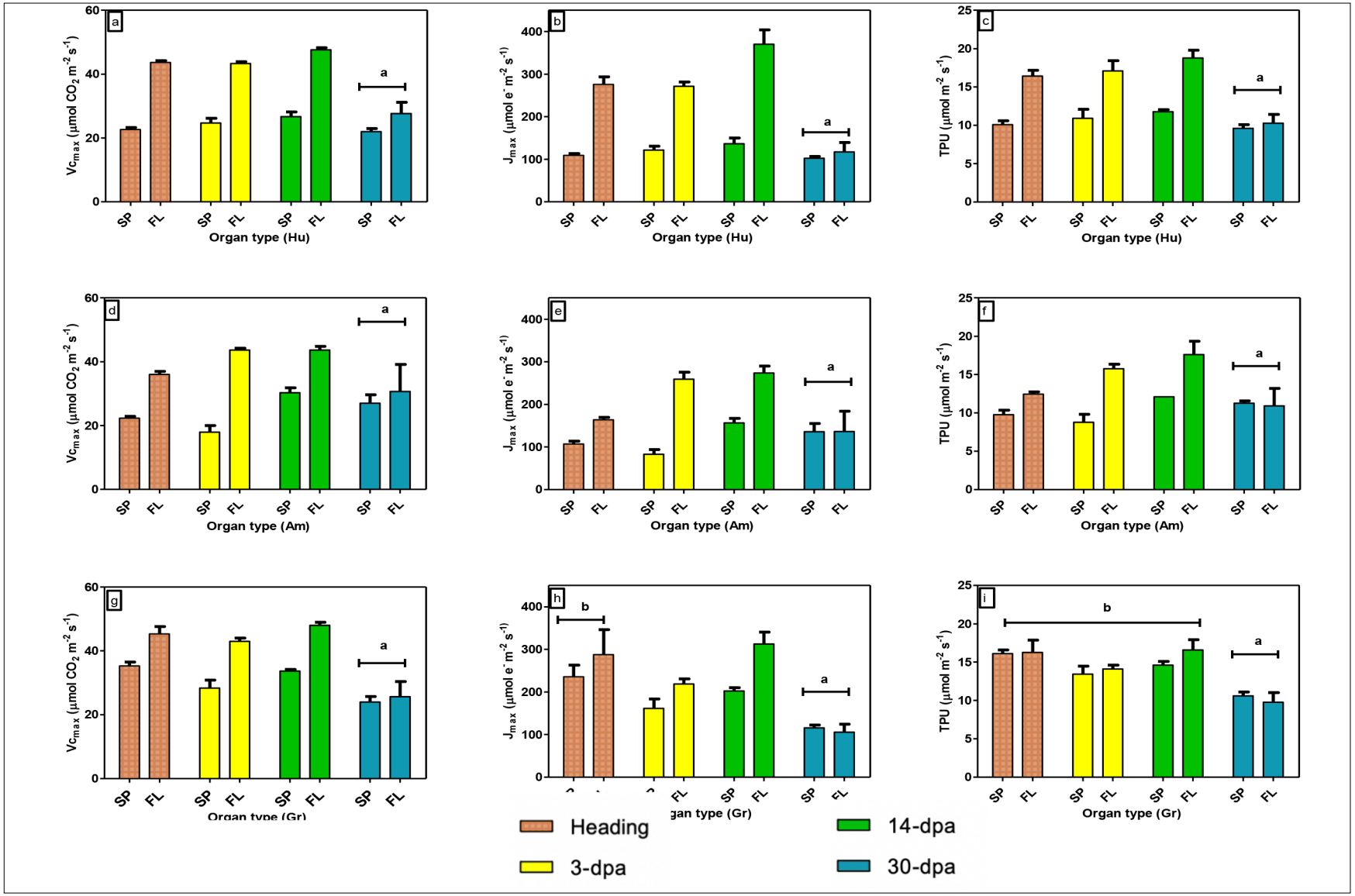
a
b
c
d
e
f
g
h
i
Vcmax (μmol CO2 m-2 s-1)
Jmax (μmol e- m-2 s-1)
TPU (μmol m-2 s-1)
SP
FL
Organ type (Hu)
Organ type (Am)
Organ type (Gr)
Heading
3-dpa
14-dpa
30-dpa

Figure 6

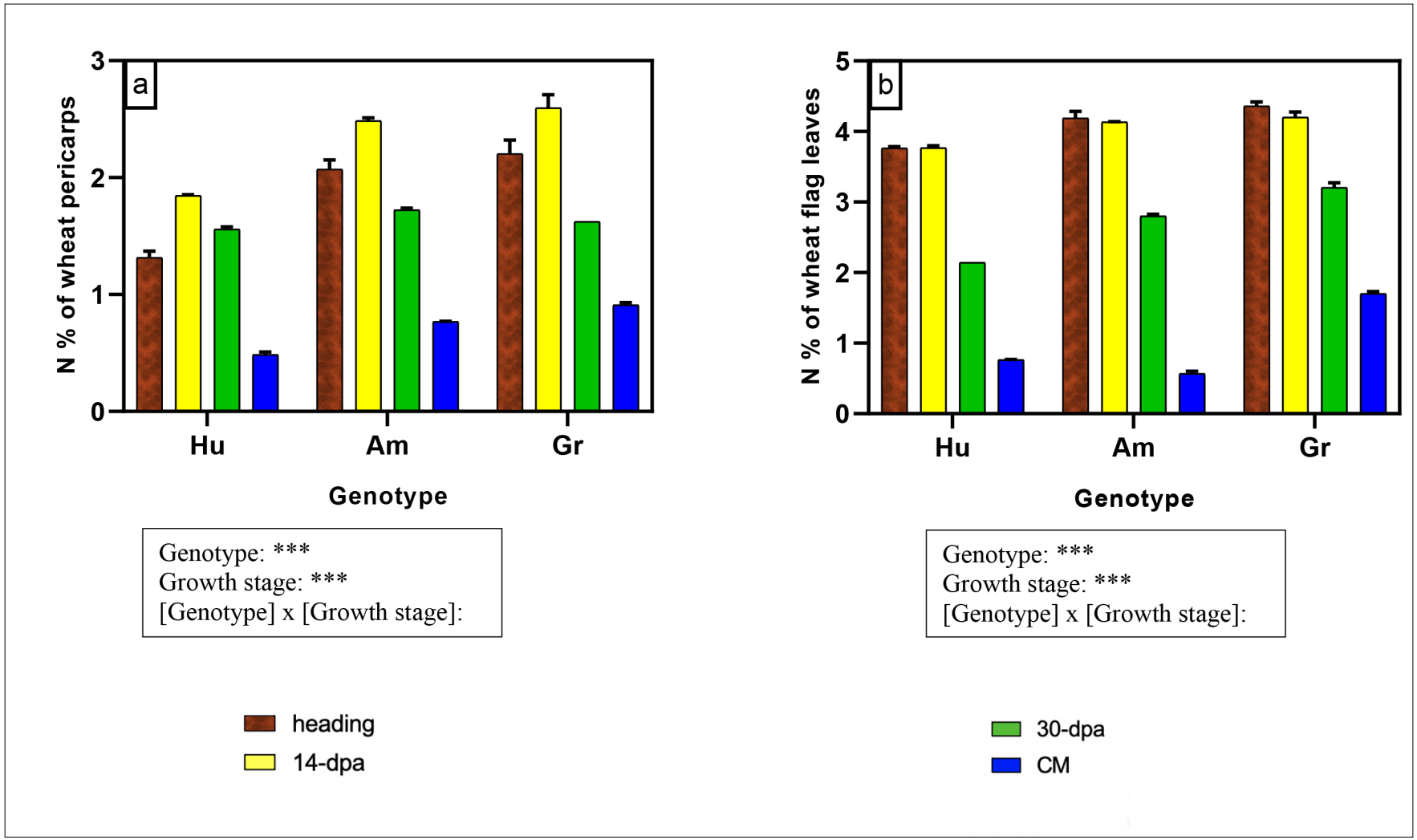
a
N % of wheat pericarps
3
2
1
0
Hu
Am
Gr
Genotype
Genotype: ***
Growth stage: ***
[Genotype] x [Growth stage]:
heading
14-dpa
b
N % of wheat flag leaves
5
4
3
2
1
0
Hu
Am
Gr
Genotype
Genotype: ***
Growth stage: ***
[Genotype] x [Growth stage]:
30-dpa
CM

Figure 7

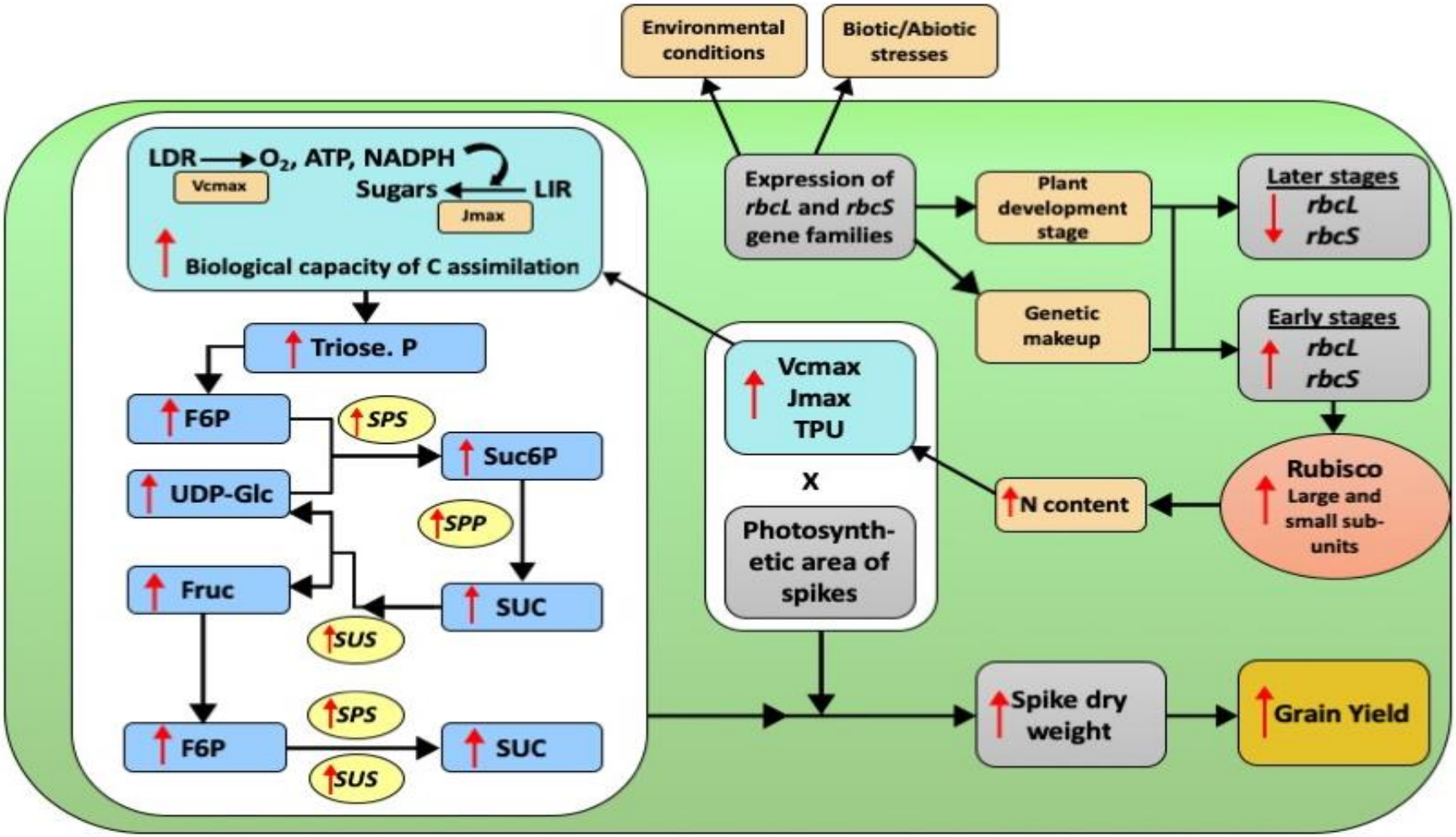
Environmental conditions
Biotic/Abiotic stresses
LDR → O_2, ATP, NADPH
Vcmax
Sugars
LIR
Jmax
Biological capacity of C assimilation
Triose. P
F6P
SPS
Suc6P
UDP-Glc
SPP
Fruc
SUC
SUS
F6P
SPS
SUS
SUC
Expression of rbcL and rbcS gene families
Plant development stage
Genetic makeup
Later stages
rbcL
rbcS
Early stages
rbcL
rbcS
Vcmax
Jmax
TPU
X
Photosynth-etic area of spikes
N content
Rubisco
Large and small sub-units
Spike dry weight
Grain Yield

Figure 8

Table 1.

Category	Trait	Growth stage/s of data collection
Growth-related traits	Total spike weight Total above ground biomass (AGB) Total biomass (TB) Plant height Total biomass without spikes (BWS)	Heading, 14-dpa, 30-dpa and Complete maturity (CM)
Photosynthesis-related traits	Photosynthesis area: total spikes (PAS) Photosynthesis area: spike, main tiller (PASM) Photosynthesis area: total flag leaves (PAFL) Photosynthesis area: flag leaf, main tiller (PAFLM) Photosynthesis area: total leaves (PAL) Photosynthesis area: total (PAT) Spike area index (SAI) Ratio between total spike area and total leaf area (PAS/ PAL)	Heading, 14-dpa and 30-dpa
Harvest-related traits	Harvest index (HI) Total harvest (TH) Spike number Tiller number	CM

Table 2.

Traits	Individual effect			Interaction effect			
	Genotype effect	Organ type effect	Growth stage effect	Genotype X Organ type	Genotype X Growth stage	Organ type X Growth stage	Genotype X Organ type X Growth stage
Vc_{max} ($\mu mol\ CO_2 m^{-2} s^{-1}$)	***	***	***	***	***	***	**
J_{max} ($\mu molem^{-2} s^{-1}$)	***	***	***	***	***	***	***
TPU ($\mu mol\ m^{-2} s^{-1}$)	***	***	***	***	***	***	**

Table 3.

Growth stage comparison		Spikes			Flag leaves		
		Traits					
stage a	stage b	Vc_{max}	J_{max}	*TPU*	Vc_{max}	J_{max}	*TPU*
Heading	3-dpa	**	**	ns	ns	ns	ns
Heading	14-dpa	**	*	*	***	***	**
Heading	30-dpa	*	**	**	***	***	***
3-dpa	14-dpa	***	***	***	**	***	**
3-dpa	30-dpa	ns	ns	ns	***	***	***
14-dpa	30-dpa	***	***	***	***	***	***

Table 4.

Genotype comparison		Spikes			Flag leaves		
		Traits					
Genotype a	Genotype b	Vc_{max}	J_{max}	*TPU*	Vc_{max}	J_{max}	*TPU*
Huandoy	Amurskaja 75	ns	ns	ns	ns	*	*
Huandoy	Greece 25	***	***	***	ns	ns	*
Amurskaja 75	Greece 25	***	***	***	ns	ns	ns

Table 5.

		Huandoy			Amurskaja 75			Greece 25		
		Mean values			Mean values			Mean values		
Growth stage	Trait	Spike	Flag leaf	Significance	Spike	Flag leaf	Significance	Spike	Flag leaf	Significance
heading	Vc_{max}	22.67	43.67	***	22.30	36.00	***	35.33	45.33	**
	J_{max}	109.00	275.67	***	106.67	164.00	***	235.67	287.33	ns
	TPU	10.10	16.43	***	9.77	15.77	**	16.10	16.27	ns
3-dpa	Vc_{max}	24.67	43.33	***	18.00	43.67	***	28.33	43.00	**
	J_{max}	121.67	271.33	***	83.00	259.00	***	161.00	218.67	*
	TPU	10.93	17.10	**	8.77	15.77	**	13.43	14.10	ns
14-dpa	Vc_{max}	26.67	47.67	***	30.33	43.67	**	33.67	48.00	**
	J_{max}	136.33	370.00	***	156.67	273.67	**	202.33	312.67	**
	TPU	11.77	18.77	***	12.10	17.60	**	14.60	16.60	ns
30-dpa	Vc_{max}	22.00	27.67	ns	27.00	30.67	ns	24.00	25.67	ns
	J_{max}	102.33	117.33	ns	135.67	136.33	ns	115.67	105.33	ns
	TPU	9.60	10.27	ns	11.27	10.93	ns	10.60	9.77	ns

Table 6.

Metabolism	Gene	Individual effect			Interaction effect			
		Genotype effect	Organ type effect	Growth stage effect	Genotype X Organ type	Genotype X Growth stage	Organ type X Growth stage	Genotype X Organ type X Growth stage
Photosynthesis	*rbcL*	*	***	***	ns	**	***	ns
	rbcS	*	***	***	**	***	***	***
Carbon	*SPS1*	*	***	**	***	***	***	***
	SUS1	***	***	*	**	**	***	ns
	SPP1	***	***	**	***	***	ns	ns

Table 7.

Gene	Expression and fold change	Stage	Relative Expression: Pericarps			Relative Expression: Flag Leaves			Fold change between organ types		
			Huandoy	**Amurskaja**	**Greece**	**Huandoy**	**Amurskaja**	**Greece**	**Huandoy**	**Amurskaja**	**Greece**
rbcS	Mean expression	heading	**5.00**	**13.94**	**14.97**	**31.06**	**26.53**	**45.87**	**6.21**	**1.90**	**3.06**
		14-dpa	**1.42**	**1.50**	**1.81**	**14.49**	**5.63**	**3.41**	**10.22**	**3.75**	**1.88**
		30-dpa	**0.74**	**0.45**	**2.29**	**4.56**	**4.77**	**2.28**	**6.16**	**10.57**	**1.00**
	Fold change between growth stages	heading and 14-dpa	**3.53**	**9.29**	**8.27**	**2.14**	**4.72**	**13.45**			
		heading and 30-dpa	**6.76**	**30.90**	**6.54**	**6.81**	**5.56**	**20.13**			
		14-dpa and 30-dpa	**1.92**	**3.33**	**0.79**	**3.18**	**1.18**	**1.50**			
rbcL	Mean expression	heading	**414.81**	**519.31**	**303.81**	**1076.24**	**1009.80**	**873.87**	**2.59**	**1.94**	**2.88**
		14-dpa	**200.51**	**113.51**	**129.63**	**314.09**	**257.41**	**231.81**	**1.57**	**2.27**	**1.79**
		30-dpa	**94.47**	**64.63**	**130.06**	**124.54**	**147.86**	**125.65**	**1.32**	**2.29**	**0.97**
	Fold change between growth stages	heading and 14-dpa	**2.07**	**4.58**	**2.34**	**3.43**	**3.92**	**3.77**			
		heading and 30-dpa	**4.39**	**8.04**	**2.34**	**8.64**	**6.83**	**6.95**			
		14-dpa and 30-dpa	**2.12**	**1.76**	**1.00**	**2.52**	**1.74**	**1.84**			

Table 8.

Gene	Expression and fold change	Stage	Relative Expression: Pericarps			Relative Expression: Flag Leaves			Fold change between organ types		
			Huandoy	Amurskaja	Greece	Huandoy	Amurskaja	Greece	Huandoy	Amurskaja	Greece
SPS1	Mean expression	heading	**0.64**	**1.31**	**1.23**	**3.68**	**6.13**	**5.51**	**5.80**	**4.67**	**4.49**
		14-dpa	**1.09**	**1.63**	**2.78**	**2.89**	**3.47**	**1.49**	**2.67**	**2.13**	**0.53**
		30-dpa	**1.42**	**0.47**	**1.41**	**8.90**	**3.06**	**1.92**	**6.28**	**6.47**	**1.36**
	Fold change between growth stages	heading and 14-dpa	**0.59**	**0.81**	**0.44**	**1.27**	**1.77**	**3.71**			
		heading and 30-dpa	**0.45**	**2.77**	**0.87**	**0.41**	**2.00**	**2.88**			
		14-dpa and 30-dpa	**0.77**	**3.44**	**1.98**	**0.33**	**1.13**	**0.78**			
SUS1	mean expression	heading	**1.27**	**2.65**	**4.23**	**4.47**	**3.31**	**4.81**	**3.51**	**1.25**	**1.14**
		14-dpa	**3.99**	**3.14**	**3.27**	**5.20**	**2.14**	**1.22**	**1.31**	**0.68**	**0.37**
		30-dpa	**2.93**	**1.57**	**2.02**	**8.36**	**4.96**	**5.13**	**2.85**	**3.16**	**2.53**
	fold change between growth stages	heading and 14-dpa	**0.32**	**0.84**	**1.29**	**0.86**	**1.55**	**3.95**			
		heading and 30-dpa	**0.43**	**1.69**	**2.09**	**0.53**	**0.67**	**0.94**			
		14-dpa and 30-dpa	**1.36**	**2.00**	**1.62**	**0.62**	**0.43**	**0.24**			
SPP1	mean expression	heading	**0.79**	**1.49**	**4.05**	**0.97**	**1.25**	**2.39**	**1.24**	**0.84**	**0.59**
		14-dpa	**0.66**	**1.70**	**2.78**	**1.50**	**0.80**	**0.80**	**2.28**	**0.47**	**0.29**
		30-dpa	**0.72**	**1.38**	**2.70**	**1.03**	**1.17**	**1.53**	**1.42**	**0.85**	**0.57**
	fold change between growth stages	heading and 14-dpa	**1.19**	**0.88**	**1.46**	**0.65**	**1.57**	**2.99**			
		heading and 30-dpa	**1.08**	**1.08**	**1.50**	**0.94**	**1.07**	**1.56**			
		14-dpa and 30-dpa	**0.91**	**1.23**	**1.03**	**1.46**	**0.68**	**0.52**			

Supplementary Table S1. List of primer sequences of genes selected for qRT-PCR

Primer abbreviation	Sequence (5'------3')	Metabolism	Reference
rbcL	F: GGCTGCAGTAGCTGCCGAATCT R: TCCCCAGCAACAGGCTCGATGT	Rubisco biosynthesis and sucrose metabolism	Vicente et al, 2015
rbcS	F: AGCCTCAGCAGCGTCAGCAAT R: CGTGGATAGGGGTGGCAGGTAAGA		
SPP1	F: GCGCACGGGAAGGAGTTTTTCTTCT R: GACCTCCGTAGACATCATCCAGCCC		
SPS1	F: AGAAGGCTCTGCCTCCCATTTGGTC R: AGGATCATCGGCTTGTGCGGGTT		
SUS1	F: GTATGTTCACCAGGGCAAGGGCA R: GGCGTCAAACTCAGCAAGCAGC		
ADP riosylation factor	F: GCTCTCCAACAACATTGCCAAC R: GCTTCTGCCTGTCACATACGC	Housekeeping genes	Vicente et al, 2015
TaActin-F	F: TTGCTGACCGTATGAGCAAG R: ACCCTCCAATCCAGACACTG		Bachir et al. 2017
TaSand-F	F: TGCCTTGCCCATAAGAAATC R: GTGCGGACCAGTTGCTTTAT		

References

Bachir, D. G., Saeed, I., Song, Q., Linn, T. Z., Chen, L. & Hu, Y.-G. 2017. Characterization and expression patterns of key C4 photosynthetic pathway genes in bread wheat (Triticum aestivum L.) under field conditions. *Journal of plant physiology*, 213**,** 87-97.

Barbottin, A., Lecomte, C., Bouchard, C. & Jeuffroy, M.-H. 2005. Nitrogen remobilization during grain filling in wheat. *Crop science,* 45**,** 1141-1150.

Bate, N. J., Rothstein, S. J. & Thompson, J. E. 1991. Expression of nuclear and chloroplast photosynthesis-specific genes during leaf senescence. *Journal of experimental botany,* 42**,** 801-811.

Battistelli, A., Adcock, M. D. & Leegood, R. C. 1991. The relationship between the activation state of sucrose-phosphate synthase and the rate of CO 2 assimilation in spinach leaves. *Planta,* 183**,** 620-622.

Baxter, C. J., Foyer, C. H., Turner, J., Rolfe, S. A. & Quick, W. P. 2003. Elevated sucrose-phosphate synthase activity in transgenic tobacco sustains photosynthesis in older leaves and alters development. *Journal of Experimental Botany,* 54**,** 1813-1820.

Bihmidine, S., Hunter Iii, C. T., Johns, C. E., Koch, K. E. & Braun, D. M. 2013. Regulation of assimilate import into sink organs: update on molecular drivers of sink strength. *Frontiers in plant science,* 4**,** 177.

Coleman, H. D., Ellis, D. D., Gilbert, M. & Mansfield, S. D. 2006. Up-regulation of sucrose synthase and UDP-glucose pyrophosphorylase impacts plant growth and metabolism. *Plant Biotechnology Journal,* 4**,** 87-101.

Coleman, H. D., Yan, J. & Mansfield, S. D. 2009. Sucrose synthase affects carbon partitioning to increase cellulose production and altered cell wall ultrastructure. *Proceedings of the National Academy of Sciences,* 106**,** 13118-13123.

Craig, J., Barratt, P., Tatge, H., Déjardin, A., Handley, L., Gardner, C. D., Barber, L., Wang, T., Hedley, C. & Martin, C. 1999. Mutations at the rug4 locus alter the carbon and nitrogen metabolism of pea plants through an effect on sucrose synthase. *The Plant Journal,* 17**,** 353-362.

Darroch, B. & Baker, R. 1990a. Grain filling in three spring wheat genotypes: statistical analysis. *Crop Science,* 30**,** 525-529.

Darroch, B. & Baker, R. J. C. S. 1990b. Grain filling in three spring wheat genotypes: statistical analysis. 30**,** 525-529.

Dean, C., Pichersky, E. & Dunsmuir, P. 1989. Structure, evolution, and regulation of RbcS genes in higher plants. *Annual review of plant biology,* 40**,** 415-439.

Dehigaspitiya, P., Milham, P., Ash, G. J., Arun-Chinnappa, K., Gamage, D., Martin, A., Nagasaka, S. & Seneweera, S. J. P. 2019. Exploring natural variation of photosynthesis in a site-specific manner: evolution, progress, and prospects. 1-18.

Demirevska, K., Zasheva, D., Dimitrov, R., Simova-Stoilova, L., Stamenova, M. & Feller, U. 2009. Drought stress effects on Rubisco in wheat: changes in the Rubisco large subunit. *Acta Physiologiae Plantarum,* 31**,** 1129.

Dillard, H. R. 2019. Global food and nutrition security: from challenges to solutions. *Food Security***,** 1-4.

Echeverria, E., Salvucci, M. E., Gonzalez, P., Paris, G. & Salerno, G. 1997. Physical and kinetic evidence for an association between sucrose-phosphate synthase and sucrose-phosphate phosphatase. *Plant physiology,* 115**,** 223-227.

Evans, J. R. & Santiago, L. S. 2014. PrometheusWiki Gold Leaf Protocol: gas exchange using LI-COR 6400. *Functional Plant Biology,* 41**,** 223-226.

Evans, L. & Rawson, H. M. 1970. Photosynthesis and respiration by the flag leaf and components of the ear during grain development in wheat. *Australian Journal of Biological Sciences,* 23**,** 245-254.

Fan, Y., Zhong, Z. & Zhang, X. 2011. Determination of photosynthetic parameters Vcmax and Jmax for a C3 plant (spring hulless barley) at two altitudes on the Tibetan Plateau. *Agricultural and Forest Meteorology,* 151**,** 1481-1487.

Farquhar, G. V., Von Caemmerer, S. V. & Berry, J. 1980. A biochemical model of photosynthetic CO2 assimilation in leaves of C3 species. *Planta,* 149**,** 78-90.

Furbank, R. T., Quick, W. P. & Sirault, X. R. 2015. Improving photosynthesis and yield potential in cereal crops by targeted genetic manipulation: prospects, progress and challenges. *Field Crops Research,* 182**,** 19-29.

Geber, M. A. & Dawson, T. E. 1997. Genetic variation in stomatal and biochemical limitations to photosynthesis in the annual plant, Polygonum arenastrum. *Oecologia,* 109**,** 535-546.

Ho, L. & Thornley, J. 1978. Energy requirements for assimilate translocation from mature tomato leaves. *Annals of Botany,* 42**,** 481-483.

Jansson, C., Vogel, J., Hazen, S., Brutnell, T. & Mockler, T. 2018. Climate-smart crops with enhanced photosynthesis. *Journal of Experimental Botany***,** ery213.

Jenner, C., Ugalde, T. & Aspinall, D. 1991. The physiology of starch and protein deposition in the endosperm of wheat. *Functional Plant Biology,* 18**,** 211-226.

Jiang, S.-Y., Chi, Y.-H., Wang, J.-Z., Zhou, J.-X., Cheng, Y.-S., Zhang, B.-L., Ma, A., Vanitha, J. & Ramachandran, S. 2015. Sucrose metabolism gene families and their biological functions. *Scientific reports,* 5**,** 17583.

Jiang, Y., Guo, W., Zhu, H., Ruan, Y. L. & Zhang, T. 2012. Overexpression of GhSusA1 increases plant biomass and improves cotton fiber yield and quality. *Plant biotechnology journal,* 10**,** 301-312.

Koch, K. 2004. Sucrose metabolism: regulatory mechanisms and pivotal roles in sugar sensing and plant development. *Current opinion in plant biology,* 7**,** 235-246.

Koch, K. E., Wu, Y. & Xu, J. 1996. Sugar and metabolic regulation of genes for sucrose metabolism: potential influence of maize sucrose synthase and soluble invertase responses on carbon partitioning and sugar sensing. *Journal of experimental botany***,** 1179-1185.

Kubis, A. & Bar-Even, A. 2019. Synthetic biology approaches for improving photosynthesis. *Journal of Experimental Botany*.

Lawlor, D., Kontturi, M. & Young, A. 1989. Photosynthesis by flag leaves of wheat in relation to protein, ribulose bis phosphate carboxylase activity and nitrogen supply. *Journal of Experimental Botany,* 40**,** 43-52.

Li, Y., Heckmann, D., Lercher, M. J. & Maurino, V. G. 2017. Combining genetic and evolutionary engineering to establish C4 metabolism in C3 plants. *Journal of experimental botany,* 68**,** 117-125.

Lunn, J. E. & Macrae, E. 2003. New complexities in the synthesis of sucrose. *Current opinion in plant biology,* 6**,** 208-214.

Makino, A., Mae, T. & Ohira, K. 1984. Relation between nitrogen and ribulose-1, 5-bisphosphate carboxylase in rice leaves from emergence through senescence. *Plant and Cell Physiology,* 25**,** 429-437.

Makino, A., Sakashita, H., Hidema, J., Mae, T., Ojima, K. & Osmond, B. 1992. Distinctive responses of ribulose-1, 5-bisphosphate carboxylase and carbonic anhydrase in wheat leaves to nitrogen nutrition and their possible relationships to CO2-transfer resistance. *Plant Physiology,* 100**,** 1737-1743.

Maydup, M. L., Antonietta, M., Guiamet, J., Graciano, C., López, J. R. & Tambussi, E. A. 2010. The contribution of ear photosynthesis to grain filling in bread wheat (Triticum aestivum L.). *Field Crops Research,* 119**,** 48-58.

Nie, G., Hendrix, D. L., Webber, A. N., Kimball, B. A. & Long, S. P. 1995. Increased accumulation of carbohydrates and decreased photosynthetic gene transcript levels in wheat grown at an elevated CO2 concentration in the field. *Plant Physiology,* 108**,** 975-983.

Nikolau, B. J. & Klessig, D. F. 1987. Coordinate, organ-specific and developmental regulation of ribulose 1, 5-bisphosphate carboxylase gene expression in Amaranthus hypochondriacus. *Plant physiology,* 85**,** 167-173.

Nomura, M., Katayama, K., Nishimura, A., Ishida, Y., Ohta, S., Komari, T., Miyao-Tokutomi, M., Tajima, S. & Matsuoka, M. 2000. The promoter of rbcS in a C3 plant (rice) directs organ-specific, light-dependent expression in a C4 plant (maize), but does not confer bundle sheath cell-specific expression. *Plant molecular biology,* 44**,** 99-106.

Paul, M. J. & Pellny, T. K. 2003. Carbon metabolite feedback regulation of leaf photosynthesis and development. *Journal of experimental botany,* 54**,** 539-547.

Poovaiah, C. R., Mazarei, M., Decker, S. R., Turner, G. B., Sykes, R. W., Davis, M. F. & Stewart, C. N. 2015. Transgenic switchgrass (Panicum virgatum L.) biomass is increased by overexpression of switchgrass sucrose synthase (PvSUS1). *Biotechnology journal,* 10**,** 552-563.

Rajala, A., Hakala, K., Mäkelä, P., Muurinen, S. & Peltonen-Sainio, P. 2009. Spring wheat response to timing of water deficit through sink and grain filling capacity. *Field Crops Research,* 114**,** 263-271.

Rangan, P., Furtado, A. & Henry, R. J. 2016a. New evidence for grain specific C4 photosynthesis in wheat. *Scientific Reports,* 6.

Rangan, P., Furtado, A. & Henry, R. J. 2016b. New evidence for grain specific C 4 photosynthesis in wheat. *Scientific reports,* 6**,** 31721.

Ruan, Y.-L., Llewellyn, D. J. & Furbank, R. T. 2003. Suppression of sucrose synthase gene expression represses cotton fiber cell initiation, elongation, and seed development. *The Plant Cell,* 15**,** 952-964.

Sasaki, Y., Nakamura, Y. & Matsuno, R. 1987. Regulation of gene expression of ribulose bisphosphate carboxylase in greening pea leaves. *Plant molecular biology,* 8**,** 375-382.

Schuler, M. L., Mantegazza, O. & Weber, A. P. 2016. Engineering C4 photosynthesis into C3 chassis in the synthetic biology age. *The Plant Journal,* 87**,** 51-65.

Seneweera, S., Makino, A., Hirotsu, N., Norton, R., Suzuki, Y. J. E. & Botany, E. 2011. New insight into photosynthetic acclimation to elevated CO2: the role of leaf nitrogen and ribulose-1, 5-bisphosphate carboxylase/oxygenase content in rice leaves. 71**,** 128-136.

Seneweera, S. P., Basra, A. S., Barlow, E. W. & Conroy, J. P. J. P. P. 1995. Diurnal regulation of leaf blade elongation in rice by CO2 (is it related to sucrose-phosphate synthase activity?). 108**,** 1471-1477.

Serrago, R. A., Alzueta, I., Savin, R. & Slafer, G. A. 2013. Understanding grain yield responses to source–sink ratios during grain filling in wheat and barley under contrasting environments. *Field Crops Research,* 150**,** 42-51.

South, P. F., Cavanagh, A. P., Lopez-Calcagno, P. E., Raines, C. A. & Ort, D. R. 2018. Optimizing photorespiration for improved crop productivity. *Journal of integrative plant biology,* 60**,** 1217-1230.

Stitt, M. 1986. Limitation of photosynthesis by carbon metabolism: I. Evidence for excess electron transport capacity in leaves carrying out photosynthesis in saturating light and CO2. *Plant Physiology,* 81**,** 1115-1122.

Stitt, M., Lunn, J. & Usadel, B. 2010. Arabidopsis and primary photosynthetic metabolism–more than the icing on the cake. *The Plant Journal,* 61**,** 1067-1091.

Suzuki, Y., Kihara-Doi, T., Kawazu, T., Miyake, C. & Makino, A. 2010. Differences in Rubisco content and its synthesis in leaves at different positions in Eucalyptus globulus seedlings. *Plant, cell & environment,* 33**,** 1314-1323.

Suzuki, Y., Makino, A. & Mae, T. 2001. Changes in the turnover of Rubisco and levels of mRNAs of rbcL and rbcS in rice leaves from emergence to senescence. *Plant, Cell & Environment,* 24**,** 1353-1360.

Suzuki, Y., Miyamoto, T., Yoshizawa, R., Mae, T. & Makino, A. 2009. Rubisco content and photosynthesis of leaves at different positions in transgenic rice with an overexpression of RBCS. *Plant, cell & environment,* 32**,** 417-427.

Tadesse, W., Halila, H., Jamal, M., El-Hanafi, S., Assefa, S., Oweis, T. & Baum, M. 2017. Role of Sustainable Wheat Production to Ensure Food Security in the CWANA region. *Journal of Experimental Biology and Agricultural Sciences,* 5**,** S15-S32.

Tambussi, E. A., Bort, J., Guiamet, J. J., Nogués, S. & Araus, J. L. 2007. The photosynthetic role of ears in C3 cereals: metabolism, water use efficiency and contribution to grain yield. *Critical Reviews in Plant Sciences,* 26**,** 1-16.

Van Bezouw, R. F., Keurentjes, J. J., Harbinson, J. & Aarts, M. G. 2019. Converging phenomics and genomics to study natural variation in plant photosynthetic efficiency. *The Plant Journal,* 97**,** 112-133.

Vicente, R., Pérez, P., Martínez-Carrasco, R., Usadel, B., Kostadinova, S. & Morcuende, R. 2015. Quantitative RT–PCR platform to measure transcript levels of C and N metabolism-related genes in durum wheat: transcript profiles in elevated [CO2] and high temperature at different levels of N supply. *Plant and Cell Physiology,* 56**,** 1556-1573.

Vu, J. C., Allen Jr, L. H. & Gesch, R. W. 2006. Up-regulation of photosynthesis and sucrose metabolism enzymes in young expanding leaves of sugarcane under elevated growth CO2. *Plant Science,* 171**,** 123-131.

Walker, A. P., Beckerman, A. P., Gu, L., Kattge, J., Cernusak, L. A., Domingues, T. F., Scales, J. C., Wohlfahrt, G., Wullschleger, S. D. & Woodward, F. I. 2014. The relationship of leaf photosynthetic traits–Vcmax and Jmax–to leaf nitrogen, leaf phosphorus, and specific leaf area: a meta-analysis and modeling study. *Ecology and evolution,* 4**,** 3218-3235.

Wang, S., Tholen, D. & Zhu, X. G. 2017. C4 photosynthesis in C3 rice: a theoretical analysis of biochemical and anatomical factors. *Plant, Cell & Environment,* 40**,** 80-94.

White, J. C. & Gardea-Torresdey, J. 2018. Achieving food security through the very small. *Nature nanotechnology,* 13**,** 627.

Wullschleger, S. D. 1993. Biochemical limitations to carbon assimilation in C3 plants—a retrospective analysis of the A/Ci curves from 109 species. *Journal of Experimental Botany,* 44**,** 907-920.

Yadav, S. S., Redden, R. J., Hatfield, J. L., Ebert, A. W. & Hunter, D. 2019. *Food Security and Climate Change,* Wiley-Blackwell.

CHAPTER 5

SITE-SPECIFIC, GENOTYPIC, AND TEMPORAL CHARACTERIZATION OF NITROGEN METABOLISM AND THE EXPRESSION OF KEY GENES OF C_4 PHOTOSYNTHESIS IN WHEAT (*Triticum aestivum* L.)

Wheat is known to be a classical C_3 plant. However, recent findings suggest that C_4-like photosynthesis may be occurring specifically in the wheat pericarps. This study was designed to investigate the site-specific, genotypic, and temporal variation of the expression of key C_4 pathway genes in pericarps and flag leaves of wheat. Along with gene expression profiling, isotopic signatures of carbon and nitrogen (N) ($\delta^{13}C$ and $\delta^{15}N$) were also determined in plant dry matter at different ontogenies to underpin the underlying photosynthetic pathway in wheat. Differences in N metabolism during grain filling was also investigated between wheat spikes and flag leaves. This chapter has been prepared as a research manuscript to be submitted to "Frontiers in Plant Science."

Site-specific, genotypic, and temporal characterization of nitrogen metabolism and the expression of key genes of C_4 photosynthesis in wheat (*Triticum aestivum* L.)

Prabuddha Dehigaspitiya[1], Anke Martin[1], Paul Milham[2], Dananjali Gamage[3], Gavin J. Ash[1], Kiruba Arun-Chinnappa[1], Seiji Nagasaka[1, 4], Kotaro Shirai [5], Saman Seneweera[1, 6]*

Affiliations

[1] Centre for Crop Health, University of Southern Queensland, Toowoomba, QLD, 4350, Australia.

[2] Hawkesbury Institute for the Environment, Western Sydney University, LB 1797 Penrith NSW, 2753, Australia.

[3]Department of Agricultural Biology, Faculty of Agriculture, University of Ruhuna, Kamburupitiya, Sri Lanka.

[4] 1-1-1, Izumino, Itakura-machi, Org-gun, Gunma, Toyo University, Japan.

[5] International Coastal Research Center, Atmosphere and Ocean Research Institute, The University of Tokyo. 5-1-5, Kashiwanoha, Kashiwa-shi, Chiba, 277-8564 Japan.

[6] National Institute of Fundamental Studies, Hanthana Road, Kandy, Sri Lanka.

E-mail addresses:

Prabuddha Dehigaspitiya: Prabuddha.DehigaspitiyageDon@usq.edu.au

Paul Milham: P.Milham@westernsydney.edu.au

Gavin Ash: Gavin.Ash@usq.edu.au

Kiruba Arun-Chinnappa: Kiruba.ArunChinnappa@usq.edu.au

Anke Martin: Anke.Martin@usq.edu.au

Dananjali Gamage: Dananjali@agbio.ruh.ac.lk

Seiji Nagasaka: nagasaka@toyo.jp

***Corresponding author**

Saman Seneweera (+61401879853)

Saman.Seneweera@usq.edu.au

Abbreviations

A – photosynthesis rate; AGB – above ground biomass; ANOVA - analysis of variance; BC - bundle sheath cell; *Ca* – ambient carbon dioxide concentration; CM – complete maturity; *Ci* – intercellular carbon dioxide concentration; *Fd-GOGAT* - Putative ferredoxin-dependent glutamate synthase; dpa – days post anthesis; *GS1a* – Glutamine synthetase (cytosolic) – GS1; *GSr1* - Glutamine synthetase (cytosolic) – GS1; *GS2a* - Glutamine Synthetase (Plastidial) – GS2; *GS2b* - Glutamine Synthetase (Plastidial) – GS2; HI – harvest index; LPA – leaf photosynthetic area; MC - mesophyll cell; MDH - malate dehydrogenase; NADH nicotinamide adenine dinucleotide; *NADH-GOGAT* - Putative NADH-dependent glutamate synthase; NADP- nicotinamide adenine dinucleotide phosphate; NADP-ME - NADP-dependent malic enzyme; NiR - Ferredoxin Nitrite Reductase; PAR - photosynthetically active radiation; PAS – photosynthetic area of total spikes; PEPC-phosphoenolpyruvate carboxylase; PPDK - pyruvate orthophosphate dikinase; Rubisco - Ribulose 1,5-bisphosphate carboxylase/oxygenase; SAI – spike area index; *SC* – stomatal conductance; SD - total spike weight; SPA/LPA - Ratio between total spike area and total leaf area; TB – total biomass; TH – total harvest; TPA - total photosynthetic area; $\delta^{13}C$ - isotopic signatures of carbon; $\delta^{15}N$ – isotopic signatures of nitrogen.

Abstract

C_4 photosynthesis is the most efficient mode of carbon (C) fixation, due to its unique biochemical and structural adaptations. However, cereals such as rice and wheat, perform C_3 photosynthesis, which is considered less efficient. As the C_4 system evolved from ancestral C_3 species, both C_3 and C_4 plants may have a similar photosynthetic genetic makeup, although there are clear differences in expression. To test this hypothesis, we elucidated site-specific, genotypic, and temporal variations of the expression of C_4 pathway and nitrogen (N) metabolism in wheat, in pericarps and flag leaves of three genotypes (Huandoy, Amurskaja 75 and Greece 25) at different growth stages. Real-time PCR was used to determine the expression variation of key genes related to the C_4 pathway (*TaPEPC_5, TaNADP-ME _1, TaPPDK_1α, TaMDH_7, TaPEPC_5ALTaPEPC_5BL*, *TaPEPC_5DL*, *TaNADP_1AS*, *TaNADP_1BS* , *TaNADP_1DS* , *TaPPDK_1αAL, TaPPDK_1αBL*, *TaPPDK_1αDL*) along with their sub-genome specificity and N metabolism (*Fd-GOGAT* , *NiR, GS2a, NADH-GOGAT* , *GSR1, GS2b, GS1a*). Carbon and N isotopic signatures ($\delta^{13}C$ and $\delta^{15}N$) of dry matter of wheat pericarps and flag leaves were measured along with their organ-specific C and N atomic ratios and were verified by phenotyping and organ-specific gas exchange parameters. Evidence of grain-specific C_4 photosynthesis in wheat was not apparent; however, there was a site-specific expression pattern of genes related to C_4 pathway enzymes in the pericarps and flag leaves of wheat. Nonetheless, in both organs, C isotopic signatures were within the C_3 range. The site-specific, genotypic, and temporal variation in the expression of genes related to N metabolism support the hypothesis that wheat pericarps may play an important role in grain yield and quality after leaf senescence. Finally, our results point to the importance of understanding the metabolic processes of wheat spikes to develop a high yielding/grain quality variety in the future.

Keywords: C and N isotopic signatures, grain photosynthesis

1. Introduction

To feed the expected population of 9.8 billion by the middle of this century, overall food production must increase by at least 60% (Crist et al., 2017). Global food demand has been sustained for a few decades by yield transformation of cereals during the green revolution between the 1950s and 1980s (Furbank et al., 2015). However, feeding the future population seems challenging without another similar transformation, as the current genetic yield potential of critical food crops has almost plateaued (Furbank et al., 2015, Taylor and Long, 2017). One of the possible solutions is an increase in crop biomass by improving photosynthetic efficiency (Kubis and Bar-Even, 2019, van Bezouw et al., 2019). Several approaches seem possible including: enhancing the activity of ribulose-1,5-bisphosphate carboxylase/oxygenase (Rubisco), the leading CO_2 fixing enzyme (Galmes et al., 2014); engineering more efficient photosynthetic pathways into critical food crops (Gao et al., 2014, Wang et al., 2014); optimizing the source and sink feedback mechanism in photosynthesis (Campany et al., 2017); reducing the barriers of mesophyll conductance to CO_2 diffusion (Xiong et al., 2017) and minimizing the incompetence of photosynthesis due to dynamic ecological aspects such as light and temperature (Vialet-Chabrand et al., 2017). However, limited understanding of the genetic background underlying photosynthesis-related processes has impeded many of these approaches to crop improvement.

The atmospheric CO_2 concentration may have decreased from over 1,000 μmol mol^{-1} to less than 200 μmol mol^{-1}, during the last 50 million years (Sage et al., 2012). The natural variations of photosynthesis which is seen in angiosperms such as C_3, crassulacean acid metabolism (CAM), C_4, and C_3-C_4 intermediates are evolutionary adaptations to the diverse states of atmospheric CO_2 concentration over time (Yamori et al., 2014, Dehigaspitiya et al., 2019). Although there are biochemical, structural, and temporal deviations in different photosynthetic pathways, the bifunctional enzyme Rubisco catalyzes the reaction of atmospheric CO_2 fixation into a stable, three-carbon intermediate. Also, Rubisco binds with atmospheric O_2 in competition with CO_2 initiating oxygenic activity of the bifunctional enzyme leading to photorespiration. Photorespiration is capable of reducing the efficiency of photosynthesis by up to 30%. To minimize the oxygenic activity of Rubisco, higher plants have evolved biochemical and structural modifications, and carbon concentration mechanisms (CCMs), as in C_4,

are one such adaptation. In C_4, the enzyme Rubisco is localized in the chloroplasts of inner bundle sheath cells (BCs), and by decarboxylation of the malate/aspartate from malic enzymes, CO_2 is liberated by increasing the CO_2 concentration by about 10-fold than in the atmosphere at the sites of Rubisco (Furbank, 2011). This allows Rubisco to perform closer to its catalytic maximum (V_{max}) by minimizing photorespiration (von Caemmerer and Furbank, 2003). This unique arrangement of C_4 photosynthesis is termed Kranz anatomy and evolved independently up to 60 times from C_3 ancestors during angiosperm evolution and is the most efficient photosynthetic pathway under current atmospheric conditions concerning the use of water, nitrogen (N), and light (Hibberd and Covshoff, 2010).

Bioengineering the C_4 pathway into C_3 cereals, such as rice and wheat, is expected to massively increase C_3 yields (Rangan et al., 2016, Wang et al., 2017). This ambitious goal would be facilitated by an enhanced understanding of the regulatory mechanisms underlying both the C_3 and C_4 pathways (Weissmann and Brutnell, 2012, Rangan et al., 2016). Until recently, the majority of the research on photosynthesis has focussed on leaves (Rangan et al., 2016, Dehigaspitiya et al., 2019). However, different modes of photosynthesis have recently been reported at various sites of the same plant, or of plants which are grown in diverse niches (Rangan et al., 2016, Bachir et al., 2017). Not only photosynthesis, but also, the other metabolic processes such as photorespiration, sucrose, and N metabolism, can also vary site-specifically (Dehigaspitiya et al., 2019). Knowledge of site-specific C_4 photosynthesis and other metabolic processes may accelerate the production of higher-yielding crop varieties by bioengineering efficient C_4 photosynthetic traits into major C_3 cereals.

Wheat (*Triticum aestivum* L.) is the second most important cereal globally, providing 20% of the daily protein and calories in the developing world (Tadesse et al., 2017). Despite the fact that wheat is a typical C_3 plant, site-specific C_4 photosynthesis may occur in developing pericarps (Rangan et al., 2016). However, the unequivocal establishment of site-specific C_4 photosynthesis in wheat requires additional biochemical and physiological evidence (Busch and Farquhar, 2016).

In this study, we test the hypothesis that site-specific C_4 photosynthesis occurs in developing pericarps of wheat by observing the genotypic, temporal, and site-specific expression of key genes of C_4 photosynthesis relative to those in flag leaves. These

data are supported by measurements of: $\delta^{13}C$ and $\delta^{15}N$ analysis; transcript abundance of key genes associated with N metabolism; the C/N atomic ratio; and growth and gas exchange.

2. Materials and methods

2.1. Plant materials and growth conditions

Three winter wheat genotypes (Huandoy, Amurskaja 75, and Greece 25) were used to investigate the site-specific changes in the expression of key genes related to C_4 photosynthesis and N metabolism in wheat. These genotypes had been used to determine the C_4 pathway expression in the developing wheat pericarps (Rangan et al., 2016). Seeds were acquired from the Australian Grain Genebank, Grains Innovation Park, Horsham, Victoria. The experiment was conducted in a glasshouse at the University of Southern Queensland, Australia (Latitude: 27° 33' 38.02" S and Longitude: 151° 55' 55.20" E) between May 2018 and October 2018. The experimental design of the glasshouse experiment was completely randomized with three replicates. Seeds were sown in pots filled with 4.2 kg of loam soil (5 seeds per pot) with a diurnal temperature range of 14°C to 22°C. The seedlings were thinned to two plants per pot fourteen days after sowing. Pots were randomized regularly to reduce the location effect of the glasshouse.

2.2. Phenotyping

Phenotypic traits measured are shown in Table 1. Leaf area measurements were taken using a LI-COR area meter (LI-COR, USA). Photosynthetic area of the wheat spikes was measured as described by (Dehigaspitiya et al chapter 2)' after which samples were dried at 60°C for 72 h and weighed.

2.3. Gas exchange measurements

To determine the genotypic, temporal and organ-specific variation of gas exchange, the rate of photosynthesis (*A*), stomatal conductance (*SC*), intercellular CO_2 concentration (*Ci*) and the ratio between *Ci* and ambient CO_2 concentration (*Ca*)

(*Ci/Ca*) was measured between wheat spikes and flag leaves in three wheat genotypes (Huandoy, Amurskaja 75, and Greece 25) across four growth stages (heading, 3-dpa, 14-dpa and 30-dpa) using LI-COR portable photosynthesis system (LI-6400xt, LI-COR, USA) coupled with a leaf chamber and a transparent conifer chamber (LI-COR, Lincoln, NE, USA 6400-05). Gas exchange measurements of spikes and flag leaves were measured as described by (Dehigaspitiya et al 2019. chapter 2) and (Evans and Santiago, 2014) respectively.

All the measurements were taken between 10.00 am and 2.00 pm. At least one hour before taking measurements, wheat plants were moved to a controlled growth cabinet (PGC-105, Percival, USA). Canopy level light intensity, relative humidity (RH) and temperature inside the growth cabinet were maintained at 1000 µmol m^{-2} s^{-1}, 70%, and 22 $^{\circ}$C respectively. Spike level temperature, air flow rate, and reference CO_2 concentration inside the leaf and conifer chambers were maintained at 22 $^{\circ}$C, 500 µmol s^{-1}, and 400 µmol mol^{-1} respectively. RH inside the conifer chamber was maintained between 50% and 70%. Rate of photosynthesis (*A*), stomatal conductance (*SC*), and intercellular CO_2 concentration (*Ci*) were obtained. Further, for wheat spikes, dark respiration was measured as described in (Dehigaspitiya et al chapter 2).

2.4. Carbon and nitrogen analysis

Oven-dried samples of wheat pericarps and flag leaves of four growth stages [heading, 14-dpa, 30-dpa and maturity (CM)] and wheat seeds at 30-dpa and CM were used for C and N analysis. Oven-dried (65°C for 72 hours) plant samples were ground using a ball mill (Tissue Lyser II, QIAGEN, Australia) to a fine powder (~100 µm). The C and N concentrations of the plant organs were analyzed using a CN analyzer (Leco CN628, USA).

2.5. Stable isotope of carbon and nitrogen analysis

Wheat pericarps and flag leaves at heading and 14-dpa were selected for stable C and N isotope ($\delta^{13}C$ and $\delta^{15}N$) analysis to investigate the differences of isotopic signatures at early and mid-reproductive stages. Oven-dried samples (65°C for 72 hours) were ground to a fine powder using a ball mill (Tissue Lyser II, QIAGEN, Australia) and

stored at -30°C. Isotopic signatures of C and N were determined using a mass spectrometer (IsoPrime100, IsoPrime, U.K.) connected to a combustion device (Vario MICRO cube elementar, Germany).

2.6. Gene expression analysis

2.6.1 Sample collection

Wheat spikes and flag leaves at heading, 14-dpa, and 30-dpa were collected for gene expression analysis. Sampling was conducted between 11.00 am and 1.00 pm. Wheat spikes and flag leaves were separated from the plant, stored in chilled storage tubes separately prior to being submerged in liquid N_2. Until total RNA extraction, samples were stored at -80 ˚C.

2.6.2 Extraction and quantification of RNA

Before extraction all mortars and pestles were chilled using liquid N_2. Approximately 300 mg (fresh weight) of the pericarp of the wheat spikes and flag leaves were used for RNA extraction. Plant materials were placed into a mortar and ground into a fine powder with liquid N_2. Then, 500 µL of Trizol® Reagent (Invitrogen by Thermo Fisher Scientific, USA) and 700 µL of TPS buffer [100 mM Tris-HCl (pH 8), 10 mM EDTA and 1 M KCl] were added to the ground samples and grinding was continued until the samples were completely homogenized. High-quality RNA was extracted according to the manufacturer's instructions of Trizol® Reagent (Invitrogen by Thermo Fisher Scientific, USA). Quantification of the extracted RNA was carried out using Qubit 3 Fluorimeter (Invitrogen by Thermo Fisher Scientific, USA) as per the manufacturer's instructions. For the cDNA synthesis, the concentration of each extracted RNA sample was adjusted to 1µg/µl.

2.6.3. cDNA Synthesis

To avoid possible contamination from genomic DNA, extracted RNA samples were treated with DNaseI, Amplification Grade (Invitrogen by Thermo Fisher Scientific, USA) according to the manufacturer's instructions. Then, a volume of 20 µl of cDNA

from each sample was synthesised using SensiFAST^{TM} cDNA synthesis kit (Catalogue No – Bio-65054, Bioline, UK) as per the manufacturer's instructions.

2.6.4. Primer Selection

Gene-specific primers of genes related to N metabolism and C_4 photosynthesis (Supplementary Table S1) were designed as per (Vicente et al., 2015, Bachir et al., 2017). Using the Primer-Blast option in the National Centre for Biotechnology Information (NCBI) website, the genes were verified for their specificity to *T. aestivum* L. Primers were sourced from Integrated DNA Technologies, Inc. (Integrated DNA Technologies Pty. Ltd, Singapore).

2.6.5. Expression analysis using real-time Quantitative PCR (qRT-PCR)

Gene expression was determined from the reaction assays carried out in 96-well plates using QuantStudio 3 quantitative real-time PCR system (Applied Biosystems, Thermo Fisher Scientific, USA). The total reaction mixture in a well (20 µL) consisted of 4 µL of diluted cDNA, 10 µL of PowerUp™ SYBR™ Green Master (Applied Biosystems from Thermo Fisher Scientific, USA), 4 µL of DEPC treated water, 1 µL of 10 mM forward primer and 1 µL of 10 mM reverse primer. The program of the thermal cycler was set at 95 $^{\circ}$C for 10 min, followed by 40 cycles at 95 $^{\circ}$C for 15 s and 60 $^{\circ}$C for 1 min. The primer efficiency of each primer was calculated using LinRegPCR v2012.3 application software. Expression analysis was carried out using the comparative threshold cycle [(C_t) $2^{-\Delta\Delta Ct}$] method.

2.7. Statistical analysis

Before analysis, the normality of the data set was tested and the data which were not normally distributed were transformed to normalize. ANOVA was carried out to determine the significance between organ types, genotypes, and growth stages (P <0.05). To determine the statistical differences between genotypes, organ types, and growth stages, Tukey's test was used. Data analysis was performed using SPSS statistical software version 23 (IBM, Armonk, NY, USA). GraphPad Prism scientific

software version 5.01 (GraphPad Software, San Diego, CA) was used for the graphical representations.

3. Results

3.1 Genotypic, temporal and organ-specific variation of gas exchange parameters

Statistically significant interactions among genotypes, growth stages, and organ types affected the combined dependent variables of gas exchange: *A* ($P < 0.001$), *SC* ($P < 0.001$), and *Ci/Ca* ($P < 0.001$) (Figure 1). However, wheat genotype did not have a statistically significant effect on C_i/C_a.

According to the multiple comparisons, *A* was significantly different among wheat genotypes (Supplementary Table S2). However, *SC* was only statistically significant between Huandoy and Amurskaja 75 and Amurskaja 75 and Greece 25 (Supplementary Table S2). Statistically significant difference for *A* was observed across most growth stage combinations [heading and 30-dpa ($P < 0.001$), 3-dpa and 14-dpa ($P < 0.05$), 3-dpa and 30-dpa ($P < 0.001$), 14-dpa and 30-dpa ($P < 0.001$)] (Supplementary Table S3). However, the difference between growth stage heading and 14-dpa was not statistically significant for all traits.

In Huandoy, growth stage 14-dpa displayed the highest values for *A* for both spikes and flag leaves (Figure 1). In contrast, in Greece 25, the highest values for *A* was exhibited at heading for both the organ types: spikes and flag leaves. In general, at early reproductive growth stages (heading to 14-dpa), *A* was significantly higher in flag leaves than in wheat spikes (Figure 1). However, at 30-dpa, the difference between spikes and flag leaves for *A* was getting reduced. Interestingly, at 30-dpa, *A* of wheat spikes were much higher than in the flag leaves for both Huandoy and Greece 25. Further, in all the instances, the *Ci/Ca* was between 0.626 and 0.81 (Figure 1).

3.2 Genotypic, temporal and organ-specific expression of genes related to the C_4 photosynthesis N metabolism

The key genes related to C_4 photosynthesis (general and genome-specific) and N metabolism (Supplementary Table S1) were tested in pericarps, and flag leaves of selected wheat genotypes at different growth stages (heading, 14-dpa and 30-dpa).

3.2.1 Expression of key genes related to the C_4 photosynthesis

The qRT-PCR using general primers for the C_4 pathway showed a statistically significant interaction effect among wheat genotype, growth stage and organ type on the relative expressions of *TaNADP-ME _1* ($P < 0.001$), *TaPEPC_5* ($P < 0.05$), *TaMDH_7* ($P < 0.01$) and *TaPPDK_1α* ($P < 0.001$) (Table 2). However, the genotypic and organ (pericarps and flag leaves) effect for *TaNADP-ME _1* expression was not statistically significant. In contrast, of the four genes, only *TaNADP-ME _1* displayed a statistically significant growth-stage effect (Table 2).

According to multiple comparisons, Amurskaja 75 and Greece 25 displayed statistically significant differences for *TaPEPC_5* ($P < 0.01$), *TaMDH_7* ($P < 0.001$) and *TaPPDK_1α* ($P < 0.001$) expression (Supplementary Table S4). In contrast, only *TaNADP-ME _1* displayed a statistically significant difference across growth stages (Supplementary table S5).

Wheat pericarps and flag leaves showed a similar expression pattern between wheat genotypes across different growth stages (Table 3). In pericarps of all three wheat genotypes, *TaPEPC_5* displayed the highest relative expression at all growth stages (Table 3). Likewise, flag leaves also showed a similar expression pattern with a few exceptions where *TaPPDK_1α* displayed the highest expression in Huandoy and Greece 25 at 14-dpa and 30-dpa respectively (Table 3). In wheat pericarps, the highest and the lowest mean relative expression for *TaPPDK_1α* was observed in Huandoy and Amurskaja 75, respectively, at 14-dpa (Table 3).

In Huandoy at all growth stages, flag leaves showed much higher relative expressions for all considered genes than in wheat pericarps. With few exceptions, the other two varieties also displayed a similar trend (Table 3).

Genome-specific primers of *TaPEPC_5*, *TaNADP-ME _1*, and *TaPPDK_1α* were used to determine the variation in genome-specific expression. Because of the relatively lower expression in most instances, the genome-specific expression analysis was not carried out for *TaMDH_7*.

When considering genome-specific analysis of *TaNADP-ME _1*, there was a statistically significant interaction among genotype, growth stage, and organ type on *TaNADP_1DS* expression (Table 2). Also, there was a statistically significant interaction between genotypes and organ types on *TaNADP_1BS* expression (Table 2). For *TaNADP_1AS*, the only significant effect was from the organ type (Table 2). Moving to multiple comparisons, the significant differences could only be seen between Huandoy and Amurskaja 75 and, Amurskaja 75 and Greece 25 for *TaNADP_1BS.* Also, *TaNADP_1BS* displayed a statistical difference between 14-dpa and 30-dpa (Supplementary Table S6).

Of three genome-specific genes of *TaNADP-ME _1*, *TaNADP_1BS* displayed the highest expression in both wheat pericarps and flag leaves, among three genotypes at all growth stages (Table 4). Mean relative expressions of *TaNADP_1AS*, *TaNADP_1BS*, and *TaNADP_1DS* along with their fold changes, are shown in Table 4.

In the genome-specific expression of *TaPEPC_5*, there was a statistically significant interaction effect between growth stage and organ type on *TaPEPC_5AL* ($P < 0.05$), *TaPEPC_5BL* ($P < 0.01$) and *TaPEPC_5DL* ($P < 0.05$) expression (Table 2). Similarly, there were statistically significant interaction effects between genotype and organ type and, genotype and growth stage on the three genome-specific genes of *TaPEPC_5* (Table 2). However, the interaction effect from the genotype, growth stage and the organ type on *TaPEPC_5AL*, *TaPEPC_5BL*, and *TaPEPC_5DL* was not statistically significant (Table 2). According to multiple comparisons, the only significant difference was observed in *TaPEPC_5AL* ($P < 0.01$) between Huandoy and Greece 25 (Supplementary Table S7). Furthermore, there was a statistically significant difference ($P < 0.05$) between heading and 14-dpa on *TaPEPC_5BL* expression (Supplementary Table S6). In most cases, in wheat pericarps and flag leaves, total expression from *TaPEPC_5AL*, *TaPEPC_5BL* and *TaPEPC_5DL* were significantly

lower than the total expression of genome-specific genes of *TaNADP-ME _1* and *TaPPDK_1α* (Table 4).

The genotype, organ type, and growth-stage had a statistically significant interaction effect on the expression of all genome-specific genes of *TaPPDK_1α* [*TaPPDK_1αAL* (*P <0.001*), *TaPPDK_1αBL* (*P <0.001*) and *TaPPDK_1αDL* (*P <0.05*)] (Table 2). Results from multiple comparisons revealed that the expression of *TaPPDK_1αAL*, *TaPPDK_1αBL*, and *TaPPDK_1αDL* was not statistically significant between Huandoy and Amurskaja 75 (Supplementary Table S6). Furthermore, there was a statistically significant difference between heading and 30-dpa on *TaPPDK_1αAL* (*P <0.001*), *TaPPDK_1αBL* (*P <0.001*) and *TaPPDK_1αDL* (*P <0.01*) expression (Supplementary Table S7). In all instances, the expression of *TaPPDK_1αBL* and *TaPPDK_1αDL* were significantly higher than the expression of *TaPPDK_1αAL* (Table 4).

3.3.2 Expression of key genes related to N metabolism

There was a statistically significant interaction effect among genotype, growth stage and organ type on *Fd-GOGAT* (*P <0.05*), *NiR* (*P <0.001*), *GS2a* (*P <0.001*), *NADH-GOGAT* (*P <0.001*), *and GSR1* (*P <0.001*) (Table 5). *GS2b* and *GS1a* had a statistically significant interaction effect with growth stage and organ type (*P<0.05* and *P <0.001*, respectively) (Table 5). Multiple comparisons revealed that Huandoy and Amurskaja 75 were statistically different for the relative expression of *NiR* (*P <0.001*), *GS2a* (*P <0.05*), and *NADH-GOGAT* (*P <0.001*) (Supplementary Table S8). Further, in all genotypes, the relative expression of *Fd-GOGAT* (*P <0.01*), *NiR* (*P <0.001*), *GS2a* (*P <0.001*), *GS1a* (*P <0.001*), and *GSR1* (*P <0.001*) differed significantly between 14-dpa and 30-dpa (Supplementary Table S9). Only *GS2a* displayed a significant difference among all considered growth stages (Supplementary Table S9).

In most cases, although the relative expression of genes of N metabolism was comparatively higher in flag leaves than in wheat pericarps (except *NADH-GOGAT*), both the organ types displayed a similar expression trend (Table 6). In both organ types, the lowest expression was from *GS2b* (Table 6). In general, the highest expression of wheat pericarps was observed from *GS2a* across all genotypes (Table

6). However, the highest expression in flag leaves varied among *Fd-GOGAT*, *GS2a*, and *GS1a* (Table 6). Both in wheat pericarps and flag leaves, the expression of *GS1a* increased from heading to 30-dpa, and this was prominent in flag leaves. In contrast, the expression of *GS2a* was much higher at heading in both organ types except flag leaves of Amurskaja 75 (Table 6).

3.3 Organ-specific $\delta^{13}C$, $\delta^{15}N$ and C/N atomic ratios

There was a statistically significant difference between wheat pericarps and flag leaves for $\delta^{15}N$ and C/N atomic ratio in all three wheat genotypes at two considered growth stages (heading and 14-dpa) (Table 7). However, except in Amurskaja 75 and Greece 25 at heading, there was no statistically significant difference between wheat pericarps and flag leaves for $\delta^{13}C$ (Table 7).

In general, in both wheat spikes and flag leaves, $\delta^{13}C$ displayed a decreasing trend with the age of the plant (heading to 14-dpa) while C/N atomic ratios were showing an increasing trend.

3.4 Phenotypic variation

3.4.1 Photosynthesis-related traits

There was a statistically significant interaction effect between genotype and growth stage on the spike photosynthetic area (SPA) ($P < 0.01$), total photosynthetic area of leaves (LPA) ($P < 0.01$), total photosynthetic area (TPA) ($P < 0.01$), spike area index (SPA/TPA) (SAI) ($P < 0.01$) and the ratio between SPA and LPA (SPA/LPA) ($P < 0.001$) (Figure 2). Genotype ($P < 0.001$) and growth stage ($P < 0.001$) had a statistically significant effect on flag leaf photosynthetic area (FPA) (Figure 2). According to multiple comparisons, Amurskaja 75 and Greece 25 were not statistically different only for SPA out of photosynthesis-related traits (Supplementary Table S10). Lastly, LPA was not statistically different between heading and 14-dpa (Supplementary Table S11).

In all genotypes, the highest SPA was observed at 30-dpa, and the highest value was shown by Huandoy (Figure 2). In contrast, the highest FPA was observed in

Amurskaja 75 (Figure 2). Also, Amurskaja 75 had the highest TPA at heading (Figure 2). However, the highest SAI was observed in Huandoy at 30-dpa (Figure 2).

3.4.2 Growth-related traits

The wheat genotype and growth stage had a statistically significant interaction effect on spike dry weight (SD) ($P < 0.001$) and total biomass (TB) ($P < 0.001$) (Figure 3). However, according to the multiple comparisons, 30-dpa and CM were not statistically different for TB (Supplementary Table S12). In all growth stages, the highest and the lowest SD was given by Huandoy and Amurskaja 75 respectively (Figure 3). Further, the highest and the lowest TB in each growth stage was observed in Amurskaja 75 and Greece25, respectively (Figure 3).

3.4.2 Harvest-related traits

For both harvest index (HI) and total harvest (TH), the genotypic effect was statistically significant ($P < 0.001$) (Figure 3). The highest values for HI and TH was observed in Huandoy (Figure 3). Amurskaja 75 showed the lowest value for HI while Greece 25, giving the lowest TH (Figure 3).

3.5 Genotypic, temporal and organ-specific variation in N concentrations in wheat

Nitrogen concentration (weight basis) in wheat interacted significantly with organ type, genotype, and growth stage ($P < 0.001$) (Figure 4). Across all genotypes at the considered growth stages (heading, 14-dpa, 30-dpa, and CM), the N concentrations were much higher in flag leaves than in wheat pericarps except for Amurskaja 75 at CM (Figure 4). Further, Greece 25 showed the highest mean N concentration for both wheat pericarps and flag leaves (Figure 4). For N concentrations, wheat pericarps and flag leaves expressed a similar pattern, which is a decreasing trend after 14-dpa (Figure 4). For all genotypes, the highest N concentrations were observed at 14-dpa for both pericarps and flag leaves (Figure 4). To determine the activity of N sinks, N concentrations of wheat seeds at 30-dpa and CM were measured. Wheat genotype and growth stage showed a statistically significant interactive effect on seed N

concentrations (Figure 4). The weight of N in the TH of a plant was calculated. The results showed a similar trend in TH with highest average N weight for Huandoy being 217.9 mg and the lowest for Greece 25 being 104.6 mg (Figure 4).

4. Discussion

4.1 Expression of key genes related to C_4 pathway site-specifically and temporally varied

In this study, we were able to report the site-specific, genotypic and temporal variation of the expression of key genes related to C_4 photosynthesis (*TaPEPC_5, TaNADP-ME _1, TaPPDK_1α,* and *TaMDH_7*). Our results supported those gene expression results of Bachir et al. (2017), which were conducted on wheat flag leaves at three different growth stages. According to Bachir et al. (2017), the expression of *TaNADP-ME _1* was relatively low compared to other C_4 like genes among genotypes. In contrast, our results show that, in most cases, both in wheat pericarps and flag leaves, the relative expression of *TaMDH_7* was the lowest (Table 3). Although wheat is known to perform C_3 photosynthesis, evidence for the existence of a C_4-like photosynthetic mechanism has been reported in developing wheat pericarps using transcriptomic and microscopy data (Rangan et al., 2016). Further, Bachir et al. (2017) characterized the expression patterns of key genes related to the C_4 pathway enzymes, including NADP-dependent malic enzyme (NADP-ME), malate dehydrogenase (MDH), pyruvate orthophosphate dikinase (PPDK), and Phosphoenolpyruvate carboxylase (PEPC) in wheat flag leaves. It is evident that not only in wheat, but also the genomes of other C_3, cereals may encode all the genes of the C_4 pathway even though they are less active (Rangan et al., 2016, Bachir et al., 2017). However, less effort has been made to utilize their functions for crop improvement (Bachir et al., 2017).

Further, our results indicated that there was no genotypic or organ-specific variation for the expression of *TaNADP-ME _1* (Table 2). Importantly too, we observed no variation in expression among growth stages for *TaPEPC_5, TaPPDK_1α,* and *TaMDH_7*. Except for a very few instances, *TaPEPC_5* was the most highly expressed of the four genes (Table 3).

The modern bread wheat (hexaploid) is a result of hybridization between diploid goat grass (DD, *Aegilops tauschii*) and cultivated tetraploid emmer wheat (AABB, *Triticum dicoccoides*) approximately 8000 years ago (Nesbitt et al., 1996). Out of three diploid progenitor sub-genomes (AA, BB, and DD) of wheat, AA and DD were from *Triticum urartu* and *Ae. tauschii* respectively, and BB was from an unknown species (Haudry et al., 2007). When considering present cultivated varieties, the nucleotide diversity of each sub-genome (A, B, and D) has noticeably declined from its ancestral populations (Haudry et al., 2007). In our study, the genome-specific expression of genes related to PEPC, NADP-ME, and PPDK C_4 enzymes was evaluated. In both organ types, across all considered growth stages, the expression of *TaNADP_1BS* was much higher than the other two genome-specific genes (*TaNADP_1AS* and *TaNADP_1DS*) indicating that in this particular instance, the B sub-genome of wheat may be accountable for the NADP-ME expression (Table 4).

In contrast, the expression of both *TaPPDK_1αBL* and *TaPPDK_1αDL* was much higher than the expression of *TaPPDK_1αAL,* indicating that both B and D sub-genomes maybe responsible for PPDK expression (Table 4). However, in flag leaves at 30-dpa, the expression of *TaPPDK_1αAL* was comparatively higher than in the other growth stages specifying a temporal variation of PPDK gene expression (Table 4). Interestingly, the expression of PPDK related genes in Greece 25 at 30-dpa was much higher than in the flag leaves of other varieties (Table 4). The reason for this observation could be at late grain filling, as PPDK may have an important role in wheat metabolic processes. Although the expression of genome-specific genes related to PEPC was comparatively lower than the other two: NADP-ME and PPDK, in most cases, from the gene expression data, we can assume that all the three (A, B and D) sub-genomes may be accountable for the PEPC expression (Table 4). Although the relative expression of key genes related to C_4 enzymes was much higher in flag-leaves than in wheat pericarps, the organ-specific variation of NADP-ME expression was comparatively lower than the organ-specific variation of PPDK and PEPC. This indicates that, although wheat pericarp is not a major photosynthetic organ, it may have the potential to perform in a more or less similar manner to the flag leaves concerning NADP-ME, PPDK, and PEPC expression. Similar to the results of Bachir et al. (2017), in our study as well, a correlation between the expression of general and genome-specific C_4 genes was not observed.

4.2 Change in nitrogen dynamics in flag leaves and wheat pericarps from heading to maturity

We observed organ-specific variation in the relative expression of *GS2a*, *GS2b*, *GS1a*, and *GSr1*: key genes which encode GS2 and GS1 isoenzyme families, between wheat spikes and flag leaves (Table 5). In both organ types, the highest *GS2a* expression was during the early reproductive stages, and there was a decreasing trend towards 30-dpa (Table 6). A similar observation was reported by Bernard et al. (2008) from a study of wheat flag leaves. The reason for this decreasing trend of *GS2a* may be due to the senescence of photosynthetic organs, which converts their roles from N-sinks to N-sources. At early reproductive stages, the relative expression of *GS2a* in flag leaves was much higher than in pericarps (Table 6). However, at 30-dpa, the difference between wheat pericarps and flag leaves for *GS2a* expression was minimum, and in some instances, it was higher in wheat pericarps (Table 6). That maybe again due to early senescence of flag leaves when compared to wheat pericarps (Figure 5).

Interestingly, in both organ types at early reproductive stages, the *GS1a* expression was comparatively lower than the *GS2a*, highlighting the site-specific variation of GS1 and GS2 (Table 6). However, in most cases at 30-dpa, the *GS1a* expression is higher than the *GS2a* both in wheat pericarps and flag leaves (Table 6). The increasing trend of *GS1a* expression towards 30-dpa was more prominent in flag leaves. Again, this may be due to the change from N-sinks to N-sources (N remobilization), which fits with the much earlier senescence of flag leaves (late senescence of wheat spikes) than spikes. According to Masclaux-Daubresse et al. (2006), the GS1 facilitates N remobilization from initial sink tissues, in this case, from flag leaves and wheat pericarps to developing sink organs: maybe to the wheat grain. That is, wheat pericarps probably become a prominent source of grain N during late grain filling or after complete leaf senescence.

N is amongst the essential elements required by plant cells to maintain protein turnover (White et al., 2015). Until senescence, plant roots are the sources of N while shoots act as sinks. At senescence, shoot tissues then become a secondary N source due to remobilization of N mainly for reproduction and growth (White et al., 2015).

In plant N assimilation, glutamate is converted into glutamine by glutamine synthetase (GS), using ammonia as a substrate. Among GS subclasses, GS1, and GS2 are

believed to have site-specific roles in N metabolism (Masclaux-Daubresse et al., 2010). The enzyme GS2 is highly abundant in photosynthetic organs such as in leaves (sinks). Further, GS2 catalyzes the primary N assimilation of ammonia and re-assimilation of respiratory ammonia. In contrast, the expression of GS1 is comparatively lower in leaf organs (Foyer and Zhang, 2011).

To integrate amino groups into amino acids which are required for protein synthesis, the GS enzymes tend to combine with two types of GOGAT (glutamate synthase) enzymes: *Fd-GOGAT* and *NADH-GOGAT* (Masclaux-Daubresse et al., 2010). According to Kamachi et al. (1992), both *Fd-GOGAT* and *NADH-GOGAT* display a site-specific localization in plants where there is an abundance of *NADH-GOGAT* at non-photosynthetic organs while a much higher profusion of *Fd-GOGAT* was detected at photosynthetic organs. Supporting this, our results also revealed that the expression of genes related to *Fd-GOGAT* is much higher than *NADH-GOGAT* gene expression both in wheat pericarps and flag leaves (Table 6). Further, the expression of genes associated with *Fd-GOGAT* is much higher in the flag leaves than in the wheat pericarps indicating chloroplastic localization (Figure 5).

Consistent with the expression of genes related to N assimilation, in our study, we observed a site-specific, genotypic, and temporal variation in N concentrations between wheat pericarps and flag leaves (Table 5). In flag leaves, there was a steady N concentration during heading and 14-dpa: the stages which generally have the highest photosynthetic activity (Table 6). In this stage, the flag leaves may be in equilibrium between the N supply and N remobilization or with minimum N remobilization. The comparatively lower expressions of genes encoding GS1 further supported our observation. The steady decrement in N concentrations from 14-dpa to CM denotes the role change of flag leaves, which is the transformation from N-sink to N-source due to N remobilization taking place during leaf senescence.

However, wheat pericarps across all genotypes showed a different pattern in N concentrations compared to the leaves (Figure 4). In spikes, N concentrations increased between heading and 14-dpa (Figure 4) indicating sink activity. Further, although N concentrations decreased between 14-dpa and 30-dpa, the decrease was not as steady as in flag leaves (Figure 4), indicating delayed senescence of wheat

spikes and delayed N remobilization compared to flag leaves. However, the flag leaf N concentrations were always much higher than the pericarps (Figure 4).

Further, the highest and the lowest N content (weight) of the total harvest was in genotype Huandoy and Greece 25, respectively (Figure 4). However, the highest grain N concentration was with variety Amurskaja 75. Hence, we can assume that although the amount of N (weight) in the total harvest higher in Huandoy, the highest grain quality was with Amurskaja 75 concerning the grain protein content.

The grain protein content is one of the most important quality parameters in cereals. The findings of ours' and others' suggest that there may have a strong interconnection between spike N metabolism and the grain protein concentrations.

4.3 Intraspecific variation in plant growth parameters, gas exchange measurements and C and N isotopic signatures

The differences in gas exchange parameters support the site-specific, genotypic, and temporal variation of plant metabolic processes already noted. In most cases, the highest *A* was at 14-dpa both in wheat pericarps and flag leaves (Figure 1). With few exceptions, the expression of genes related to PEPC and NADP-ME was also higher in early reproductive stages (between heading and 14-dpa) (Table 3 and 4). The presence of much higher N concentrations in pericarps and flag leaves during early to mid-reproductive stages is consistent with the photosynthetic rates (Figure 1 and 4).

In photosynthetic organs, C_i /C_a is an indication of the CO_2 concentration at the intercellular air spaces in comparison to that of the atmosphere (Feng, 1998). In our study, the C_i/C_a was 0.62–0.85 for both wheat spikes and flag leaves (Figure 1). Although there were organ-specific and temporal variations, the range is consistent with organs performing C_3 photosynthesis.

There are two naturally occurring C isotopes in the atmosphere: ^{12}C, which is the most abundant (98.9%) and ^{13}C (1.1%). During photosynthetic carbon fixation, along with underlying photosynthetic pathway, plants discriminate one stable C isotope over another (Caemmerer et al., 2014). Further, a strong positive correlation between C isotope discrimination values (C isotopic signatures) and C_i /C_a has been reported (Farquhar et al., 1982, Caemmerer et al., 2014). The $\delta^{13}C$ signatures of wheat spikes

(dry matter) were -27% to -31% while flag leaves had values of -28% to -31%. Except for Amurskaja 75 at 14-dpa, we did not observe a statistically significant difference for $\delta^{13}C$ between wheat pericarps and flag leaves (Table 7). Thus we infer that the wheat pericarps and flag leaves may both be performing C_3 photosynthesis. However, determining the photosynthetic pathway by looking at the C isotopic signature of plant dry matter may be inaccurate, as part of dry matter of the considered plant organ is derived from the C fixation of other photosynthetic organs rather than the current photosynthates of a particular organ.

Although there are some limitations, C isotopic signature of plant dry matter reveals information about the changes in chemical, physical, and metabolic processes of photosynthesis (Farquhar et al., 1982). In general, C isotopic signature of C_3 organs varies between -21% and -35% while in C_4, the isotopic signature of C varies between -9% and -20% (Badeck et al., 2005). Further various other factors related to plant respiration also affect the C isotopic signature of plant dry matter (Caemmerer et al., 2014). Therefore, to get a better understanding of the underlying carbon metabolism of plant organs, along with C isotopic signatures, other methods such as gas exchange measurements, chemical, and molecular assays are needed.

4.4 Growth Parameters

Not only grain biomass but also total biomass may be important in breeding programs (Villegas et al., 2001). For example, a relationship has been reported between plant total biomass and grain yield in bread wheat during anthesis (Teulat et al., 1997, Villegas et al., 2001). Consistent with this proposition, we observed a moderate positive correlation between TB and SD ($r = 0.65$, $P < 0.05$); however, there wasn't a positive correlation between the total photosynthetic area and the TB.

The SD among different growth stages gives a clue about the temporal variation of grain filling in wheat. In our study, the highest grain biomass accumulation was observed between 14-dpa and 30-dpa (Figure 2), which is consistent with the results of Jenner et al. (1991). Finally, to get an overall understanding of plant C and N metabolism, intense phenotyping along with molecular and biochemical analysis is increasingly important.

5. Conclusion

We found no strong evidence for site-specific C_4 photosynthesis in wheat; however, genotypic temporal and site-specific variations in the expression key C_4 pathway genes were observed. Further, we reported the site-specific, genotypic and temporal changes in the mechanisms of C and N metabolism. Our results support the idea the that metabolic processes of wheat spikes may play a significant role in grain filling and in grain protein content.

Conflict of interest

The authors declare that this study was conducted in the absence of any commercial relationships that could lead to any potential conflict of interest.

Acknowledgment

This work was supported by the University of Southern Queensland (USQ), Australia and the USQ Strategic Research Fund. PD is supported by a USQ International Stipend Research Scholarship and USQ International Fees Research Scholarship. Analysis of C and N isotopic signatures as supported by Motohiro Ito (Toyo University) and Yu Takahata (The Graduate University for Advanced Studies).

List of Figures

List of Tables and Supplementary Tables

Table.7. Comparison of N and C isotopic signatures and C and N atomic ratios between wheat pericarps and flag leaves. Abbreviations: $\delta^{15}N$, N isotopic signature; $\delta^{13}C$, C isotopic signature; C/N atomic ratio, atomic ratio of C and N; ns, not significant; *, *P <0.01*; ***, *P <0.001*.

Supplementary Table S1. Primer abbreviations, references and sequences.

Supplementary Table S2. Photosynthesis (*A*), stomatal conductance (*SC*) and the ratio between intercellular to ambient CO_2 concentrations of wheat pericarps and flag leaves of three wheat genotypes. Summary of multiple comparisons. Abbreviations: ns, not significant; **, $P < 0.01$; ***, $P < 0.001$.

Supplementary Table S3. Variation of photosynthesis (*A*), stomatal conductance (*SC*) and the ratio between intercellular to ambient CO_2 concentrations between wheat pericarps and flag leaves of different growth stages. Summary of multiple comparisons. Abbreviations: ns, not significant; **, $P< 0.01$; ***, $P < 0.001$.

Supplementary Table S4. Multiple comparisons of selected genes of the C_4 pathway between different wheat genotypes. Summary of multivariate analyses. Abbreviations: ns, not significant; *, $P < 0.05$; **, $P < 0.01$; ***, $P < 0.001$.

Supplementary Table S5. Multiple comparisons of selected genes of the C_4 pathway between different growth stages in wheat. Summary of multivariate analyses. Abbreviations:14-dpa, fourteen days post-anthesis; 30-dpa, thirty days post-anthesis; ns, not significant; *, $P < 0.05$; **, $P < 0.01$; ***, $P < 0.001$.

Supplementary Table S6. Multiple comparisons of selected genes of the C_4 pathway between different wheat genotypes. Summary of multivariate analyses. Abbreviations: ns, not significant; *, $P < 0.05$; **, $P < 0.01$; ***, $P < 0.001$.

Supplementary Table S7. Multiple comparisons of selected genes of the C_4 pathway between different growth stages in wheat. Summary of multivariate analyses. Abbreviations: 3-dpa, three days post-anthesis; 14-dpa, fourteen days post-anthesis; 30-dpa, thirty days post-anthesis; ns, not significant; *, P <0.05; **, P <0.01; ***, P <0.001.

Supplementary Table S8. Multiple comparisons of selected genes of N metabolism between different wheat genotypes. Summary of multivariate analyses. Abbreviations: ns, not significant; *, P <0.05; **, P <0.01; ***, P <0. 001.

Supplementary Table S9. Multiple comparisons of selected genes of N metabolism between different growth stages in wheat. Summary of multivariate analyses. Abbreviations:14-dpa, fourteen days post-anthesis; 30-dpa, thirty days post-anthesis; ns, not significant; *, P <0.05; **, P <0.01; ***, P <0.001.

Supplementary Table S10. Photosynthesis-related physiological traits of wheat pericarps and flag leaves of three wheat genotypes at different growth stages. Summary of multiple comparisons. Abbreviations: ns, not significant; **, P <0.01; ***, P <0.001; SPA, photosynthetic spike area; FPA, flag leaf photosynthetic area; LPA, photosynthetic area of the total leaves; TPA, total photosynthetic area; SAI (transformed), spike area index.

Supplementary Table S11. Photosynthesis-related physiological traits of wheat pericarps and flag leaves of three wheat genotypes at different growth stages. Summary of multiple comparisons. Abbreviations: ns, not significant; **, P <0.01; ***, P <0.001; SPA, photosynthetic spike area; FPA, flag leaf photosynthetic area; LPA, photosynthetic area of the total leaves; TPA, total photosynthetic area; SAI, spike area index.

Supplementary Table S12. Growth-related physiological traits at different growth stages. Results of multiple comparisons. Abbreviations: ns, not significant; ***, *P* <0.001; SD, spike dry weight; TB, total biomass; HI, harvest index; TH, total harvest.

Supplementary Table S13. Growth-related physiological traits of wheat genotypes. Results of multiple comparisons are shown. Abbreviations: ***, *P* <0. 001; Hu, Huandoy; Am, Amurskaja 75; Gr, Greece 25; SD, spike dry weight; TB, total biomass; HI, harvest index; TH, total harvest.

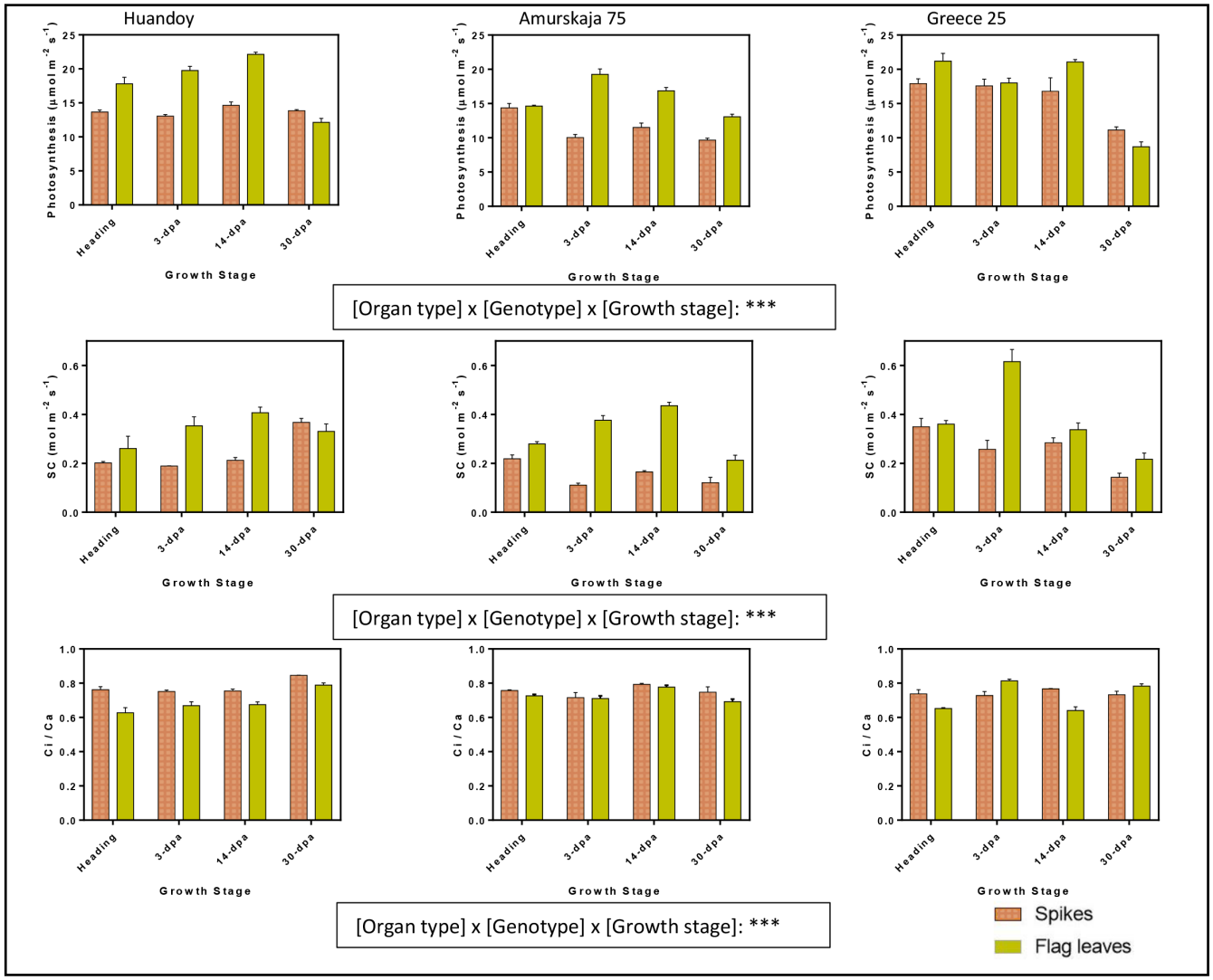
Huandoy
Amurskaja 75
Greece 25
Photosynthesis (µmol m-2 s-1)
SC (mol m-2 s-1)
Ci / Ca
Heading
3-dpa
14-dpa
30-dpa
Growth Stage
[Organ type] x [Genotype] x [Growth stage]: ***
[Organ type] x [Genotype] x [Growth stage]: ***
[Organ type] x [Genotype] x [Growth stage]: ***
Spikes
Flag leaves

Figure 1

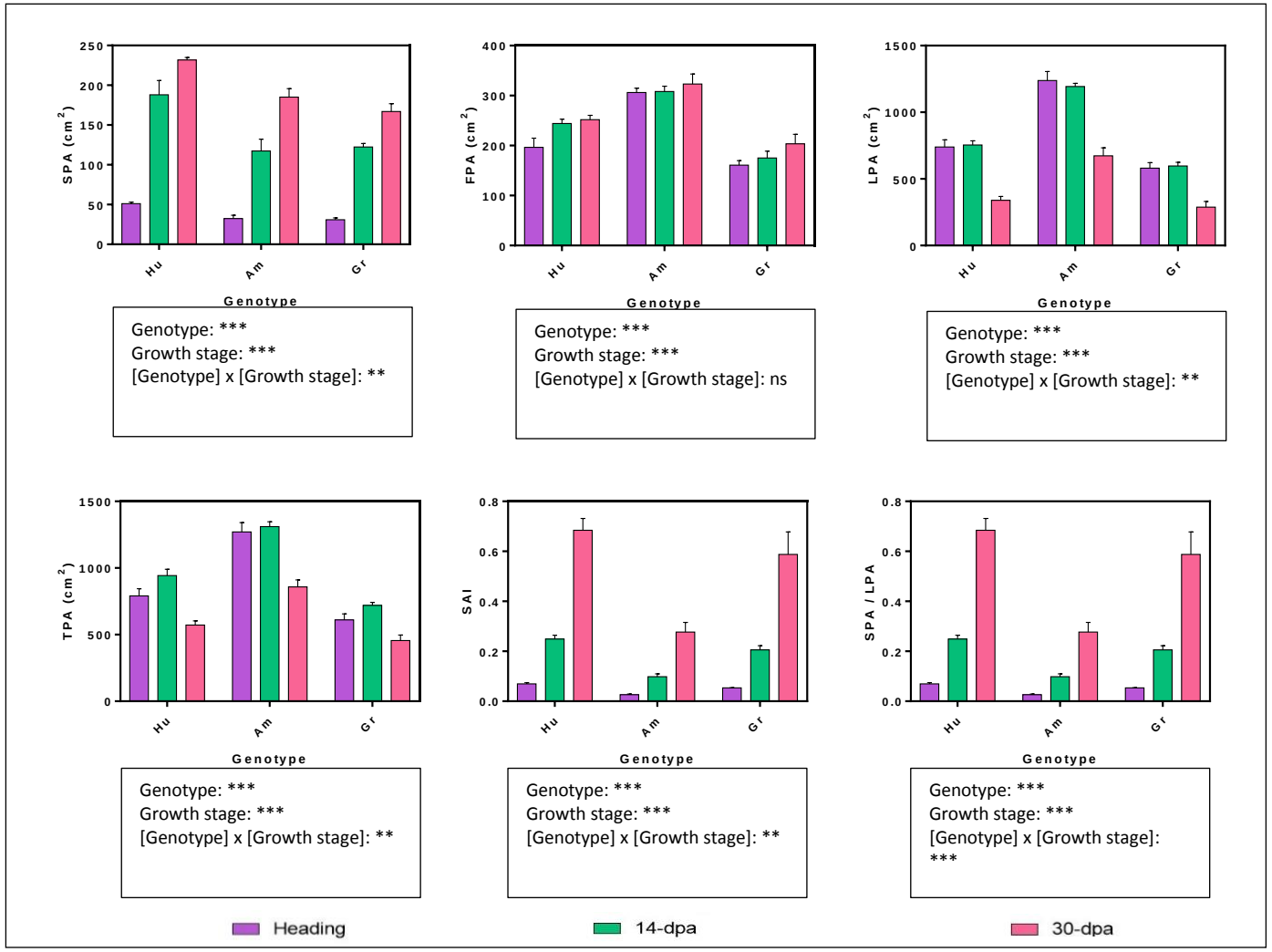
SPA (cm²)
Hu
Am
Gr
Genotype
Genotype: ***
Growth stage: ***
[Genotype] x [Growth stage]: **
FPA (cm²)
Genotype: ***
Growth stage: ***
[Genotype] x [Growth stage]: ns
LPA (cm²)
Genotype: ***
Growth stage: ***
[Genotype] x [Growth stage]: **
TPA (cm²)
Genotype: ***
Growth stage: ***
[Genotype] x [Growth stage]: **
SAI
Genotype: ***
Growth stage: ***
[Genotype] x [Growth stage]: **
SPA / LPA
Genotype: ***
Growth stage: ***
[Genotype] x [Growth stage]: ***
Heading
14-dpa
30-dpa

Figure 2

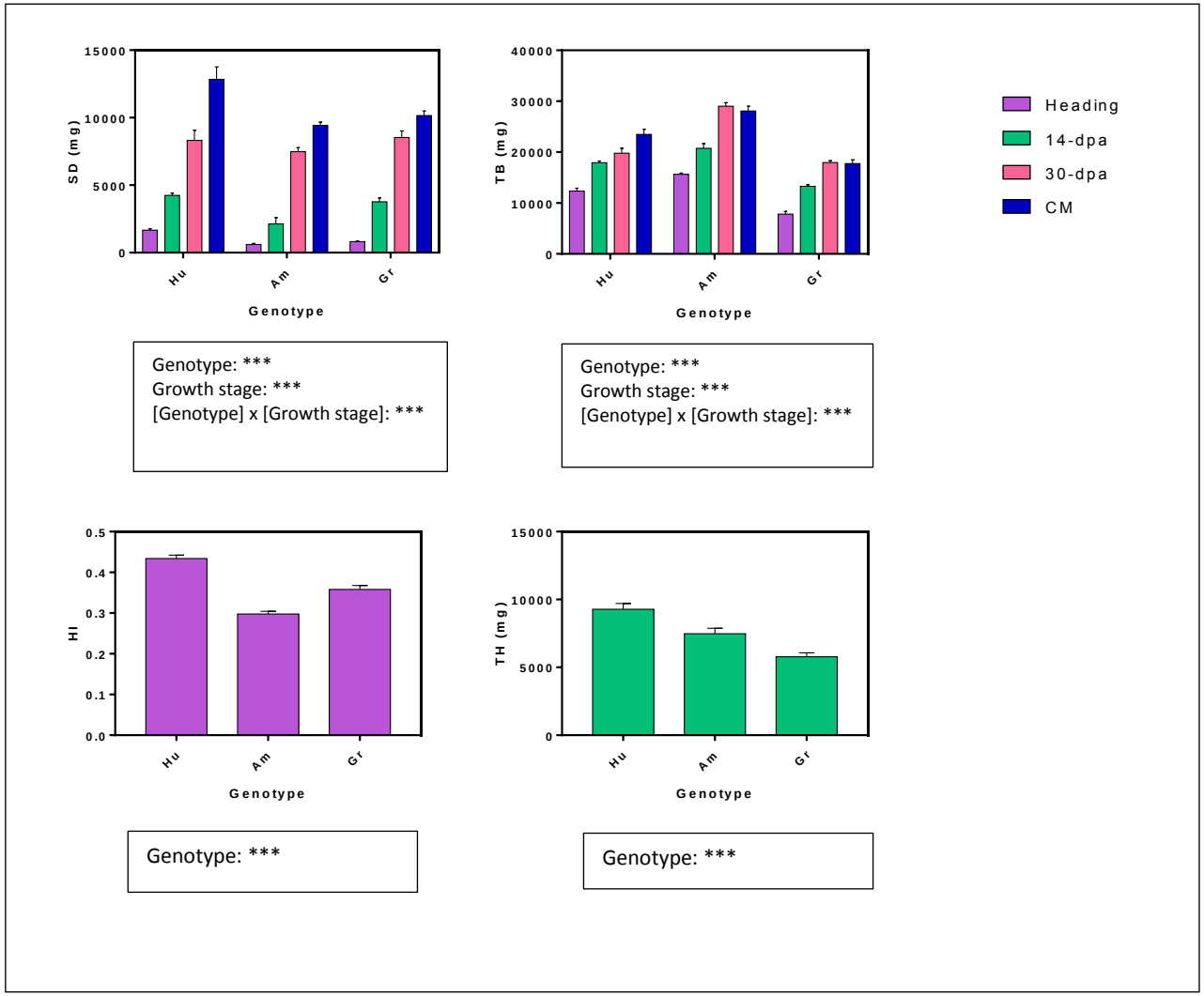
SD (mg)
15000
10000
5000
0
Hu
Am
Gr
Genotype
Genotype: ***
Growth stage: ***
[Genotype] x [Growth stage]: ***
TB (mg)
40000
30000
20000
10000
0
Hu
Am
Gr
Genotype
Genotype: ***
Growth stage: ***
[Genotype] x [Growth stage]: ***
Heading
14-dpa
30-dpa
CM
HI
0.5
0.4
0.3
0.2
0.1
0.0
Hu
Am
Gr
Genotype
Genotype: ***
TH (mg)
15000
10000
5000
0
Hu
Am
Gr
Genotype
Genotype: ***

Figure 3

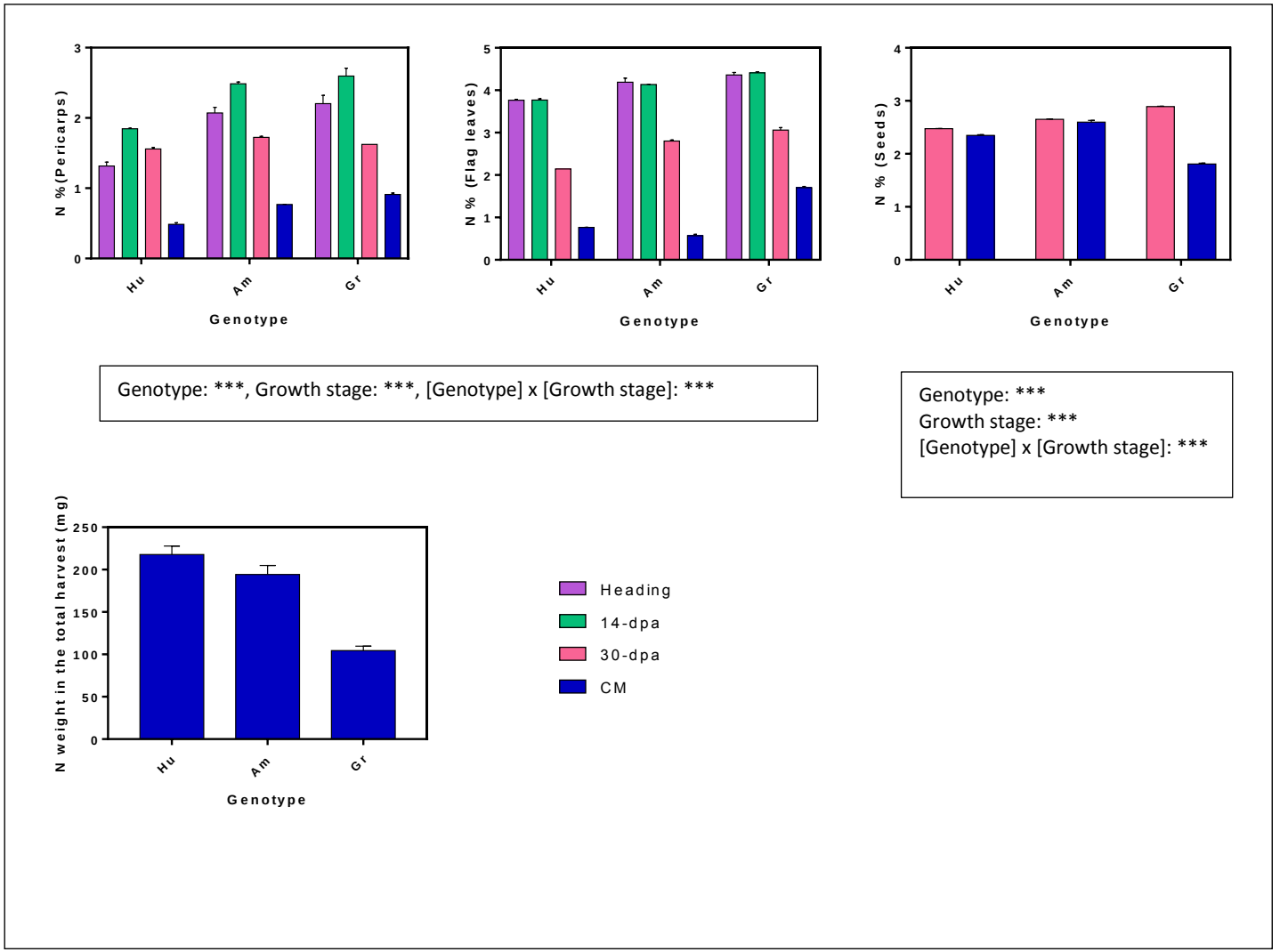
N %(Pericarps)
Hu
Am
Gr
Genotype
N % (Flag leaves)
Hu
Am
Gr
Genotype
N % (Seeds)
Hu
Am
Gr
Genotype
Genotype: ***, Growth stage: ***, [Genotype] x [Growth stage]: ***
Genotype: ***
Growth stage: ***
[Genotype] x [Growth stage]: ***
N weight in the total harvest (mg)
Hu
Am
Gr
Genotype
Heading
14-dpa
30-dpa
CM

Figure 4

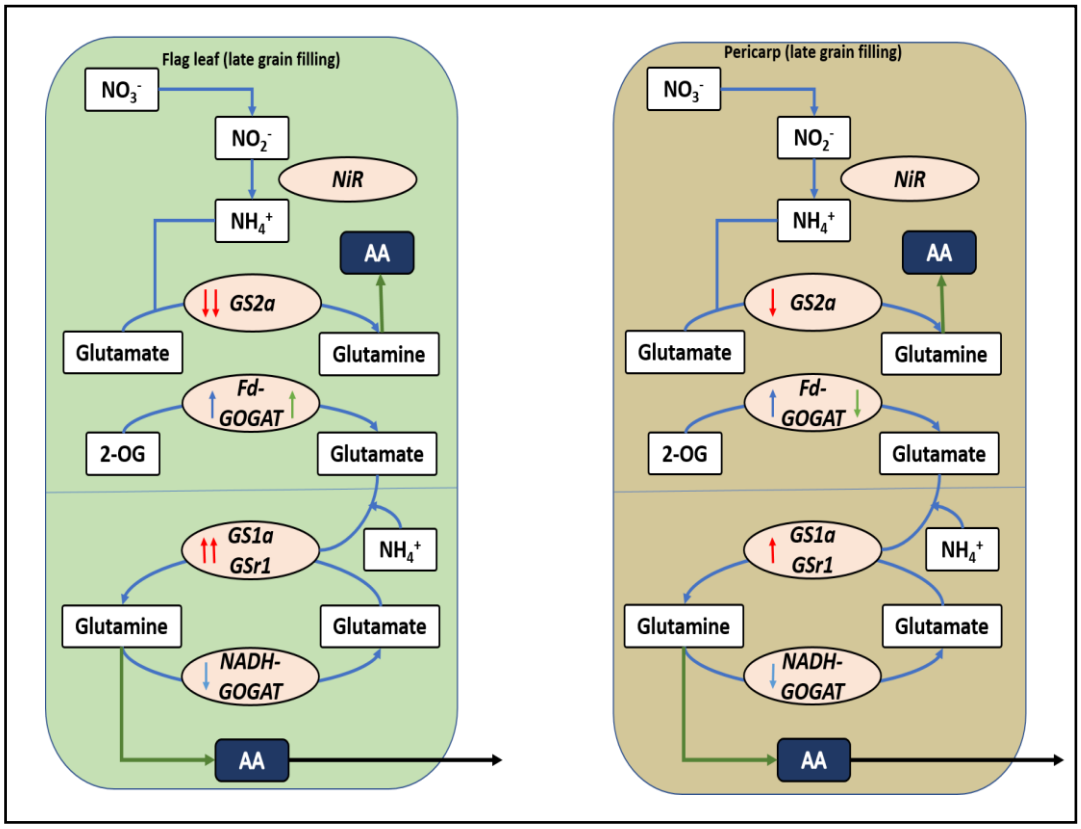
Flag leaf (late grain filling)
NO3-
NO2-
NiR
NH4+
AA
GS2a
Glutamate
Glutamine
Fd-GOGAT
2-OG
Glutamate
GS1a GSr1
NH4+
Glutamine
Glutamate
NADH-GOGAT
AA
Pericarp (late grain filling)
NO3-
NO2-
NiR
NH4+
AA
GS2a
Glutamate
Glutamine
Fd-GOGAT
2-OG
Glutamate
GS1a GSr1
NH4+
Glutamine
Glutamate
NADH-GOGAT
AA

Figure 5

Table 1.

Category	Trait	Growth stage/s of data collection
Growth-related traits	Total spike weight (SD) Total biomass (TB)	Heading, 14-dpa, 30-dpa and Complete maturity (CM)
Photosynthesis-related traits	Photosynthetic area: total spikes (SPA) Photosynthetic area: total flag leaves (FPA) Photosynthetic area: total leaves (LPA) Photosynthetic area: total (TPA) Spike area index (SAI) Ratio between total spike area and total leaf area (SPA/LPA)	Heading, 14-dpa and 30-dpa
Harvest-related traits	Harvest index (HI) Total harvest (TH)	CM

Table 2.

Gene	Individual effect			Interaction effect			
	Genotype	Growth stage	Organ	Genotype X Growth stage	Genotype X Organ	Growth stage X Organ	Genotype X Growth stage X Organ
TaNADP-ME_1	ns	***	ns	**	**	***	***
TaPEPC_5	**	ns	***	ns	**	ns	*
TaMDH_7	***	ns	**	**	***	ns	**
TaPPDK_1α	***	ns	***	**	***	ns	***
TaNADP-1AS	ns	ns	*	ns	ns	ns	ns
TaNADP-1BS	***	*	**	*	**	***	ns
TaNADP-1DS	ns	***	***	*	ns	ns	**
TaPEPC-5AL	**	ns	**	*	**	*	ns
TaPEPC-5BL	ns	*	***	**	***	**	ns
TaPEPC-5DL	ns	*	***	*	**	*	ns
TaPPDK-1αAL	***	***	***	***	***	***	***
TaPPDK-1αBL	*	***	***	***	***	***	***
TaPPDK-1αDL	ns	**	***	*	***	*	*

Table 3.

Gene	Growth Stage	Mean Relative Expression: Pericarps			Mean Relative Expression: Flag Leaves		
		Hu	Am	Gr	Hu	Am	Gr
TaNADP-ME_1	Heading	1.22	2.57	2.63	2.15	0.66	0.98
	14-dpa	0.95	0.68	0.88	1.41	1.46	0.57
	30-dpa	0.81	1.60	0.66	0.86	2.06	1.80
TaPEPC_5	Heading	1.70	3.65	3.17	6.62	1.76	5.97
	14-dpa	2.70	1.73	3.38	4.61	3.97	7.03
	30-dpa	2.11	3.13	1.92	4.52	3.77	4.26
TaMDH_7	Heading	0.18	0.65	1.31	0.63	0.45	2.33
	14-dpa	0.53	0.52	1.42	1.05	1.02	1.57
	30-dpa	0.57	1.72	0.69	1.13	0.62	2.00
TaPPDK_1α	Heading	0.89	0.74	1.80	5.65	1.17	4.39
	14-dpa	2.23	0.41	1.93	5.27	1.59	3.44
	30-dpa	1.36	1.35	1.06	2.88	2.02	5.90

Table 4.

Gene	Growth Stage	Mean Relative Expression: Pericarps			Mean Relative Expression: Flag Leaves		
		Hu	Am	Gr	Hu	Am	Gr
TaNADP-1AS	Heading	0.04	0.15	0.01	0.00	0.02	0.04
	14-dpa	0.03	0.00	0.02	0.00	0.01	0.01
	30-dpa	0.03	0.03	0.06	0.00	0.00	0.00
TaNADP-1BS	Heading	27.56	25.09	12.53	7.41	6.98	6.31
	14-dpa	14.92	17.76	8.33	9.12	28.97	11.62
	30-dpa	12.29	16.17	5.74	5.62	12.21	11.43
TaNADP-1DS	Heading	0.06	0.18	0.10	0.13	0.15	0.38
	14-dpa	0.01	0.01	0.02	0.12	0.12	0.05
	30-dpa	0.02	0.01	0.02	0.02	0.18	0.06
TaPEPC-5AL	Heading	1.96	1.53	1.30	1.35	1.08	2.19
	14-dpa	1.28	1.40	1.71	1.22	2.32	3.71
	30-dpa	1.20	1.65	1.31	1.19	2.97	2.97
TaPEPC-5BL	Heading	2.98	1.69	1.17	1.68	1.68	2.16
	14-dpa	1.83	1.89	1.38	1.74	4.08	4.96
	30-dpa	2.09	2.02	0.96	2.43	3.50	2.60
TaPEPC-5DL	Heading	2.48	1.95	1.31	2.69	2.79	2.29
	14-dpa	1.78	2.32	1.52	2.54	3.83	6.16

	30-dpa	**2.17**	**2.29**	**1.12**	**2.27**	**2.78**	**3.14**
	Heading	**0.08**	**0.14**	**0.07**	**0.43**	**0.17**	**0.14**
TaPPDK-1αAL	**14-dpa**	**0.25**	**0.26**	**0.22**	**0.17**	**0.35**	**0.11**
	30-dpa	**0.30**	**0.45**	**0.37**	**1.73**	**7.62**	**32.35**
	Heading	**4.27**	**12.16**	**6.31**	**21.06**	**21.00**	**15.41**
TaPPDK-1αBL	**14-dpa**	**10.63**	**9.05**	**11.84**	**14.51**	**18.75**	**12.69**
	30-dpa	**14.81**	**7.59**	**8.03**	**26.46**	**42.15**	**69.91**
	Heading	**10.82**	**13.33**	**9.29**	**22.03**	**19.44**	**29.88**
TaPPDK-1αDL	**14-dpa**	**26.34**	**23.00**	**11.64**	**25.90**	**32.22**	**26.49**
	30-dpa	**19.78**	**15.64**	**11.32**	**23.55**	**34.06**	**59.19**

Table 5.

Gene	Individual effect			Interaction effect			
	Genotype	Growth stage	Organ	Genotype X Growth stage	Genotype X Organ	Growth stage X Organ	Genotype X Growth stage X Organ
Fd-GOGAT	**	**	***	ns	*	**	*
NiR	***	***	***	***	***	***	***
GS2a	*	***	***	**	ns	***	***
GS2b	**	***	ns	*	ns	**	ns
NADH-GOGAT	***	ns	*	ns	ns	**	***
GS1a	*	***	***	ns	ns	***	ns
GSR1	*	***	*	***	**	***	***

Table 6.

Gene	Stage	Mean Relative Expression: Pericarps			Mean Relative Expression: Flag Leaves		
		Hu	Am	Gr	Hu	Am	Gr
FD-Gogat	Pre A	7.10	13.35	8.27	40.60	26.06	32.50
	14dpa	8.11	5.50	7.28	27.59	33.77	14.23
	30dpa	10.30	5.36	5.42	53.62	37.20	31.47
NIR	Pre A	0.53	0.30	0.19	5.07	1.62	3.53
	14dpa	0.46	0.51	0.39	2.67	4.83	1.64
	30dpa	1.23	1.43	0.30	4.43	14.76	2.36
GS2A	Pre A	17.97	27.46	24.40	29.22	19.21	36.05
	14dpa	10.21	5.58	6.43	16.90	43.19	20.79
	30dpa	5.20	7.75	7.56	7.37	8.93	4.92
GS2B	Pre A	0.11	0.21	0.24	0.12	0.11	0.19
	14dpa	0.03	0.04	0.06	0.07	0.12	0.11
	30dpa	0.05	0.04	0.06	0.05	0.06	0.03
NADH-Gogat	Pre A	0.88	2.23	1.84	0.45	0.73	0.61
	14dpa	0.68	1.22	2.31	0.51	3.05	0.69
	30dpa	1.11	1.89	1.17	0.37	1.90	2.09
GS1A	Pre A	0.64	2.62	2.88	7.86	6.02	2.63
	14dpa	2.92	4.28	5.66	10.09	13.46	7.03
	30dpa	11.20	7.50	4.70	49.31	50.20	38.73
GSR1	Pre A	1.41	1.08	1.32	0.86	0.67	1.09
	14dpa	2.39	1.73	1.51	1.53	1.45	0.90
	30dpa	1.90	1.46	1.31	1.82	3.05	7.37

Table 7.

Variety	Growth Stage	Comparison between wheat pericarps and flag leaves		
		$\delta^{15}N$	**$\delta^{13}C$**	**C/N atomic ratio**
Huandoy	Heading	*****	ns	***
	14-dpa	*******	ns	***
Amurskaja 75	Heading	*******	***	***
	14-dpa	*******	ns	***
Greece 25	Heading	*******	***	***
	14-dpa	*****	ns	***

Supplementary Table S1.

Primer abbreviation	Sequence (5'------3')	Metabolism	Reference
NiR	F: AACCTCCTCTCCTCCTACATCA R: CCTAGGAAGGTTGGTGATGGC	N metabolism	Vicente et al, 2015
Fd-GOGAT	F: CGGCAATGGAGGCTGAGCAACA R: TGAGCCTGCTCGATGGTCACTGT		
GS2a	F: CTCATGGTGTGTTGCGAACC R: GGTCCTCCAGGTATCCTTTGC		
GS2b	F: TGAAGGAAACGAGCGGAGAC R: CTCGCCCCACACGAATAGAG		
NADH-GOGAT	F: GCCATTGAATCAGTTCCAGGGCCAC R: GCCAGCACCTGAGCTTTCCTGATG		
GS1a	F: AGGTCATCGTGGATGCCGTGGA R: TTTGCGACGCCCCAGCTGAA		
GSr1	F: AAGGGCTACTTCGAGGACCGCA R: ATGATCTGGCGGCGGTAGGCAT		
TaPEPC_5	F: CAGGGTGAAGTTATCGAGCAG R: ACTTGGCTTTCTCTTGGATGG	C4 pathway	Bachir et al. 2017
TaNADP-ME _1	F: CTCTACATCAGCCTCAAGGAC R: CGTTGAGCAATGTCTCGTTG		
TaPPDK_1α	F: CAGGCTTGGTATTTCGTATC R: CTGCTCTGCTATCTCATCT		
TaMDH_7	F: CGATTGCTGCTGAGATTC R: CAGCGTTCTGTATCCTCT		
TaPEPC_5AL	F: TGCTGTGGGCCTTGTATC R: CAAGTACGACTGACAAACAGATTAG	Genome specific C_4 pathway	Bachir et al. 2017
TaPEPC_5BL	F: GTATCTCAGCGGATGTTGCT R: GGAGTACATTGTTAAGTGTTCCAAG		
TaPEPC_5DL	F: GTATCTCAGCGGATGTTGCT R: CACCCAATCCAGTACATTGTTA		
TaNADP_1AS	F: CTGCCCTCCATGTTCGTTT R: AGAGACAGAGAGAGGGAGAGA		
TaNADP_1BS	F: TTCAGCGACGCAACCTAAA R: ACCTCGACACGGATAGACA		
TaNADP_1DS	F: CCGACCACCTTCTTCAATCC R: TCGTTCGTTACCCATGACAAA		
TaPPDK_1αAL	F: CAACGACACCGACCTCAT R: ATACTTGTTCGCTCTCGGACT		
TaPPDK_1αBL	F: ACCGACCTCACTGCCAAT R: TGTACTTGTTCGCTCTCGGA		
TaPPDK_1αDL	F: GTTGGTGCATCTGGTGAAGATA R: GCACAGATAATCGCCACCTT		

TaActin-F	F: TTGCTGACCGTATGAGCAAG R: ACCCTCCAATCCAGACACTG		Bachir et al. 2017
TaSand-F	F: TGCCTTGCCCATAAGAAATC R: GTGCGGACCAGTTGCTTTAT	Housekeeping genes	

Supplementary Table S2.

Genotype Comparison		**Traits**		
Genotype a	**Genotype b**	**A**	**SC**	**C_i/C_a**
Huandoy	Amurskaja 75	***	**	ns
Huandoy	Greece 25	*	ns	ns
Amurskaja 75	Greece 25	***	***	ns

Supplementary Table S3.

Growth stage comparison		Traits		
Growth stage a	**Growth stage b**	**A**	**SC**	**Ci/Ca**
Heading	3-dpa	ns	*	ns
Heading	14-dpa	ns	ns	ns
Heading	30-dpa	***	*	***
3-dpa	14-dpa	*	ns	ns
3-dpa	30-dpa	***	***	**
14-dpa	30-dpa	***	***	*

Supplementary Table S4.

Genotype Comparison		Genes			
Genotype a	**Genotype b**	***TaNADP-ME_1***	***TaPEPC_5***	***TaMDH_7***	***TaPPDK_1α***
Huandoy	Amurskaja 75	ns	ns	ns	***
Huandoy	Greece 25	ns	ns	***	ns
Amurskaja 75	Greece 25	ns	**	***	***

Supplementary Table S5.

Growth stage Comparison		Genes			
Growth stage a	**Growth stage b**	***TaNADP-ME_1***	***TaPEPC_5***	***TaMDH_7***	***TaPPDK_1α***
Heading	14-dpa	***	ns	ns	ns
Heading	30-dpa	**	ns	ns	ns
14-dpa	30-dpa	*	ns	ns	ns

Supplementary Table S6.

Genotype		Genes								
Genotype a	**Genotype b**	***TaNADP-1AS***	***TaNADP-1BS***	***TaNADP-1DS***	***TaPEPC-5AL***	***TaPEPC-5BL***	***TaPEPC-5DL***	***TaPPDK-1αAL***	***TaPPDK-1αBL***	***TaPPDK-1αDL***
Huandoy	Amurskaja	ns	**	ns	ns	ns	ns	ns	ns	ns
Huandoy	Greece	ns	ns	ns	**	ns	ns	***	*	ns
Amurskaja	Greece	ns	***	ns	ns	ns	ns	**	ns	ns

Supplementary Table S7.

Growth stage		Genes								
Growth stage a	**Growth stage b**	***TaNADP-1AS***	***TaNADP-1BS***	***TaNADP-1DS***	***TaPEPC-5AL***	***TaPEPC-5BL***	***TaPEPC-5DL***	***TaPPDK-1αAL***	***TaPPDK-1αBL***	***TaPPDK-1αDL***
Heading	14-dpa	ns	ns	***	ns	*	ns	ns	ns	*
Heading	30-dpa	ns	ns	***	ns	ns	ns	***	***	**
14-dpa	30-dpa	ns	*	ns	ns	ns	ns	***	***	ns

Supplementary Table S8.

Genotype		Genes						
Genotype a	**Genotype b**	***FD-GOGAT***	***NiR***	***GS2a***	***GS2b***	***NADH-GOGAT***	***GS1a***	***GSR1***
Huandoy	Amurskaja	ns	***	*	ns	***	ns	ns
Huandoy	Greece	**	*	ns	**	***	ns	ns
Amurskaja	Greece	ns	***	ns	ns	*	ns	*

Supplementary Table S9.

Growth stage		Genes						
Growth stage a	**Growth stage b**	***FD-GOGAT***	***NiR***	***GS2a***	***GS2b***	***NADH-GOGAT***	***GS1a***	***GSR1***
Heading	14-dpa	*	ns	***	***	ns	ns	ns
Heading	30-dpa	ns	***	***	***	ns	***	***
14-dpa	30-dpa	**	***	***	ns	ns	***	***

Supplementary Table S10.

Genotype		Traits					
Genotype a	Genotype b	**SPA**	**FPA**	**LPA**	**TPA**	**SAI**	**SPA/LPA**
Huandoy	Amurskaja	***	***	***	***	***	***
Huandoy	Greece	***	***	***	***	**	**
Amurskaja	Greece	ns	***	***	***	***	***

Supplementary Table S11.

Genotype		Traits					
Genotype a	Genotype b	**SPA**	**FPA**	**LPA**	**TPA**	**SAI**	**SPA/LPA**
Heading	14-dpa	***	*	ns	**	***	***
Heading	30-dpa	***	***	***	***	***	***
14-dpa	30-dpa	***	*	***	***	***	***

Supplementary Table S12.

Growth stage comparison		Traits	
Growth stage a	Growth stage b	**SD**	**TB**
Heading	14-dpa	***	***
Heading	30-dpa	***	***
Heading	CM	***	***
14-dpa	30-dpa	***	***
14-dpa	CM	***	***
30-dpa	CM	***	ns

Supplementary Table S13.

Genotype		Traits	
Genotype a	Genotype b	**SD**	**TB**
Huandoy	Amurskaja	***	***
Huandoy	Greece	***	***
Amurskaja	Greece	***	***

References

Bachir, D. G., Saeed, I., Song, Q., Linn, T. Z., Chen, L. & Hu, Y.-G. J. J. O. P. P. 2017. Characterization and expression patterns of key C4 photosynthetic pathway genes in bread wheat (Triticum aestivum L.) under field conditions. 213**,** 87-97.

Badeck, F. W., Tcherkez, G., Nogues, S., Piel, C. & Ghashghaie, J. J. R. C. I. M. S. a. I. J. D. T. T. R. D. O. U. T. T. M. R. I. M. S. 2005. Post-photosynthetic fractionation of stable carbon isotopes between plant organs—a widespread phenomenon. 19**,** 1381-1391.

Bernard, S. M., Møller, A. L. B., Dionisio, G., Kichey, T., Jahn, T. P., Dubois, F., Baudo, M., Lopes, M. S., Tercé-Laforgue, T. & Foyer, C. H. J. P. M. B. 2008. Gene expression, cellular localisation and function of glutamine synthetase isozymes in wheat (Triticum aestivum L.). 67**,** 89-105.

Busch, F. A. & Farquhar, G. D. J. P. P. 2016. Poor evidence for C4 photosynthesis in the wheat grain. 172**,** 1357-1357.

Caemmerer, S. V., Ghannoum, O., Pengelly, J. J. & Cousins, A. B. J. J. O. E. B. 2014. Carbon isotope discrimination as a tool to explore C4 photosynthesis. 65**,** 3459-3470.

Campany, C. E., Medlyn, B. E. & Duursma, R. a. J. T. P. 2017. Reduced growth due to belowground sink limitation is not fully explained by reduced photosynthesis. 37**,** 1042-1054.

Crist, E., Mora, C. & Engelman, R. J. S. 2017. The interaction of human population, food production, and biodiversity protection. 356**,** 260-264.

Dehigaspitiya, P., Milham, P., Ash, G. J., Arun-Chinnappa, K., Gamage, D., Martin, A., Nagasaka, S. & Seneweera, S. J. P. 2019. Exploring natural variation of photosynthesis in a site-specific manner: evolution, progress, and prospects. 1-18.

Evans, J. R. & Santiago, L. S. J. F. P. B. 2014. PrometheusWiki gold leaf protocol: gas exchange using LI-COR 6400. 41**,** 223-226.

Farquhar, G. D., O'leary, M. H. & Berry, J. a. J. F. P. B. 1982. On the relationship between carbon isotope discrimination and the intercellular carbon dioxide concentration in leaves. 9**,** 121-137.

Feng, X. J. O. 1998. Long-term c i/c a response of trees in western North America to atmospheric CO 2 concentration derived from carbon isotope chronologies. 117**,** 19-25.

Foyer, C. & Zhang, H. 2011. *Annual Plant Reviews, Nitrogen Metabolism in Plants in the Post-genomic Era*, John Wiley & Sons.

Furbank, R. T., Quick, W. P. & Sirault, X. R. J. F. C. R. 2015. Improving photosynthesis and yield potential in cereal crops by targeted genetic manipulation: prospects, progress and challenges. 182**,** 19-29.

Furbank, R. T. J. J. O. E. B. 2011. Evolution of the C4 photosynthetic mechanism: are there really three C4 acid decarboxylation types? 62**,** 3103-3108.

Galmes, J., Kapralov, M. V., Andralojc, P. J., Conesa, M. À., Keys, A. J., Parry, M. A., Flexas, J. J. P., Cell & Environment 2014. Expanding knowledge of the R ubisco kinetics variability in plant species: environmental and evolutionary trends. 37**,** 1989-2001.

Gao, X., Wang, C., Cui, H. J. P. S. & Behavior 2014. Identification of bundle sheath cell fate factors provides new tools for C3-to-C4 engineering. 9**,** 319-27.

Haudry, A., Cenci, A., Ravel, C., Bataillon, T., Brunel, D., Poncet, C., Hochu, I., Poirier, S., Santoni, S., Glémin, S. J. M. B. & Evolution 2007. Grinding up wheat: a massive loss of nucleotide diversity since domestication. 24**,** 1506-1517.

Hibberd, J. M. & Covshoff, S. J. a. R. O. P. B. 2010. The regulation of gene expression required for C4 photosynthesis. 61**,** 181-207.

Jenner, C., Ugalde, T. & Aspinall, D. J. F. P. B. 1991. The physiology of starch and protein deposition in the endosperm of wheat. 18**,** 211-226.

Kamachi, K., Yamaya, T., Hayakawa, T., Mae, T. & Ojima, K. J. P. P. 1992. Vascular bundle-specific localization of cytosolic glutamine synthetase in rice leaves. 99**,** 1481-1486.

Kubis, A. & Bar-Even, A. J. J. O. E. B. 2019. Synthetic biology approaches for improving photosynthesis. 70**,** 1425-1433.

Masclaux-Daubresse, C., Daniel-Vedele, F., Dechorgnat, J., Chardon, F., Gaufichon, L. & Suzuki, A. J. a. O. B. 2010. Nitrogen uptake, assimilation and remobilization in plants: challenges for sustainable and productive agriculture. 105**,** 1141-1157.

Masclaux-Daubresse, C., Reisdorf-Cren, M., Pageau, K., Lelandais, M., Grandjean, O., Kronenberger, J., Valadier, M.-H., Feraud, M., Jouglet, T. & Suzuki, A. J. P. P. 2006. Glutamine synthetase-glutamate synthase pathway and glutamate dehydrogenase play distinct roles in the sink-source nitrogen cycle in tobacco. 140**,** 444-456.

Nesbitt, M. J. H. W. P. T. C., Underutilized, U. O. & Crops, N. 1996. From staple crop to extinction? The archaeology and history of hulled wheat. 1-100.

Rangan, P., Furtado, A. & Henry, R. J. J. S. R. 2016. New evidence for grain specific C 4 photosynthesis in wheat. 6**,** 31721.

Sage, R. F., Sage, T. L. & Kocacinar, F. J. a. R. O. P. B. 2012. Photorespiration and the evolution of C4 photosynthesis. 63**,** 19-47.

Tadesse, W., Halila, H., Jamal, M., El-Hanafi, S., Assefa, S., Oweis, T., Baum, M. J. J. O. E. B. & Sciences, A. 2017. Role of Sustainable Wheat Production to Ensure Food Security in the CWANA region. 5**,** S15-S32.

Taylor, S. H. & Long, S. P. J. P. T. O. T. R. S. B. B. S. 2017. Slow induction of photosynthesis on shade to sun transitions in wheat may cost at least 21% of productivity. 372**,** 20160543.

Teulat, B., Monneveux, P., Wery, J., Borries, C., Souyris, I., Charrier, A. & This, D. J. N. P. 1997. Relationships between relative water content and growth parameters under water stress in barley: a QTL study. 137**,** 99-107.

Van Bezouw, R. F., Keurentjes, J. J., Harbinson, J. & Aarts, M. G. J. T. P. J. 2019. Converging phenomics and genomics to study natural variation in plant photosynthetic efficiency. 97**,** 112-133.

Vialet-Chabrand, S., Matthews, J. S., Simkin, A. J., Raines, C. A. & Lawson, T. J. P. P. 2017. Importance of fluctuations in light on plant photosynthetic acclimation. 173**,** 2163-2179.

Vicente, R., Pérez, P., Martínez-Carrasco, R., Usadel, B., Kostadinova, S., Morcuende, R. J. P. & Physiology, C. 2015. Quantitative RT–PCR platform to measure transcript levels of C and N metabolism-related genes in durum wheat: transcript profiles in elevated [CO2] and high temperature at different levels of N supply. 56**,** 1556-1573.

Villegas, D., Aparicio, N., Blanco, R. & Royo, C. J. a. O. B. 2001. Biomass accumulation and main stem elongation of durum wheat grown under Mediterranean conditions. 88**,** 617-627.

Von Caemmerer, S. & Furbank, R. T. J. P. R. 2003. The C 4 pathway: an efficient CO 2 pump. 77**,** 191.

Wang, L., Czedik-Eysenberg, A., Mertz, R. A., Si, Y., Tohge, T., Nunes-Nesi, A., Arrivault, S., Dedow, L. K., Bryant, D. W. & Zhou, W. J. N. B. 2014. Comparative analyses of C 4 and C 3 photosynthesis in developing leaves of maize and rice. 32**,** 1158.

Wang, S., Tholen, D., Zhu, X. G. J. P., Cell & Environment 2017. C4 photosynthesis in C3 rice: a theoretical analysis of biochemical and anatomical factors. 40**,** 80-94.

Weissmann, S. & Brutnell, T. P. J. C. O. I. B. 2012. Engineering C4 photosynthetic regulatory networks. 23**,** 298-304.

White, A. C., Rogers, A., Rees, M. & Osborne, C. P. J. J. O. E. B. 2015. How can we make plants grow faster? A source–sink perspective on growth rate. 67**,** 31-45.

Xiong, D., Flexas, J., Yu, T., Peng, S. & Huang, J. J. N. P. 2017. Leaf anatomy mediates coordination of leaf hydraulic conductance and mesophyll conductance to CO2 in Oryza. 213**,** 572-583.

Yamori, W., Hikosaka, K. & Way, D. a. J. P. R. 2014. Temperature response of photosynthesis in C 3, C 4, and CAM plants: temperature acclimation and temperature adaptation. 119**,** 101-117.

CHAPTER 6

A COMPARATIVE PROTEOMIC ANALYSIS OF WHEAT (*Triticum aestivum* L.) AT MODERATELY HIGH TEMPERATURE

Wheat is amongst the most sensitive crop species to heat stress. Of the different metabolic processes, photosynthesis is the most affected by heat stress in wheat. Although flag leaf metabolism of wheat induced by moderately high temperatures has been well characterized changes in spike metabolism have not been well documented. Findings from previous studies (Chapter 4 and Chapter 5) demonstrated the importance of spike carbon and nitrogen metabolism in determining grain quality and quantity. In this study, a comparative proteomic analysis was conducted to determine the changes in key metabolic processes that govern grain quality and quantity using pericarps of two wheat genotypes under different temperature regimes. Biochemical and phenotypic data were used to support the molecular results. Genotypic variation in spike responses to high temperatures was detected. This study has been prepared as a research manuscript to be submitted to "Journal of Experimental Botany".

A comparative proteomic analysis of wheat (*Triticum aestivum* L.) at moderately high temperature

Prabuddha Dehigaspitiya[1], Anke Martin[1], Paul Milham[2], Gavin J. Ash[1], Dananjali Gamage[3], Kolin Harinda Rajapaksha[4], Saman Seneweera[1, 5]*

Affiliations

[1] Centre for Crop Health, University of Southern Queensland, Toowoomba, QLD, 4350, Australia.

[2] Hawkesbury Institute for the Environment, Western Sydney University, LB 1797 Penrith NSW, 2753, Australia.

[3] Department of Agricultural Biology, Faculty of Agriculture, University of Ruhuna, Sri Lanka.

[4] Department of Biochemistry and Genetics, La Trobe Institute for Molecular Life Science, La Trobe University, Bundoora, Australia.

[5] National Institute of Fundamental Studies, Hanthana Road, Kandy, Sri Lanka.

E-mail addresses:

Prabuddha Dehigaspitiya: Prabuddha.DehigaspitiyageDon@usq.edu.au
Anke Martin: Anke.Martin@usq.edu.au
Paul Milham: P.Milham@westernsydney.edu.au
Gavin Ash: Gavin.Ash@usq.edu.au
Dananjali Gamage: Dananjali@agbio.ruh.ac.lk
Kolin Harinda Rajapaksha: K.Rajapaksha@latrobe.edu.au

***Corresponding author**

Saman Seneweera (+61401879853)
Saman.Seneweera@usq.edu.au

Abbreviations

A – photosynthesis rate; AGB – above ground biomass; ANOVA - analysis of variance; *Ca* – ambient carbon dioxide concentration; CM – complete maturity; *Ci* - intercellular carbon dioxide concentration; DAH- days after heading; *Fd-GOGAT* - Putative ferredoxin-dependent glutamate synthase; dpa – days post anthesis; *g* – stomatal conductance; *GS1a* – Glutamine synthetase (cytosolic) – GS1; *GSr1* - Glutamine synthetase (cytosolic) – GS1; *GS2a* - Glutamine Synthetase (Plastidial) – GS2; *GS2b* - Glutamine Synthetase (Plastidial) – GS2; HI – harvest index; GW – grain weight; LPA – leaf photosynthetic area; MC - mesophyll cell; MDH - malate dehydrogenase; NADH nicotinamide adenine dinucleotide; NADH-GOGAT - Putative NADH-dependent glutamate synthase; NADP- nicotinamide adenine dinucleotide phosphate; NADP-ME - NADP-dependent malic enzyme; NiR - Ferredoxin Nitrite Reductase; PAR - photosynthetically active radiation; PAS – photosynthetic area of total spikes; PEPC- phosphoenolpyruvate carboxylase; PPDK - pyruvate orthophosphate dikinase; Rubisco - Ribulose 1,5-bisphosphate carboxylase/oxygenase; *rbcL* - Ribulose 1,5 –bisphosphate carboxylase/oxygenase (large sub unit); rbcS - Ribulose 1,5 – bisphosphate carboxylase/oxygenase (small sub unit); SAI – spike area index; SDM - spike dry weight of main tiller; SDT – total spike weight; *SPP1* - Sucrose Phosphate Phosphatase 1; *SPS1* - Sucrose Phosphate Synthase 1; *SUS1* - Sucrose Synthase type 1; TB – total biomass; TH – total harvest; TPA - total photosynthetic area; $\delta^{13}C$ - isotopic signatures of carbon; δ^{15} N - isotopic signatures of nitrogen.

Abstract

Knowledge of the changes in crop metabolism in response to moderately high temperatures is essential for crop improvements for future climates. Wheat is a globally important crop and changes in flag leaf of wheat induced by moderately high temperatures have been characterized. However, less attention has been paid to the changes in spike metabolism during grain filling in response to temperature. To address this knowledge gap, we observed the differences in vital metabolic processes in wheat spikes of two wheat genotypes (Huandoy and Amurskaja 75), with contrasting spike nitrogen (N) metabolism, grown at two temperature regimes after heading. A comparative proteomic analysis was carried out to elucidate the mechanistic responses in wheat spikes in response to moderately high temperatures. Key genes associated with Rubisco biosynthesis, sucrose metabolism, N metabolism, and the C_4 photosynthesis were investigated. In addition, isotopic signatures of carbon (C) and N, along with phenotyping, and spike gas exchange were investigated. At moderately high temperature, grain yield decreased by 60% in Huandoy and increased by 5% in Amurskaja 75. Proteomics analysis identified 458 proteins common to both genotypes, and of these, 12% and 23% were significantly affected in Huandoy and Amurskaja 75, respectively. These proteins belonged predominantly to the antioxidant defence system and upregulation was greater in Huandoy than in Amurskaja 75, indicating a greater heat stress of Huandoy than Amurskaja 75. The relative effect of moderately high temperature on upregulation of the antioxidant defence system between the genotypes is consistent with the effects on grain yield. Proteomic studies further revealed that along with antioxidant defence system, other metabolic processes such as photosynthesis, energy production and protein synthesis significantly affected at elevated temperatures. The finding that Amurskaja 75 is a relatively heat resistant variety makes it a candidate for crop improvement programs for future climate scenarios.

Keywords. Moderate heat stress, nitrogen assimilation, sucrose metabolism, spike photosynthesis

1. Introduction

Wheat (*Triticum aestivum* L.), accounts for one-third of the global annual cereal production, with an estimate of 735 million tons, which provides approximately 21% of the world's daily dietary protein intake (Shiferaw et al., 2013). With a projected population of 9.8 billion by 2050, demand for wheat is estimated to increase by at least 50% (Li et al., 2017). To cater for this demand, the annual yield increment of wheat has to be boosted by at least 1.6% compared to the current 1% (Tadesse et al., 2017). The green revolution sustained global food demand between the 1950s and 1980s. However, reaching future food production targets seems challenging without another breakthrough, as genetic yield potential of most of the current cereals has reached its maximum (Wang et al., 2017, Dehigaspitiya et al., 2019). The aim of nourishing the future world has become even more challenging because of the adverse effects of climate change, including water scarcity and global warming (Yadav et al., 2019). It has been estimated that mean atmospheric temperatures could increase by of 1.5–5.8°C by the end of this century (Farooq et al., 2011).

Since the middle of the 20th century, more severe floods, droughts and extreme temperature events have been recorded in many regions of the world (Reduction, 2013, Lesk et al., 2016). When these extreme weather events occur in agricultural areas they can cause significant damage to crop and food system infrastructure, threatening global food security (Lesk et al., 2016). In the recent past, nearly one-quarter of total damage and losses due to extreme climatic events were associated with the agricultural sector in the developing world (Lesk et al., 2016), and these disasters are likely to become a more frequent occurrence in the future. Increasing global temperatures have become a significant factor with the potential to destabilize the global food system (Asseng et al., 2015). However, the effects of extreme temperatures on crop production and the global food system are yet to be fully quantified (Lesk et al., 2016).

Adverse effects of heat stress on wheat include floret abortion, pollen sterility, tissue dehydration, lower CO_2 assimilation with decreased phenology, and increased photorespiration (Kaše and Čatský, 1984, Wahid et al., 2007, Farooq et al., 2011). Of these, photosynthesis is the biological process that is most sensitive to high temperatures (Wahid et al., 2007). Along with photosynthesis and sucrose metabolism, it may be worthwhile to investigate the metabolism of nitrogen (N), which is

responsible for grain protein, a prominent grain quality factor. Increases in the atmospheric temperature cause changes in membrane fluidity, metabolism, protein conformation and assembly of the cytoskeleton (Ruelland et al., 2010). Furthermore, those changes trigger adaptive metabolic processes at the cellular level to minimize heat stress damage, such as the expression of heat shock proteins (Wahid et al., 2007). The intensity of these protective measures may vary genotypically. Therefore, combining conventional morphological, physiological and molecular approaches with wheat proteomic investigations of the photosynthetic organs may reveal new knowledge about acclimation to elevated temperatures that could lead to the development of adaptive crop varieties for future climates.

Wheat is highly susceptible to high temperature or heat stress (Satorre and Slafer, 1999). According to Lesk et al. (2016), the reduction in the national cereal production in Canada was approximately 9–10% due to drought and extreme heat due not only to reduced yield per unit area, but also to reduced harvested area. Heat stress is a function of the rate and the magnitude of temperature increase, as well as the duration of exposure (Wahid et al., 2007). Asseng et al. (2011) reported that high temperatures alone could have large negative impacts on cropping systems. The influence of high temperature on wheat yield differs profoundly depending on the phenological stage, and is most damaging during the reproductive and grain filling phase (Farooq et al., 2011). The optimum temperatures for wheat heading and grain filling are 12–22°C, and prolonged exposure to higher temperatures can depress the yield (Tewolde et al., 2006, Farooq et al., 2011).

Metabolic activities of wheat pericarps may play a vital role in grain filling, yield, and grain quality (Rangan et al., 2016, Dehigaspitiya et al., 2019), and spikes may contribute 10–44% to the total grain photosynthates (Dehigaspitiya et al., 2019). This is particularly important when plant experience stresses like moderately high temperatures. To test the hypothesis that high temperatures/ moderately high temperatures affect the wheat pericarps, and the effect of moderately high temperature varies between genotypes, a comparative proteomic analysis was carried out. Besides, we studied the effect of elevated temperature on the photosynthesis, sucrose metabolism, and N assimilation in developing spikes of two wheat genotypes known to differ in spike N metabolism.

2. Materials and methods

2.1. Plant materials and growth conditions

Seeds of two bread wheat varieties (Huandoy and Amurskaja 75) were obtained from the Australian Grains Gene Bank, the Grains Innovation Park, Horsham, Victoria. These wheat genotypes had been used in transcriptomic studies for C_4-like gene expression by Rangan et al. (2016). Further, these two genotypes displayed significant differences in spike N metabolism (chapter 5). Experiments were conducted in identical controlled growth cabinets (PGC-165 105, Percival, USA) at the University of Southern Queensland, Toowoomba, Australia. The experiment was a complete randomized design with three replicates in a controlled environment. Five seeds were sown in each pot filled with 4 kg of loam soil. The pots were placed in growth cabinets and the initial environmental conditions were a 14-h photoperiod with a light intensity of 700–800 μmol m^{-2} s^{-1}, and temperatures of 22°C (day) and 12°C (night). The relative humidity inside the growth cabinets was maintained at ~70%. Two weeks after sowing seedlings were thinned to two uniform plants per pot. To minimize the location effect inside the growth cabinets, pots were randomized weekly. When heading commenced, pots were allocated to two separate growth cabinets: one remained at of 22°C (day) and 12°C (night) and the other at the elevated temperature (+8°C from the control). The environmental conditions of the two growth cabinets (heat treatment and control) are indicated in Supplementary Tables S1 and S2.

2.2. Gas exchange measurements

Before taking measurements, plants were allowed to stabilize in the dark for about 30 min by turning off the light source in the growth cabinet. Gas exchange measurements were made on wheat spikes ten days after heading (10-DAH). The measurements were carried out during the middle of the photoperiod using a portable photosynthesis system (LI-6400XT, LI-COR, USA) coupled with a transparent conifer chamber (LI-COR, Lincoln, NE, USA 6400-05). The reference CO_2 concentration and the airflow rate inside the conifer chamber were maintained at 400 μmol mol^{-1} and 500 μmol s^{-1} respectively. Spike temperature was maintained at the relevant growth temperature. Relative humidity inside the conifer chamber was maintained at 50–70%. The rate of photosynthesis (A), intercellular CO_2 concentration (C_i), stomatal conductance (g) and

the transpiration rate were measured for each genotype at each temperature regime. After gas exchange measurements, dark respiration was measured using a portable photosynthesis system (LI-6400XT, LI-COR, USA) coupled with a transparent conifer chamber (LI-COR, Lincoln, NE, USA 6400-05) with the same settings as in Chapter 3.

2.3. Phenotyping and N concentration

At 10-DAH and maturity (CM), a subset of plants grown at each heat regime was harvested and oven-dried at 65°C for 72 h to determine the dry weights of spikes of the main tiller (SDM), dry weights of flag leaves of the main tiller (FDM), seed dry weight of spike of the main tiller (SDSM), hundred grain weight, number of spikes per plant (SN), total spike weight (SDT), total above-ground biomass (AGB), total above ground biomass without spikes (ABWS), harvest index (HI).

2.4. Carbon and nitrogen isotopic signatures and atomic ratios

The oven-dried pericarps and flag leaves (2.3) were ground in a ball mill (Tissue Lyser II, QIAGEN, Australia) to a fine powder (~100 μm) and stored at -30°C prior to C and N analysis. Stable C and N isotope signatures ($\delta^{13}C$ and $\delta^{15}N$) and the C/N atomic ratios of the samples were determined using a mass spectrometer (MS) (IsoPrime100, IsoPrime, U.K.) coupled to a combustion analyser (Vario MICRO cube, Elementar, Germany) at the Tokyo university, Japan as described by (Le et al., 2017).

2.5. Sample collection for proteomics and gene expression analysis

At 10-DAH, wheat spikes of the main tiller were separated from the plant at the end of the 6^{th} hour of a total photoperiod of 12 h, placed into a chilled tube and quickly submerged in liquid N_2. Samples were stored at -80°C prior to total RNA and total soluble protein extraction.

2.6. Analysis of the pericarp proteome

2.6.1 Extraction and purification of total soluble proteins

For the total protein extraction, 300 mg of wheat pericarps were separated from the wheat spikes and ground using liquid N_2 and homogenized with 500 µL of modified RIPA solubilizing buffer [10 mM Tris-HCl (pH 8.0, 1mM EDTA, 0.5% sodium deoxycholate, 0.1% SDS, 140 mM NaCl 216 and 1 mM PMSF]. The homogenate was vortexed, sonicated three times, incubated at 37°C for 30 min on a mechanical shaker, then centrifuged at 18 000 rpm for 10 min. Proteins in the supernatant were quantified using microplate bicinchoninic acid (BCA) protein assay kit (Thermo Fisher Scientific, USA) according to the manufacturer's instructions. Desalting of the samples was conducted using Zeba spin columns according to the manufacturer's instructions.

2.6.2 Precipitation of total proteins

For protein precipitation, 400 µL of methanol was added to 100 µL of protein solution, mixed thoroughly and centrifuged at 9000 rpm for 10 sec. After adding100 µL of chloroform, samples were again centrifuged at 9000 rpm for 10 sec. Three-hundred µL of double-distilled H_2O was added to the mixture and again centrifuged at 9000 rpm for 1 min after which phase separation could be observed, i.e. the bottom chloroform phase, the middle protein phase, and the upper aqueous phase. After removing the upper aqueous phase, 300 µL of methanol was added, mixed thoroughly and centrifuged at 9000 rpm for 2 min to precipitate proteins. After removing the supernatant, the precipitated protein pellet was air-dried and used in proteomic analysis.

2.6.3 Proteome analysis

The extracted protein samples were analysed using liquid chromatography-mass spectrometry (LC-MS/MS) at the Comprehensive Proteomic Platform, La Trobe Institute for Molecular Science, La Trobe University, Australia, as described by (Lowe et al., 2015).

From the precipitated protein sample, 50 μg was resuspended in 100 μL of 8 M urea and allowed to reduce for 5 h after adding 1 μL of 200 mM tris (2-carboxyethyl) phosphine (TCEP). Then, 4 μL of 1 M iodoacetamide (IAA) was added to the mixture and alkylated for 1 h at 25°C in the dark. Duel-step trypsin digestion was performed by adding 1 μg of trypsin (Promega, Madison WI, USA) and 900 μL of 50 mM TRIS to the samples and retaining overnight at 37°C, followed by adding another 1 μg of trypsin and an additional 4-h incubation period at 37°C.

The solution of digested proteins was dried using SpeedVac centrifugation. Dried proteins were resuspended in 100 μL of 1% (v/v) formic acid centrifuged at 14 000 rpm for 2 min. Extraction was performed using Empore reverse-phase extraction disks (SDB-XC reversed-phase material, 3M) as described by (Ishihama et al., 2006), with the following modifications. Before the tryptic peptides were bound to the membrane, 50 μL of 80% (v/v) acetonitrile (ACN), 0.1% (w/v) and trifluoroacetic acid (TFA) were used to condition the membrane followed by washing with 50 μL of 0.1% TFA. The bound peptides were eluted by 50 μL 80% (v/v) ACN, 0.1% (w/v) TFA, and dried using a SpeedVac centrifuge.

For the LC-MS/MS analysis, 2 μg of dried peptides were taken and reformed into a final volume of 10 μL by adding 0.1% TFA and 2% ACN (buffer A). The solution was loaded into a trap column (C18 PepMap 100 μm i.d. × 2 cm trapping 276 columns, Thermo-Fisher Scientific) at a rate of 5 μL min^{-1} for 6 min before switching the pre-column in-line with the analytical column (Easy-Spray 75 μm i.d. × 50 cm, Thermo-Fisher Scientific). Starting from 5% of buffer B (0.1% formic acid, 80% ACN) and increasing to 60% over 300 min, the peptide separation was conducted at 250 nL min^{-1} using a linear CAN gradient with buffer A (0.1% formic acid, 2% ACN).

Data were acquired from Orbitrap Elite (Thermo-Fisher Scientific) in data-dependent acquisition mode and a m/z scan range of 300–1500 Da. Collision-induced dissociation (CID) MS/MS spectra were determined for the 20 most intense ions. Repeat count, duration, and exclusion list size was set at 1, 90 sec and 500, respectively for dynamic exclusion parameters with disabling the early expiration. The rest of the Orbitrap settings were as follows: MS scan at 120 000 resolution, maximum injection time 150 ms, automatic gain control (AGC) target 1×10^6, CID at 35% energy for a maximum injection time of 150 ms with AGT target of 5000. The Orbitrap Elite

functioned in dual analyser mode and MaxQuant software (version 1.6) was used for spectra analysis. Andromeda peptide search engine, combined with MaxQuant environment with *Triticum aestivum* proteome, downloaded from the UniProt database were used for protein identification and quantification.

2.7 Gene expression analysis

2.7.1 RNA extraction, quantification, and cDNA synthesis

Approximately 300 mg of wheat pericarps were ground using liquid N_2, and the ground samples were homogenized with 500 µL of Trizol® Reagent (Invitrogen, Thermo Fisher Scientific, USA) and 700 µL of TPS buffer [100 mM TRIS-HCl (pH 8), 10 mM EDTA and 1 M KCl]. RNA was extracted according to the manufacturer's instructions (Invitrogen, Thermo Fisher Scientific, USA). Extracted RNA was quantified using a Qubit 3 Fluorimeter (Invitrogen, Thermo Fisher Scientific, USA) as per the manufacturer's instructions. The concentration of each RNA sample was adjusted to 1 µg/µL. RNA samples were treated with DNaseI, Amplification Grade (Invitrogen, Thermo Fisher Scientific, USA) according to the manufacturer's instructions. cDNA (20 µL) was synthesized from each RNA sample using SensiFAST^{TM} cDNA synthesis kit (Catalogue No – Bio-65054, Bioline, UK) as per the manufacturer's instructions.

2.7.2 Primer Selection and expression analysis (qRT-PCRT)

Genome-specific primers of wheat, related to N metabolism, sucrose metabolism, Rubisco biosynthesis, and the C_4 pathway were identified from the published literature (Vicente et al., 2015, Bachir et al., 2017) (Supplementary Table S3). Gene specificity of those primers to *T. aestivum* L. was tested using the Primer-Blast option at the National Centre for Biotechnology Information (NCBI) website. Primers were sourced from Integrated DNA Technologies, Inc. (Integrated DNA Technologies Pty. Ltd, Singapore).

Gene expression was determined from the reactions carried out in 96-well plates using QuantStudio 3 quantitative, real-time PCR system (Applied Biosystems, Thermo Fisher Scientific, USA). The composition of the reaction mixture in a well was 4 µL of diluted cDNA, 4 µL of DEPC treated water, 10 µl of PowerUp™ SYBR™ Green

Master (Applied Biosystems from Thermo Fisher Scientific, USA), 1 µL of 10 mM reverse primer and 1 µL of 10 mM forward primer. The thermal cycler program was set as 95°C for 10 min, followed by 40 cycles of 95°C for 15 s, and 60°C for 1 min. LinRegPCR v2012.3 application software was used to calculate the efficiency of each primer. Gene expression was determined using the comparative threshold cycle [(C_t) $2^{-\Delta\Delta Ct}$] method.

2.8 Statistical analysis

Before analysis, normality of the data sets was determined, and the data sets that were not normally distributed were transformed. To determine the significance between treatments and genotypes, analysis of variance was carried out at a significance level of $P < 0.05$. Data analysis was conducted using SPSS statistical software version 23 (IBM, Armonk, NY, USA). Gene expression data were transformed into a $\log_2$ scale for normality. Statistical analysis of proteomics data was performed using the R programming language. Graphical representations used GraphPad Prism scientific software version 7 (GraphPad Software, San Diego, CA).

3. Results

3.1 Genotypic variation of growth responses to elevated temperature

At 10-DAH statistically significant interactions (*P <0.001*) occurred between genotype and growth temperature on both the dry weight of the spike on the main tiller (SDM) (*P <0.01*) and on 100-grain weight (100 GW) (Figure 1). However, there was no statistically significant interaction between genotype and temperature on the dry weight of the flag leaf of the main tiller (FDM) (Figure 1). In Huandoy and Amurskaja 75 at 10-DAH, the increase of SDM at the higher temperature was 53.8% and 25.6%, and the corresponding 100 GW increase was 268% and 192% (Figure 1).

At maturity, SDMT ($P <0.01$), total spike weight (SDT) ($P <0.05$), total harvest (TH) ($P <0.01$) and harvest index (HI) ($P <0.001$) exhibited statistically significant interactions between genotype and growth temperature. In contrast, spike number, above-ground biomass (AGB), and AGB without harvest did not display significant interactions (Figure 2). A 7.1% and 25.7% SN reduction was observed in Huandoy

and Amurskaja 75, respectively at the higher growth temperature. In Huandoy, at moderately high temperature there was a 60% decrease in HT and a 5% HT increment in Amurskaja 75 (Figure 2). Amurskaja 75 displayed a 15% increase in HI at moderately high temperature, while Huandoy had a 28% decrease (Figure 2). Both Huandoy and Amurskaja showed a decrease of AGB and AGB without harvest at the higher temperature.

3.2 Genotypic variation of gas exchange parameters at elevated temperature

At 10-DAH, the rates of spike photosynthesis (A) and of spike respiration in the dark (DR) were stimulated significantly under higher temperature in both the genotypes (Huandoy and Amurskaja 75) (Figure 3). At elevated temperature, the increment of A was much greater in Huandoy (40%) than in Amurskaja 75 (4.5%) (Figure 3).

There were statistically significant interactions between genotype and growth temperature on A (P <0.01) and intercellular CO_2 concentration (C_i) (P <0.001) (Figure 3). The highest DR was observed with Huandoy at moderately high temperature (41%). On the other hand, the increase of DR in Amurskaja 75 at the higher temperature was 62%. Further, wheat genotype and growth stage did not interact on DR or stomatal conductance (SC) (Figure 3).

3.3. Site-specific variation in N concentrations to moderately high temperature

There was a statistically significant (P <0.001) interactions between wheat genotype and growth temperature on N concentrations of wheat pericarps and flag leaves at 10-DAH (Figure 4). However, there were no significant interactions between genotype and growth temperature on grain N concentrations (Figure 4). In Huandoy, there was a decrement of mean N concentrations in wheat pericarps, seeds, and flag leaves at moderately high temperature, which were 30%, 9%, and 19%, respectively. In contrast, for Amurskaja 75, the mean N concentrations of flag leaves increased by 6%. Although there was a decrement of mean N concentrations of pericarps and seeds of Amurskaja 75 at moderately high temperature, that difference was comparatively smaller in Huandoy (Figure 4).

3.4. Genotypic and site-specific variation in δ ^{13}C and δ ^{15}N

Wheat genotype, organ type, and growth temperature displayed statistically significant interactions (P <0.001) for δ ^{13}C and C/N atomic ratio. However, δ ^{15}N was not statistically different for genotypic, organ type, and heat-treatment interactions. In Huandoy, both δ ^{15}N and C:N atomic ratio showed an increasing trend in wheat pericarps and flag leaves at moderately high temperature while isotopic signatures of C (δ ^{13}C) decreased (Figure 5). Although the pericarps of Amurskaja 75 exhibited a similar expression pattern to Huandoy, in most cases, the flag leaves of Amurskaja 75 acted differently. In all instances, C isotopic signatures (δ ^{13}C) were between the ranges of organs, which perform C_3 photosynthesis.

3.5. Effect of moderately high temperature and genotype on the expression of genes associated with Rubisco biosynthesis and sucrose metabolism

The mean relative expression of *rbcS* was statistically different among wheat genotypes (P <0.001) and the growth temperature (P <0.001) (Table 1). However, there was no statistically significant interaction effect between genotype and growth temperature on the *rbcS* expression (Table 1). In addition, the relative expression of *rbcL* also differed between genotypes (P <0.05) (Table 1). Generally, the expression of *rbcL* is much higher than that of *rbcS* at both temperature regimes (Table 2).

In Huandoy, the relative expression of both *rbcS* and *rbcL* was down-regulated 0.7 and 0.6 log fold at high temperature (Table 2). However, there was a 0.1 log fold upregulation in the *rbcL* expression in Amurskaja 75 (Table 2). In all the instances, the expression of *rbcS* and *rbcL* in Huanday is comparatively greater than in Amurskaja 75 (Table 2).

Of the three sucrose metabolism genes, *SPP1*, *SPS1*, and *SUS1*, only expression of *SUS1* and *SPP1* had statistically significant interactions between genotype and growth temperature (Table 1). In Huandoy, expression of *SPP1*, *SPS1*, and *SUS1* was upregulated at high temperature (0.09, 0.60 and 0.04-log fold upregulation, respectively) while expression was downregulated in Amurskaja 75 (Table 3).

3.6. Effect of moderately high temperature and genotype on the expression of key genes related to C_4 photosynthesis

There were statistically significant interactions between wheat genotype and growth temperature on the combined dependent variables: *TaPPDK_1α* (*P <0.001*), *TaPEPC_5* (*P* <0.001) and *TaMDH_7* (*P* <0.001), although *TaNADP-ME _1* was not statistically different (Table 1). In Huandoy, the relative expression of *TaNADP-ME _1*, *TaPPDK_1α, TaPEPC_5,* and *TaMDH_7* increased 0.12, 1.08, 0.89, and 1.82-log fold increase respectively at high temperature (Table 4). In contrast, in Amurskaja 75, high temperature down-regulated the relative expression of all measured C_4 pathway genes (Table 4). Independent of temperature, Huandoy had the highest expression of *TaPPDK_1α*, while Amurskaja 75 had the highest expression of *TaPEPC_5* (Table 4).

3.7. Effect of moderately high temperature and genotype on nitrogen metabolism in pericarps

Wheat genotype and the growth stage showed a statistically significant interaction effect on the expression of *NADH-GOGAT* (*P<0.05*), *GS1a* (*P<0.05*), *GS2a* (*P<0.01*) and *NiR* (*P* <0.001) (Table 1). Further, the expression of *Fd-GOGAT* and *GS2b* was genotypically varied (Table 1). In Huandoy, only *GS1a* expression displayed an upregulation, with a 0.4 log-fold increase at high temperature (Table 5). In contrast, the expression of both *GS2a* and *GS2b* were upregulateds in Amurskaja 75 (Table 5). In Amurskaja 75, the highest downregulation was observed in the *NiR* expression at high temperature with a 2.7 log-fold decrease (Table 5).

3.8. Effect of moderately high temperature on the pericarp proteome

From the extracted protein samples of wheat pericarps, overall, 458 different protein types were identified from proteomics analysis, which were common to both Huandoy and Amurskaja 75. The differently expressed proteins (significantly) were grouped, based on the metabolic pathway to which they belonged (Figures 6 and 7). In Huandoy, of the 458 proteins, only 54 (11.8% of the total) were significantly affected by high temperature, of which 28 were upregulated and 26 downregulated (Table 6).

Among the 54 different expressed protein types, 27 were characterized (Table 6). Of them the highest proportion (11.3%) were from the antioxidant defence system (Figure 6). The characterized proteins, changes in expression, and statistical significance are shown in Table 6.

In Amurskaja 75, of the 458 proteins, 105 (23%) were significantly affected at moderately high temperature. Of these, 54 proteins (51%) were upregulated (Table 7). Of the significantly affected proteins 38 were characterized (Table 7) and again these were mainly part of the antioxidant defence system (Figure 7).

Among proteins which were found to be significantly affected by moderately high temperature, 27 were common for both Huandoy and Amurskaja 75, of which 14 were characterized. Of these, seven protein types displayed a similar expression pattern across both genotypes: *glutathione-S-transferase 19E50, chloroplast acetyl-CoA carboxylase (fragment), phosphoribulokinase, 40S ribosomal protein S30* were upregulated and *cytochrome b559 subunit alpha (PSII reaction center subunit V), proteasome subunit alpha type,* and *UMP-CMP kinase (deoxycytidylate kinase) (CK) (dCMP kinase) (uridine monophosphate/cytidine monophosphate kinase) (UMP/CMP kinase) (UMP/CMPK)* were down-regulated at moderately high temperature. The expression pattern of the remaining seven proteins differed between Huandoy and Amurskaja 75.

4. Discussion

4.1. Growth traits affected by moderately high temperature

For both genotypes at 10-DAH, there were increases in SDM and 100 GW at moderately high temperature after heading (Figure 1) and at maturity, there were reductions in SN, SDT, AGB, and AGB without harvest (Figure 2). These results are consistent with previous findings in wheat (Saini and Aspinall, 1982, Ferris et al., 1998, Gibson and Paulsen, 1999). The influence of moderately high temperature on harvest related traits depends on the growth stage at which the high temperature occurs (Farooq et al., 2011), i.e. temperatures above 20°C in the reproductive phase cause yield loss due to pollen sterility, floret abortion, lower CO_2 assimilation, dehydration of reproductive organs, and increased photorespiration (Saini and Aspinall, 1982,

Porter and Gawith, 1999, Farooq et al., 2011). High temperature reduced the duration between heading and maturity by increasing the rate of spike development. This is associated with a reduced number of spikelets, and thus total yield (Porter and Gawith, 1999). For instance, the reduction of grain number in a spike by approximately 4% was observed for every 1°C increase between 15–22°C from anthesis to 30-days post-anthesis (30-dpa) (Fischer, 1985). Further, grain weight reduced by ~1.5 mg day^{-1} for every 1°C increase between 15–22°C (Shpiler and Blum, 1986). With the high temperature, the enzymatic activities involved in starch biosynthesis and deposition are hindered, and reduced starch deposition in the grain is the main reason for reduced harvest as starch accounts for about 70% of the dry weight of wheat grain (Jenner, 1994). In this study, the accelerated growth rates at moderately high temperature may be the reason for obtaining much higher SDM and 100 GW values at 10-DAH than at the lower temperature.

We observed a substantial genotypic variation in growth-related traits due to moderately high temperature. Of the different growth parameters, marked genotypic variation was shown in TH, that is although harvest decreased significantly in Huandoy it increased in Amurskaja 75, and HI displayed a similar pattern. Although high temperature generally causes a reduction in the wheat harvest, others too have reported significant genotypic variation (Freeha et al., 2008, Farooq et al., 2011). Consequently, we suggest that Amurskaja 75 may be useful in breeding programs for heat tolerance.

4.2. Spike photosynthesis affected by moderately high temperature

Both genotypes displayed an increase in the rate of spike photosynthesis, respiration in the dark and stomatal conductance at moderately high temperature (Figure 3), although the effect of *A* was not statistically significant in Amurskaja 75. Similarly, an increase in the rate of CO_2 assimilation with the increase in temperature of up to 30°C was reported in cotton (Wise et al. (2004), and Shah et al. (2003) state that the photosynthesis in mature plants is not severely affected by moderately high temperature in the absence of water stress.

In plants, photosynthesis is the most sensitive biological process to high temperature (Wahid et al., 2007). In wheat, spike photosynthesis may play a vital role in grain

filling although it is less well studied (Dehigaspitiya et al., 2019). The reduction in CO_2 assimilation at high temperature and how it affects crop productivity has been investigated for decades (Wise et al., 2004). Previously, the reactions in photosystem II (PSII) including photosystem I (PSI) mediated electron transfer was considered as the most temperature-sensitive component in photosynthesis (Berry and Bjorkman, 1980). However, recent findings revealed that there was no significant inhibition in PSII under moderate heat stress (< 40°C) although there were substantial photosynthesis reductions (Sharkey and Environment, 2005, Farooq et al., 2011). Currently, it is believed that the deactivation of Rubisco due to the loss of activity of Rubisco activase is the main reason for photosynthesis inhibition at moderately high temperature (35-40°C) (Salvucci et al., 2001). The nett rate of photosynthesis at moderately high temperature can be decreased by increased photorespiration because of the changes in kinetic properties of Rubisco and the changes in CO_2 and O_2 solubility (Ogren, 1984). In this study, the reason for not observing a photosynthesis reduction at moderately high temperature may be due to the maximum temperature that we used (30°C) which was not sufficient to inhibit the activity of PSI, PSII, and Rubisco. However, increased respiration rates in the dark and photorespiration may account for the final yield reduction in Huandoy. In addition, there was a clear genotypic variation in gas exchange parameters at moderately high temperature. Supporting the substantial yield loss in Huandoy at moderately high temperature, much higher respiration rates were also observed in the dark with Huandoy than in Amurskaja 75.

In our study, in most cases, the isotopic signatures of C and N ($\delta\,^{13}C$ and $\delta\,^{15}N$) did not display a significant variation when they were grown at moderately high temperature, although there were genotypic and organ-specific changes. According to our results, in all instances, the isotopic signatures of C were within the range of C_3 photosynthesis. Thus, we can assume that the mode of photosynthesis or the selectivity of CO_2 in photosynthesis may not be affected by moderately high temperature. However, this observation may not lead to any deliberation as to when the plants were introduced to moderately high temperature as the flag leaves had already initiated. In addition, part of the dry matter of the considered organ may be from the photosynthate of other photosynthetic organs rather than its own C fixation. Of the two genotypes, Amurskaja 75 displayed the lesser variation in C and N isotopic signatures ($\delta\,^{13}C$ and

δ ^{15}N) at moderately high temperature. During photosynthetic C fixation along with underlying photosynthetic pathway of the photosynthetic organ, plants discriminate two types of CO_2 which were composed of the two naturally occurring C isotopes (^{12}C and ^{13}C) (Caemmerer et al., 2014). Although there are some limitations, isotopic signatures of plant dry matter are widely used to determine the underlying mechanism of C assimilation in plants (Farquhar et al., 1982, Caemmerer et al., 2014).

4.3. Expression of genes related to Rubisco biosynthesis affected by moderately high temperature

We did not observe a statistically significant interaction between genotype and growth temperature on the expression of *rbcS* and *rbcL* at 10-DAH; nonetheless, the individual effects of genotype and growth temperature on *rbcS* expression were significant (Table 1). Of the two genes, expression of *rbsS* was strongly reduced by elevated temperature in both genotypes (Table 2). In Huandoy, moderately high temperature decreased the expression of *rbcL* by 35%. A similar expression pattern in *rbcS* was previously observed in flag leaves of wheat grown at two different temperature regimes (Almeselmani et al. 2012). These authors also reported a genotypic variation in expression of both *rbcS* and *rbcL*.

The enzyme Rubisco governs the light-saturated C fixation under current atmospheric conditions and plays a vital role in both C and N metabolism in higher plants (Suzuki et al., 2009). As wheat spikes play an important role in grain filling and thus the total yield, it is vital to study the metabolic processes, including Rubisco biosynthesis in wheat pericarps (Dehigaspitiya et al., 2019). Rubisco consists of eight large and small subunits and *rbcL*; a single gene in the chloroplast codes for the large subunit while *rbcS*; a multigene family at the nucleus is coding for the small subunit (Suzuki et al., 2009). The abundance of *rbcS* and *rbcL* in a photosynthetic organ is an indirect measurement for the amount of Rubisco present in that organ (Suzuki et al., 2010). According to our results, the transcript abundance of both *rbcS* and *rbcL* was higher in Huandoy than Amurskaja 75 at both temperature regimes displaying a genotypic variation similar to the study of Almeselmani et al. (2012). In Huandoy, although there was a decrease in *rbcL* expression at moderately high temperature, Amurskaja 75 displayed an increment. A similar expression pattern was observed by Almeselmani

et al. (2012) from a study conducted using flag leaves of heat resistant wheat varieties at different temperature regimes. In addition, supporting our observation of *rbcL* expression, the N concentrations of wheat pericarps of Amurskaja 75 did not display a decrement when exposed to moderately high temperature, whereas there was a significant decrease in Huandoy.

4.4. Expression of genes associated with the sucrose metabolism affected by moderately high temperatures

In wheat pericarps expression of key genes of sucrose metabolism varied between genotypes at the elevated temperature. The importance of knowledge of sucrose metabolism in wheat pericarps for crop improvement was explained by Dehigaspitiya et al. (2019). It has been proposed that at least nine enzymes are involved in sucrose metabolism including fructokinase, invertase, hexokinase, phosphoglucomutase, UDP-glucose purophosphorylase, phosphoglucose isomerase, (UDPGP), sucrose phosphate phosphatase (SPP), sucrose synthase (SUS), and sucrose phosphate synthase (SPS) (Jiang et al., 2015). However, in this study, we considered only the mRNA abundance of SPS, SUS, and SPP as they may play significant roles in sucrose biosynthesis. Of the above three genes, both *SUS1* and *SPP1* displayed a significant interaction from genotype and growth temperature.

Sucrose is the main transport carbohydrate in most plants, and it forms the interface between C production at the source and assimilation in sink tissues; consequently the amount of sucrose present in a photosynthetic organ represents the balance between these processes (Baxter et al., 2003). The enzyme SPS is considered the main rate-limiting enzyme of sucrose synthesis and SPS is responsible also for catalysing the reactions of sucrose-6-phosphate biosynthesis from UDP-glucose and fructose-6-phosphate (Lunn and MacRae, 2003). In addition, SPP catalyses the final step of sucrose biosynthesis by hydrolysing sucrose-6-phosphate (Jiang et al., 2015). Because of the strong interdependence, it is believed that both SPP and SPS act together as a multi-enzyme complex in sucrose metabolism (Echeverria et al., 1997). A correlation between the rate of photosynthesis and the rate of sucrose biosynthesis in photosynthetic organs was suggested (Stitt, 1986, Battistelli et al., 1991). Consistent with this proposition, in Huandoy, we also observed slightly higher expression of *SPS1*

and *SPP1* at elevated temperature with the increase of photosynthesis. However, the expression of *SPS1* and *SPP1* did not increase in Amurskaja 75 (Table 3) as the rate of photosynthesis did not increase at elevated temperature. The higher expression of *SPS1* and *SPP1* may be an indication of an increased sucrose biosynthesis in wheat pericarps at elevated temperature. This sucrose has to be transported to sink tissues of the plant for storage. However, the biomass reduction of Huandoy at elevated temperature suggests that although the C assimilation is high at elevated temperature, nett C assimilation was reduced. This may be due to inefficiencies such as higher respiration rates and site-specific inefficiencies, for instance, low photosynthetic rates in other photosynthetic organs such as the leaves as well as increased rate of photorespiration and respiration.

Concerning sucrose metabolism in higher plants, sucrose is degraded by either SUS or sucrose invertase. Sucrose invertases catalyses the conversion of sucrose into fructose and glucose while under SUS, sucrose is converted into UDP-glucose (Jiang et al., 2015). Besides, SUS is mainly involved in the biosynthesis of sugar polymers such as cellulose and starch and biosynthesis of energy (ATP: Adenosine Tri-Phosphate) (Coleman et al., 2009, Ruan et al., 2010). In our study, the relative expression of *SUS1* displayed a genotypic variation at moderately high temperature, which was in Huandoy; there was an increase in *SUS1* expression while Amurskaja 75 showed a decrease. Further, out of three genes of sucrose metabolism, *SUS1* expression was the highest.

4.5. Nitrogen metabolism affected by moderately high temperature

The expression of key genes of N metabolism changed in response to moderately high temperature (Tables 1 and 5). Of the seven genes tested, only *NADH-GOGAT* and *NiR* were significantly changed by the growth temperature, and only four interacted significantly with genotype and growth temperature (Table 1). In N metabolism, *GS2a, GS2b, GS1a,* and *GSr1* encode for the GS2 and GS1 isoenzyme families. In general, the expression of *GS2a* is much higher in N-sinks, i.e., immature photosynthetic organs (Bernard et al., 2008). With the age of a plant organ, the relative expression of *GS2a* decreases. In our study, expression of *GS2a* declined at elevated temperature in Huandoy. This may be due to temperature induced differences in tissue

maturity even though all the samples were taken at 10-DAH. Until senescence, plant shoots act as N-sinks while roots act as sources. When the photosynthetic organ senesces it changes from a N-sink to a source that is remobilized for grain/reproduction (Bernard et al., 2008). However, in Amurskaja 75, there was no apparent decrease in the relative expression of *GS2a* at elevated temperature. Our gene expression results were supported by the observation that at elevated temperature pericarps of Huandoy had lowered N concentrations. Moreover, consistent with the *GS2a* expression, there was no apparent decrease in N concentrations of pericarps of Amurskaja 75 at moderately high temperature.

N metabolism in wheat pericarps may play an important role in grain protein content (Dehigaspitiya et al., 2019). In plant N metabolism, glutamine synthetase (GS) converts glutamate into glutamine using ammonia as a substrate. A few subclasses of GS have been identified, and among them, GS1 and GS2 are believed to have site-specific roles in N metabolism. Generally, the expression of GS2 is higher in N-sinks, such as photosynthetic organs and it catalyzes the primary N assimilation of ammonia and re-assimilation of respiratory ammonia (Bernard et al., 2008). However, the expression of GS1 is relatively lower in sink organs (Bernard et al., 2008). Combining with two types of GOGAT (glutamate synthase) enzymes: *Fd-GOGAT* and *NADH-GOGAT*, GS integrates amino groups into amino acids in protein synthesis (Masclaux-Daubresse et al., 2010). Similar to GS enzymes, both *Fd-GOGAT* and *NADH-GOGAT* display a site-specific localization in their expression where there is an abundance of *Fd-GOGAT* in photosynthetic organs while a much higher profusion of *NADH-GOGAT* is localized in non-photosynthetic organs (Kamachi et al., 1992). Consistent with this proposition, our results exhibited site-specific variation in the expression of GOGAT enzymes in pericarps such that there were significantly higher expressions in *Fd-GOGAT* than *NADH-GOGAT*.

4.6. Expression of key genes associated with the C_4 pathway affected by moderately high temperature

At moderately high temperature, the expression of key C_4 pathway genes in the two wheat genotypes varied (Table 1). These results are similar to those for wheat flag leaves (Bachir et al. 2017). We generally found significant interaction effects between

genotype and growth temperature on expression of *TaPEPC_5*, *TaPPDK_1α,* and *TaMDH_7*. Interestingly, the expression pattern of four C_4 pathway genes was contrary between the genotypes. For instance, in Huandoy, the mean relative expression of *TaPEPC_5*, *TaNADP-ME _1*, *TaPPDK_1α,* and *TaMDH_7* increased at elevated temperature, while expression decreased in Amurskaja 75. In both genotypes, the lowest expression was with *TaMDH_7* independent of temperature (Table 4).

Wheat is a classic C_3 cereal. However, recent findings of Rangan et al. (2016) suggest the existence of a C_4-like photosynthetic pathway in developing wheat pericarps. Bachir et al. (2017) characterized the expression of genes related to the main C_4 pathway enzymes including phosphoenolpyruvate carboxylase (PEPC), NADP-dependent malic enzyme (NADP-ME), malate dehydrogenase (MDH), and pyruvate orthophosphate dikinase (PPDK). Although we observed expression of C_4 pathway genes in developing wheat pericarps, a definitive inference would require supporting evidence from other metabolic processes. This merits further research because of the potential benefits to crop productivity (Bachir et al., 2017, Rangan et al., 2016).

4.7. The proteome of the wheat pericarp affected by moderately high temperature

Of the 458 protein types we identified that were common to both Huandoy and Amurskaja 75, only 12% and 23% were significantly affected by elevated temperature in Huandoy and Amurskaja 75, respectively. Genotypic variation of grain proteome at high temperature was reported by Majoul et al. (2003, 2004). Of the different proteins, a considerable amount was uncharacterized. The characterized proteins that were marked different were grouped based on their metabolic functions, including: carbohydrate metabolism, photosynthesis, protein synthesis, and post-translational modifications, antioxidant defence, energy production, signal transduction, gene expression (transcription) and nitrogen assimilation. In both genotypes, the greatest number of significantly affected proteins belonged to the antioxidant defence system.

Reactive oxygen species (ROS) are activated or partially reduced forms of oxygen ($O_2^{\cdot -}$, H_2O_2, $^1O_2$). ROS in plants can be considered as unavoidable by-products of aerobic metabolism, originating about 2.7 billion years ago with the oxygen-evolving photosynthetic pathways (Mittler et al., 2011). Although ROS are considered as

harmful by-products of plant metabolism which cause oxidative damage to cell membranes (by lipid peroxidation), proteins, nucleotides, and even oxidative destruction of cells, they also act as signal transduction molecules that regulate different pathways during plant acclimation to abiotic stresses (Choudhury et al., 2017). Thus plants have their own set of ROS-producing and ROS-scavenging pathways in subcellular compartments (Choudhury et al., 2017). The antioxidant defence system consisting of ROS detoxifying proteins is one such ROS-scavenging pathway (Mittler et al., 2004).

In Huandoy, we observed upregulation of proteins related to the antioxidant defence system and other stress coping proteins (Table 6), including: g*lutathione-S-transferase 19E50, dirigent protein, glutathione S-transferase, ascorbate peroxidase (fragment), Harpin binding protein 1* and *protein disulfide-isomerase* at elevated temperature indicating a stress response. Further, 11% of the significantly affected proteins in response to moderately high temperature were categorized as parts of the antioxidant defence system (Figure 6). However, in Amurskaja 75, of 105 significantly affected proteins, only eight were grouped into the antioxidant defence system and only five were upregulated (Table 7). This genotypic difference indicates that Huandoy was experiencing greater heat stress than Amurskaja 75. This observation is further supported by the effect of moderately high temperature on relative yield. However, of the proteins significantly affected by elevated temperature, 49%, and 64% were uncharacterized in Huandoy and Amurskaja 75, respectively at the time of the study, which may substantially mask the overall picture.

Consistent with the much higher photosynthetic rates of Huandoy at elevated temperature, *fructose-bisphosphate aldolase* was upregulated. This protein is responsible for C fixation and sucrose metabolism and has functions in both glycolysis and Calvin cycle, *Chloroplast acetyl-CoA carboxylase (Fragment),* and *Phosphoribulokinas*; a protein in Calvin cycle which converts ribulose 5 phosphate to ribulose-1, 5-bisphosphate. Likewise, in Amurskaja 75, the following proteins were upregulated: *phosphoribulokinase, photosystem II polypeptide (fragment)*; protein which contributes to PSII light-harvesting, *photosystem I iron-sulfur center (PSI-C) (photosystem I subunit VII) (PsaC)*; a protein responsible for photochemical activity including electron acceptance and transport, *chloroplast acetyl-CoA carboxylase,* a protein involved in fatty acid metabolism and *geranylgeranyl hydrogenase*; a protein

involved in the production of chlorophyll. Supporting the higher respiration rates at elevated temperature, few proteins of the energy pathway were upregulated, i.e., in Huandoy *phosphoglycerate kinase*; a protein involved in glycolysis and in Amurskaja 75, *succinate dehydrogenase [ubiquinone] flavoprotein subunit- mitochondrial* and *glyceraldehyde-3-phosphate dehydrogenase* showed upregulation. Of the significantly affected proteins in Huandoy at elevated temperature, 9% were related to protein synthesis and post-translational modifications, 4% were in plant signalling, 8% were responsible for transcriptional regulation, and 2% were associated with N metabolism. Likewise, in Amurskaja 75, of the significantly affected proteins, 7%, 4%, 7%, and 1% belonged to protein synthesis and post-translational modifications, plant signalling, transcriptional regulation, and N metabolism, respectively.

There were numerous uncharacterized proteins that may have significant roles in wheat metabolism in response to moderately high temperatures. For instance, in both genotypes, the uncharacterised protein *A0A1D5U621_WHEAT* displayed the highest upregulation, but the function or the metabolic pathway attached was unknown. The inability to characterize protein roles is a significant challenge to determining the complete spike responses to elevated temperature.

Conclusion

The results of this study confirm that elevated temperature has a significant influence on major metabolic processes in wheat pericarps and that the impact varied genotypically. Of the two varieties, Amurskaja 75 had the greater resistance to moderately high temperature. Of significantly affected proteins in both genotypes, the highest proportion was associated with the ROS-scavenging pathway. However, a significant number of proteins are yet to be characterized and, this has become a challenge when determining overall plant responses to elevated temperature.

Conflict of interest

The authors declare no conflict of interest

Acknowledgement

The University of Southern Queensland, Australia, funded this study. The proteomics analysis as supported by La Trobe Comprehensive Proteomics Platform (La Trobe University, Melbourne, Australia). Analysis of C and N isotopic signatures as supported by Motohiro Ito (Toyo University) and Yu Takahata (The Graduate University for Advanced Studies).

List of Figures

Figure 7. Protein categories of Amurskaja 75 which were significantly affected by elevated temperature.

List of Tables and Supplementary Tables

Table 1. The effect of wheat genotype (Huandoy and Amurskaja 75), growth temperature, and their interactions, on the expression of genes related to Rubisco biosynthesis, sucrose metabolism, nitrogen metabolism, and C_4 pathway enzymes in wheat pericarps in response to elevated temperature. Abbreviations: ns, not significant; *, P <0.05; **, P <; 0.01; ***, P <0.001.

Table 2. Heat-map of transcript abundance of key genes related to Rubisco biosynthesis in wheat pericarps in response to elevated temperature. Data presented are log_2 mean values of relative expression. At relative expressions, shades of red denote relatively higher expression, shades of yellow denote average expression and shades of green denotes relatively low expression. Abbreviations: C, control (normal temperature); HT, elevated temperature.

Table 3. Heat-map of transcript abundance of key genes related to sucrose metabolism in wheat pericarps in response to elevated temperature. Data presented are mean values of relative expression. At relative expressions, shades of red denote relatively higher expression, shades of yellow denote average expression and shades of green denote relatively low expression. Abbreviations: C, control (low temperature); HT, elevated temperature.

Table 4. Heat-map of transcript abundance of key genes related to C_4 pathway enzymes in wheat pericarps in response to elevated temperature. Data presented are mean values of relative expression. At relative expressions, shades of red denote relatively higher expression, shades of yellow denote average expression and shades of green denote relatively low expression. Abbreviations: C, control (low temperature); HT, elevated temperature.

Table 5. Heat-map of transcript abundance of key genes related to nitrogen metabolism in wheat pericarps in response to elevated temperature. Data presented are mean values of relative expression. At relative expressions, shades of red denote relatively higher expression, shades of yellow denote average expression and shades of green denote relatively low expression. Abbreviations: C, control (low temperature); HT, elevated temperature.

Table 6. Significantly affected characterized proteins of Huandoy and their metabolic pathways. Abbreviations: *, P <0.05; **, P <; 0.01; ***, P <0.001.

Table 7. Significantly affected characterized proteins of Amursjaka 75 and their metabolic pathways. Abbreviations: *, P <0.05; **, P <; 0.01; ***, P <0.001.

Supplementary Table S1. Atmospheric conditions of the low-temperature growth cabinet.

Supplementary Table S2. Atmospheric conditions of the elevated temperature growth cabinet.

Supplementary Table S3. List of primer sequences of genes selected for qRT-PCR

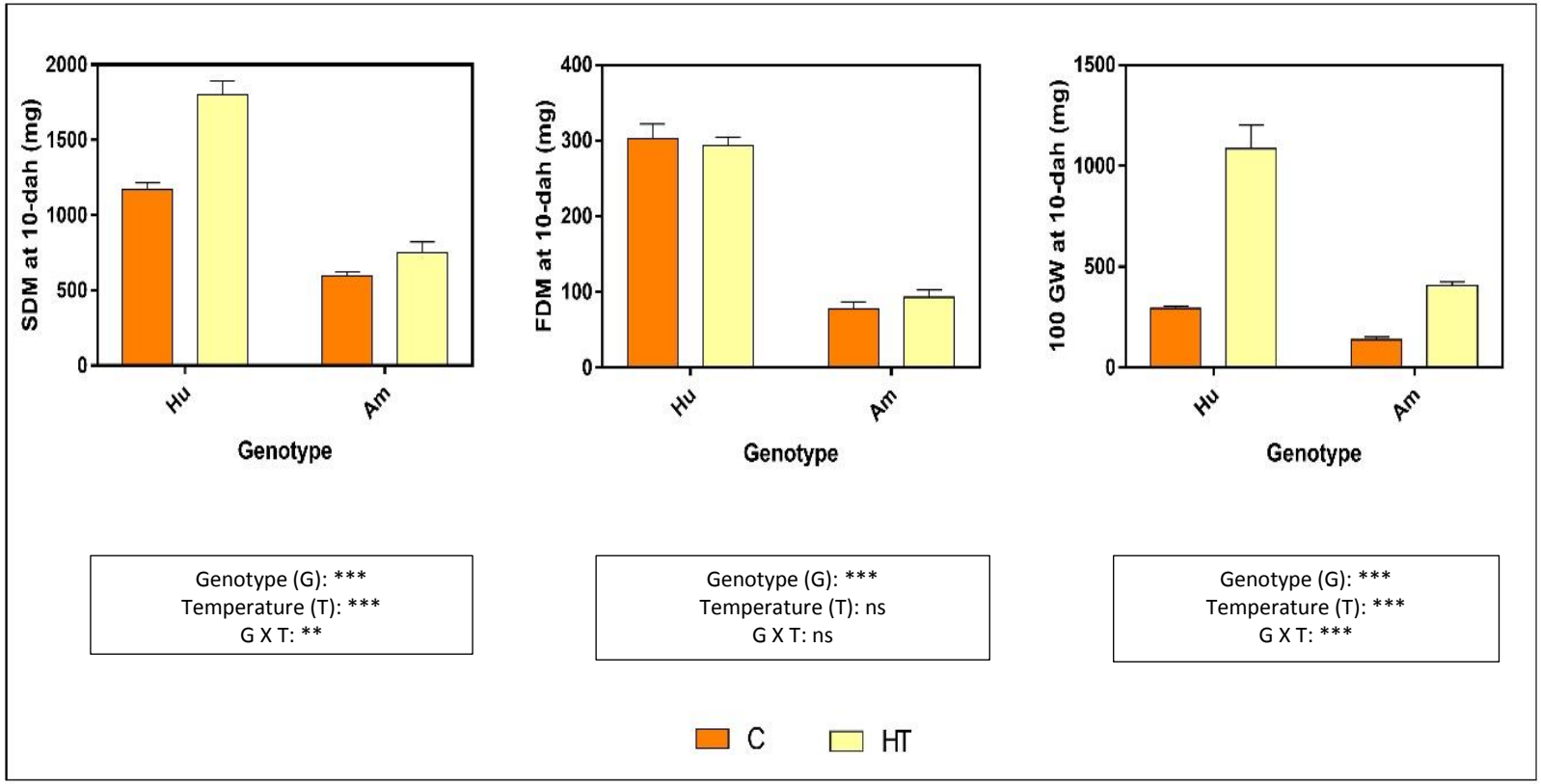
SDM at 10-dah (mg)
2000
1500
1000
500
0
Hu
Am
Genotype
Genotype (G): ***
Temperature (T): ***
G X T: **
FDM at 10-dah (mg)
400
300
200
100
0
Hu
Am
Genotype
Genotype (G): ***
Temperature (T): ns
G X T: ns
100 GW at 10-dah (mg)
1500
1000
500
0
Hu
Am
Genotype
Genotype (G): ***
Temperature (T): ***
G X T: ***
C
HT

Figure 1

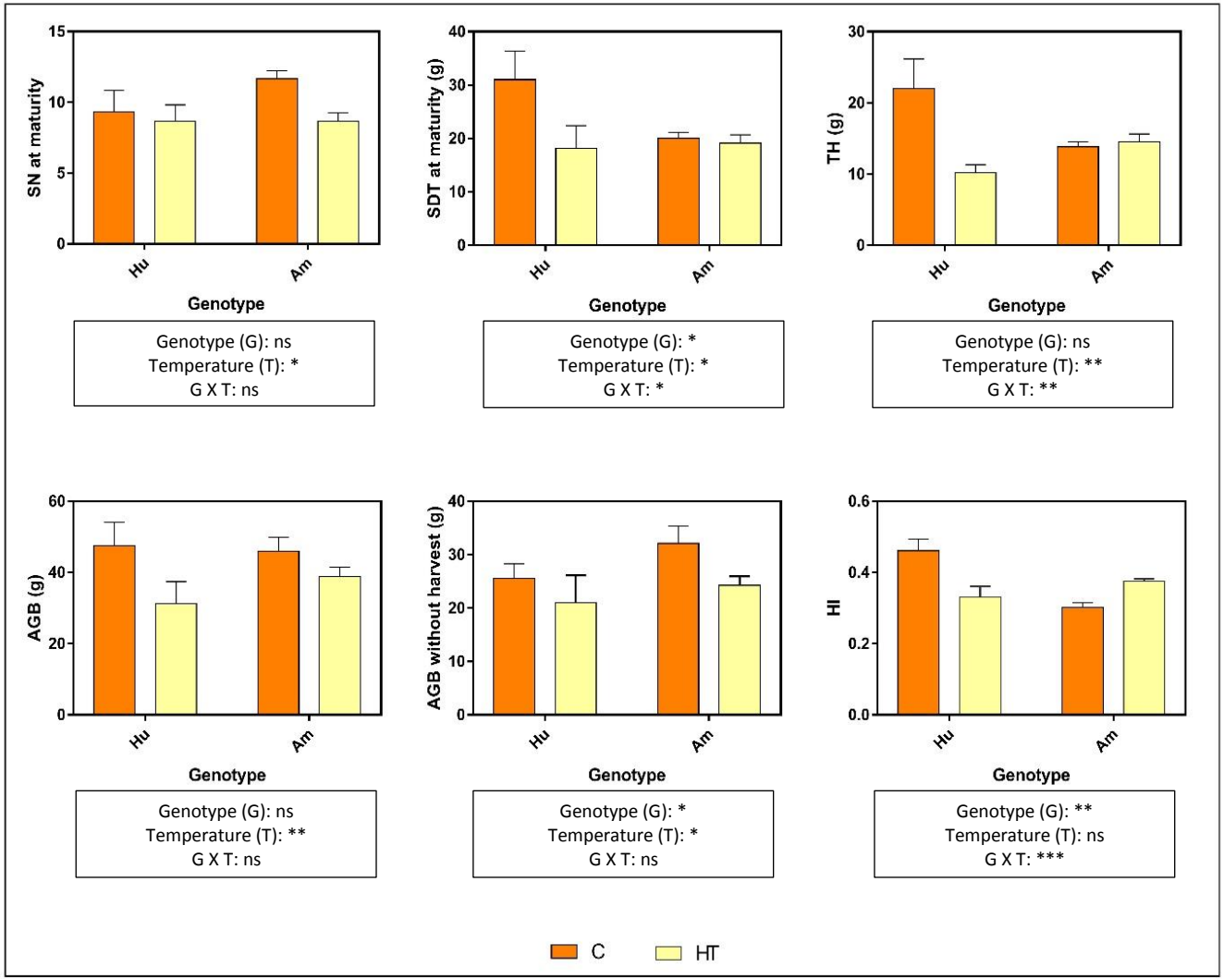
SN at maturity
Genotype
Hu
Am
Genotype (G): ns
Temperature (T): *
G X T: ns
SDT at maturity (g)
Genotype (G): *
Temperature (T): *
G X T: *
TH (g)
Genotype (G): ns
Temperature (T): **
G X T: **
AGB (g)
Genotype (G): ns
Temperature (T): **
G X T: ns
AGB without harvest (g)
Genotype (G): *
Temperature (T): *
G X T: ns
HI
Genotype (G): **
Temperature (T): ns
G X T: ***
C
HT

Figure 2

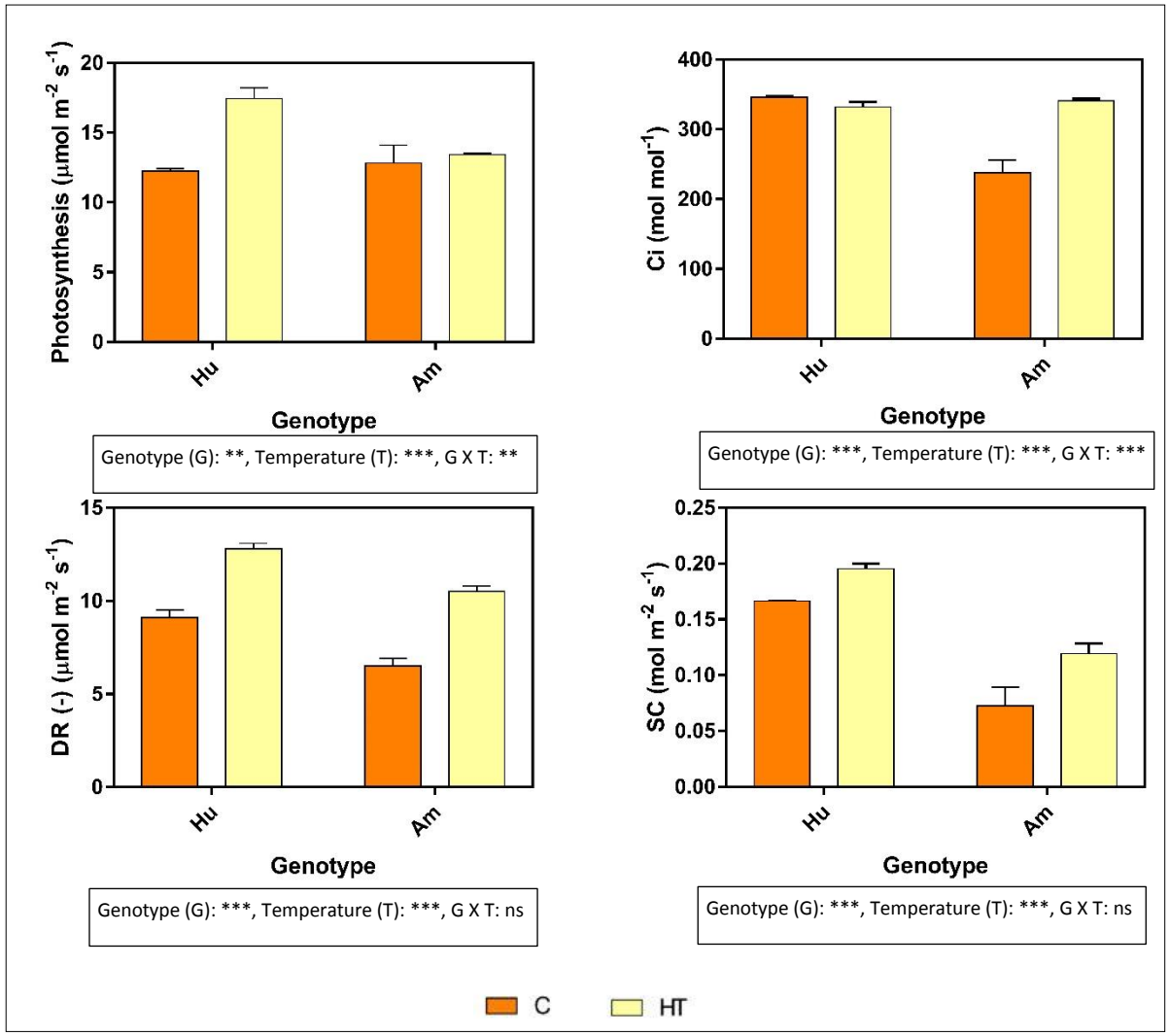
Photosynthesis (µmol m-2 s-1)
20
15
10
5
0
Hu
Am
Genotype
Genotype (G): **, Temperature (T): ***, G X T: **
Ci (mol mol-1)
400
300
200
100
0
Hu
Am
Genotype
Genotype (G): ***, Temperature (T): ***, G X T: ***
DR (-) (µmol m-2 s-1)
15
10
5
0
Hu
Am
Genotype
Genotype (G): ***, Temperature (T): ***, G X T: ns
SC (mol m-2 s-1)
0.25
0.20
0.15
0.10
0.05
0.00
Hu
Am
Genotype
Genotype (G): ***, Temperature (T): ***, G X T: ns
C
HT

Figure 3

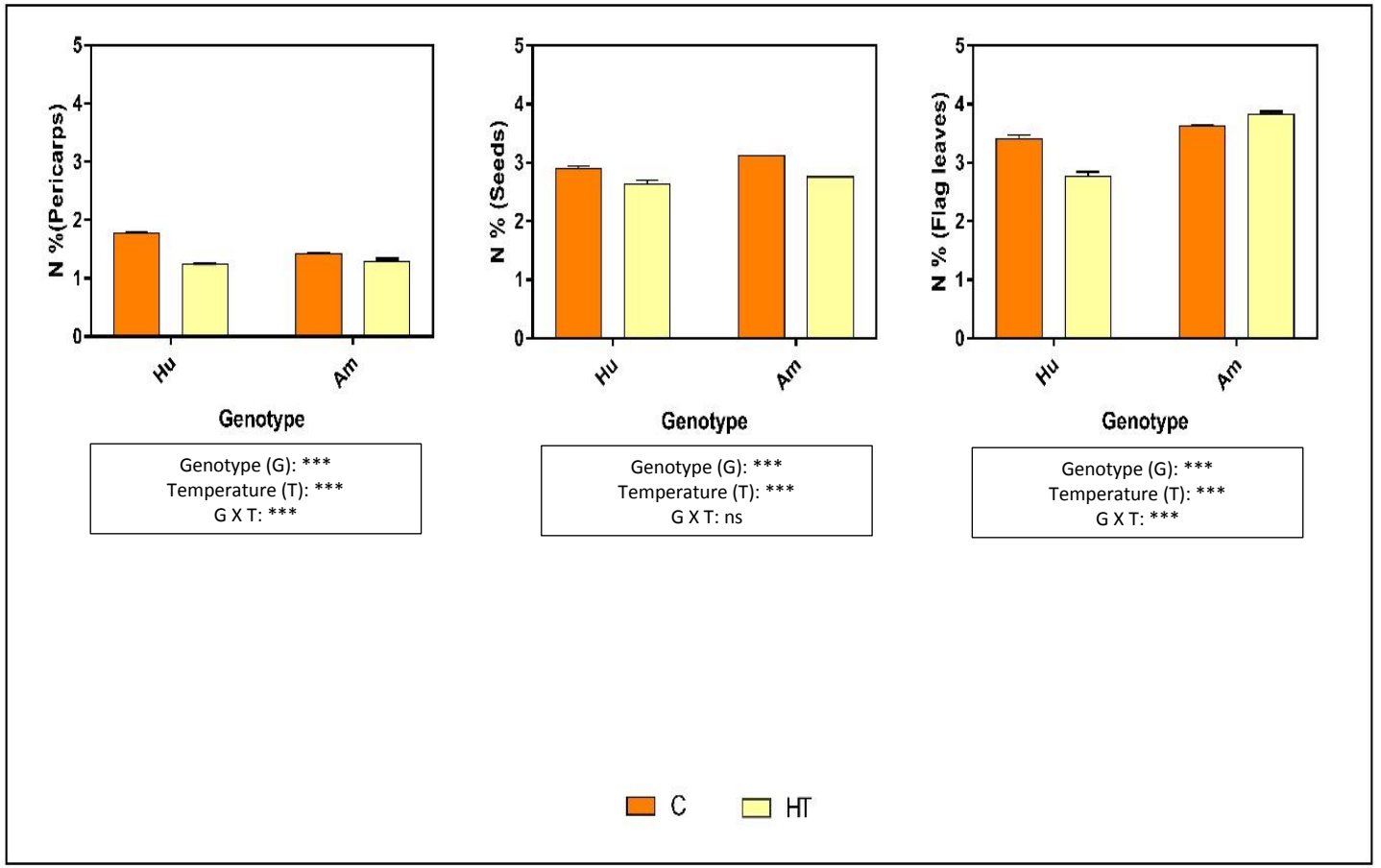
N %(Pericarps)
N % (Seeds)
N % (Flag leaves)
0
1
2
3
4
5
Hu
Am
Genotype
Genotype (G): ***
Temperature (T): ***
G X T: ***
Genotype (G): ***
Temperature (T): ***
G X T: ns
Genotype (G): ***
Temperature (T): ***
G X T: ***
C
HT

Figure 4

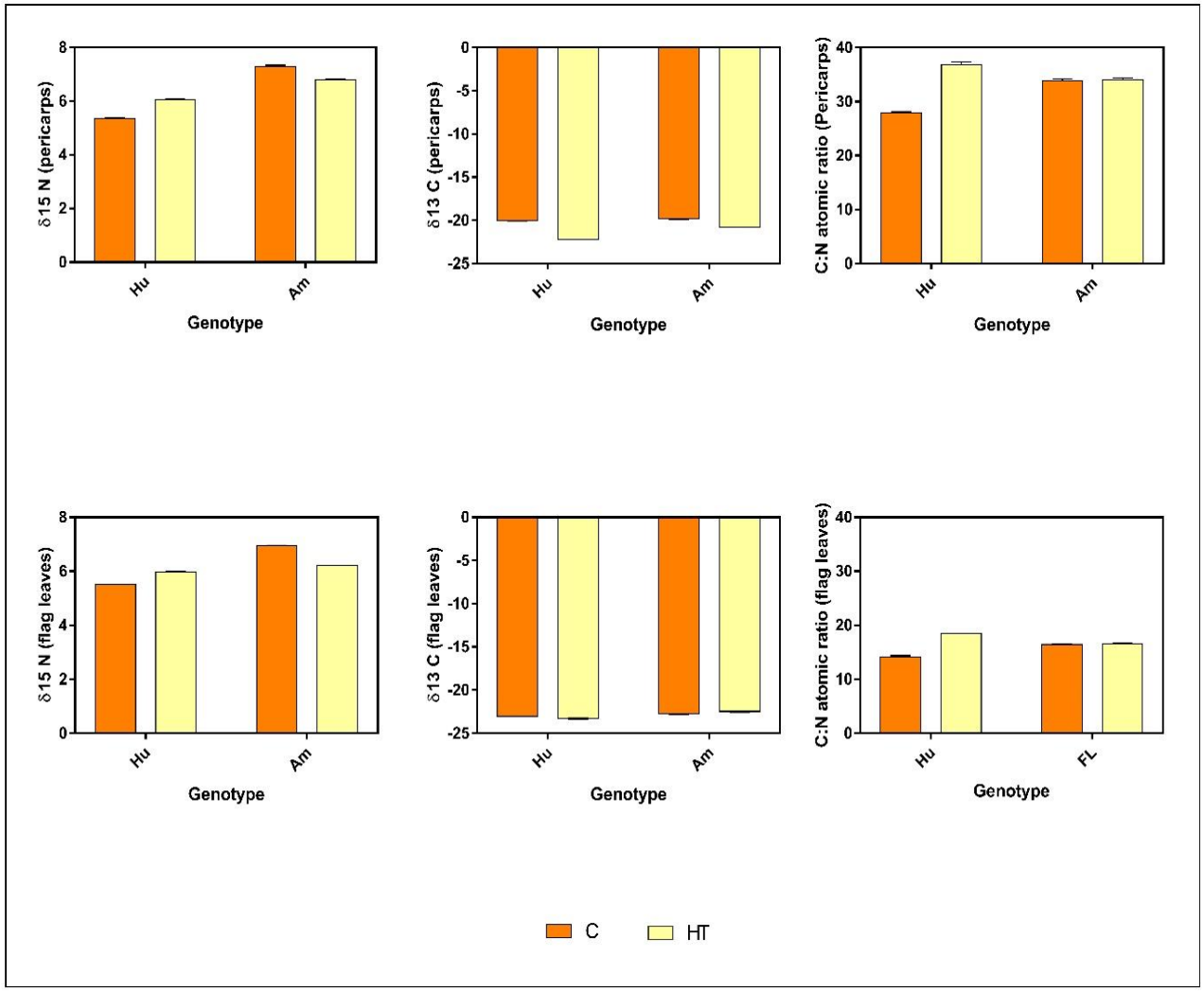
δ15 N (pericarps)
δ13 C (pericarps)
C:N atomic ratio (Pericarps)
δ15 N (flag leaves)
δ13 C (flag leaves)
C:N atomic ratio (flag leaves)
Hu
Am
FL
Genotype
C
HT

Figure 5

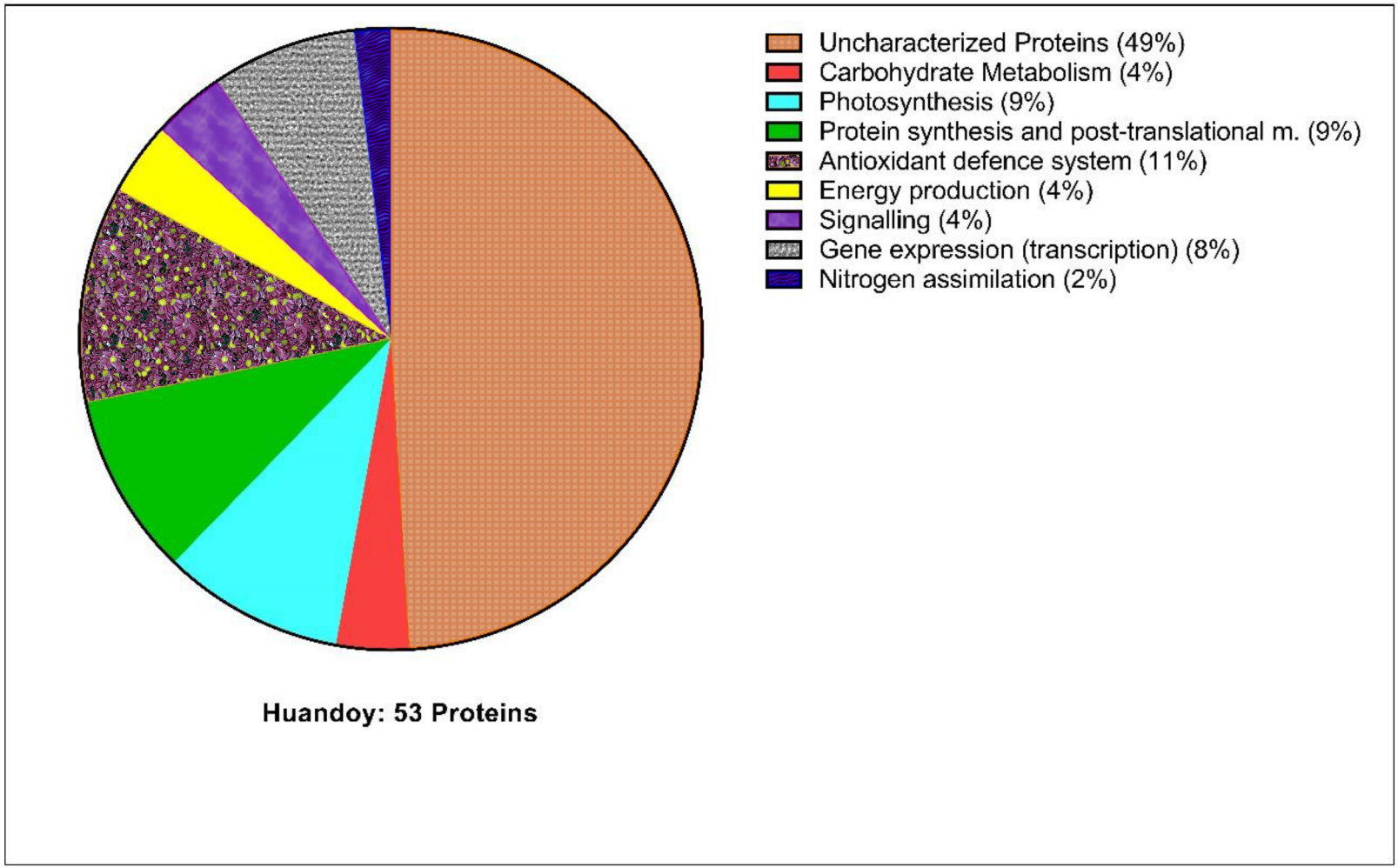
Uncharacterized Proteins (49%)
Carbohydrate Metabolism (4%)
Photosynthesis (9%)
Protein synthesis and post-translational m. (9%)
Antioxidant defence system (11%)
Energy production (4%)
Signalling (4%)
Gene expression (transcription) (8%)
Nitrogen assimilation (2%)
Huandoy: 53 Proteins

Figure 6

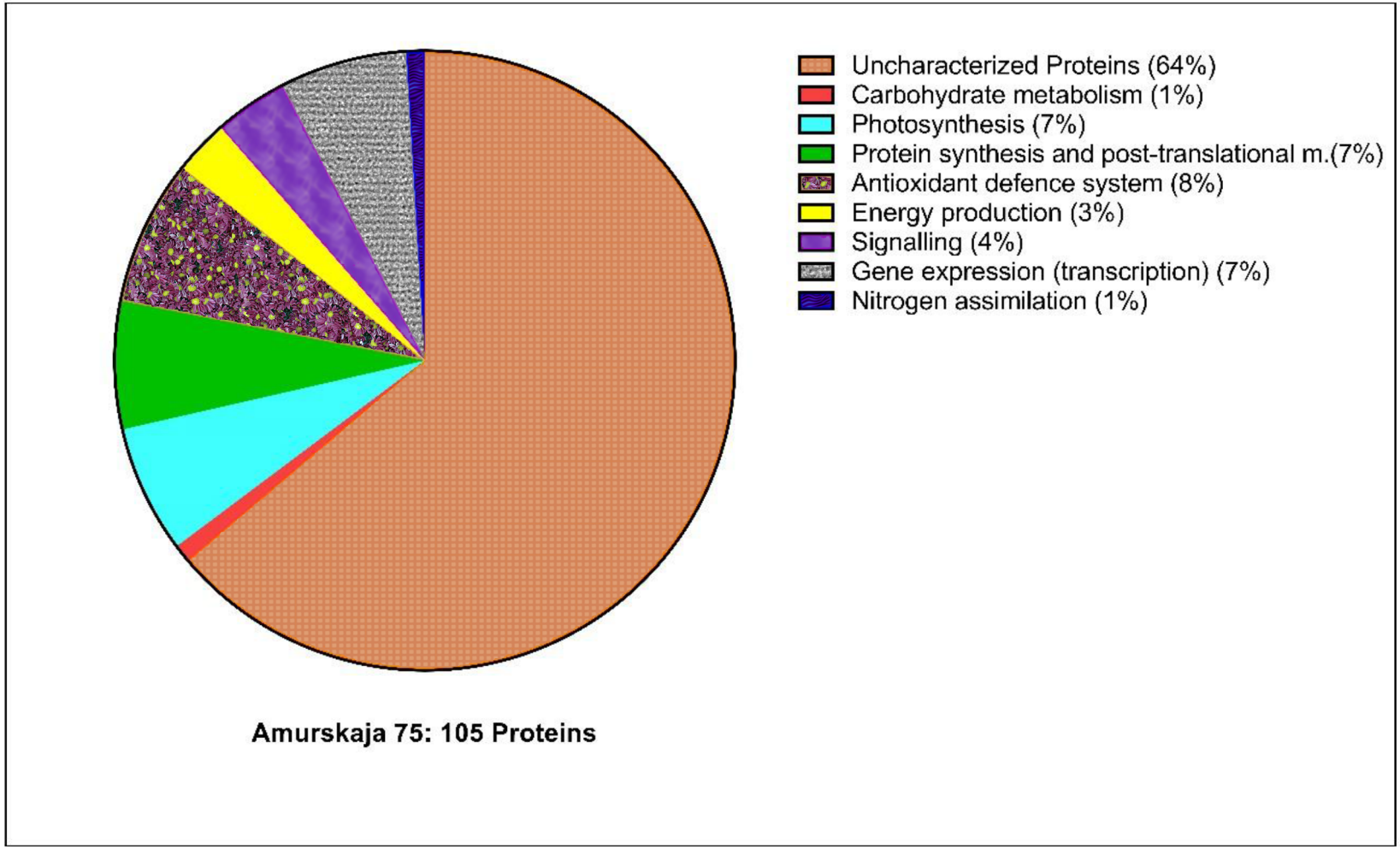
Uncharacterized Proteins (64%)
Carbohydrate metabolism (1%)
Photosynthesis (7%)
Protein synthesis and post-translational m.(7%)
Antioxidant defence system (8%)
Energy production (3%)
Signalling (4%)
Gene expression (transcription) (7%)
Nitrogen assimilation (1%)
Amurskaja 75: 105 Proteins

Figure 7

Table 1

Metabolic pathway	Gene	Significance		
		Genotype	Growth Temperature	Genotype X Growth Temperature
Rubisco biosynthesis	*rbcS*	***	***	ns
	rbcL	*	ns	ns
Sucrose metabolism	*SPS1*	ns	ns	ns
	SUS1	***	ns	***
	SPP1	ns	ns	*
Nitrogen metabolism	*NADH-GOGAT*	*	*	*
	GS1a	*	ns	*
	GSr1	ns	ns	ns
	Fd-GOGAT	*	ns	ns
	GS2a	ns	ns	**
	GS2b	*	ns	ns
	NiR	***	***	***
C_4 pathway enzymes	*TaNADP-ME_1*	ns	ns	ns
	TaPPDK_1α	**	ns	***
	TaPEPC_5	*	ns	***
	TaMDH_7	*	ns	***

Table 2

Gene Name	Relative expression				Log2 fold change	
	Huandoy		Amurskaja 75		Huandoy	Amurskaja75
	C	HT	C	HT	HT - C	HT - C
rbcS	6.73	6.02	5.78	4.81	-0.71	-0.97
rbcL	12.55	11.91	11.72	11.83	-0.64	0.11

Table 3.

Gene Name	Relative expression				Log2 fold change	
	Huandoy		Amurskaja 75		Huandoy	Amurskaja75
	C	HT	C	HT	HT - C	HT - C
SPS1	1.77	1.85	2.33	1.99	0.09	-0.34
SUS1	3.28	3.87	3.28	2.46	0.59	-0.82
SPP1	1.32	1.37	1.44	0.87	0.04	-0.57

Table 4

Gene Name	Relative expression				Log2 fold change	
	Huandoy		Amurskaja 75		Huandoy	Amurskaja75
	C	HT	C	HT	HT - C	HT - C
TaNADP-ME_1	-0.53	-0.41	0.21	-0.41	0.12	-0.61
TaPPDK_1α	0.28	1.36	0.88	-0.21	1.08	-1.09
TaPEPC_5	-0.21	0.69	1.36	0.12	0.89	-1.25
TaMDH_7	-2.70	-0.87	-0.43	-1.83	1.82	-1.40

Table 5

Gene Name	Relative expression				Log2 fold change	
	Huandoy		Amurskaja 75		Huandoy	Amurskaja75
	C	HT	C	HT	HT - C	HT - C
NADH-GOGAT	0.41	-0.26	0.37	0.33	-0.66	-0.04
GS1a	1.05	1.43	2.24	1.35	0.37	-0.89
GSr1	0.27	0.26	0.17	0.03	-0.01	-0.14
Fd-GOGAT	2.63	2.63	3.23	2.89	0.00	-0.34
GS2a	3.26	2.58	2.63	2.85	-0.68	0.22
GS2b	-3.64	-4.07	-4.26	-4.14	-0.42	0.11
NiR	-1.09	-1.72	-2.03	-4.75	-0.63	-2.73

Table 6

Accession No	Protein names and metabolic pathway	Fold change at elevated temperature	P value
	Carbohydrate metabolism		
W5FL09	Fructose-bisphosphate aldolase (EC 4.1.2.13)	**0.67**	*
A0A1D5RVB3	Phosphotransferase (EC 2.7.1.-)	**-0.37**	*
	Photosynthesis		
Q6XW17	Photosystem II polypeptide (Fragment)	**-0.52**	**
A0A1D5UBN5	UMP-CMP kinase (EC 2.7.4.14) (Deoxycytidylate kinase) (CK) (dCMP kinase) (Uridine monophosphate/cytidine monophosphate kinase) (UMP/CMP kinase) (UMP/CMPK)	**-0.40**	**
Q5S744	Chloroplast acetyl-CoA carboxylase (EC 6.4.1.2) (Fragment)	**0.48**	*
A0A1D6DFN1	Phosphoribulokinase (EC 2.7.1.19)	**0.32**	*
S4Z0B1	Cytochrome b559 subunit alpha (PSII reaction center subunit V)	**-0.41**	*
	Protein synthesis and post translational modifications		
U5HTD8	Ribosomal protein S20	**0.61**	**
A0A1D5RXH7	Proteasome subunit alpha type (EC 3.4.25.1)	**-0.50**	**
W5BPU1	40S ribosomal protein SA	**0.52**	*
W5C3H4	Proteasome subunit alpha type (EC 3.4.25.1)	**0.51**	*
A0A1D6CDN7	40S ribosomal protein S30	**0.43**	*
	Antioxidant defense system		
Q8LGN5	Glutathione-S-transferase 19E50	**0.60**	**
W5EC14	Dirigent protein	**1.25**	**
Q9SP56	Glutathione S-transferase	**0.44**	*
C3VQ52	Ascorbate peroxidase (Fragment)	**0.47**	*
Q5QJA5	Harpin binding protein 1	**-0.36**	*
A0A1D5X7C5	Protein disulfide-isomerase (EC 5.3.4.1)	**0.40**	*

	Energy production		
A0A1D5ZJM0	Cytochrome b-c1 complex subunit 7	**-0.75**	**
A0A1D6RDZ8	Phosphoglycerate kinase (EC 2.7.2.3)	**0.37**	*
	Signaling		
C0SPI3	Polyphenol oxidase	**0.38**	*
A0A1D5ZA24	Clathrin heavy chain	**0.36**	*
	Gene expression (transcription)		
A0A1D5Z8I6	Histone H4	**-0.49**	**
A0A1D5SHX1	Tubulin beta chain	**0.59**	*
W5A3G5	Profilin	**-0.51**	*
A0A1D5XQ86	Alanine--tRNA ligase (EC 6.1.1.7) (Alanyl-tRNA synthetase) (AlaRS)	**0.34**	*
	Nitrogen assimilation		
A0A1D6AQA7	Glutamine synthetase	**0.51**	**

Table 7

Accession No	Protein names	Fold Change at elevated temperature	P Value
	Carbohydrate metabolism		
A0A1D5YRW6	Fructose-bisphosphate aldolase (EC 4.1.2.13)	**-0.31**	*
	Photosynthesis		
Q45FE7	Geranylgeranyl hydrogenase	**0.46**	**
Q5S744	Chloroplast acetyl-CoA carboxylase (EC 6.4.1.2) (Fragment)	**0.43**	*
A1YV22	Photosystem I iron-sulfur center (EC 1.97.1.12) (9 kDa polypeptide) (PSI-C) (Photosystem I subunit VII) (PsaC)	**0.40**	*
S4Z0B1	Cytochrome b559 subunit alpha (PSII reaction center subunit V)	**-0.47**	*
Q6XW17	Photosystem II polypeptide (Fragment)	**0.41**	*
A0A1D6DFN1	Phosphoribulokinase (EC 2.7.1.19)	**0.31**	*
A0A1D5UBN5	UMP-CMP kinase (EC 2.7.4.14) (Deoxycytidylate kinase) (CK) (dCMP kinase) (Uridine monophosphate/cytidine monophosphate kinase) (UMP/CMP kinase) (UMP/CMPK)	**-0.29**	*
	Protein synthesis and post translational modifications		
A0A1D6CDN7	40S ribosomal protein S30	**0.74**	**
A0A1D6C4Q5	60S acidic ribosomal protein P0	**-0.52**	**
A0A1D5XUJ3	40S ribosomal protein S21	**-0.48**	*
S4Z9J2	30S ribosomal protein S7, chloroplastic	**-0.43**	*
A0A1D5RXH7	Proteasome subunit alpha type (EC 3.4.25.1)	**-0.35**	*
W5C3H4	Proteasome subunit alpha type (EC 3.4.25.1)	**0.50**	*
A0A1D5S805	60S ribosomal protein L36	**0.42**	*
	Antioxidant defense system		
Q8LGN5	Glutathione-S-transferase 19E50	**0.82**	***
Q9LD25	Phenylalanine ammonia lyase (Fragment)	**-0.93**	***

A0A1D6RKR9	Isocitrate dehydrogenase [NADP] (EC 1.1.1.42)	**0.52**	**
W5CQ97	Cysteine proteinase inhibitor	**0.47**	**
Q8GZB9	Putative ascorbate peroxidase (Fragment)	**-0.41**	*
A0A1D6RUV7	Dirigent protein	**-0.51**	*
W5GUI9	Phenylalanine ammonia-lyase (EC 4.3.1.24)	**0.43**	*
Q9S8F6	Glycosylated protein disulfide isomerase homolog (Fragment)	**0.30**	*
	Energy production		
A0A1D5YL67	Glyceraldehyde-3-phosphate dehydrogenase (EC 1.2.1.-)	**0.84**	**
A0A1D5YWR2	Succinate dehydrogenase [ubiquinone] flavoprotein subunit, mitochondrial (EC 1.3.5.1)	**0.78**	**
S4Z0A5	ATP synthase epsilon chain, chloroplastic (ATP synthase F1 sector epsilon subunit) (F-ATPase epsilon subunit)	**-0.54**	*
	Signaling		
A0A1D5T1D8	SHAGGY-like kinase	**0.58**	**
A0A1D6S3V8	Cysteine synthase (EC 2.5.1.47)	**0.91**	*
D2KZ12	3-ketoacyl-CoA thiolase-like protein	**0.51**	*
C0SPI3	Polyphenol oxidase	**-0.41**	*
	Gene expression (transcription)		
A0A1D6RGU8	Importin subunit alpha	**-0.77**	**
Q9FXQ9	TaWIN1	**0.57**	**
A0A1D5X443	Low temperature-responsive RNA-binding protein	**-0.65**	**
O81331	Vacuolar invertase (EC 3.2.1.26) (Fragment)	**0.45**	**
A0A1D5U4G9	Adenosylhomocysteinase (EC 3.3.1.1)	**-0.44**	*
A0A1D5XQ86	Alanine--tRNA ligase (EC 6.1.1.7) (Alanyl-tRNA synthetase) (AlaRS)	**0.38**	*
A4K4Z1	Tubulin alpha chain	**0.51**	*
	Nitrogen assimilation		
A0A1D6AQA7	Glutamine synthetase	**0.40**	*

Supplementary Table S1. Atmospheric conditions of the low-temperature growth cabinet

Growth cabinet one: low temperature		
Hours	**Light intensity**	**Temperature °C**
0-4	Off	14
4-5	On (20%)	16
5-6	On (30%)	18
6-7	On (50%)	20
7-17	On (60%)	22
17-18	On (50%)	20
18-19	On (30%)	18
19-20	On (20%)	16
20-23	Off	14

Supplementary Table S2. Atmospheric conditions of the elevated temperature growth cabinet.

Hours	**Light intensity**	**Temperature °C**
0-4	Off	22
4-5	On (20%)	24
5-6	On (30%)	26
6-7	On (50%)	28
7-17	On (60%)	30
17-18	On (50%)	28
18-19	On (30%)	26
19-20	On (20%)	24
20-23	Off	22

Supplementary Table S3. List of primer sequences of genes selected for qRT-PCR

Primer abbreviation	Sequence (5'------3')	Metabolism	Reference
NiR	F: AACCTCCTCTCCTCCTACATCA R: CCTAGGAAGGTTGGTGATGGC	N metabolism	Vicente et al, 2015
Fd-GOGAT	F: CGGCAATGGAGGCTGAGCAACA R: TGAGCCTGCTCGATGGTCACTGT		
GS2a	F: CTCATGGTGTGTTGCGAACC R: GGTCCTCCAGGTATCCTTTGC		
GS2b	F: TGAAGGAAACGAGCGGAGAC R: CTCGCCCCACACGAATAGAG		
NADH-GOGAT	F: GCCATTGAATCAGTTCCAGGGCCAC R: GCCAGCACCTGAGCTTTCCTGATG		
GS1a	F: AGGTCATCGTGGATGCCGTGGA R: TTTGCGACGCCCCAGCTGAA		
GSr1	F: AAGGGCTACTTCGAGGACCGCA R: ATGATCTGGCGGCGGTAGGCAT		
TaPEPC_5	F: CAGGGTGAAGTTATCGAGCAG R: ACTTGGCTTTCTCTTGGATGG	C_4 pathway enzymes	Bachir et al. 2017
TaNADP-ME _1	F: CTCTACATCAGCCTCAAGGAC R: CGTTGAGCAATGTCTCGTTG		
TaPPDK_1α	F: CAGGCTTGGTATTTCGTATC R: CTGCTCTGCTATCTCATCT		
TaMDH_7	F: CGATTGCTGCTGAGATTC R: CAGCGTTCTGTATCCTCT		
rbcL	F: GGCTGCAGTAGCTGCCGAATCT R: TCCCCAGCAACAGGCTCGATGT	Rubisco biosynthesis and sucrose metabolism	Vicente et al, 2015
rbcS	F: AGCCTCAGCAGCGTCAGCAAT R: CGTGGATAGGGGTGGCAGGTAAGA		
SPP1	F: GCGCACGGGAAGGAGTTTTTCTTCT R: GACCTCCGTAGACATCATCCAGCCC		
SPS1	F: AGAAGGCTCTGCCTCCCATTTGGTC R: AGGATCATCGGCTTGTGCGGGTT		
SUS1	F: GTATGTTCACCAGGGCAAGGGCA R: GGCGTCAAACTCAGCAAGCAGC		
ADP riosylation factor	F: GCTCTCCAACAACATTGCCAAC R: GCTTCTGCCTGTCACATACGC	Housekeeping genes	Vicente et al, 2015
TaActin-F	F: TTGCTGACCGTATGAGCAAG R: ACCCTCCAATCCAGACACTG		Bachir et al. 2017
TaSand-F	F: TGCCTTGCCCATAAGAAATC R: GTGCGGACCAGTTGCTTTAT		

References

Almeselmani, M., Deshmukh, P. & Chinnusamy, V. J. P. S. 2012. Effects of prolonged high temperature stress on respiration, photosynthesis and gene expression in wheat (Triticum aestivum L.) varieties differing in their thermotolerance. 6**,** 25-32.

Asseng, S., Ewert, F., Martre, P., Rötter, R. P., Lobell, D. B., Cammarano, D., Kimball, B., Ottman, M. J., Wall, G. & White, J. W. J. N. C. C. 2015. Rising temperatures reduce global wheat production. 5**,** 143.

Asseng, S., Foster, I. & Turner, N. C. J. G. C. B. 2011. The impact of temperature variability on wheat yields. 17**,** 997-1012.

Bachir, D. G., Saeed, I., Song, Q., Linn, T. Z., Chen, L. & Hu, Y.-G. J. J. O. P. P. 2017. Characterization and expression patterns of key C4 photosynthetic pathway genes in bread wheat (Triticum aestivum L.) under field conditions. 213**,** 87-97.

Battistelli, A., Adcock, M. D. & Leegood, R. C. J. P. 1991. The relationship between the activation state of sucrose-phosphate synthase and the rate of CO 2 assimilation in spinach leaves. 183**,** 620-622.

Baxter, C. J., Foyer, C. H., Turner, J., Rolfe, S. A. & Quick, W. P. J. J. O. E. B. 2003. Elevated sucrose-phosphate synthase activity in transgenic tobacco sustains photosynthesis in older leaves and alters development. 54**,** 1813-1820.

Bernard, S. M., Møller, A. L. B., Dionisio, G., Kichey, T., Jahn, T. P., Dubois, F., Baudo, M., Lopes, M. S., Tercé-Laforgue, T. & Foyer, C. H. J. P. M. B. 2008. Gene expression, cellular localisation and function of glutamine synthetase isozymes in wheat (Triticum aestivum L.). 67**,** 89-105.

Berry, J. & Bjorkman, O. J. a. R. O. P. P. 1980. Photosynthetic response and adaptation to temperature in higher plants. 31**,** 491-543.

Caemmerer, S. V., Ghannoum, O., Pengelly, J. J. & Cousins, A. B. J. J. O. E. B. 2014. Carbon isotope discrimination as a tool to explore C4 photosynthesis. 65**,** 3459-3470.

Choudhury, F. K., Rivero, R. M., Blumwald, E. & Mittler, R. J. T. P. J. 2017. Reactive oxygen species, abiotic stress and stress combination. 90**,** 856-867.

Coleman, H. D., Yan, J. & Mansfield, S. D. J. P. O. T. N. a. O. S. 2009. Sucrose synthase affects carbon partitioning to increase cellulose production and altered cell wall ultrastructure. 106**,** 13118-13123.

Dehigaspitiya, P., Milham, P., Ash, G. J., Arun-Chinnappa, K., Gamage, D., Martin, A., Nagasaka, S. & Seneweera, S. J. P. 2019. Exploring natural variation of photosynthesis in a site-specific manner: evolution, progress, and prospects. 1-18.

Echeverria, E., Salvucci, M. E., Gonzalez, P., Paris, G. & Salerno, G. J. P. P. 1997. Physical and kinetic evidence for an association between sucrose-phosphate synthase and sucrose-phosphate phosphatase. 115**,** 223-227.

Farooq, M., Bramley, H., Palta, J. A. & Siddique, K. H. J. C. R. I. P. S. 2011. Heat stress in wheat during reproductive and grain-filling phases. 30**,** 491-507.

Farquhar, G. D., O'leary, M. H. & Berry, J. a. J. F. P. B. 1982. On the relationship between carbon isotope discrimination and the intercellular carbon dioxide concentration in leaves. 9**,** 121-137.

Ferris, R., Ellis, R., Wheeler, T. & Hadley, P. J. a. O. B. 1998. Effect of high temperature stress at anthesis on grain yield and biomass of field-grown crops of wheat. 82**,** 631-639.

Fischer, R. J. T. J. O. a. S. 1985. Number of kernels in wheat crops and the influence of solar radiation and temperature. 105**,** 447-461.

Freeha, A., Abdul, W., Farrukh, J., Muhammad, A. J. I. J. O. A. & Biology 2008. Influence of foliar applied thiourea on flag leaf gas exchange and yield parameters of bread wheat (Triticum aestivum) cultivars under salinity and heat stresses. 10**,** 619-626.

Gibson, L. & Paulsen, G. J. C. S. 1999. Yield components of wheat grown under high temperature stress during reproductive growth. 39**,** 1841-1846.

Ishihama, Y., Rappsilber, J. & Mann, M. J. J. O. P. R. 2006. Modular stop and go extraction tips with stacked disks for parallel and multidimensional Peptide fractionation in proteomics. 5**,** 988-994.

Jenner, C. J. F. P. B. 1994. Starch synthesis in the kernel of wheat under high temperature conditions. 21**,** 791-806.

Jiang, S.-Y., Chi, Y.-H., Wang, J.-Z., Zhou, J.-X., Cheng, Y.-S., Zhang, B.-L., Ma, A., Vanitha, J. & Ramachandran, S. J. S. R. 2015. Sucrose metabolism gene families and their biological functions. 5**,** 17583.

Kamachi, K., Yamaya, T., Hayakawa, T., Mae, T. & Ojima, K. J. P. P. 1992. Vascular bundle-specific localization of cytosolic glutamine synthetase in rice leaves. 99**,** 1481-1486.

Kaše, M. & Čatský, J. J. B. P. 1984. Maintenance and growth components of dark respiration rate in leaves of C 3 and C 4 plants as affected by leaf temperature. 26**,** 461-470.

Le, D. Q., Tanaka, K., Dung, L. V., Siau, Y. F., Lachs, L., Kadir, S. T. S. A., Sano, Y. & Shirai, K. J. R. S. I. M. S. 2017. Biomagnification of total mercury in the mangrove lagoon foodweb in east coast of Peninsula, Malaysia. 16**,** 49-55.

Lesk, C., Rowhani, P. & Ramankutty, N. J. N. 2016. Influence of extreme weather disasters on global crop production. 529**,** 84.

Li, Y., Heckmann, D., Lercher, M. J. & Maurino, V. G. J. J. O. E. B. 2017. Combining genetic and evolutionary engineering to establish C4 metabolism in C3 plants. 68**,** 117-125.

Lowe, R. G., Mccorkelle, O., Bleackley, M., Collins, C., Faou, P., Mathivanan, S. & Anderson, M. J. F. I. P. S. 2015. Extracellular peptidases of the cereal pathogen Fusarium graminearum. 6**,** 962.

Lunn, J. E. & Macrae, E. J. C. O. I. P. B. 2003. New complexities in the synthesis of sucrose. 6**,** 208-214.

Majoul, T., Bancel, E., Triboï, E., Ben Hamida, J. & Branlard, G. J. P. 2003. Proteomic analysis of the effect of heat stress on hexaploid wheat grain: Characterization of heat-responsive proteins from total endosperm. 3**,** 175-183.

Majoul, T., Bancel, E., Triboï, E., Ben Hamida, J. & Branlard, G. J. P. 2004. Proteomic analysis of the effect of heat stress on hexaploid wheat grain: characterization of heat-responsive proteins from non-prolamins fraction. 4**,** 505-513.

Masclaux-Daubresse, C., Daniel-Vedele, F., Dechorgnat, J., Chardon, F., Gaufichon, L. & Suzuki, A. J. a. O. B. 2010. Nitrogen uptake, assimilation and remobilization in plants: challenges for sustainable and productive agriculture. 105**,** 1141-1157.

Mittler, R., Vanderauwera, S., Gollery, M. & Van Breusegem, F. J. T. I. P. S. 2004. Reactive oxygen gene network of plants. 9**,** 490-498.

Mittler, R., Vanderauwera, S., Suzuki, N., Miller, G., Tognetti, V. B., Vandepoele, K., Gollery, M., Shulaev, V. & Van Breusegem, F. J. T. I. P. S. 2011. ROS signaling: the new wave? 16**,** 300-309.

Ogren, W. L. J. a. R. O. P. P. 1984. Photorespiration: pathways, regulation, and modification. 35**,** 415-442.

Porter, J. R. & Gawith, M. J. E. J. O. A. 1999. Temperatures and the growth and development of wheat: a review. 10**,** 23-36.

Rangan, P., Furtado, A. & Henry, R. J. J. S. R. 2016. New evidence for grain specific C 4 photosynthesis in wheat. 6**,** 31721.

Reduction, U. J. G. a. R. O. D. R. 2013. From shared risk to shared value: the business case for disaster risk reduction.

Ruan, Y.-L., Jin, Y., Yang, Y.-J., Li, G.-J. & Boyer, J. S. J. M. P. 2010. Sugar input, metabolism, and signaling mediated by invertase: roles in development, yield potential, and response to drought and heat. 3**,** 942-955.

Ruelland, E., Zachowski, A. J. E. & Botany, E. 2010. How plants sense temperature. 69**,** 225-232.

Saini, H. & Aspinall, D. J. a. O. B. 1982. Abnormal sporogenesis in wheat (Triticum aestivum L.) induced by short periods of high temperature. 49**,** 835-846.

Salvucci, M. E., Osteryoung, K. W., Crafts-Brandner, S. J. & Vierling, E. J. P. P. 2001. Exceptional sensitivity of Rubisco activase to thermal denaturation in vitro and in vivo. 127**,** 1053-1064.

Satorre, E. H. & Slafer, G. A. 1999. *Wheat: ecology and physiology of yield determination*, CRC Press.

Shah, N., Paulsen, G. J. P. & Soil 2003. Interaction of drought and high temperature on photosynthesis and grain-filling of wheat. 257**,** 219-226.

Sharkey, T. D. J. P., Cell & Environment 2005. Effects of moderate heat stress on photosynthesis: importance of thylakoid reactions, rubisco deactivation, reactive oxygen species, and thermotolerance provided by isoprene. 28**,** 269-277.

Shiferaw, B., Smale, M., Braun, H.-J., Duveiller, E., Reynolds, M. & Muricho, G. J. F. S. 2013. Crops that feed the world 10. Past successes and future challenges to the role played by wheat in global food security. 5**,** 291-317.

Shpiler, L. & Blum, A. J. E. 1986. Differential reaction of wheat cultivars to hot environments. 35**,** 483-492.

Stitt, M. J. P. P. 1986. Limitation of photosynthesis by carbon metabolism: I. Evidence for excess electron transport capacity in leaves carrying out photosynthesis in saturating light and CO2. 81**,** 1115-1122.

Suzuki, Y., Kihara-Doi, T., Kawazu, T., Miyake, C., Makino, A. J. P., Cell & Environment 2010. Differences in Rubisco content and its synthesis in leaves at different positions in Eucalyptus globulus seedlings. 33**,** 1314-1323.

Suzuki, Y., Miyamoto, T., Yoshizawa, R., Mae, T., Makino, A. J. P., Cell & Environment 2009. Rubisco content and photosynthesis of leaves at different positions in transgenic rice with an overexpression of RBCS. 32**,** 417-427.

Tadesse, W., Halila, H., Jamal, M., El-Hanafi, S., Assefa, S., Oweis, T., Baum, M. J. J. O. E. B. & Sciences, A. 2017. Role of Sustainable Wheat Production to Ensure Food Security in the CWANA region. 5**,** S15-S32.

Tewolde, H., Fernandez, C., Erickson, C. J. J. O. A. & Science, C. 2006. Wheat cultivars adapted to post-heading high temperature stress. 192**,** 111-120.

Vicente, R., Pérez, P., Martínez-Carrasco, R., Usadel, B., Kostadinova, S., Morcuende, R. J. P. & Physiology, C. 2015. Quantitative RT–PCR platform to measure transcript levels of C and N metabolism-related genes in durum wheat: transcript profiles in elevated [CO2] and high temperature at different levels of N supply. 56**,** 1556-1573.

Wahid, A., Gelani, S., Ashraf, M., Foolad, M. R. J. E. & Botany, E. 2007. Heat tolerance in plants: an overview. 61**,** 199-223.

Wang, S., Tholen, D., Zhu, X. G. J. P., Cell & Environment 2017. C4 photosynthesis in C3 rice: a theoretical analysis of biochemical and anatomical factors. 40**,** 80-94.

Wise, R., Olson, A., Schrader, S., Sharkey, T. J. P., Cell & Environment 2004. Electron transport is the functional limitation of photosynthesis in field-grown Pima cotton plants at high temperature. 27**,** 717-724.

Yadav, S. S., Redden, R. J., Hatfield, J. L., Ebert, A. W. & Hunter, D. 2019. *Food Security and Climate Change*, Wiley-Blackwell.

CHAPTER 7

GENERAL DISCUSSION, CONCLUSION AND FUTURE DIRECTIONS

7.1 General Discussion

Wheat is considered a classical C_3 cereal based on its leaf photosynthesis, yet evidence is mounting that a different mode of photosynthesis may operate in wheat spikes, raising the possibility of manipulating this physiological trait for future crop improvement (Dehigaspitiya et al., 2019). Other vital metabolic processes such as nitrogen (N) assimilation and sucrose metabolism could also vary site-specifically and may have significant roles in grain quality and quantity. To test these hypotheses I investigated site-specific, genotypic and temporal variation in carbon assimilation and other photosynthesis-related processes in wheat using wheat spikes and flag leaves of three wheat genotypes (Huandoy, Amurskaja 75 and Greece25) at different growth stages [heading, three days post-anthesis (3-dpa), fourteen days post-anthesis (14-dpa), thirty days post-anthesis (30-dpa) and maturity (CM)].

A major initial technical hurdle for the study was to measure the gas exchange parameters of wheat spikes. This was difficult because spikes differ structurally and physiologically from leaves for which most gas exchange protocols are designed. The LI-COR conifer chamber (6400-05) is designed to connect with LI-COR 6400 portable photosynthesis system to determine gas exchange parameters of short needle conifers in a chamber environment where humidity, temperature, and CO_2 are controlled by LI-COR 6400. In Chapter 3, I optimized a methodology of analysing gas exchange of wheat spikes using the LI-COR portable photosynthesis system coupled with LI-COR conifer chamber, using an external light source. I provided two methods of calculating the photosynthetic area of wheat spikes, which is a vital piece of information when determining gas exchange parameters of photosynthetic organs. Together these developments enabled me to calculate the biological capacity of carbon assimilation (Vc_{max} and J_{max}) of wheat spikes at different growth stages using carbon dioxide response (A-C_i) curves (Chapter 3). This method can be extended in

phenotyping and determining the gas exchange of other photosynthetic organs such as rice panicles.

Chapter 4 integrated the site-specific, genotypic, and temporal variation of the photosynthesis in wheat (Chapter 3) with biochemical, and molecular approaches focussing on wheat spikes and flag leaves. Molecular-level changes in photosynthesis and sucrose metabolism were investigated using the expression of key genes of Rubisco biosynthesis (*rbcL* and *rbcS*) and sucrose metabolism (*SPS1, SUS1*, and *SPP1*). The results confirmed the hypothesis of site-specific photosynthesis and significant genotypic, site-specific, and temporal variations in the biological capacity of carbon assimilation. The highest biological capacity of carbon assimilation both in wheat spikes and flag leaves was at 14-dpa. The highest biomass accumulation in wheat spikes was also between 14-dpa and 30-dpa. During early to mid-grain filling (heading to 14-dpa), wheat flag leaves displayed a significantly higher Vc_{max} and J_{max} than wheat spikes. Interestingly, at late grain filling (30-dpa), there was a steady decrease in the biological capacity of carbon assimilation of wheat flag leaves and the difference in Vc_{max} and J_{max} between spikes and flag-leaves was not significantly different, maybe due to early leaf senescence. This again supports my hypothesis of much higher spike contribution to crop yield than leaves specifically at late grain filling stage. Results of phenotyping further supported this observation (Chapter 4). Although there were quantitative differences in the expression of *rbcS* and *rbcL*, both organ types (pericarps and flag leaves) displayed a similar expression pattern across genotypes which was much higher expression at heading and a gradual decrease towards 30-dpa. In both organ types, the *rbcL* expression was much higher than the *rbcS* abundance. As the key enzyme of carbon assimilation, Rubisco plays a vital role in photosynthesis and is accountable for a significant proportion of the N content of a photosynthetic organ (Suzuki et al., 2001). Further, a strong correlation between Vc_{max} and the N content of a photosynthetic organ has also been reported (Walker et al., 2014). Consistent with this proposition, I also observed the highest Vc_{max} at 14-dpa, the stage which showed the highest organ N concentrations. Although the *rbcS* and *rbcL* expression was comparatively lower at 14-dpa than heading, organ-specific N concentrations suggested the maximum Rubisco content was at 14-dpa possibly due to low Rubisco degradation rates during heading to 14-dpa. In addition, I found a marked, organ-specific, variation in expression of *SPS1*, *SUS1,* and *SPP1* along with

genotypic and temporal variation, indicating changes in sucrose metabolism. At 14-dpa, positive correlations between the biological capacity of carbon assimilation of wheat spikes and *SPS1* and *SPP1* were observed. The growth stage heading and the 14-dpa were the most photosynthetically active stages of wheat spikes. Interestingly, the relative expression of *SPS1* and *SPP1* was maximal at those stages, suggesting an increased sucrose biosynthesis in the wheat pericarp, which leads to high carbon assimilation. Phenotyping revealed that the greatest biomass accumulation after heading took place in wheat spikes, consistent with the idea that the C assimilated during the high photosynthetic activity of wheat spikes was directly translocated to the endosperm, contributing in a major way to grain filling.

Chapter 5 investigated the site-specific expression pattern of key C_4 pathway genes during grain filling and determined site-specific variation in nitrogen metabolism. While this experiment did not directly demonstrate C_4 photosynthesis in wheat pericarps, there was a site-specific, genotypic, and temporal variation in the expression of key genes of the C_4 pathway (*TaNADP-ME _1*, *TaPEPC_5*, *TaPPDK_1α*, and *TaMDH_7*). These genes encode for: NADP-dependent malic enzyme (NADP-ME), phosphoenolpyruvate carboxylase (PEPC), pyruvate orthophosphate dikinase (PPDK) and malate dehydrogenase (MDH). Of these genes, in most instances, the highest and the lowest relative expression was with *TaPEPC_5* and *TaMDH_7*, respectively. Wheat is composed of three diploid progenitor sub-genomes (AA, BB, and DD). To gain an overall idea of the expression pattern, the sub-genome specificity of C_4 pathway genes was also tested. The higher expressions of *TaNADP_1BS* suggested that sub-genomes B was mainly accountable for the NADP-ME expression. In contrast, both B and D sub-genomes were responsible for PPDK expression. Even though there was a minimum expression, all sub-genomes of wheat (A, B and D) were responsible for PEPC expression. Isotopic signatures of C ($\delta^{13}C$) in a photosynthetic organ (dry matter) provide clues about the underlying C metabolism. In this study, the C isotopic signatures of wheat spikes and flag leaves were between -27% and -31%. Further, in most cases, site-specific variation in C isotopic signatures was not observed. From these results, I suggested that wheat spikes and flag leaves probably perform the same photosynthetic mode, i.e. C_3. However, determining the photosynthetic pathway based on $\delta^{13}C$ of dry matter may be inaccurate as part of dry matter is imported from other photosynthetic organs.

There was an organ-specific variation in the expression of *GS2a, GS2b, GS1a,* and *GSr1*: key genes which encode GS2 and GS1 isoenzyme families of N metabolism in plants. In both spikes and flag leaves, the maximum relative expression of *GS2a* was at the early reproductive stages and showed a decreasing trend towards late grain filling showing a temporal variation. This expression pattern is an indication for the organ senescence over time, which convert their roles from N-sinks to secondary N-sources. The organ-specific difference I observed in *GS2a* expression was probably due to early senescence of flag leaves as compared to pericarps. The steady increase of *GS1a* expression towards 30-dpa in flag leaves further point toward the fact that the role change in the N metabolism (N remobilization) and much earlier flag leaf senescence compared to pericarps, as GS1 facilitates N remobilization from initial sink tissues to developing sink organs (endosperms) (Masclaux-Daubresse et al., 2006). My results further suggested that the N remobilization of flag leaves starts much earlier than in the wheat pericarps implying the importance of spike N metabolism for grain protein content at the late grain filling stage. To integrate the amino groups into amino acids in protein synthesis, GS enzymes tend to combine with two types of GOGAT (glutamate synthase) enzymes: *Fd-GOGAT* and *NADH-GOGAT,* which show a site-specific localization. Supporting the chloroplastic localization, the expression of genes associated with *Fd-GOGAT* was much higher in flag leaves than in the wheat pericarps. Consistent with the gene expression, organ-specific N concentrations also showed genotypic and temporal variation, supporting much earlier leaf senescence than in wheat spikes. Analysis of grain N content revealed that although the maximum grain N content (mass) per plant was with Huandoy, the maximum grain N concentration was with Amurskaja 75 indicating highest grain quality in Amurskaja 75.

Chapter 6 tested the effect of elevated temperature on spike photosynthesis and other related metabolic processes on varieties Huandoy and Amurskaja 75 at ten days after heading (10-dah). At elevated temperature, grain yield increased by 5% in Amurskaja 75 and decreased by 60% in Huandoy. Gene expression differed between genotypes showing a significant genotypic variation in spike metabolism in response to elevated temperature. According to the proteomics studies, most of the differentially expressed proteins at high temperatures belonged to the antioxidant defense system, photosynthesis, protein synthesis, and energy production. This indicates that along

with the changes in carbon assimilation in wheat pericarps, other metabolic processes such as N and energy pathways also differed in response to high temperatures. Of the differentially expressed proteins, those related to antioxidant defense system were more significant in Huandoy than in Amurskaja 75, indicating that Huandoy was under greater heat stress than Amurskaja 75. Upregulation of proteins related to the antioxidant defense system is an indication of excessive production of reactive oxygen species (ROS). Although ROS have important roles in plant metabolism, including intercellular signaling, excessive ROS production causes oxidative damage (Choudhury et al., 2017). My observation of the expression of proteins related to antioxidant defense system was consistent with the effects on grain yield. In both genotypes, there were numerous uncharacterized proteins which may have performed significant roles in spike metabolism in response to heat stress.

7.2 Conclusions and future directions

The most severe limitation of previous attempts to measure gas exchange parameters (A-Ci curves) of wheat spikes was the requirement of an appropriate chamber which can accommodate wheat spikes and the inability to control the chamber environment precisely. My novel solution optimized in Chapter 3, with a LI-COR portable photosynthesis system coupled with the conifer chamber, could with minor changes be utilized also to analyse gas exchange parameters of other three-dimensional photosynthetic organs, such as rice panicles, fruits, and stems. Further, the optimized area calculation protocol is equally widely applicable. A-Ci curves generated using the above protocol, coupled with other molecular techniques, facilitated observation of mechanistic variation behind the site-specific, genotypic, and temporal changes of photosynthesis and other key metabolic processes in three genotypes of wheat under controlled conditions. The observations allow the proposal of a mechanism of spike contribution to grain filling at leaf senescence.

Nonetheless, more needs to be done to test these findings, e.g. by using more genotypes and growth stages in the field. Knowledge from such studies might open new leads to yield enhancement in economically important C_3 cereals. By mounting a lighted conifer chamber (Li-COR, Lincoln, Nebraska, USA 6400-22L) we can

eliminate the necessity of an external light source for gas exchange measurements. In addition, it may also necessary to identify efficient photosynthetic traits through microscopy since I could not identify strong evidence for the existence of C_4 like photosynthetic pathway in wheat from gene expression and carbon isotopic signatures. There was however site-specific, genotypic and temporal variation in the expression of key C_4 pathway genes, which is worthy of further investigation. In addition, I demonstrated the importance of spike N metabolism for grain protein content specifically during leaf senescence, and identified Amurskaja 75 as a genotype with high grain protein concentration. I investigated the expression only of key genes of each metabolic pathway: new experiments should conduct an in-depth transcriptomic analysis through microarray and make observations at more developmental stages.

Lastly, changes in the proteome of wheat pericarps allowed me to identify the key metabolic pathways affected at high temperatures. However, of the significantly affected proteins, there were numerous uncharacterized proteins which may have prominent roles in plant metabolism. It is essential to characterize the wheat proteome in the future to underpin the mechanistic changes which occur not only at heat stress but also during other biotic and abiotic stresses. Huandoy displayed the highest upregulation of proteins related to antioxidant defence system indicating heat stress. Molecular and physiological findings point to the fact that of the two genotypes, Amurskaja 75 was a heat resistant variety and a possible candidate for crop improvement programs for future climates.

References

Aben SK, Seneweera SP, Ghannoum O, Conroy JPJFPB (1999) Nitrogen requirements for maximum growth and photosynthesis of rice, Oryza sativa L. cv. Jarrah grown at 36 and 70 Pa CO2 26:759-766

Alexandratos N, Bruinsma J (2012) World agriculture towards 2030/2050: the 2012 revision

Choudhury, F. K., Rivero, R. M., Blumwald, E. & Mittler, R. J. T. P. J. 2017. Reactive oxygen species, abiotic stress and stress combination. 90**,** 856-867.

Crist E, Mora C, Engelman RJS (2017) The interaction of human population, food production, and biodiversity protection 356:260-264

Dehigaspitiya P et al. (2019) Exploring natural variation of photosynthesis in a site-specific manner: evolution, progress, and prospects:1-18

Dehigaspitiya, P., Milham, P., Ash, G. J., Arun-Chinnappa, K., Gamage, D., Martin, A., Nagasaka, S. & Seneweera, S. J. P. 2019. Exploring natural variation of photosynthesis in a site-specific manner: evolution, progress, and prospects. 1-18.

Evans JR, Santiago LSJFPB (2014) PrometheusWiki gold leaf protocol: gas exchange using LI-COR 6400 41:223-226

Furbank RT, Quick WP, Sirault XRJFCR (2015) Improving photosynthesis and yield potential in cereal crops by targeted genetic manipulation: prospects, progress and challenges 182:19-29

Lesk C, Rowhani P, Ramankutty NJN (2016) Influence of extreme weather disasters on global crop production 529:84

Li H et al. (2017) Exogenous melatonin confers salt stress tolerance to watermelon by improving photosynthesis and redox homeostasis 8:295

Masclaux-Daubresse, C., Reisdorf-Cren, M., Pageau, K., Lelandais, M., Grandjean, O., Kronenberger, J., Valadier, M.-H., Feraud, M., Jouglet, T. & Suzuki, A. J. P. P. 2006. Glutamine synthetase-glutamate synthase pathway and glutamate dehydrogenase play distinct roles in the sink-source nitrogen cycle in tobacco. 140**,** 444-456.

Peterhansel C et al. (2013) Engineering photorespiration: current state and future possibilities 15:754-758

Rangan P, Furtado A, Henry RJJSr (2016) New evidence for grain specific C 4 photosynthesis in wheat 6:31721

Sanchez-Bragado R, Molero G, Reynolds MP, Araus JLJJoeb (2014) Relative contribution of shoot and ear photosynthesis to grain filling in wheat under good agronomical conditions assessed by differential organ δ13C 65:5401-5413

Sanchez-Bragado R, Molero G, Reynolds MP, Araus JLJJoeb (2016) Photosynthetic contribution of the ear to grain filling in wheat: a comparison of different methodologies for evaluation 67:2787-2798

Shewry PRJJoeb (2009) Wheat 60:1537-1553

Shiferaw B, Smale M, Braun H-J, Duveiller E, Reynolds M, Muricho GJFS (2013) Crops that feed the world 10. Past successes and future challenges to the role played by wheat in global food security 5:291-317

Suzuki, Y., Makino, A., Mae, T. J. P., Cell & Environment 2001. Changes in the turnover of Rubisco and levels of mRNAs of rbcL and rbcS in rice leaves from emergence to senescence. 24**,** 1353-1360.

Wahid A, Gelani S, Ashraf M, Foolad MRJE, botany e (2007) Heat tolerance in plants: an overview 61:199-223

Walker, A. P., Beckerman, A. P., Gu, L., Kattge, J., Cernusak, L. A., Domingues, T. F., Scales, J. C., Wohlfahrt, G., Wullschleger, S. D., Woodward, F. I. J. E. & Evolution 2014. The relationship of leaf photosynthetic traits–Vcmax and Jmax–to leaf nitrogen, leaf phosphorus, and specific leaf area: a meta-analysis and modeling study. 4**,** 3218-3235.